uOttawa

CFD and Experimental Investigation of Dense Jet Interaction with Cross-flows for Sustainable Coastal Outfall Design and Environmental Impact Mitigation

by

Mostafa Taherian

Thesis submitted to the University of Ottawa
in partial fulfillment of the requirements for the
Doctorate in Philosophy degree in Civil Engineering

Department of Civil Engineering
Faculty of Engineering
University of Ottawa

Abstract

The scarcity and security of freshwater are becoming critical global concerns. Seawater reverse osmosis (SWRO) desalination is a promising solution to supply clean water sustainably; however, it produces hypersaline by-products that need to be safely disposed of in ambient environments. The direct discharge of dense effluents can lead to significant environmental issues, including water quality degradation and marine life disruption. A widely accepted method for mitigating these impacts is to use submerged offshore diffusers designed to rapidly dilute effluents to near-background levels, thus minimizing environmental harm. For an optimal design, it is essential to understand the influence of the ambient hydrodynamic forces and discharge characteristics on their performance.

Realistic coastal environments are dynamic and dominated by flowing currents, turbulence, and shear, which complicate the interaction between buoyant discharges and cross-flow currents. This interaction, known as buoyant jet in cross-flow (JICF), highlights the need for accurate predictions of jet flow behavior and mixing while presenting considerable challenges. Therefore, a deeper understanding and more precise design guidelines for these outfalls are crucial. This thesis represents the first attempt to experimentally and numerically simulate dense discharges with various source inclinations, issuing perpendicular cross-flow currents with 3D trajectories.

First, a comprehensive review of the developments and applications of buoyant JICFs and computational fluid dynamics (CFD) modeling of outfall discharges was conducted to identify existing knowledge gaps. The review revealed deficiencies in understanding the combined effects of different flowing current strengths and nozzle inclinations on the discharge performance, warranting further investigation. Although CFD methods for simulating outfall discharges have advanced, their application to buoyant JICFs is still in the early stages, presenting significant opportunities for further research.

Second, laser-induced fluorescence (LIF) experiments were conducted to examine the effects of the flowing current strength and nozzle inclination on dense jets discharging perpendicular to the cross-flows. Nozzle angles of 30°, 45°, and 60° and various cross-flow Froude numbers ($u_r F$, where u_r is the ratio of ambient cross-flow to jet velocity and F is the jet-densimetric Froude number) were studied to assess the 3D jet trajectories and concentration distributions. Empirical equations describing the jet dilution and geometrical characteristics were derived. The findings showed that the 60° jet achieved dilutions of over 50% and 20%, on average,

more than those of the 30° and 45° jets, respectively, due to its longer trajectory and greater expansion. These results challenge previous reports that dilution is insensitive to nozzle angles between 40°-70° in stationary ambient water and highlight the 60° jet's sensitivity to changes in $u_r F$ compared to shallower angles.

Third, a numerical study was conducted using the OpenFOAM finite-volume model. The accuracy of the model was verified by comparing the results from four Reynolds-averaged Navier-Stokes (RANS) simulations—standard k-ε, realizable k-ε, k-ω shear stress transport (SST), and Launder-Reece-Rodi (LRR)—with experimental data from the literature. The realizable k–ε and LRR schemes showed strong potential for simulating the flow behavior and dilution performance of dense JICFs due to their incorporation of realizability assumptions and Reynolds stress transport equations, respectively. In addition, the modeling approach successfully visualized the evolution of a time-averaged counter-rotating vortex pair (CRVP) along the jet trajectory.

Fourth, the large eddy simulation (LES) modeling technique with OpenFOAM was used to reproduce our LIF experimental results for the 60° dense jets, which demonstrated superior mixing performance. Simulations were extended to a broader range of cross-flow Froude numbers, identifying three regimes: jet-dominated, regular cross-flow, and strong cross-flow-dominated. The LES results aligned well with the experimental data, confirming LES as a reliable method for capturing the complex flow behavior and dilution characteristics of dense JICFs.

This research provides valuable insights for protecting coastal water bodies and improving the design and operational efficiency of submerged dense outfall systems. It underscores the importance of understanding the interaction between varying current strengths and discharge inclinations to optimize outfall performance in dynamic environments. Furthermore, the research discusses and highlights the capabilities of different CFD modeling approaches for outfall engineering design.

Publications Included in this Thesis

The following publications have been produced as a result of this research and are included in this thesis:

- **Taherian, M.,** Mohammadian, A. (2021). Buoyant Jets in Cross-flows: Review, Developments, and Applications. Journal of Marine Science and Engineering, 9 (1), 61.
  https://www.mdpi.com/2077-1312/9/1/61
  Incorporated within Chapter 2.
- **Taherian, M.**, Saeidi Hosseini, S. A. R., Mohammadian, A., Ferrari, S., Roberts, P. J. (2024). Laboratory study on inclined desalination discharges in perpendicular cross-flow. Desalination, 583, 117719.
  https://www.sciencedirect.com/science/article/abs/pii/S0011916424004302
  Incorporated within Chapter 3.
- **Taherian, M.**, Saeidi Hosseini, S. A. R., Mohammadian, A. (2022). CFD Numerical Simulation of Submerged Dense Jets in Cross-flows. In Proceedings of the 39th IAHR World Congress, Granada, Spain.
  https://www.iahr.org/library/infor?pid=20964
  Incorporated within Chapter 4.
- **Taherian, M.**, Mohammadian, A., Goodarzi, D., Saeidi Hosseini, S. A. R. Large Eddy Simulation Study on the Mixing Behavior of Inclined Dense Jets in Cross-flow. (This paper will be submitted in a couple of weeks in the Desalination Journal.)
  Incorporated within Chapter 5.
- **Taherian, M.**, Saeidi Hosseini, S. A. R., Mohammadian, A. (2022). Overview of outfall discharge modeling with a focus on turbulence modeling approaches. In Advances in Fluid Mechanics: Modelling and Simulations (pp. 139-177). Singapore: Springer Nature Singapore.
  https://link.springer.com/chapter/10.1007/978-981-19-1438-6_4
  Incorporated within Appendix.

Other Publications during Candidature

The following publications have been produced during my Ph.D. study at the University of Ottawa:

- Behzad, E., Rennie, C., Mohammadian, A. **Taherian., M**. (Submitted). Experimental Investigation of Positively Buoyant Surface Jet in Confluence Regions. Environmental Processes.
  https://www.researchsquare.com/article/rs-4870938/v1
- Saeidi Hosseini, S. A. R., **Taherian, M.**, Mohammadian, A., Ferrari, S., Roberts, P. J. (2023). Mixing behavior of multiport diffusers with nonuniform port orientations. Desalination, 567, 116962.
  https://www.sciencedirect.com/science/article/abs/pii/S0011916423005945
- Saeidi Hosseini, S. A. R., **Taherian, M.**, Mohammadian, A. (2022). Large Eddy Simulation of Multiple Inclined Brine Discharges. In Proceedings of the 39th IAHR World Congress, Granada, Spain.
  https://www.iahr.org/library/infor?pid=21201
- Attari, M., **Taherian, M.**, Mohammadian, A. (2022). A New Approach for the Determination of Best Field Measurement Points to Estimate Manning's Roughness Coefficient in Natural Rivers. In Proceedings of the 39th IAHR World Congress, Granada, Spain.
  https://www.iahr.org/library/infor?pid=21545
- Attari, M., **Taherian, M.**, Hosseini, S. M., Niazmand, S. B., Jeiroodi, A., Mohammadian, A. (2020). A simple and robust method for identifying the distribution functions of Manning's roughness coefficient along a natural river, Journal of Hydrology, 595, 125680.
  https://www.sciencedirect.com/science/article/abs/pii/S0022169420311410

Table of Contents

List of Figures

List of Tables

List of Abbreviations

3D	Three-Dimensional
AI	Artificial Intelligence
AIZ	Allocated Impact Zone
ARC	Advanced Research Computing
CFD	Computational Fluid Dynamics
CCD	Charge-Coupled Device
DES	Detached Eddy Simulation
DNS	Direct Numerical Simulation
DPSS	Diode-Pumped Solid-State
EPA	Environmental Protection Agency
EU	European Union
EVM	Eddy Viscosity Model
INBJ	Inclined Negative Buoyant Jet
LES	Large Eddy Simulation
LIF	Laser-Induced Fluorescence
LMZ	Legal Mixing Zone
LRR	Launder, Reece, and Rodi
MAPE	Mean Absolute Percentage Error
MGGP	Multigene Genetic Programming
NPDES	National Pollutant Discharge Elimination System
OpenFOAM	Open Field Operation and Manipulation
RANS	Reynolds-Averaged Navier-Stokes
RNG	Re-Normalization Group
RSM	Reynolds Stress Model
SGGP	Single-Gene Genetic Programming

SGS	Subgrid-Scale
SST	Shear Stress Transport
USEPA	United States Environmental Protection Agency
WFD	Water Framework Directive
WALE	Wall-Adapting Local Eddy-viscosity
ZID	Zone of Initial Dilution

List of Symbols

θ	Discharge Initial Angle [º]
φ	Angle Difference Between Adjacent Ports [º]
$\emptyset(t)$	Instantaneous Variable [depends on the variable]
$\overline{\emptyset}$	Mean Component of An Instantaneous Variable [depends on the variable]
$\emptyset'(t)$	Fluctuating Component of An Instantaneous Variable [depends on the variable]
ϕ_{ij}	Pressure-Strain Parameter []
α	Volume Fraction []
Δ	LES Filter Size []
ρ	Local Density [kg/m^3]
ρ_0	Effluent Density [kg/m^3]
ρ_a	Ambient Density [kg/m^3]
ε_{ij}	Turbulence Dissipation Rate Parameter [m^2/s^3]
ν_t	Turbulent Eddy Viscosity [m^2/s]
μ	Dynamic Viscosity [N.s/m^2]
μ_t	Turbulent Viscosity [N.s/m^2]
τ_{ij}	Stress Tensor []
Ω_{ij}	Transport Term by Rotation []

Π_{ij}	Transport Term by Turbulent Pressure-Strain Interactions []
δ_{ij}	Kronecker Delta []
D, d or d_0	Nozzle Diameter [m]
U_0 or U	Jet Velocity [m/s]
F_r	Froude Number []
F_d or F_0	Jet Densimetric Froude Number []
Q	Volume Flux [m/s]
M	Kinematic Momentum Flux [N/m^2]
B	Buoyancy Flux [N/(m^2.s)]
q_0	Volume Flux Per Unit Length [1/s]
m_0	Kinematic Momentum Flux Per Unit Length [N/m^3]
b_0	Buoyancy Flux Per Unit Length [N/(m.s)]
g	Gravitational Acceleration [m/s^2]
g_0'	Reduced Gravitational Acceleration [m/s^2]
l_Q and l_M	Jet Length Scales [m]
S_i	Impact Point Dilution []
S_r	Return Point Dilution []
S_c	Dilution Corresponds to Maximum Centerline Height []
S_n	Near Field Dilution []
x_i	Impact Point Location [m]
x_r	Return Point Location [m]
x_c	Horizontal Distance Corresponds to Maximum Centerline Height [m]
x_n	Near Field Location [m]
y_t	Terminal Rise Height [m]
y_c	Maximum Centerline Height [m]
y_l	Thickness Of Spreading Layer [m]

C_0	Initial Concentration [mg/L]
C_i	Impact Point Concentration [mg/L]
$\tilde{c}$	Concentration
C	Local Concentration [mg/L]
$t, \tilde{t}$	Time [s]
$H\ or\ h$	Fluid Column Height [m]
D_{ab}	Molecular Diffusivity [m^2/s]
S_C	Turbulent Schmidt Number [m^2/s]
$\overline{u_i' u_j'}$	Reynolds Stress [m^2/s^2]
D_{ij}^T	Turbulent Diffusion Parameter []
D_{ij}^v	Viscous Diffusion Parameter []
P_{ij}	Production Rate Parameter []
R_{ij}	Reynolds Stress [m^2/s^2]
$\bar{u}_i$	Filtered Velocity Field [m/s]
$\bar{p}$	Filtered Pressure Field [$kg/(m.s^2)$]

1 Introduction and Study Objectives

1.1 General Background

The growing global concern over freshwater scarcity, driven by population growth, economic expansion, changing consumption patterns, and increasing demand for irrigated agriculture, has led to a greater reliance on seawater reverse osmosis (SWRO) desalination technologies as a sustainable solution [1–3]. However, this process generates hypersaline byproducts that are discharged into the marine environment. Being denser than ambient seawater, these brine effluents sink to the ocean floor, negatively impacting water quality and threatening benthic ecosystems by creating "salty deserts" that inhibit marine life and reduce biodiversity [4,5]. In addition, brine discharges can disrupt near-shore recreational areas and destabilize ambient flow by increasing turbidity and altering water salinity and temperature [4], see Figure 1-1. Research has shown that brine discharges are particularly harmful in the near-field of the discharge point, requiring effective solutions for quick dispersion and dilution [4,6].

To mitigate these impacts, strict regulatory standards, such as those set by the US Environmental Protection Agency (EPA) [7] and EU Water Framework Directive (WFD)[8], must be adhered to during the design, implementation, and monitoring of outfall systems. Regulations typically focus on controlling salinity levels at specified distances from discharge points to ensure minimal environmental harm. For example, the US National Pollutant Discharge Elimination System (NPDES) governs the discharge of wastewater and thermal effluents into rivers, lakes, and coastal waters, thereby ensuring compliance with environmental standards [2].

A widely accepted approach to safely manage brine and thermal effluent discharges is the use of offshore diffusers [9,10]. These systems discharge effluents in the form of turbulent buoyant jets from diffuser ports or nozzles at upward angles and high velocities, thereby promoting rapid mixing with ambient water and enhancing dilution to near-background levels [11]. Figure 1-2 illustrates a typical setup for discharging brine effluents from a diffuser outfall system. The turbulent entrainment process, driven by velocity gradients between the jet and the surrounding water, is critical for the effective dispersion of effluents [12]. Prior research has shown that diffuser installations can significantly improve brine dispersion. For example, studies from desalination plants in Spain demonstrated a 17-fold increase in dilution at

distances of 1 km from the outfall when using diffusers [13]. Hence, by leveraging efficient outfall discharge systems and adhering to regulatory guidelines, we can reduce the ecological impact of these discharges and protect the marine environment.

Figure 1-1 Brine entering the Mediterranean, 300 meters off the coast of Israel

(Image: Hagai Nativ / Alamy; Adopted from Dialogue Earth)

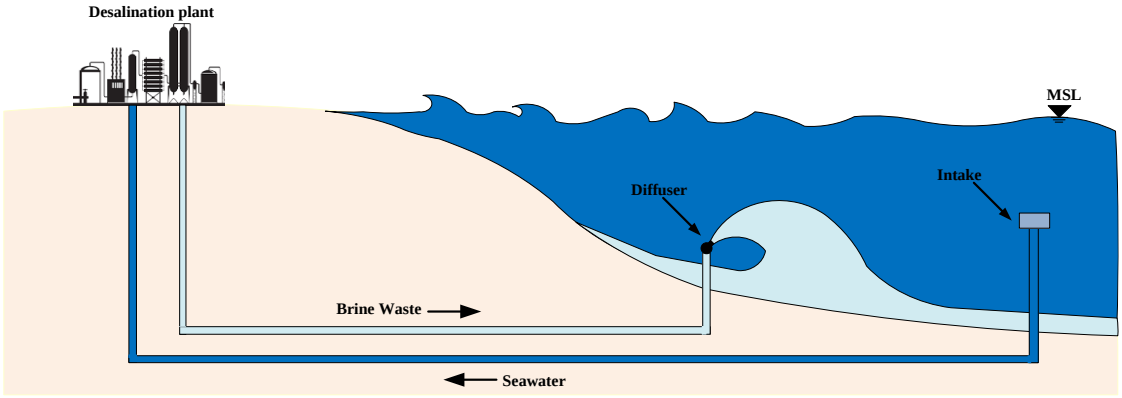

Figure 1-2 A Typical layout of a desalination plant discharge system

1.2 Mixing Behavior of the Desalination Discharges

A clear understanding of effluent discharge behavior is closely tied to the definitions and distinctions between the key terms associated with outfall mixing. Table 1-1 provides the terminology commonly used in this context. To explain the mixing process, consider a jet discharge with an initial angle of θ_0 relative to the horizontal, nozzle diameter of D, and port height of h_0, which releases effluent with a density of ρ_0, concentration of C_0, and discharge velocity of U_0 into a stagnant receiving environment with ambient density ρ_a ($< \rho_0$), concentration C_a, and flow depth H_a. As illustrated in Figure 1-3, this type of outfall discharge typically undergoes mixing in the two primary regions.

Table 1-1 Outfall mixing and mixing zone terminology [14]

Term	Definition
Mixing Zone or Allocated Impact Zone (AIZ)	Refers to an area in which rapid mixing occurs and the numeric water quality criteria can go beyond what is allowed, although the intense toxic conditions have to be halted. Certain water quality provisions must be followed at the end of the AIZ.
Regulatory Mixing Zone or Legal Mixing Zone (LMZ)	As defined by the appropriate regulatory authority, can be a length, an area, or a volume of the receiving water bodies.
Near-Field or Hydrodynamic Mixing Zone	The zone where mixing is only induced by the processes resulting from the outfall. Near-field characteristics are closely dependent on the discharge parameters, and are under the control of the designer.
Far-Field	The ambient oceanic turbulence is the reason for the mixing processes in this region. Far-field mixing is not controlled by the engineer.
Initial Dilution	General terminology for the quick mixing occurring in the proximity of the outfall.
Zone of Initial Dilution (ZID)	Refers to a small zone in the immediate vicinity of the diffuser where dilution is mainly induced by both the momentum and buoyancy of the discharge.

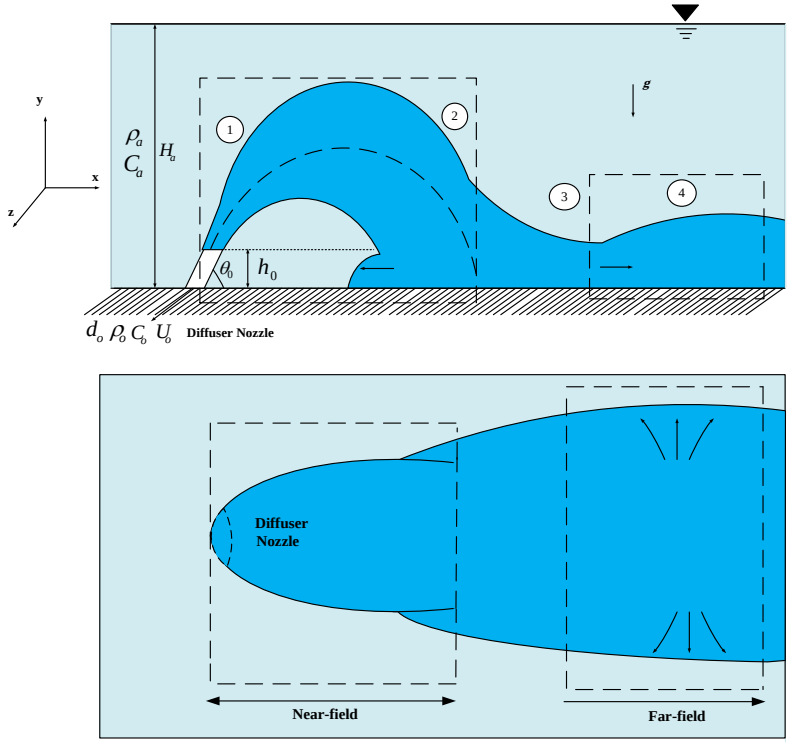

Figure 1-3 Jet discharge: Near-field and far-field regions

The first region, known as the near field, is located close to the discharge point. This region is characterized by intense initial mixing, which is heavily influenced by the design of the discharge configuration and the properties of both the effluent and ambient environment. The goal of designing a brine discharge system is to maximize the dilution in the near field. Here, the dilution rate is very high due to vigorous mixing caused by the initial buoyancy and momentum of the high-velocity discharge interacting with the surrounding water. In this region, mixing and flow dynamics are governed by small spatial and temporal scales (on the order of meters and minutes, respectively). According to [11], the near field extends until the point where self-induced turbulence dissipates due to the influence of induced density stratification, although the exact boundary is not universally defined.

The second region, known as the far-field, lies beyond the near-field and farther from the discharge point or diffuser. In this region, the effluent behaves as a density current moving along the ocean floor. Self-induced turbulence diminishes, and mixing primarily occurs due to ambient turbulence, resulting in a much lower dilution rate than that in the near field. In the far-field, mixing and flow dynamics are dominated by larger spatial and temporal scales (on the order of kilometers and hours) [15].

The mixing process of a brine jet discharge can be more precisely divided into four distinct regions, as illustrated in Figure 1-3. In region (1), the jet momentum governs its upward trajectory due to the initial inclined velocity, which decreases until the point of maximum jet height, where the momentum and buoyancy forces are balanced. In region (2), buoyancy becomes the dominant force, causing the jet to descend toward the seabed, where further dilution occurs as the effluent spreads. Region (3), the transition zone or "spreading layer," extends between the impact point and the far-field region. Finally, in region (4), the far-field effluent continues as a density current along the ocean bottom [15].

1.3 Key Factors Influencing the Performance of Desalination Discharges

Multiple factors, including the configuration of the jet discharge and the ambient hydrodynamic forces of the receiving environment, influence the design and performance of turbulent buoyant jets [14,16]. One of the key aspects of the jet design is the discharge angle, which can vary from 0° (horizontal) to 90° (vertical). Inclined jets, typically preferred due to their horizontal momentum components, are especially advantageous in shallow waters near shorelines as they help prevent surface impact and improve dilution [11,17,18].

Buoyant jets can be discharged into both stationary and dynamic water environments depending on the ambient hydrodynamic conditions. Discharges into stationary water bodies have been the primary focus of jet design research, as they represent a simple scenario for the mixing and dilution of outfall discharge [2]. The early studies by Zeitoun et al. [19] identified 60° as the most efficient angle for achieving maximum dilution, a finding supported by Roberts et al. [11] and Kikkert et al. [20], although slight variations in the results have been reported depending on the study and methods used. Jirka [21] challenged the standard 60° angle, suggesting that a 45° discharge may offer a slightly better terminal rise dilution, although later research by Oliver et al. [22] reaffirmed the effectiveness of the 60° angle in terms of return point dilution. Other studies by Papakonstantis et al. [23,24], Lai and Lee [25], and Abessi and Roberts [17] argued that in stationary ambient conditions, the dilution performance of discharges remains relatively insensitive to variations in discharge angles within the range of 40° to 70°.

While the majority of research has focused on stationary environments, real-world conditions, especially in coastal areas, are typically dynamic, with factors such as flowing currents, turbulence, and shear coming into play [12]. Discharges into these dynamic environments introduce additional complexity, particularly in terms of the initial mixing behavior and jet trajectory. In flowing waters, discharges may experience co-flow, counter-flow, or cross-flow conditions. A co-flow or counter-flow refers to a scenario in which the jet aligns with or opposes the ambient current, creating a two-dimensional flow pattern [26]. In contrast, when the current is perpendicular to the discharge, a more complex interaction occurs, known as buoyant jet in cross-flow (JICF) [27].

In cross-flow conditions, the interaction between the jet and ambient water results in the deflection of the jet along the flow direction, creating a three-dimensional, unsteady, and nonlinear mixing process [28]. The interaction resembles the flow around a circular cylinder, with momentum and energy exchanges occurring between the jet and boundary shear layer of the cross-flow [29]. This dynamic leads to extended jet trajectories and enhanced mixing, making it crucial to understand and predict the behavior of JICFs for optimal jet design. A schematic of the flow geometry for a JICF is provided in Figure 1-4. Based on the explanations provided above, a more comprehensive understanding of the discharge behavior from different nozzle orientations in cross-flow currents is necessary to develop improved predictive models and more precise design guidelines.

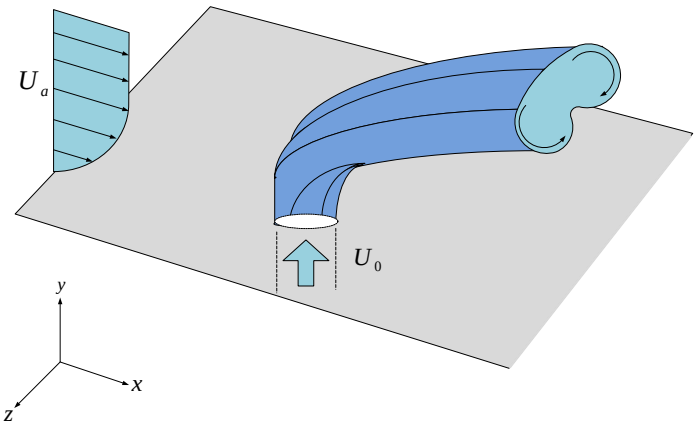

Figure 1-4 A simple schematic of flow geometry for a JICF

(U_a and U_0 are the ambient flow and jet flow velocities, respectively)

1.4 Research Questions

This study was planned to enhance the understanding of desalination discharge behaviors in terms of geometrical features and dilution characteristics in the near-field zone of cross-flow receiving environments by addressing the following research questions:

1) What are the primary gaps in understanding the dense discharge behavior in dynamic receiving environments, as identified through a comprehensive literature review of buoyant JICFs? In addition, what vortical structures can be anticipated in such outfall discharge scenarios?
2) What are the key limitations of the available modeling techniques for simulating buoyant JICFs and how can these be addressed in future research?
3) What are the main parameters in determining the dilution properties and trajectory of the jet while dealing with dense JICF outfalls?
4) How does the discharge trajectory of dense jets respond to cross-flow currents?
5) How do varying the cross-flow strengths and nozzle inclinations affect the mixing performance and trajectory of dense JICFs?
6) What are the differences in flow behavior and dilution performance between jets discharged at 30°, 45°, and 60° angles, and the behavior of which discharge inclinations is more sensitive to cross-flow conditions?

7) How effective is LES modeling in capturing the complex flow dynamics and dilution characteristics of dense JICFs and how does it compare to conventional RANS approaches?
8) What are the flow regimes observed in dense JICFs under varying cross-flow conditions and how can these regimes be categorized based on jet-dominated, regular cross-flow, and strong cross-flow dynamics?
9) What roles do counter-rotating vortex pairs (CRVPs) play in the mixing behavior of dense jets and how powerful are numerical models in the visualization of their evolution?
10) What kind of design instructions can be provided to reduce the ecological impact of these discharges and protect marine environments?

1.5 Research Objectives and Significance

Optimizing the design of marine outfall discharges to minimize environmental impacts is important for adhering to regulatory demands. As discussed in Section 1.3, an ambient receiving environment that typifies realistic oceanic conditions is rarely stationary and is often characterized by flowing currents and turbulence. Although engineers can adjust the properties of brine effluent and determine the discharge depth and diffuser design, they have no control over the ambient conditions of the receiving ocean environment. Therefore, these types of outfall discharges, known as buoyant JICFs, are worthy of in-depth study.

The primary objective of this research is to advance the understanding of dense effluent discharges from SWRO desalination plants in dynamic coastal environments, where complex interactions with cross-flow currents play a critical role in the dilution and dispersion of hypersaline by-products. To address existing gaps in knowledge and improve outfall system design, this thesis focuses on the following key objectives:

1) **Comprehensive Review and Knowledge Gap Identification**: Conduct an in-depth review of the developments in buoyant JICFs and CFD modeling of outfall discharges. This study aims to identify the limitations of the current understanding, particularly regarding the combined effects of flowing currents and nozzle inclination on dense discharge behavior.

2) **Experimental Investigation Using Laser-Induced Fluorescence (LIF)**: Perform LIF experiments to analyze how variations in current strength and nozzle inclination (30°,

45°, 60°) affect the 3D trajectories and concentration distributions of dense jets. The goal is to derive empirical relationships that accurately describe the jet dilution performance and geometric characteristics, with a focus on optimizing the design configurations for improved mixing.

3) **Numerical Simulations Using RANS Modeling Approaches**: Develop and validate CFD models to assess the accuracy of different RANS turbulence closure models (standard k-ε, realizable k-ε, k-ω shear stress transport (SST), and Launder-Reece-Rodi (LRR)) in predicting the flow behavior of dense JICFs. These simulations aim to reproduce the experimental findings and extend the analysis to broader conditions, capturing the range of mixing regimes and performance across various cross-flow Froude numbers.

4) **Application of Large Eddy Simulation (LES)**: Utilize LES modeling to explore the intricate flow dynamics and mixing performance of dense discharges at different cross-flow strengths and identify flow regimes that govern discharge behavior. This provides further insights into the roles of CRVPs and other critical flow structures.

To achieve the above objectives, LIF experimental techniques and practical CFD simulations using the open-source Open Field Operation and Manipulation (OpenFOAM) software will be considered as the main methodologies for determining the mixing behavior and performance of submerged dense JICFs. Overall, these findings will aid in the design of effective outfall systems, ensuring the safe disposal of hypersaline effluents in an environmentally responsible manner.

The outcomes of this research are significant for several reasons:

- **Environmental Protection**: By enhancing our understanding of how dense effluents interact with coastal currents, this research provides crucial insights for minimizing the adverse environmental impacts of desalination brine discharges. Improved outfall designs can reduce harm to marine ecosystems, prevent degradation of water quality, and protect coastal biodiversity.
- **Engineering Applications**: This study highlights the importance of diffuser design and operational parameters such as nozzle angle and cross-flow velocity in optimizing the performance of submerged outfalls. This will guide future engineering practices to ensure compliance with environmental regulations and to achieve more efficient discharge systems.

- **Advancement of CFD Modeling**: This research underscores the potential of CFD techniques, particularly LES, for accurately simulating the complex behavior of buoyant JICFs. The verification of numerical models with experimental data contributes to the development of reliable tools for outfall design and performance assessment in current flowing environments.

1.6 Novelty and Contribution of the Research

This thesis presents several novel contributions to the study of buoyant JICFs, particularly in the context of dense discharge systems. This study explores both experimental and computational approaches to address existing knowledge gaps and improve the design and performance of submerged outfall systems in dynamic marine environments. The key contributions of this study are as follows:

1) **Addressing Knowledge Gaps in Buoyant JICFs**: The literature review conducted as part of this research identifies critical gaps in the understanding of buoyant JICFs, particularly the combined effects of the discharge angle and current strength on mixing performance. This study contributes to filling these gaps by systematically exploring these effects through both experimental and numerical methods. This also highlights the need for more precise design guidelines for submerged diffusers in dynamic coastal environments, where the interaction between ambient currents and discharges significantly influences environmental outcomes.

2) **First Experimental Simulation of Dense JICFs with Varied Source Inclinations**: This study is the first to experimentally simulate dense discharges with varying nozzle inclinations (30°, 45°, and 60°) into perpendicular cross-flow currents. The LIF imaging approach provides 3D visualizations of the jet trajectories and concentration distributions, leading to a better understanding of the interaction between dense jets and flowing ambient currents. This study challenges previous assumptions that dilution is insensitive to nozzle angles between 40° and 70° in static water and highlights the sensitivity of a 60° jet to changes in current strength, offering new insights for optimal outfall design.

3) **Introduction of Empirical Equations for Dilution and Geometrical Characteristics**: The research derived empirical equations that describe the dilution and geometrical characteristics of dense jets under varying flow conditions. This is particularly important for improving the prediction of mixing behavior in real-world

coastal environments where currents and turbulence are prominent. These equations can serve as practical tools for engineers designing outfall systems, helping to mitigate environmental impacts by optimizing the discharge angles and velocities.

4) **Evaluation of RANS Models for Dense JICFs**: The study provides an evaluation of several RANS turbulence models, including the standard k-ε, realizable k-ε, k-ω SST, and LRR. By comparing the performance of these models against experimental data, the research identified the realizable k–ε and LRR models as particularly promising for simulating dense JICFs. This comparison represents one of the first attempts to assess the applicability of different RANS models for this specific flow scenario and offers valuable guidance for future CFD-based outfall studies.

5) **First LES Model of Inclined Dense JICFs**: This thesis is the first study to apply the LES technique to dense JICFs. LES was used to replicate the experimental results for a 60° jet, and the simulations were extended to a broader range of cross-flow Froude numbers. The LES approach successfully captured complex flow dynamics, including the formation of a CRVP, and revealed three distinct mixing regimes: jet-dominated, regular cross-flow-dominated, and strong cross-flow-dominated. These findings not only validate LES as a powerful tool for outfall design, but also provide deeper insights into the behavior of dense discharges under varying flow conditions.

6) **Implications for Environmental Protection and Outfall Design**: The insights gained from this research have practical implications for protecting coastal water bodies and minimizing the environmental impact of dense effluent discharge. By improving the understanding of how discharge characteristics such as nozzle inclination and current strength affect mixing and dilution, this study provides valuable data for optimizing the design of SWRO outfalls and other industrial effluent discharge systems. This research also emphasizes the importance of using advanced CFD techniques, such as LES, to achieve better accuracy in predicting the discharge behavior in real-world conditions.

In summary, this thesis attempts to make significant advancements in both experimental and computational studies on buoyant JICFs, contributing to the development of more efficient and environmentally sustainable outfall systems. The novel insights and methods presented herein are expected to guide future research and engineering practices in the field of coastal effluent discharge management.

1.7 Thesis Outline

This thesis is organized as a sequence of review and technical papers and is divided into six chapters, see Figure 1-5 presenting the thesis outline diagram. Following the current chapter (Chapter 1), **Chapter 2** sets the stage for understanding the complex interactions between buoyant jets and ambient flowing currents, forming the foundation for the research objectives and significance of this study. It reviews the existing research, highlights the flow structures and mixing behaviors of jets in cross-flows, and identifies research gaps, aiming to enhance predictive methods and design guidelines for outfall systems. This chapter has been published in the *Journal of Marine Science and Engineering*.

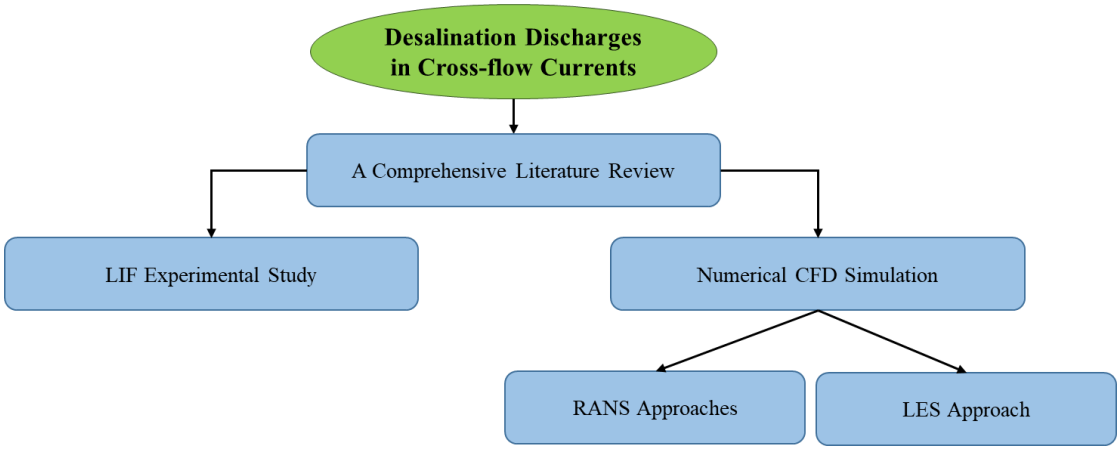

Figure 1-5 Thesis Outline Diagram

Chapter 3 focuses on the experimental investigation using LIF to study the effects of varying nozzle inclinations and cross-flow strengths on dense jets. Detailed empirical equations are derived to describe the dilution and geometric characteristics of the jets. The findings demonstrate significant differences in dilution performance based on jet inclination, challenging previous assumptions in the literature and offering new insights into optimal outfall configurations. This chapter was published in the *Desalination Journal*.

Chapter 4 details numerical simulations using OpenFOAM's finite volume technique to model the behavior of dense JICFs. This chapter compares the performance of different RANS turbulence models, including standard k–ε, realizable k–ε, k–ω SST, and LRR, with experimental data from the literature. This highlights the strengths and limitations of each model in predicting the flow behavior and mixing characteristics of dense jets, contributing to the development of more accurate CFD tools for outfall design. This chapter was presented in the *Proceedings of the 39th IAHR World Congress*.

Chapter 5 extends the numerical work by applying the LES technique to simulate 60° inclined dense jets under a wide range of cross-flow conditions. The LES results are validated against our experimental data presented in Chapter 3, and three distinct flow regimes are identified: jet-dominated, regular cross-flow-dominated, and strong cross-flow-dominated. This chapter offers novel insights into the complex flow structures and mixing processes that occur in real-world discharge scenarios and provides essential guidelines for designing environmentally sustainable outfall systems. Chapter 5 is presented as a technical article and will be submitted to the *Desalination Journal* as a continuation of a previous study published in the same journal.

Chapter 6 summarizes the key contributions of this research and discusses future directions for improving the management and design of dense effluent discharge systems in coastal environments.

Finally, an overview of outfall discharge modeling, with a focus on turbulence modeling approaches, is presented in **Appendix A**. In particular, this section explains the environmental regulations, outfall discharge analysis, turbulence modeling approaches, and pros and cons of each turbulence model. In addition, prominent numerical studies on the simulation of single and multiple jets and their conclusions are presented in various tables. This chapter was published as part of a book chapter in *Advances in Fluid Mechanics, Modelling, and Simulations* (Springer Nature Publishers). **Appendix B** also presents photographs of the experimental test setup and equipment employed in this research.

1.8 List of Publications (form the thesis)

- **Taherian, M.,** Mohammadian, A. (2021). Buoyant Jets in Cross-flows: Review, Developments, and Applications. Journal of Marine Science and Engineering, 9 (1), 61. https://www.mdpi.com/2077-1312/9/1/61
- **Taherian, M.**, Saeidi Hosseini, S. A. R., Mohammadian, A., Ferrari, S., Roberts, P. J. (2024). Laboratory study on inclined desalination discharges in perpendicular cross-flow. Desalination, 583, 117719. https://www.sciencedirect.com/science/article/abs/pii/S0011916424004302
- **Taherian, M.**, Saeidi Hosseini, S. A. R., Mohammadian, A. (2022). CFD Numerical Simulation of Submerged Dense Jets in Cross-flows. In Proceedings of the 39th IAHR World Congress, Granada, Spain.

https://www.iahr.org/library/infor?pid=20964

- **Taherian, M.**, Mohammadian, A., Goodarzi, D., Saeidi Hosseini, S. A. R. Large Eddy Simulation Study on the Mixing Behavior of Inclined Dense Jets in Cross-flow. (This paper will be submitted in a couple of weeks in the Desalination Journal.)
- **Taherian, M.**, Saeidi Hosseini, S. A. R., Mohammadian, A. (2022). Overview of outfall discharge modeling with a focus on turbulence modeling approaches. In Advances in Fluid Mechanics: Modelling and Simulations (pp. 139-177). Singapore: Springer Nature Singapore. https://link.springer.com/chapter/10.1007/978-981-19-1438-6_4

1.9 References

[1] J. Kucera, Desalination: water from water, 2nd Edition, John Wiley and Sons Inc., 2019. https://doi.org/10.1002/9781119407874.

[2] T.M. Missimer, B. Jones, R.G. Maliva, Intakes and Outfalls for Seawater Reverse-Osmosis Desalination Facilities: Innovations and Environmental Impacts, Springer, New York, 2015. https://doi.org/10.1007/978-3-319-13203-7.

[3] U. Caldera, C.B.-W.R. Research, undefined 2017, Learning curve for seawater reverse osmosis desalination plants: capital cost trend of the past, present, and future, Wiley Online Library 53 (2017) 10523–10538. https://doi.org/10.1002/2017WR021402.

[4] R. Einav, F. Lokiec, Environmental aspects of a desalination plant in Ashkelon, Desalination 156 (2003) 79–85. https://doi.org/10.1016/S0011-9164(03)00328-X.

[5] P. Palomar, I.J. Losada, Desalination in Spain: Recent developments and recommendations, Desalination 255 (2010) 97–106. https://doi.org/10.1016/J.DESAL.2010.01.008.

[6] A. Hashim, M. Hajjaj, Impact of desalination plants fluid effluents on the integrity of seawater, with the Arabian Gulf in perspective, Desalination 182 (2005) 373–393. https://doi.org/10.1016/J.DESAL.2005.04.020.

[7] U. States Environmental Protection Agency, Water Quality Standards Handbook: Second Edition, (1994).

[8] P.A.. Chave, The EU water framework directive, IWA Publishing, (2001).

[9] A. Ramakanth, M.J. Davidson, R.I. Nokes, Laboratory study to quantify lower boundary influences on desalination discharges, Desalination 529 (2022). https://doi.org/10.1016/j.desal.2022.115641.

[10] E. Gungor, P.J.W. Roberts, Experimental studies on vertical dense jets in a flowing current, Journal of Hydraulic Engineering 135 (2009) 935–948. https://doi.org/10.1061/(ASCE)HY.1943-7900.0000106.

[11] P.J.W. Roberts, A. Ferrier, G. Daviero, Mixing in Inclined Dense Jets, Journal of Hydraulic Engineering 123 (1997) 693–699. https://doi.org/10.1061/(asce)0733-9429(1997)123:8(693).

[12] Baum, M. Jeffrey, Dense jet behaviour in dynamic receiving environments, The University of Queensland, 2019. https://doi.org/10.14264/UQL.2019.247.

[13] Á. Loya-Fernández, L.M. Ferrero-Vicente, C. Marco-Méndez, E. Martínez-García, J.J. Zubcoff Vallejo, J.L. Sánchez-Lizaso, Quantifying the efficiency of a mono-port diffuser in the dispersion of brine discharges, Desalination 431 (2018) 27–34. https://doi.org/10.1016/J.DESAL.2017.11.014.

[14] S. Jenkins, J. Paduan, P.J.W. Roberts, D. Schlenk, J. Weis, Management of brine discharges to coastal waters recommendations of a science advisory panel (Tech. Report No. 694), Southern California Coastal Water Research Project, Costa Mesa, CA, USA, 2012. ftp://207.141.116.145/pub/download/DOCUMENTS/TechnicalReports/694_BrinePanelReport.pdf (accessed October 25, 2020).

[15] P. Palomar, Inigo. J., Impacts of Brine Discharge on the Marine Environment. Modelling as a Predictive Tool, Desalination, Trends and Technologies (2011). https://doi.org/10.5772/14880.

[16] S.A.R. Saeidi Hosseini, M. Taherian, A. Mohammadian, S. Ferrari, P.J.W. Roberts, Mixing behavior of multiport diffusers with non-uniform port orientation, Desalination 567 (2023). https://doi.org/10.1016/j.desal.2023.116962.

[17] O. Abessi, P.J.W. Roberts, Effect of Nozzle Orientation on Dense Jets in Stagnant Environments, Journal of Hydraulic Engineering 141 (2015) 06015009. https://doi.org/10.1061/(asce)hy.1943-7900.0001032.

[18] H. Kheirkhah Gildeh, A. Mohammadian, I. Nistor, Inclined dense effluent discharge modelling in shallow waters, Environmental Fluid Mechanics 21 (2021) 955–987. https://doi.org/10.1007/s10652-021-09805-6.

[19] M.A. Zeitoun, W.F. McIlhenny, R.O. Reid, C.-M. Wong, W.F. Savage, W.W. Rinne, C.L. Gransee, Conceptual designs of outfall systems for desalting plants, Research and Development Progress Rep. 550, Office of Saline Water, Washington DC, USA, 1970. http://hdl.handle.net/2027/mdp.39015078505149 (accessed October 26, 2020).

[20] G.A. Kikkert, M.J. Davidson, R.I. Nokes, Inclined Negatively Buoyant Discharges, Journal of Hydraulic Engineering 133 (2007) 545–554. https://doi.org/10.1061/(asce)0733-9429(2007)133:5(545).

[21] G.H. Jirka, Improved discharge configurations for brine effluents from desalination plants, Journal of Hydraulic Engineering 134 (2008) 116–120. https://doi.org/10.1061/(ASCE)0733-9429(2008)134:1(116).

[22] C.J. Oliver, M.J. Davidson, R.I. Nokes, Predicting the near-field mixing of desalination discharges in a stationary environment, Desalination 309 (2013) 148–155. https://doi.org/10.1016/j.desal.2012.09.031.

[23] I.G. Papakonstantis, G.C. Christodoulou, P.N. Papanicolaou, Inclined negatively buoyant jets 1: Geometrical characteristics, Journal of Hydraulic Research 49 (2011) 3–12. https://doi.org/10.1080/00221686.2010.537153.

[24] I.G. Papakonstantis, G.C. Christodoulou, P.N. Papanicolaou, Inclined negatively buoyant jets 2: Concentration measurements, Journal of Hydraulic Research 49 (2011) 13–22. https://doi.org/10.1080/00221686.2010.542617.

[25] C.C.K. Lai, J.H.W. Lee, Mixing of inclined dense jets in stationary ambient, Journal of Hydro-Environment Research 6 (2012) 9–28. https://doi.org/10.1016/j.jher.2011.08.003.

[26] M. Jiang, A.W.K. Law, S. Zhang, Mixing behavior of 45° inclined dense jets in currents, Journal of Hydro-Environment Research 18 (2018) 37–48. https://doi.org/10.1016/j.jher.2017.10.008.

[27] M.J. Baum, B. Gibbes, Field-Scale Numerical Modeling of a Dense Multiport Diffuser Outfall in Crossflow, Journal of Hydraulic Engineering 146 (2020) 1–16. https://doi.org/10.1061/(ASCE)HY.1943-7900.0001635.

[28] C.C.K. Lai, J.H.W. Lee, Initial mixing of inclined dense jet in perpendicular crossflow, Environmental Fluid Mechanics 14 (2014) 25–49. https://doi.org/10.1007/s10652-013-9290-7.

[29] J. Chang, Y. Du, X. Shao, Y. Zhao, S. Zheng, Investigation and analysis of vortex and application of jet in crossflow, Case Studies in Thermal Engineering 14 (2019) 0–6. https://doi.org/10.1016/j.csite.2019.100459.

2 Buoyant Jets in Cross-flows: Review, Developments, and Applications[1]

Abstract

Significant environmental effects from the use of marine outfall discharges have led to increased efforts by both regulatory bodies and research groups to minimize the negative impacts of discharges on the receiving water bodies. Understanding the characteristics of discharges under conditions representative of marine environments can enhance the management of discharges and mitigate the adverse impacts to marine biota. Thus, special attention should be given to ambient cross-flow effects on the mixing behaviors of jet discharges. A buoyant jet in cross-flow has different practical applications, such as film cooling and dilution, and provides a higher mixing capability in comparison with free jets or discharges into stationary environments. The main reason for this is believed to be the existence of various complicated vortical structures, including a counter-rotating vortex pair, as the jet expands downstream. Although tremendous research efforts have been devoted to buoyant jets issuing into cross-flows over the past five decades, the mixing process of effluent at the discharge point is not yet well comprehended because of the highly complex fluid interactions and dispersion patterns involved. Therefore, there is a need for a deeper understanding of buoyant jet in cross-flows (JICFs) in order to obtain better predictive methods and more accurate design guidelines. The main aims of this study are: (i) to establish the background behind the subject of buoyant jet in cross-flows, including the flow structures resulting from the interaction of jets and cross-flows and the impacts of current on mixing and transport behavior; (ii) to present a summary of relevant experimental and numerical research efforts; and finally (iii) to identify and discuss research gaps and future research directions.

Keywords: Marine outfalls; Buoyant jets; Environmental impacts; Jet in cross-flow; Vortical structures; Counter-rotating vortex pair.

[1] This chapter has been published as: Taherian, M., Mohammadian, A. (2021). Buoyant Jets in Cross-flows: Review, Developments, and Applications. Journal of Marine Science and Engineering, 9 (1), 61.

2.1 Introduction and Background

Currently, the worldwide growth of effluent discharges into receiving water bodies has become a critical concern as a consequence of industrialization and rapid population increase [1,2]. Effluent discharges can be either in the form of brine discharge as a by-product of desalination plants or in the form of thermal discharge, which corresponds to some industrial activities including thermal power plants and mining. The former has a wide range of applications typically in arid and semi-arid countries, while the latter has broad applications in countries such as Canada [2]. In most relevant engineering applications such as seawater desalination plants, the discharge is almost always as a turbulent buoyant jet (containing both buoyancy and momentum fluxes) [3,4]. This is caused by the difference between the density of the jet and the receiving water body due to differences in salinity, temperature, or chemical composition [4,5].

Regardless of type, these effluents can be harmful to the environments they are released into. Decreases in water quality, destruction of marine habitats, and damage to near-shore recreational sites represent some of the adverse impacts on the environment. Therefore, it is necessary to study effluent outfall characteristics and designs for the purpose of minimizing their environmental impacts while adhering to regulatory demands. In this situation, utilizing buoyant jets may be a practical remedy which is capable of improving effluent discharges' mixing and dispersion in the receiving waters. Several experimental, analytical, and numerical studies have focused on the topic of buoyant jets' mixing within the receiving water bodies (e.g., [4,6–10]).

The interaction of multiple factors relevant to the discharge and receiving water bodies determines the dilution, dispersion, and even biological impacts of effluent discharges. Generally, three main types of factors should be considered when evaluating the environmental risk of a discharge, including [11]:

(i) discharge characteristics (such as type of discharge structure and effluents);

(ii) receiving environment characteristics (such as topography and other physical and biological characteristics), and;

(iii) forcing functions (such as currents and waves).

Regarding the interplay with ambient hydrodynamic forces, buoyant jets can be discharged into two main types of receiving water, namely stationary and dynamic environments. Discharges into stationary environments, which is the usual basis for the design of turbulent

buoyant jets as well as the worst case in terms of mixing and dilution [2], has been the main focus of previous studies since the 1970s. Several improvements have been obtained for this type of discharge over the last few decades. For example, in the literature [8,12–21], a general agreement has been noted for the optimal design of effluent discharges, with inclined jets yielding greater mixing and dilution than vertical ones. Particularly with the selection of a 60° inclination angle, it is generally believed that the highest dilution may be achieved at the return point, with a few exceptions.

However, the oceanic receiving environment is rarely stationary, and the impact of an ambient cross-flow on the mixing process of effluent discharges at the discharge point should be well comprehended because of the highly complex fluid interactions and dispersion patterns involved [22]. Investigations have shown that the flowing current influence mainly results in the extension of the jet trajectory as well as the enhancement of jet-mixing [23–26].

Basically, the jet in cross-flow (JICF) or transverse jet is related to a jet of fluid being ejected from a nozzle and interacting with the ambient fluid flowing across the nozzle exit [27,28], with both the jet and the cross-flow being changed after their interaction [29]. The flow characteristics of the cross-flow after being hindered by the jet can be interpreted similarly to those of a flow around a circular cylinder. In addition, due to the influence of the cross-flow, the jet gets deflected, and an energy and momentum exchange between the jet and the boundary shear-layer zone of the cross-flow takes place [27]. Highly complex three-dimensional, unsteady, and nonlinear flows are generated because of the interaction between the cross-flow and the jet [22]. As a result, the understanding and control of JICFs are of significant interest.

JICFs have a wide variety of practical applications, including plume dispersion, film cooling for combustors and turbines, and discharges of sewage and industrial effluents into channels and natural rivers [22,27,30]. JICFs have also gained considerable attention in many experimental and numerical studies in fluid mechanics due to their capability to provide higher mixing in comparison with free jets [22,31]. This is mostly attributed to the existence of various complicated vortical structures resulting from the interaction of the jet and cross-flow as the jet expands downstream [28,30,32]. It should be noted that most of the previous studies on the formation and evolution of vortical structures have involved using buoyant JICF applications involving film cooling. Thus, using this knowledge can also help in understanding the impacts of vortical structures on mixing behaviors in dilution applications.

Fifty years of JICF research was explored in a study by Margason [33], and several more achievements have been made in this field since then. Although significant research efforts have recently been devoted to buoyant jets issuing into cross-flows, a deficiency in comprehension of their discharge behavior in dynamic receiving environments still remains [34].

A review of buoyant JICFs is thus helpful in providing general principles and better knowledge in order to improve the understanding of the mixing behavior of buoyant jets and their performance under more realistic oceanic conditions (i.e., dynamic environments). Generally, two main focuses have drawn researchers' attention in the study of buoyant JICFs, including the flow structures due to the interaction of jets and cross-flows and the effects of flowing currents on the mixing and transport behavior in near- and far-field regions. In order to protect the receiving water bodies and enhance the management of discharges, such information is of significant importance. Thus, the objectives of this review study are: (i) to understand buoyant JICF flow structures and mixing and transport behaviors; (ii) identify the critical issues obtained from the experimental and numerical fields for these flow structures and mixing and transport behaviors; and (iii) highlight a range of knowledge gaps regarding future research directions.

The rest of this paper is organized as follows. Section 2.2 presents the most practical engineering applications introduced for buoyant JICFs and some of the influencing factors that should be considered in their design. Theoretical analysis, experimental techniques, and numerical modeling, which are the applicable assessment approaches to investigate the interactions of buoyant jets and cross-flows, are reviewed in Sections 2.3, 2.4, and 2.5, respectively. In Section 2.6, the existence of different vortical structures as significant structures that can be formed and evolved in the flow field of buoyant JICFs is discussed. Then, the entrainment and mixing mechanisms involved in buoyant JICFs are explained in Section 2.7. Section 2.8 deals with the experimental and numerical research efforts to understand the flow structures and mixing behaviors of buoyant JICFs. Finally, a summary of relevant research gaps and concluding remarks are identified and presented in Sections 2.9 and 2.10, respectively.

2.2 Engineering Applications of Buoyant JICF

There are many essential engineering applications introduced for buoyant JICFs, such as film cooling of gas turbine blades, fuel atomization in scramjets, and applications involving dilution [27]. According to the main goal expected, various jet penetration levels are needed which can be achieved by the changes in the ratios of jet to cross-flow velocity ($r = \frac{U_0}{U_a}$; U_0 is the jet discharge velocity and U_a is the ambient flow velocity) and jet to cross-flow momentum flux ($J = \frac{\rho_0}{\rho_a} r$; ρ_0 is the jet discharge density and ρ_a is the ambient flow density) [30,35]. For instance, the jet penetration levels and molecular mixing of the jet with its surrounding field are expected to be high for applications involving dilution, since the momentum flux ratio often exceeds 25 or even J >100 [30]. However, the momentum flux ratio is relatively low (often J <5 or J <1), for film cooling applications in order to be able to thermally protect turbine blades [30]. In addition, when it comes to engineering design of buoyant JICFs, the velocity ratio can be introduced as an important aspect of lateral jet-flow structures [27].

In the following sections, an introduction to two of the most practical engineering applications of buoyant JICFs, namely film cooling and brine water dilution, will be briefly presented.

2.2.1 Film Cooling

In film cooling applied in gas turbines, the coolant jet is injected into the hot cross-flow while requiring to be attached to the wall. The coolant then generates a thin layer over the turbine blades which protects the surface from direct exposure to the hot cross-flow [27]. Also, the cooling medium interacts with the main stream to eliminate some of the heat [36]. The Reynolds number, velocity ratio, turbulence, hole geometry, inclination angle, and density ratio are among the effective parameters while studying the film cooling performance. Consequently, studies on this application should be shifted from uni-variate to multi-variate assessments. Mechanisms of the JICF's vortical structure formation should also be considered in order to get closer to the realistic working conditions [27].

2.2.2 Dilution

Brackish water discharges (as dense jets) into a flowing water body emitted by osmotic power plants have remarkable environmental impacts and undergo complex mixing processes [4,37]. Accordingly, a deep knowledge of the interaction between the discharge system and the receiving body is required to investigate the mixing process as well as the potential

environmental effects. A definition schematic of a dense jet discharge into a receiving water body and the relevant key dimensional properties are given in Figure 2-1. The dense jet discharges an effluent with a density of ρ_0 and a velocity of U_0 through a round nozzle with a diameter of D, an angle relative to the horizontal of θ, and a port height of z_0 into the receiving environment with a depth of H, a fluid density of ρ_a, and a uniform ambient flow velocity of U_a.

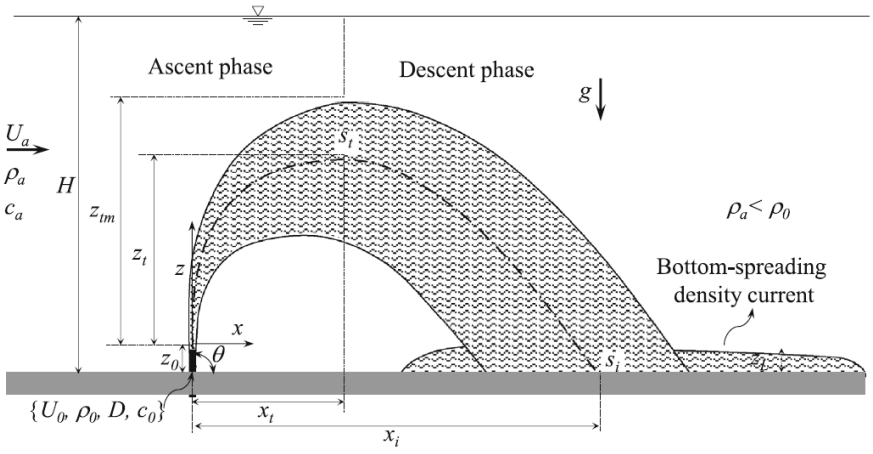

Figure 2-1 Definition sketch of a dense jet in a water body [37]

(g is the acceleration due to gravity, c_0 is the initial jet fluid conductivity, and c_a is the ambient fluid conductivity ($c_a < c_0$))

According to the literature [4,12,37–39], the behavior of a dense jet issuing into a cross-flow can generally be classified into two phases: the rapid ascent and gradual descent phases. Apart from the influence of the cross-flow, the jet's movement is governed by the interplay of discharge buoyancy and momentum forces [40]. As the jet rises, the negative impact of buoyancy forces on the jet's vertical penetration leads to a reduction in its momentum before it begins to sink. The jet peaks its maximum terminal height (z_{tm}) and its maximum centerline height (z_t) at a downstream distance of x_t with a centerline peak dilution of S_t. Then, the jet gradually falls during the descent phase due to the downward buoyancy forces until impacting at distance x_i with dilution S_i. A laterally bottom-spreading density current forms after the jet impact point, resulting in further dilution because of the flow entrainment. Finally, the turbulent jet collapses under the effect of density-induced stratification, characterizing the end of the near-field zone [2,4], and the ambient turbulence and diffusion mainly dominate further dilution beyond this zone (i.e., at the far-field boundary) [41].

It is worthwhile to mention that apart from utilizing negatively inclined dense jet as one of the important mixing applications of buoyant JICFs, they can be also designed as positively

inclined jets for the discharge of heated cooling-water from the power plants or even as surface discharge of treated effluents from industrial and municipal wastewater plants. A uniform mixing field is anticipated for these types of mixing applications.

Thus, using various flow field assessment approaches would be beneficial based on the importance of abovementioned engineering applications. In the following section, different aspects that should be considered when theoretically analyzing the flow behaviors of buoyant JICFs will be discussed.

2.3 Theoretical Analysis

2.3.1 Initial Flow Characteristics of Jet

The analysis of jet primary flow characteristics has been well established in the literature [42–44]. For a jet discharged from a port with a cross-sectional area of A_0, with the kinematic viscosity of v_0, and considering $g_0' = g(\rho_0 - \rho_a)/\rho_a$ as the initial modified acceleration due to gravity, the source fluxes, including discharge volume flux (Q_0), the momentum flux (M_0), and the buoyancy flux (B_0), can be characterized as listed in Table 2-1.

Table 2-1 Definition of primary flow characteristics of jet

Flow Characteristics	**Definitions**	**Eq.**
Discharge Volume Flux	$Q_0 = U_0 A_0$	(2-1)
Discharge Momentum Flux	$M_0 = U_0 Q_0$	(2-2)
Discharge Buoyancy Flux	$B_0 = g_0' Q_0$	(2-3)
Jet-densimetric Froude Number	$F = {U_0}/{\sqrt{g_0' D}}$	(2-4)
Jet Reynolds Number	$Re_0 = {U_0 D}/{v_0}$	(2-5)

2.3.2 Dynamic Length Scales of Jet

Different transition processes occur as a jet enters a cross-flow. In the zone of flow establishment (i.e., the zone close to the nozzle port known as ZOFE), there is a transformation between the initial flow velocity distribution into a strongly sheared jet-like velocity distribution. The discharge momentum force mainly dominates the flow regime, and the effect of buoyancy force can be ignored in the jet-like zone. Subsequently, the flow regime changes into a plume-like zone. The jet bends toward the direction of cross-flow as its momentum decreases, and the effects of the buoyancy force and secondary flow mainly control the mixing

process in this plume-like zone [41]. Moreover, it should be noted that the excess concentration and velocity profiles have a Gaussian distribution in the jet-like zone, while these profiles follow an almost uniform distribution in the plume-like zone [41].

In order to obtain the relevant length scales, the introduced fluxes in Table 2-1 can be combined with U_a as the mean ambient cross-flow velocity. It can be summarized that [4,5,23,37,39]:

- l_M, which is the jet-to-plume length scale, measures the length over which flow transforms from the momentum dominated zone (jet-like) to a buoyancy dominated zone (plume-like).
- l_m is the jet-to-cross-flow length scale, indicating the length over which the transition from a weakly deflected region to a strongly deflected one occurs. At this distance, the cross-flow dominates and causes the jet to begin to sink.
- l_Q is the discharge length scale and determines the length over which the entrained ambient volumetric flux becomes roughly equal to the source volumetric flux. The dynamic influence of the source volumetric flux is insignificant for lengths exceeding l_Q.
- l_b is the plume-to-cross-flow (buoyancy) length scale and specifies the vertical location at which the ambient flow strongly affects the plunging plume.

The importance of the introduced length scales has been well described in many studies [23,39,43,45]. Table 2-2 lists the definitions of the dynamic length scales of jets. As well, Figure 2-2 presents the definition sketch of introduced length scales in stagnant and cross-flow receiving environments.

Table 2-2 Introduction of the dynamic length scales of jets

Types of Scale	**Length Scales**	**Eq.**
Jet-to-plume Length Scale	$l_M = {M_0^{3/4}}/{B_0^{1/2}}$	(2-6)
Jet-to-cross-flow Length Scale	$l_m = {M_0^{1/2}}/{U_a}$	(2-7)
Discharge Length Scale	$l_Q = {Q_0}/{M_0^{1/2}}$	(2-8)
Plume-to-cross-flow (Buoyancy) Length Scale	$l_b = {B_0}/{U_a^3}$	(2-9)

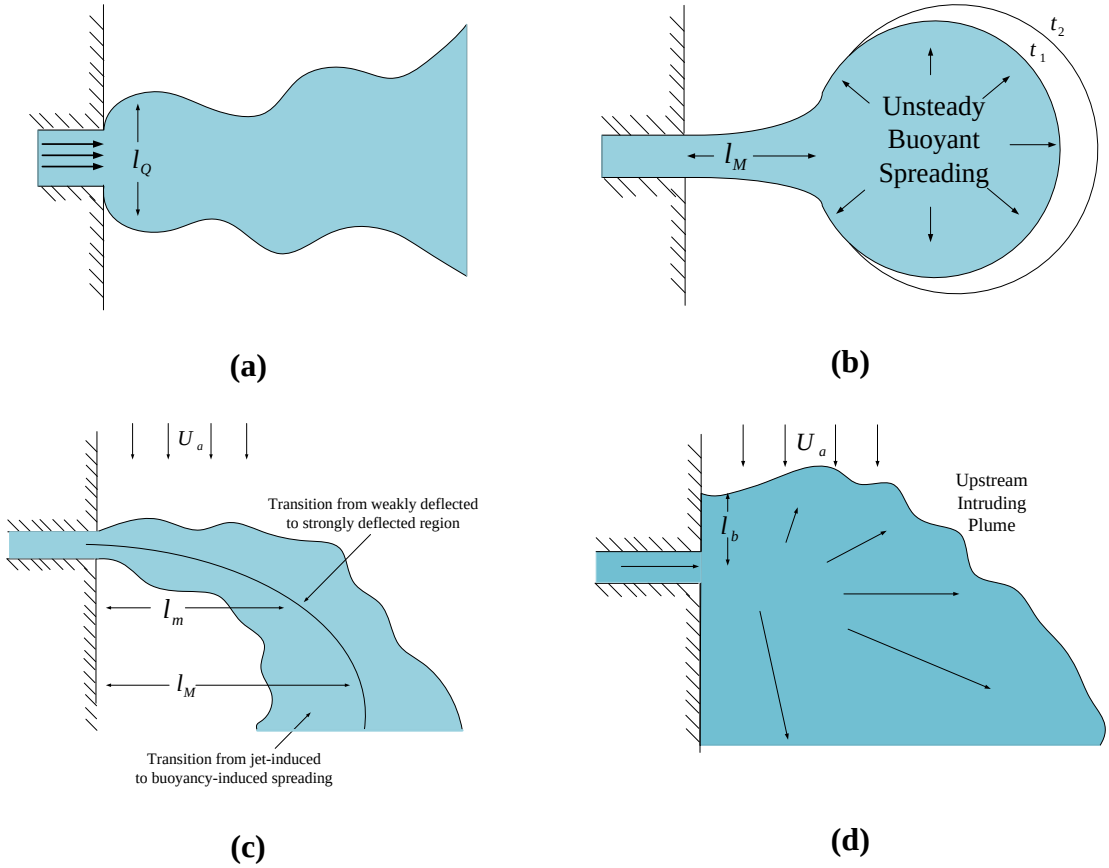

Figure 2-2 Representation of introduced length scales in stagnant (**a** and **b**), and cross-flow (**c** and **d**) ambient water environments

2.3.3 Cross-flow Ambient Conditions

A cross-flow buoyant jet can be classified into four various asymptotic regimes according to the dominance of the buoyancy, momentum, or cross-flow on the jet-mixing characteristics [46] (see Figure 2-3):

- Momentum Dominated Near-Field (MDNF) ($z/l_m << 1$): if the effect of initial jet momentum is important in a jet discharge
- Momentum Dominated Far-Field (MDFF) ($z/l_m >> 1$): if the effect of cross-flow becomes important in a jet discharge
- Buoyancy Dominated Near-Field (BDNF) ($z/l_b << 1$): if the effect of initial plume buoyancy is important in a plume discharge
- Buoyancy Dominated Far-Field (BDFF) ($z/l_b >> 1$): if the effect of cross-flow becomes important in a plume discharge

It should be noted that z is the vertical distance.

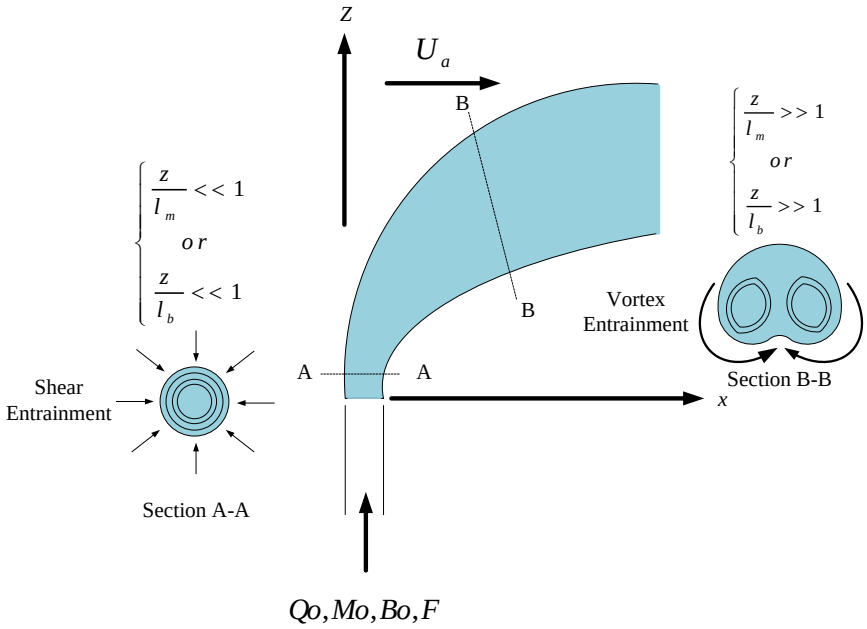

Figure 2-3 Flow regimes of a cross-flow buoyant jet

2.3.4 Dimensional Analysis

In order to quantify the effect of cross-flow on a jet's trajectory and dilution properties, a semi-empirical evaluation can be applied as a practical approach [24,44]. The background for this analytical approach was established by Roberts and Toms [23]. For dimensional analysis of buoyant discharges into cross-flows, two main assumptions are taken into account. First, the discharges are fully turbulent, and viscosity effects are not considered. Second, a Boussinesq buoyancy approximation for a buoyancy-driven flow is applied (i.e., $(\rho_a - \rho_0) \ll \rho_a$).

For the case of a buoyant JICF, any dependent parameters, including the geometric scales of the flow (ζ such as x_i, x_t, z_t, and z_{tm}) and the jet dilution properties (S such as S_i and S_t), can be expressed as a function of the jet and cross-flow characteristics [23,39]:

$$\zeta, S = f(Q_0, B_0, M_0, U_a, \phi, \theta) \tag{2-10}$$

where ϕ is the angle of cross-flow relative to the discharge propagation at the source (if $\phi < 90^\circ$ counter-flow and if $\phi > 90^\circ$ co-flow), and all other parameters are defined in Sections 2.2.2 and 2.3.1. A velocity scale (U_c) can be also defined by applying the momentum and buoyancy fluxes, as below [4,39]:

$$U_c = {B_0^{1/2}}\Big/{M_0^{1/4}} \tag{2-11}$$

Following dimensional analysis and using the definitions for the velocity and length scales, the relationship for the geometric scales of flow trajectory can be written as:

$$\frac{\zeta}{l_M} = f(\frac{l_M}{l_Q}, \frac{U_a}{U_c}, \phi, \theta) \tag{2-12}$$

In addition, the modified acceleration due to gravity ($g' = g(\rho - \rho_a)/\rho_a$) can be taken as the dependent parameter to derive an expression for the jet dilution properties given that the Boussinesq assumption is valid. Thus, following the dimensional analysis and considering $S = g'/g'_0 = (\rho - \rho_a)/(\rho_0 - \rho_a)$, the relationship for the dilution properties can be expressed as:

$$S\frac{l_Q}{l_M} = f(\frac{l_M}{l_Q}, \frac{U_a}{U_c}, \phi, \theta) \tag{2-13}$$

For a round turbulent jet with a nozzle diameter of *D*, some equivalencies can be noted:

$$\frac{l_M}{l_Q} = (\frac{\pi}{4})^{-1/4}F;\ \ \frac{U_a}{U_c} = (\frac{\pi}{4})^{-1/4}u_r F;\ \ l_M = (\frac{\pi}{4})^{1/4}DF \tag{2-14}$$

where u_r is the ratio of ambient to jet velocity ($u_r = U_a/U_0$). As a result, Eqs. (12) and (13) can be rewritten in terms of the jet-densimetric Froude number ($F = {U_0}\Big/{\sqrt{g'_0 D}}$) and the ratio of ambient to jet velocity considering the equivalencies stated in Eq. (2-14):

$$\frac{\zeta}{DF}, \frac{S}{F} = f(F, u_r F, \phi, \theta) \tag{2-15}$$

where the parameter of $u_r F$ can be defined as cross-flow based Froude number. Moreover, following dimensional analysis, the derivation obtained in Eq. (2-15) can be expanded to the scenario of multiport discharges in an ambient cross-flow, with L_p as the port-spacing:

$$\frac{\zeta}{DF}, \frac{S}{F} = f(F, u_r F, \frac{L_p}{DF}, \phi, \theta) \tag{2-16}$$

Figure 2-4 illustrates instantaneous views of the interplay between the jet trajectory and the direction of the cross-flow. According to Eqs. (2-15) and (2-16), three main points should be highlighted:

- The jet dilution parameters scale with *F*, and the trajectory parameters scale with *DF*.
- In the case of $F \gg 1$ (or $l_Q \ll l_M$), the dynamic impact of the source volumetric flux may be ignored, and accordingly $\frac{l_M}{l_Q}$ or *F* does not show individually in the list of dependent parameters. Although works done by Roberts and Toms [23] and Gungor

and Roberts [39] recommend that the jet-densimetric Froude number should be greater than about 20 for dense buoyant jets in order to neglect the effect of the source volumetric flux, the question of how large the F value would exactly be still needs further investigation.

- For the case of single-port discharges, the value of $u_r F$, and for the case of multi-port discharges, the values of $u_r F$ and $\frac{L_p}{DF}$, play a key role in determining the jet's dilution properties and trajectory.

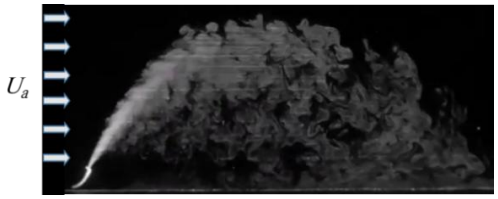

(a)

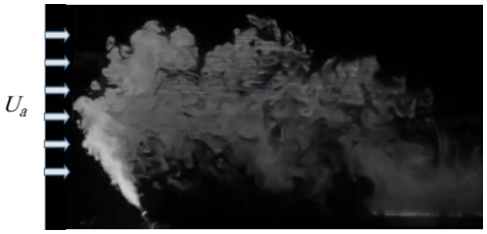

(b)

Figure 2-4 Buoyant jet trajectory behaviors in: **(a)** uniform co-flow receiving environment retrieved from [47], and **(b)** uniform counter-flow receiving environment retrieved from [48]

While the semi-empirical approach has facilitated a general basis for the regulation and design of outfall discharges, the accurate application of this approach may be limited to providing a wide range of empirical and field data [40,49]. As well, some key points regarding hydrodynamic transport complexities may be disregarded in the process of coefficient analysis using time-averaged measurements. Therefore, an introduction to common experimental methods that can help to accurately analyze the flow behavior of buoyant JICFs is essential.

2.4 Experimental Techniques

Small-scale experimental studies have played an essential role in the current development of knowledge of desirable buoyant jets. Within the past 50 years, different techniques have been applied to study jet-mixing in receiving water environments and to measure flow concentrations and velocity distributions. Significant improvements in the experimental

techniques have been achieved from the research (e.g., [13,23,42,50]), in which probe-sampling and conductivity-based techniques were applied, to studies (e.g., [15,16]) in which image-based techniques such as light attenuation (LA) as a non-invasive spatiotemporal concentration measurement technique have been used, and in recent experimental investigations (e.g., [12,21,24,41,51]) in which laser-induced fluorescence (LIF), three-dimensional LIF (3DLIF), and particle image velocimetry (PIV) have been employed.

In experimental studies, the visualization of flows can be done as simply as by adding dye to discharge systems. Currently, optical measurement methods are used, as not only are they non-intrusive techniques to measure jet trajectory and concentration, they can also provide measured values exactly at the same time in an area without any additional error caused by interpolation or extrapolation.

The most notable optical measurement methods for concentration are LA and LIF. In these techniques, a fluorescent tracer dye is added to the flow, and subsequently a laser causes the dye to fluoresce and emit light which is captured by a camera. By using an appropriate calibration method, quantitative tracer concentrations can be achieved from the images. The concentration distributions in the flows can also be demonstrated by applying the color-coded images. Furthermore, particle tracking velocimetry (PTV) and PIV have both been used in the literature for velocity distribution measurements. It is worthwhile to mention that with a lengthwise movement of the camera and nozzle port along the flume, reproduction of cross-flow currents can be obtained. This is a common method for reproducing cross-flows in LIF and PIV experimental systems [12,41].

With the introduced experimental techniques, the concentration and velocity fields can be completely characterized, and the findings can be employed to calibrate and verify complex computational fluid dynamics (CFD) numerical models. Thus, these recent experimental system enhancements have also opened the doors to utilizing different numerical methods in buoyant JICF studies.

2.5 Numerical Modeling: Jet Integral Models and CFD Methods

With the advancements in computational architecture over the past two decades, the ability to predict discharge behaviors with high accuracy has been improved [52]. Numerical modeling is considered as a flexible approach to facilitate the analysis of outfall discharges' impacts by coupling near- and far-field hydrodynamic models. Integral jet models and jet flow modeling

using CFD tools are two of the most practical methods for the assessment of jet-mixing behaviors [40,52,53]. Visual Plumes [54], JetLag [55,56], and CorJet [57] are among the mixing tools based on integral jet models. These models assume that a jet's velocity profiles are Gaussian and axisymmetric without radial changes, accordingly simplifying the governing mass and momentum conservation equations. Palomar et al. [58] compared the applications of different commercial tools (including CorJet, JetLag, and UM3) based on integral jet models for the prediction of terminal rise height (z_t) and jet dilution at impact point (S_i) resulting from discharges into a dynamic ambient environment. Comparison of simulation and experimental results demonstrated 30-40% discrepancies for the prediction of z_t and 30-55% deviations for the prediction of S_i when the studied jets issued into a cross-flow. Consequently, the inability of integral jet models to resolve and capture re-entrainment and lower boundary effects such as mixing after plume impact point [40], as well as complex interactions between the jet and ambient flow [52], has caused some restrictions for their applicability on buoyant JICFs.

Numerical CFD methods, in contrast, have recently shown considerable capabilities for overcoming the deficiency of integral models and resolving most of the complex behaviors of outfall discharges [40,59]. In CFD computations, the set of partial differential equations of momentum and continuity (known as Navier-Stokes (NS) equations) are solved numerically, with some turbulence closure approximations. These approximations, generally involved in turbulence models, lead to solving NS equations at less computational cost. Various kinds of turbulence modeling approaches have been presented for employment in outfall discharge simulations. Reynolds-averaged Navier-Stokes (RANS) and large eddy simulation (LES) are two of the most practical modeling approaches. The RANS models with various closures including k–ε, k–ω, and Launder-Reece-Rodi (LRR) are based on time-averaging methods, while the LES models with different closures such as standard Smagorinsky and dynamic Smagorinsky model (DSM) are based on filtering instead of averaging. By defining a filter size, motion scales smaller than a given size are modeled using sub-grid scale (SGS) model, and motion scales larger than the filter size are computed by solving the instantaneous NS equations [2,60]. Comparison of these two modeling approaches for the prediction of jet behavior shows that the RANS is relatively easy to implement and computationally inexpensive approach, but cannot be accurate within the entire flow field. On the other hand, the LES has a higher accuracy, as it directly computes large scale eddies, but has a higher computational cost and its relevant small-scale turbulence theory still needs development for complex geometries.

Numerous CFD studies have been carried out to analyze buoyant jet discharges into stagnant receiving environments by using the RANS modeling approach [3,61–73]. In addition, Zhang et al. [60,74] and Jiang et al. [75] applied the LES modeling approach to simulate dense jet discharges. They reported significant accuracy in the prediction of impact distance and dilution compared to the results presented by Palomar et al. [58] using integral jet models. This accuracy is mainly attributed to the capability of the LES approach to resolve coherent eddy structures in a plume-like zone. More recently, Mohammadian et al. [52] presented a review on CFD modeling of effluent discharges which provides valuable insight into the design of buoyant jets by using the CFD technique. These studies confirm the advancement in CFD simulations from the Reynolds-averaged approach to large-eddy and hybrid approaches.

Although several CFD studies have focused on the vortical structures generated due to the interaction between the jet and the cross-flow (reviewed in Section 2.8.2), ambient hydrodynamic influences on mixing and transport of effluent and diffuser configuration are less covered in the CFD literature. Hence, considering the great promise in the use of CFD method for the simulation of outfall discharges, its application to buoyant JICFs remains in its infancy, and significant opportunities are still awaiting.

2.6 Vortical Structures

2.6.1 Introduction

A complex interaction between the jet and the cross-flow results in the formation of complicated vortical structures, which are the paramount physical phenomena appearing in a JICF [27]. As shown in Figures 2-5 and 2-6, a counter-rotating vortex pair (CRVP), shear-layer and/or ring-like, hairpin, hanging, horseshoe, and tornado-like wake vortices are the vortical structures introduced in the JICF.

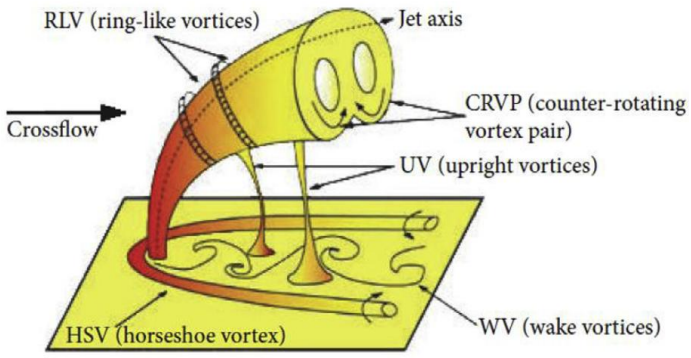

Figure 2-5 Vortical structures in a JICF [76]

According to the flow visualization, Fric and Roshko [77] presented four fundamental vortical structures involved in a JICF (see Figure 2-6):

(i) Horseshoe vortex forming upstream of the jet exit,

(ii) Jet shear-layer generated at the windward interface of the jet/cross-flow,

(iii) Unsteady wake vortices beneath the detached jet, and

(iv) A CRVP.

Among these, the time-averaged defined CRVP is taken into account as the most important structure for the mixture and entrainment between the jet and cross-flow [22].

The time-averaged behavior of a JICF (under the conditions $Re_0 = 5000$ and $r = 5.7$) obtained from a direct numerical simulation (DNS) which resolves all temporal and spatial turbulence scales is also illustrated in Figure 2-7. As is obvious, the contours of the mean velocity show that the jet gets deflected in the direction of the cross-flow, and then the jet becomes wider toward the leeward side of the center streamline (as it moves downstream) than toward the windward side. Furthermore, the cross-section of the jet develops from its circular shape to generate the CRVP [28]. The local mean vorticity reaches its maximum at the CRVP's center. Based on the center streamline, therefore, the jet trajectory penetrates deeper into the cross-flow compared with a trajectory based on the vorticity [78].

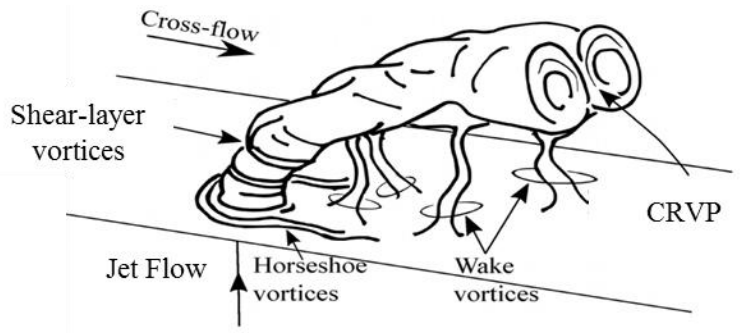

Figure 2-6 Schematic of the four fundamental vortical structures evolved in a JICF as presented by Fric and Roshko [77]

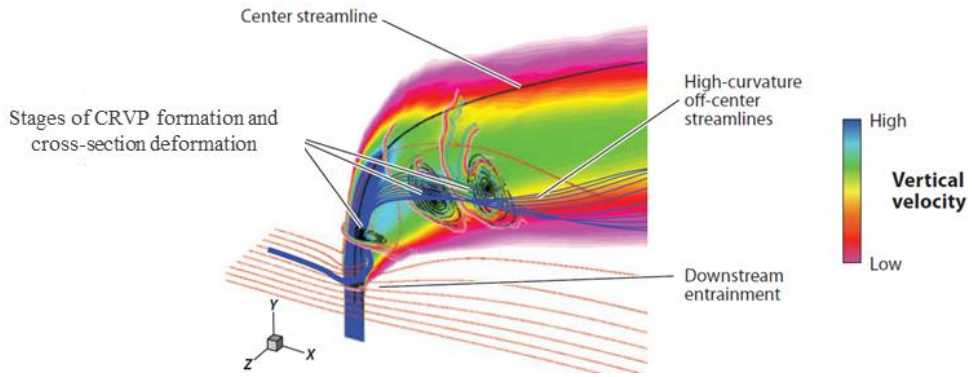

Figure 2-7 Contours of vertical velocity displayed on the symmetry plane [28,79]

In contrast, the instantaneous behavior of jets is unsteady. An adverse pressure gradient occurs on the windward side of the nozzle because of the high-pressure zone above the jet exit generated by the cross-flow. This in turn results in deceleration of the jet fluid at high velocity ratios as well as separation inside the nozzle at low velocity ratios [28,80,81]. The cross-flow boundary layer then separates ahead of the jet and helps to accelerate the jet toward the streamwise direction. As a result, the jet shear-layer is skewed. Moreover, the jet shear-layer vortices can be seen on the windward side of the jet (see Figure 2-8a). This type of vortex is highly unsteady and identical to the Kelvin-Helmholtz rollers in regular jets, which cannot be considered in a time-averaged solution [28].

The vortex structures are all connected to each other, since they originate and are affected by the interaction between the cross-flow and the jet flow. Due to their spatial and temporal coherence, these complex vortical structures also cannot be taken as random. That is why they are sometimes called coherent structures [82]. Visualizations of the different introduced flow structures are shown in Figure 2-8. The main identified coherent vortex systems will be discussed in the following sections.

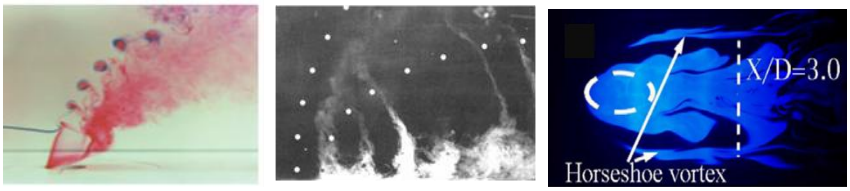

(a) **(b)** **(c)**

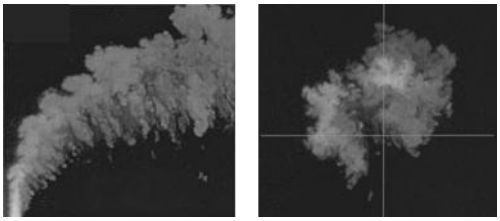

(d) **(e)**

Figure 2-8 Visualization of various instantaneous flow structures:

(a) shear-layer vortices [80]; **(b)** tornado-like wake vortices [77]; **(c)** horseshoe vortices upstream of the jet [22]; and **(d, e)** instantaneous CRVP visualization of jet fluid for r = 10.0 (Panels d and e taken from Smith and Mungal [83])

2.6.2 CRVP and Jet Shear-Layer Vortices

Many of the global characteristics of a JICF can be predicted and found on the basis of the CRVP dynamics [30]. The CRVP is highly asymmetric and unsteady at any given point in time [28] (see Figure 2-8d and e). During the past few decades, the generation and evolution of this structure have been a matter of debate, and different mechanisms have been proposed in this regard.

Broadwell and Breidenthal [84] suggested that the CRVP is a global flow feature of the far-field zone and fundamentally arises from the impulse associated with the jet. However, these results were different from the general agreement that the CRVP might be formed by the vortex sheet emanating from the jet nozzles [6,80,85]. Kelso et al. [80] presented a mechanism for the "tilting and folding" of the jet shear-layer for the interpretation of CRVP formation. The superposition of the cross-flow and the shear-layer vorticity leads to a tilting of the upstream part of the ring oriented with the mean curvature of the jet and a tilting/folding of the downstream part of the ring aligned with the jet movement. A schematic of how a vortex ring may be distorted to generate a CRVP is given in Figure 2-9.

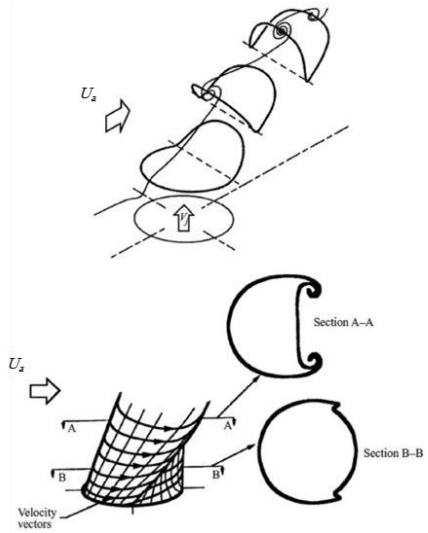

Figure 2-9 Interpretation of JICF tilting, folding, and reorientation of shear-layer vortex rings and eventual formation of CRVP taken from Kelso et al. [80]

In another study, Yuan et al. [86] suggested that quasi-stable hanging vortices generated at the lateral edge of the jet and formed in the skewed mixing layers are the reason for CRVP formation. The vortex strength is transported by the hanging vortices toward the leeward side of the jet. Because of the compressive stress, vortex breakdown takes place, and subsequently the CRVP is formed. This interpretation was also confirmed by the experimental study by Lim et al. [87]. However, Cortelezzi and Karagozian [32] performed numerical simulations through a vortex-based method which supported the CRVP formation mechanism offered by Kelso et al. [80]. Moreover, using a vortex-element simulation, Marzouk and Ghoniem [88] concluded that the planar vortex rings initially created in the proximity of the jet exit may stretch upward on the leeward side. The vorticity is then aligned in the direction of the cross-flow, thus leading to the formation of a CRVP. Muppidi and Mahesh [81] also presented a pressure-based interpretation through the use of a two-dimensional model problem, and suggested that a circular “out-of-plane flow” region may interact with an “in-plane cross-flow” and then evolve into a CRVP. Hence, the exact formation process of a CRVP is still debatable according to the literature review, while the origin of this vortex structure is ascribed to the jet shear-layer in roughly all these explanations [82]. Table 2-3 highlights the research efforts with regard to the prediction of CRVP origin formation.

Shear-layer vortices are unsteady structures that may be formed due to the Kelvin–Helmholtz instability of the ring-shaped shear-layer which separates from the circular jet nozzle. In fact, the shear-layer contains the source of the CRVP and generates the roll-up of the trailing and leading edges [82] (see Figure 2-10).

Table 2-3 Highlighted research efforts regarding CRVP formation origin

Origin of the CRVP Formation	**Methods**	**Remarks**	**Ref.**
Tilting and folding of the jet shear-layer vortices	Experimental visualization	Jet to cross-flow velocity ratios ranging from 2.0 to 6.0 and Reynolds number based on the cross-flow velocity and jet diameter in the range of 440 to 6,200	[80]
Hanging vortices in the skewed mixing layer	LES	Two different jet to cross-flow velocity ratios (r = 2.0 and 3.3) and low Reynolds numbers based on the cross-flow velocity and jet diameter (Re = 1,050 and 2,010)	[86]
Hairpin vortices	LES	Low blowing ratios* (BR = 0.5 and 1.0) and high Reynolds numbers based on the cross-flow velocity and jet diameter (Re = 11,100 and 22,200)	[89]
Interaction of the shear-layer vortices and the cross-flow	LES	Low jet to cross-flow velocity ratios between 0.1 and 0.48	[90]
Origins of the CRVP could somehow be changed with the blowing ratio	Experimental visualization	Different blowing ratios	[91]
Hairpin vortices	LES	Comparatively low blowing ratios	[92]
Hanging vortices and rear vortices		Comparatively high blowing ratios	
Hairpin vortices	LES and experimental visualization (LIF and PIV)	At relatively low jet to cross-flow velocity ratios	[22]
Coherent structures within the jet nozzle		At relatively high jet to cross-flow velocity ratios	

* Blowing Ratio (BR) = $\rho_0 U_0 / \rho_a U_a$

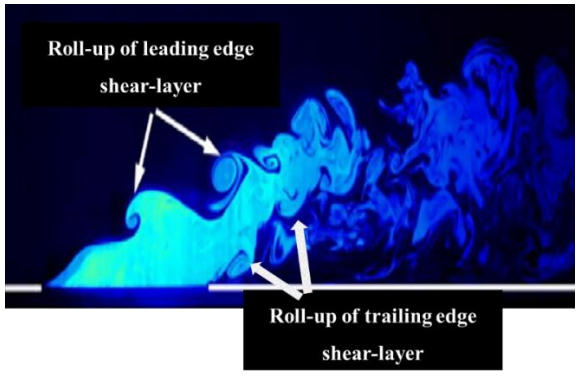

Figure 2-10 Two independent vortices in the jet shear-layer structure obtained from a LIF visualization [22]

2.6.3 Horseshoe and Wake Vortices

Horseshoe vortices appear upstream of the leading edge of the jet and are prolonged toward the downstream [28]. The horseshoe vortices are flow structures similar to those that can be observed at the base of a flow around a cylinder [82] (see Figure 2-11). These vortices form owing to the existence of an adverse pressure gradient upstream of the jet which may be encountered in the cross-flow boundary layer. Then, the boundary layer separates and generates the spanwise vortices which move around the jet [28]. Horseshoe vortices can be considered to have a mean flow feature that persists stationary around the nozzle of the jet; however, this type of vortex exhibits unsteadiness [93].

Krothapalli et al. [94], through a study of the vortices upstream of a rectangular JICF, reported that the formation and roll-up of horseshoe vortices can be periodic. Kelso and Smits [93] also concluded that the vortex system may be steady, oscillate, or even coalesce according to the value of the velocity ratio. Both the mentioned research confirmed the similarity between the unsteadiness of the horseshoe and wake vortex systems [28].

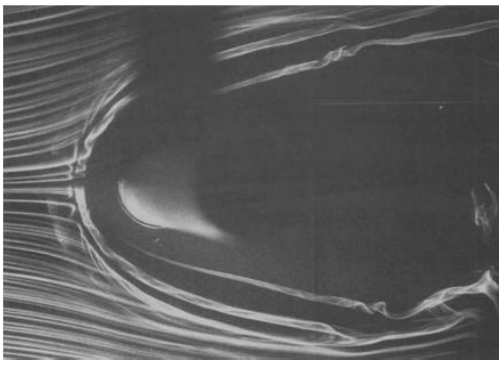

Figure 2-11 Plan view of horseshoe vortex around a cylinder [77]

Wake vortices, which can be observed as vertical tornado-like structures, are inherently transient vortices that connect the emanating jet core and the wall boundary [82]. These vortices are the most unknown and intricate among these four fundamental vortical structures. Results have demonstrated that the formation of wake vortices can be considered as different from vortex-shedding behind cylinders, so that the cross-flow exhibits no separation from the jet and also does not show vorticity-shedding in the wake, in contrast to wakes behind solid bodies [77,82]. Wake vortices expanding from the wall side to the leeward side of the jet (see Figure 2-8b and c) originate due to the separation of the wall boundary layer of the cross-flow channel [28,82]. It should be noted that this boundary layer separation takes place on the sides of the jet, owing to the adverse pressure gradient [82].

As a result, although CRVP and horseshoe vortices have a mean flow characterization in addition to unsteady components, the shear-layer and wake vortices are both naturally unsteady and will be removed from the velocity measurements by averaging over time [77].

2.6.4 Hairpin Vortices: A Distinct Vortical Structure at Low Velocity Ratios

Apart from the four fundamental vortical structures, the interaction of the cross-flow and the jet at low velocity ratios (often less than 1) may result in another flow structure called a hairpin vortex [28]. Due to the opposite signs of vorticity at the leading edge of the pipe exit and the vorticity of the cross-flow boundary layer, a hairpin structure may be created. The boundary layer's vorticity at low velocity ratios has the capability of overwhelming the leading-edge vorticity, leading to vorticity basically being shed from the trailing edge. At higher Reynolds numbers, the hairpin vortices are unstable as they develop gradually, while at low Reynolds numbers, these structures become coherent and periodic. Thus, the hairpin vortices are not detectable if the flow visualization occurs in the streamwise or even the symmetry plane [28,95,96] (see Figure 2-12).

(a) **(b)**

Figure 2-12 Hairpin vortices visualization:

(a) hairpin structure for a JICF at r = 1.0 taken from Sau and Mahesh [96]; and **(b)** instantaneous LIF visualization of hairpin structure at r = 0.5 taken from Dai et al. [22]

2.6.5 Recirculation Zone and Coanda Attachment Effect

In addition to the formation of different vortical structures, recirculation zone and Coanda attachment phenomena may also appear when a buoyant jet issues into a cross-flow. To be more specific, the movement of a JICF is restricted if a solid surface in the near-field exists, and a recirculation zone may form in the wake downstream. Figure 2-13 presents a schematic plan view of recirculation zone formation for a surface side discharge into a cross-flow receiving environment. Also, if the jet discharges in the proximity of a solid boundary in the near-field, the Coanda attachment effect may appear. Here, the jet flows alongside the nearby solid boundary before it becomes free from the attachment effect. In this situation, the

combined effects of the ambient cross-flow pressure resulting from the cross-flow being blocked from passing under the jet as well as recirculation because of the interaction with the near bank can cause jet flow attachment. This attachment effect is more likely to occur when the jet discharges into shallow water. Therefore, it is recommended that the shallowness factor and velocity ratio should both be considered as important factors for control of the Coanda attachment effect [97]. In terms of mixing applications and outfall discharge design, regions with such a strong near-field interaction effect should be avoided due to their minimally dilutive characteristics.

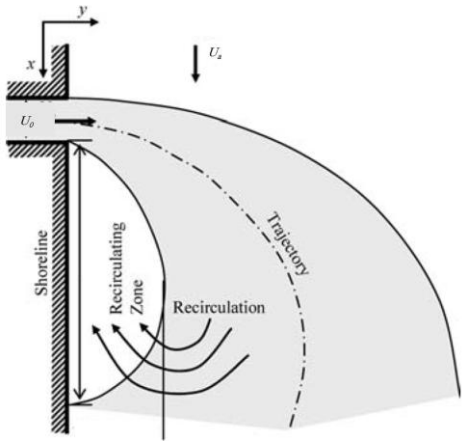

Figure 2-13 Plan view of recirculating zone formation in a JICF [97]

2.7 Entrainment, Mixing, and Trajectory in JICF

For a JICF, the entrainment mechanism becomes much more complicated. Close to the discharge point, there is shear entrainment due to a high-velocity gradient between the jet and the ambient. After the jet is bent by the ambient cross-flow, the vortex entrainment dominates, then the ambient cross-flow is drawn into the jet through the action of a pair of CRVP [32,98].

A JICF can be considered as better than a free jet at mixing and entraining with the surrounding fluid [28]. The decay in the centerline velocity and the jet fluid concentration of a JICF is more rapid in the near-field zone compared to a free jet, while slower in the far-field zone [83,99]. Comparison of free and transverse jets also shows that the former has maximum velocity and concentration at the axis of symmetry, while for the latter, as the CRVP fully develops, the peak concentration and velocity locations do not coincide [28].

The relationship of the CRVP to the mixing characteristics of the transverse jet has drawn considerable interest over many decades. Considering the relationship between the CRVP and mixing enhancement, Smith and Mungal [83] concluded that the improved mixing in the jet's

near-field zone may be attributed to the structural formation of the CRVP rather than its fully developed form. Consequently, the nature of the CRVP and its initiation are significant features of JICFs.

Improvement of the cross-flow entrainment in the proximity of the jet and the corresponding improvement of the molecular mixing of the two fluids are the most important practical benefits of using a JICF in many environments. For instance, the transverse jets can be utilized in high-speed air-breathing applications, in which the extent of penetration of the jet is of particular importance. It should be considered that for this type of application, rapid completion of the reaction process is mandatory due to the high speeds of the air entering the combustion chamber [30]. Therefore, the mixing with cross-flows, rapid fuel penetration, and ignition and combustion processes, which are some of the advantages of transverse jets, are highly desirable for this purpose [30,100].

Three ways to define the jet trajectory have been presented using the jet centerline, the locus of maximum concentration, and the locus of maximum velocity. Yuan and Street [86] compared these and argued that they have the same behavior, despite the fact that the computed trajectories may vary. Cambonie et al., [101] in their study, introduced CRVP trajectories in a way that can be calculated for any velocity ratio. Their results showed that both the CRVP and jet trajectory behave in the same manner when parameters change. This outcome is to be anticipated because the CRVP is a structure generated by the jet, and it seems that the CRVP trajectory follows the jet's centerline trajectory. The CRVP trajectory does not start at the jet exit and is lower than the jet trajectory, as shown in Figure 2-14. Additionally, it is not possible for both types of trajectory to follow a power-law and keep that parallelism due to the fact that the jet and CRVP trajectories are parallel in the far-field zone. Since CRVP trajectories are affected by the momentum ratio, jet diameter, and boundary layer thickness, a new scaling was applied in the study by Cambonie et al. [101].

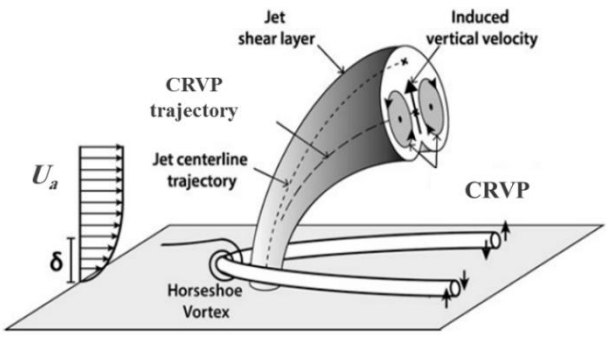

Figure 2-14 Schematic of the CRVP and jet centerline trajectories in JICF (δ is the boundary layer thickness) [101]

2.8 Research Efforts on Flow Structures and Mixing Behaviors of Buoyant JICFs

The interaction between a jet and the cross-flow leads to a highly complex, three-dimensional, nonlinear and unsteady flow, making it an essential issue in several experimental, theoretical, and numerical studies in fluid mechanics during the past few decades [22]. Reviews on this subject can also be found in the studies by Margason [33], Mahesh [28], and Karagozian [30,35]. In addition, the effects of flowing currents on the mixing and transport behaviors of buoyant JICFs have attracted considerable attention in the literature. Therefore, a summary of some selected studies in both the experimental and numerical fields can provide a better picture of the current knowledge on the flow structures and mixing behaviors of buoyant JICFs.

2.8.1 Experimental Studies

Experimental studies on the near-field zone in the late 20th century showed that a CRVP may be generated by the vortex sheet emanating from a jet nozzle [6,80,85,99]. As one of the first studies in this regard, Pratte and Baines [102] carried out experimental research on jet trajectories extracted under various jet to cross-flow velocity ratios (r). Ramsey and Goldstein [103] also performed an experimental study through the use of flow visualization and hot-wire anemometry measurements of JICF with low values of r that can be applied in film-cooling applications. Among other early JICF experiments, Kamotani and Greber [104] examined high momentum ratios (J = 15–60), and reported mean velocity and temperature distribution measurements for hot-jet injection by using hot-wire anemometry and thermocouple measurements.

Andreopoulos and Rodi [6] performed an experimental investigation of JICF for different low velocity ratios (r = 0.5, 1.0, 2.0) using three hot-wire probes and obtained turbulent kinetic energy data, mean velocity components, and three Reynolds shear stress component measurements. Three distinct regions of turbulent kinetic energy are demonstrated through their measurements, including:

- Over the jet nozzle region, where the turbulence is produced from the strong velocity gradients and jet deflection,
- The immediate downstream region, where the velocity gradient normal to the wall generates kinetic energy,

- And the farther downstream region, where the turbulence decays as velocity gradients diminish.

In addition, their results indicated that cross-flow velocities may even affect the flow inside the nozzle carrying the jet stream. This can be considered as an essential issue when the inlet boundary conditions are treated in unsteady simulation of JICFs.

In other studies, Smith et al. [83,105] carried out passive scalar mixing experiments using the PLIF technique on JICFs at various r varying from 5 to 25. According to the scalar concentration decay rate, their results indicated that the flow features are uniform and can be categorized into the near- and far-field regions for very high values of r (about r = 10 to 25). Moreover, the CRVP developed in the near-field zone and subsequently progressed to be fully formed in the far-field region.

Su and Mungal [106] carried out simultaneous measurements of the scalar field and 2D-velocity field using PLIIF and PIV for r = 5.7 and Re_0 = 5000, and emphasized the flow developing in the near-field region. Cárdenas et al. [76] applied simultaneously LIF and PIV methods, and measured the scalar concentration and the Reynolds stress fields. From their research, the effect of CRVP formation on the value of flow fluctuating quantities such as turbulence-intensities and Reynolds-fluxes was identified remarkable, thereby influencing the flow mixing behavior. Later, Galeazzo et al. [107] also employed the same experimental set-up to determine the turbulent mixing and the Reynolds flux vector within a JICF at a velocity ratio of 4. Additionally, in a number of studies, this experimental set-up has been applied with different r values for the purpose of numerical model validation as well as the analysis of scalar mixing [108–110].

Coletti et al. [111] experimentally studied a turbulent inclined JICF relevant for film-cooling applications. Their results indicated that the mean flow is governed by the CRVP aligned in the streamwise direction, bringing the cross-flow fluid into proximity with the wall. The stream-tube issued by the hole is stretched and folded by the CRVP, which enhances the surface for mass exchange with the cross-flow. Additionally, in the first few diameters downstream of the injection, the jet entrainment is slightly increased by the evolution of the CRVP; however, further downstream, the vicinity of the wall prevents this process. Consequently, unlike vertical JICFs, the leeward and windward sides contribute equally to the entrainment (see Figure 2-15). Recently, the flow characteristics resulting from the turbulent mixing of surface buoyant JICFs were experimentally examined by Gharavi et al. [41]. Using a PIV technique, they concluded

that the vortex in a surface buoyant JICF may resemble one of the vortices in a CRVP of submerged JICF, since the water surface may work as a plane of symmetry.

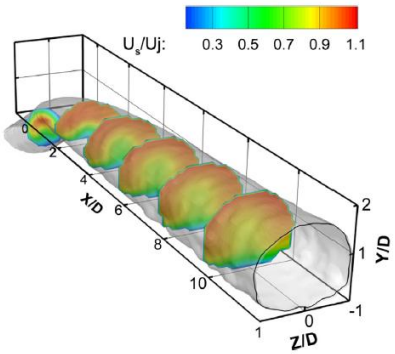

Figure 2-15 Iso-surface of 5% concentration, with cross-sections perpendicular to the jet centerline (color-coded by jet velocity) [111]

Several laboratory research efforts have also contributed to a better understanding of buoyant JICF mixing applications involving dilution. As discussed in Section 2.3.4, the effect of ambient velocity on jet-mixing behavior is not significant when $u_r F \ll 1.0$. Conversely, the jet dilution is mainly affected by the ambient velocity and the jet trajectory is bent downstream when $u_r F \gg 1.0$. An increase in both the jet impact dilution and distance (S_i and x_i) generally occurs with an increase in ambient co-flowing currents; however, for the investigation of jet characteristics in ambient counter-flowing currents, a critical threshold for the $u_r F$ parameter should be identified. In this situation, the horizontal impact distance decreases with the increase in ambient counter-flowing currents until a specific value of $u_r F$ is reached, at which point the jet falls back on itself, causing significantly impaired dilution. After this critical threshold, the jet trajectory will impact farther downstream of the nozzle. For instance, this critical threshold for a JICF with a discharge angle of 60° has been reported to be around $u_r F \sim 0.67$ [51,112].

Using a 3DLIF technique, Gungor and Roberts [39] studied the behavior of vertical dense jets under the impact of flowing currents, and their results showed that the rise height is almost constant and that jet impact dilution and distance increase with the growth of current speeds within the tested range of $u_r F$ values. They also predicted that the near-field dilution may be higher than the jet impact dilution by less than about 100% because of the additional mixing in the bottom layer. However, the dependency of near-field dilution and magnitude on current speed remained an open question in their study. Figure 2-16 shows a general sketch of the effects of flowing current on vertical dense jet behavior.

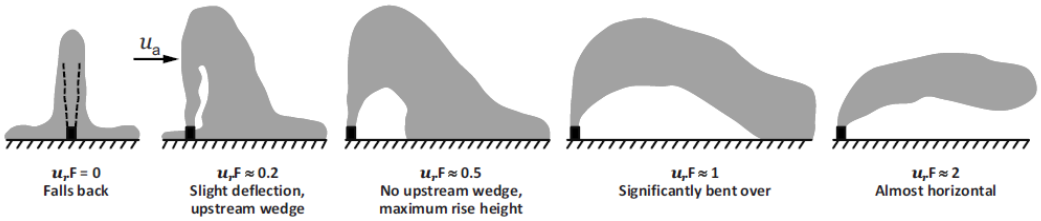

Figure 2-16 General flow characteristics for a vertical dense jet issuing into cross-flow with different values of u_rF [39]

In addition, Lai and Lee [24] studied inclined dense jets in perpendicular cross-flows and showed that the mixing behavior is governed by the cross-flow based Froude number, so that the mixing is jet-dominated and governed by shear entrainment when $u_rF < 0.8$, and mixing is dominated by vortex entrainment when $u_rF \geq 0.8$. Jiang et al. [113] also conducted an experimental study of 45º inclined dense jets in both co-flowing and counter-flowing currents by using the planar LIF technique. The aim of their study was to present more quantitative details on the influence of current on the mixing behavior of inclined dense jets. It should be mentioned that despite the importance of plume interaction with the bottom boundary upon impact, the bottom effect was neglected in the study by Jiang et al. [113] through the use of suspended configuration of jet discharge.

Recently, Ben Meftah et al. [4,37] experimentally examined a dense jet issued into a cross-flow. The flow velocity fields demonstrated that the jet can be characterized with two different jet vortex structures, i.e., the rapidly ascending region (jet-like mixing) and the gradually descending phase (plume-like mixing). A strong amount of dilution would occur during the initial rising region, so that more than 85% of the jet's salinity was decreased over a downstream distance of order 6*D*. The experimental results confirmed the formation and evolution of a CRVP within the jet cross-section with opposite rotational direction for each phase, which had not been proved in previous literature [39]. The jet flow field also indicated a rise of the vertical dispersion coefficient and a reduction of the longitudinal one, which may lead to augmentation of the jet width.

Table 2-4 summarizes the outcomes from some prominent studies over the past five decades, in which the effects of flowing current on the mixing behavior of single dense jets were experimentally explored. Although most research efforts have been conducted on singular dense jets in dynamic receiving environments, multiport diffusers are also used for brine disposal in field applications, such as at the Perth seawater desalination plant in Australia. The only systematic experimental study found in the literature for the assessment of dilution

behavior of multiport discharges in an ambient cross-flow environment was carried out by Abessi and Roberts [51]. Using a 3DLIF technique, the effects of port spacing ($0.26 < \frac{L_p}{DF} < 7.7$) and cross-flow parameter ($0.67 < u_r F < 8.0$) on multiport diffuser mixing behavior with a discharge angle of 60° were investigated, and as shown in Figure 2-17, the flow fields differed considerably for narrowly and widely spaced jets (particularly at relatively low current speeds), so that for closely spaced ports and $u_r F < 0.78$, combined effects of jet merging and Coanda interactions were observed. Contrary to experiments with stationary environments [114], in which the results became independent of port spacing for $\frac{L_p}{DF} > 2.0$, no independent threshold was identified in the scenario dealing with flowing current environments. Accordingly, further studies are required to provide a better understanding of multiport diffuser mixing behavior when influenced by ambient cross-flows.

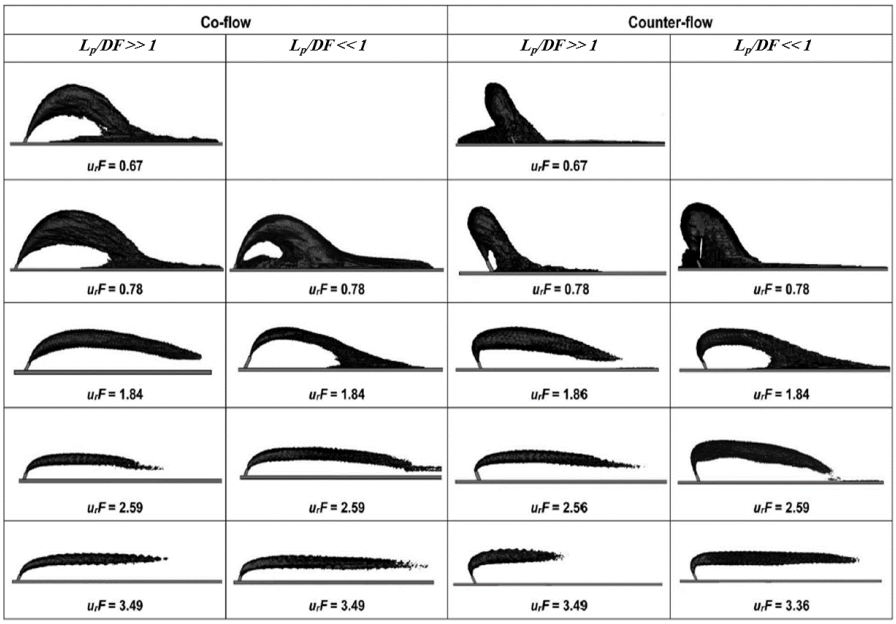

Figure 2-17 Effect of ambient current speeds on general flow characteristics of one-sided multiport diffusers with narrow and wide port spacings [51]

Table 2-4 Highlighted research efforts on the mixing behavior of single dense jets impacted by flowing current

Discharge Angle	**Effect of Cross-flow**	**Experimental Techniques**	**Outcomes and Remarks**	**Ref.**
60° and vertical	Co-flow $3.5 < u_r F < 5$ $F = 50$	Conductivity-based technique	In the jet region in which the jet momentum flux is dominated, the dilution amount increased independently of the cross-flow effect. Beyond the jet region, the dilution was enhanced with increased cross-flow velocity.	[42]

45°, 60°, and vertical	Co-flow $0.5 < u_r F < 8.04$	Conductivity-based technique	Comparison with the integral models presented by Fan [115] and Abraham [116] showed the inability of these models to accurately predict dilution and trajectory properties. The velocity ratio, jet Froude number, and discharge angle were identified as the effective parameters; however, their relationships were not defined.	[50]
45°, 60°, and vertical	$\phi = 90^{\circ}$ $0.18 < u_r F < 1.63$ $11.7 < F < 21.2$	Thermal-based technique and photogrammetry	The effects of different discharge angles were not significant on the dilution amount for the conditions examined.	[117]
60° and vertical	$0^{\circ} < \phi < 180^{\circ}$ $0 < u_r F < 1.87$	Photogrammetry and fluorometry technique	For a jet Froude number less than 25, the effect of source volumetric flux could be ignored. By increasing the angle of cross-flow relative to the discharge propagation at the source (ϕ), the dilution increased as well. The performance of inclined jets was generally preferable compared to vertical ones due to the lower terminal rise height obtained as well as taking advantage of a horizontal momentum component.	[23]
60° and vertical	Co-flow $0.36 < u_r F < 2.12$	Planar LIF technique	With a rise in ambient cross-flow velocity, gravitational detrainment in the jet region was decreased.	[118]
Vertical	$0.21 < u_r F < 0.92$ $19.0 < F < 24$	3DLIF technique	At low ambient current speeds ($u_r F \sim 0.2$), the ascending and descending flow phases were nearly vertical; however, at higher ambient current speeds ($u_r F \sim 0.5$), the rising flow was more vertical and the falling flow more gradual, leading to impacts farther downstream (see Figure 2-18a and b). At high ambient current speeds ($u_r F \sim 0.9$), a kidney-shaped concentration distribution was observed for the falling flow phase because of the formation of two counter-rotating vortices (see Figure 2-18c and d). It was recommended that entrainment models be applied with more caution for the prediction of dilution amounts.	[39]

60°	Co-flow $0.33 < u_rF < 1.07$	LA and techniques	LIF	Mixing and transport in the intermediate field (laterally buoyant spreading region after the jet impacts on the bottom boundary) were studied. The lateral spread was dominated by both inertia and buoyancy, and increased as $x^{2/3}$ with downstream distance.	[25]
45°	Co-flow ($\phi = 0^{\circ}$) and counter-flow ($\phi = 180^{\circ}$) $0.10 < u_rF < 3.26$	Planar technique	LIF	The mixing behavior was classified into current-dominated and dense-jet-dominated regimes (see Figure 2-19). For co- and counter-flowing currents, when $u_rF < 1.0$, the jet trajectory mainly depended on the characteristics of the source discharge, and the ambient current showed little impact. Also, the dimensionless coefficients (such as *z/DF* and *S/F*) were nearly independent of u_rF. However, for both kinds of flowing currents, outside this range, the mixing was mainly governed by the currents, and the characteristics mostly depended on the value of u_rF.	[113]

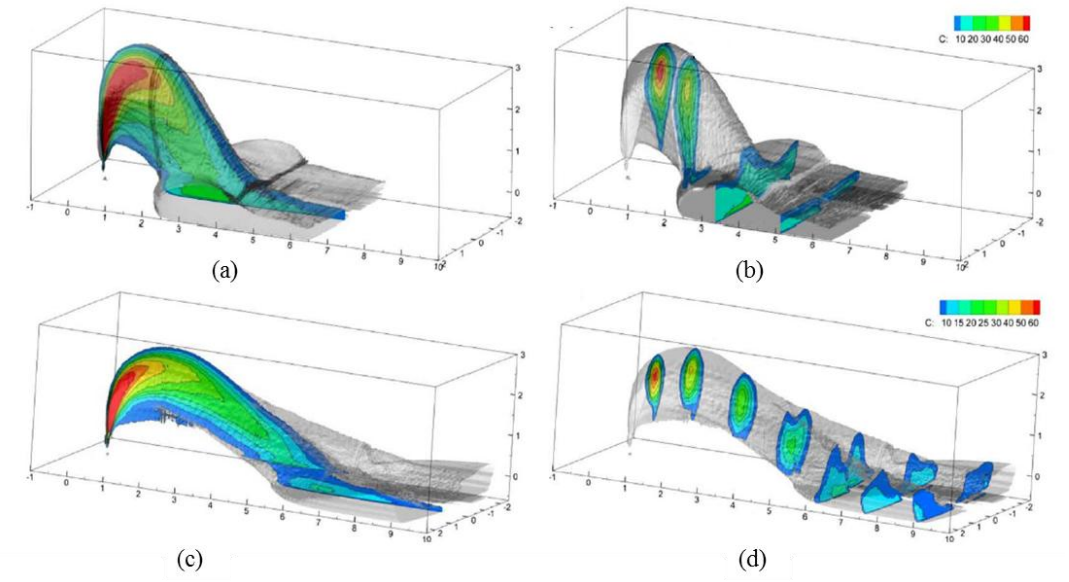

Figure 2-18 3DLIF images of a vertical dense JICF for $u_rF \sim 0.5$ (**a** and **b**), $u_rF \sim 0.9$ (**c** and **d**) [39]

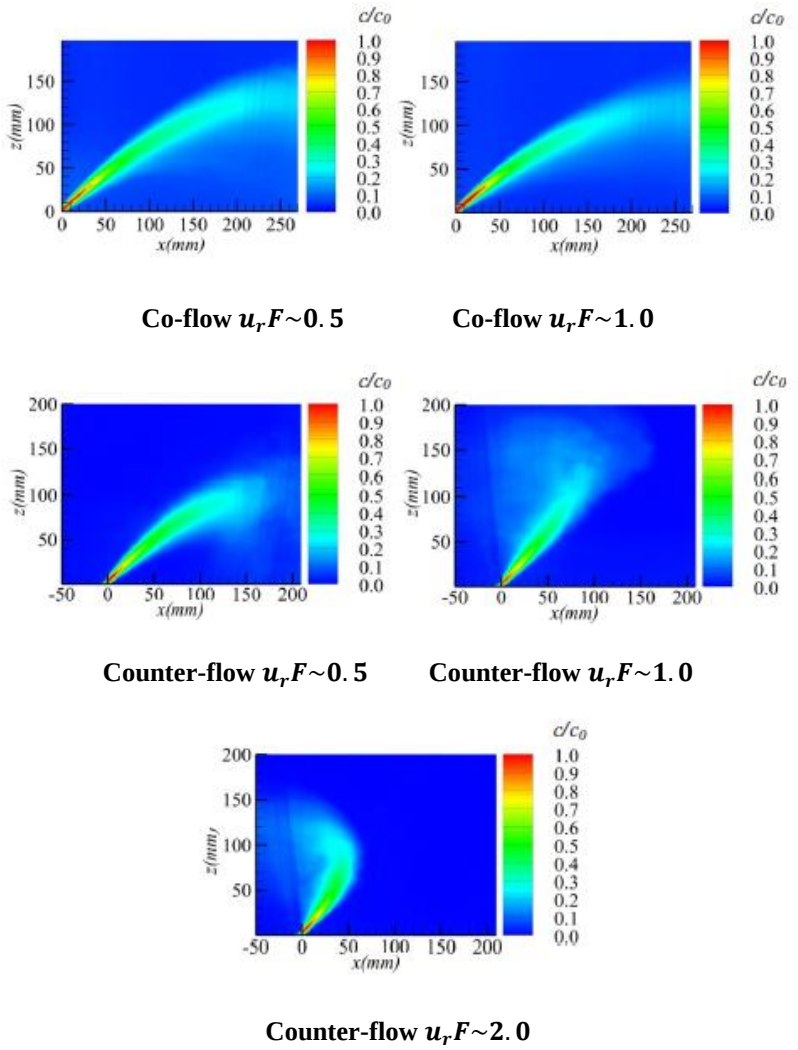

Figure 2-19 Time-averaged concentration contours of an inclined dense jet in co- and counter-flowing currents [113]

2.8.2 Numerical Studies

Patankar et al. [119] used the standard k–ε model for turbulence closure approximation in one of the earliest CFD analyses of the JICF issue, and their predictions validated the experimental mean velocity measurements in the cross-flow direction with an acceptable accuracy. Alvarez et al. [120], in a more in-depth CFD study of the JICF, used the k–ε model and a second-moment closure model to numerically simulate the experimental tests from Andreopoulos and Rodi's [6] and Ramsey and Goldstein's [103] studies. From their research, the experimental results were in a more reasonable agreement with the second-moment closure model in comparison with the k–ε model, particularly near the wall boundary condition. However, the turbulent kinetic energy and the turbulent statistics for the velocity field could not be accurately predicted with either model, apart from the mean velocity components.

Jones and Wille [121] carried out the first LES study on JICF and compared three different SGS stress models, including the standard Smagorinsky model with a constant model coefficient, a one-equation transport model for sub-grid kinetic energy, and a DSM. The results were compared with the JICF experimental case studies by Chen and Hwangt [122]. Both adaptive and non-adaptive grids were applied, neither of which could improve the obtained results. Despite some variations with the turbulent eddy viscosity values, the velocity fields were generally predicted in the same manner using all three SGS stress models.

In another study, Yuan et al. [86] performed an LES on a JICF for r = 2.0 and 3.3. They reproduced the experimental case of Sherif and Pletcher [123] by a locally dynamic SGS stress model, demonstrated that the hanging vortices in the skewed mixing layer is the origin of CRVP formation. Their study was more focused on vortex structure recognition, and the results showed very good agreement between the LES and experimental data for the velocity field.

The formation and evolution of CRVPs in JICFs were examined by Cortelezzi and Karagozian [32] by using a three-dimensional vortex element method. The numerical simulation results were consistent with the ideas described in the experimental study by Kelso et al. [80] and confirmed the rolling-up and interaction phenomena for the vortices from previous experiments. A detailed analysis of the role of the CRVP in the entrainment and blending was also performed.

Schlüter and Schönfeld [124] validated their applied LES on JICF mixing with limited experimental data by using two different SGS stress models, namely the standard Smagorinsky and filtered Smagorinsky models. Comparison with experimental results indicated that the filtered Smagorinsky model's predictions performed more accurate than the unfiltered one; however, due to the limited data used for model validation, there is a need for more comprehensive study in this regard. The influence of steady and unsteady inlet boundary conditions was investigated by Majander and Siikonen [125] through the use of the constant-coefficient Smagorinsky model. Despite the fact that the unsteady inlet boundary condition led to a stronger flow reversal at the leeward side of the jet, only a slight difference was observed in these two methods.

Later, Galeazzo et al. [107] compared the applications of LES and RANS simulations for a JICF test case at r = 4.15. Their predictions indicated the advantage of using the LES over the RANS, particularly in the prediction of Reynolds stress terms. In order to make a comparison between the performance of the DSM and the unsteady RANS (URANS) model, the

experimental configuration explored by Cárdenas et al. [76] was also modeled by Galeazzo et al. [126]. The results of the DSM showed a great accuracy for the prediction of the scalar mixing field compared to the URANS model. This could be attributed to the fact that LES can resolve the scalar transport using vortex structures better than URANS simulations. Figure 2-20 shows the ability of LES, URANS, and RANS simulation methods in capturing the formation and evolution of coherent structures. In Figure 2-21, the two dimensional plots of mean velocity component (U) and specific Reynolds stress component ($\overline{u'u'}$) are compared with the results obtained by PIV measurements.

As discussed in Section 2.2.6, the flow structures in JICFs may not be limited to those four common types of vortices with changes in the value of velocity ratios, and may contain different formation mechanisms as well [22]. The literature review shows that the instantaneous simulation methods have played an important role in the accurate prediction of different types of vortices in JICFs. For example, Tyagi and Acharya [89] could clearly identify for the first time the hairpin vortices at low velocity ratios of 0.5-1 through an LES method and introduced this type of vortical structure as the origin of the CRVP. Fawcett et al. [91] and Sakai et al. [92] also argued that a jet's structure may change with the velocity ratio.

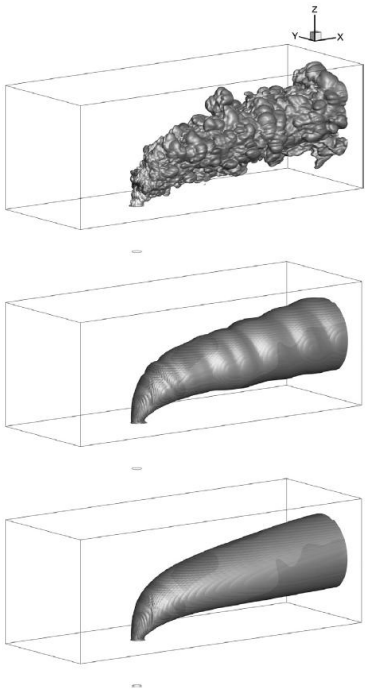

Figure 2-20 Comparing the ability of different simulation methods from top to bottom, LES, URANS, and RANS for the prediction of coherent structures [126]

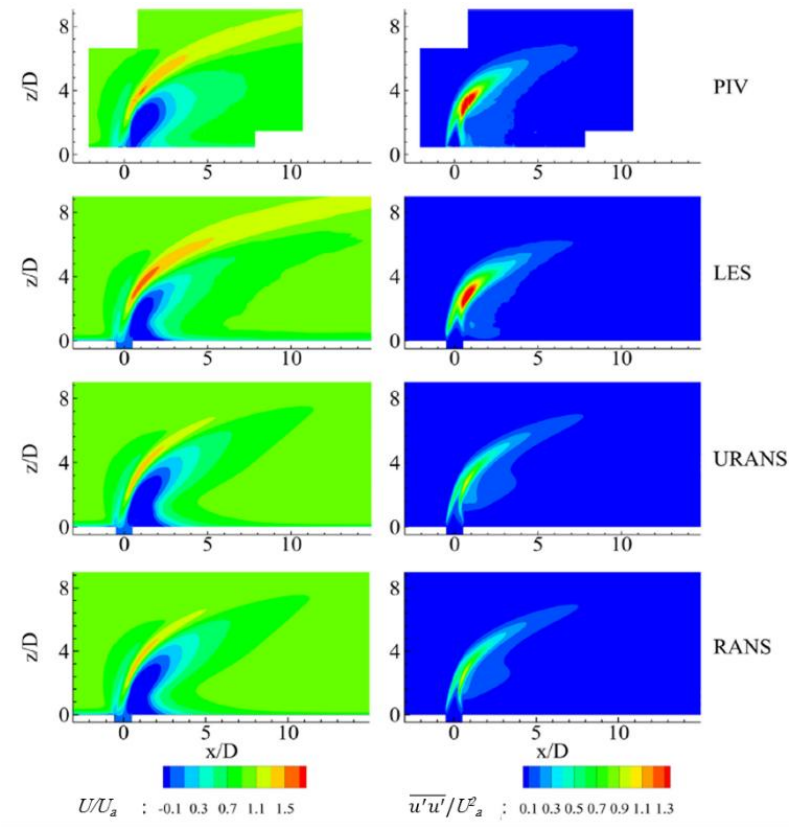

Figure 2-21 Two-dimensional maps of mean velocity component (U/U_a) and specific Reynolds stress component ($\overline{u'u'}/U_a^2$) at the symmetry plane [126]

Sakai et al. [92] investigated a series of LESs with an inclined jet issuing into a cross-flow and how the vortical structures may impact the evolution of the CRVP at various blowing ratios (*BR*). They showed that the hairpin vortices might be considered as dominant vortices when the *BR* was comparatively low. However, a pair of hanging vortices, rear vortices, vertical streaks, and jet shear-layer vortices were consecutively generated as the *BR* increased. The CRVP also originated in hairpin vortices when the *BR* was low, while originating in the hanging vortices and rear vortices when the *BR* was high (see Figures 2-22 and 2-23). The difference in the vortex formation might be due to the different pressure gradients in the downstream and the upstream shear-layers.

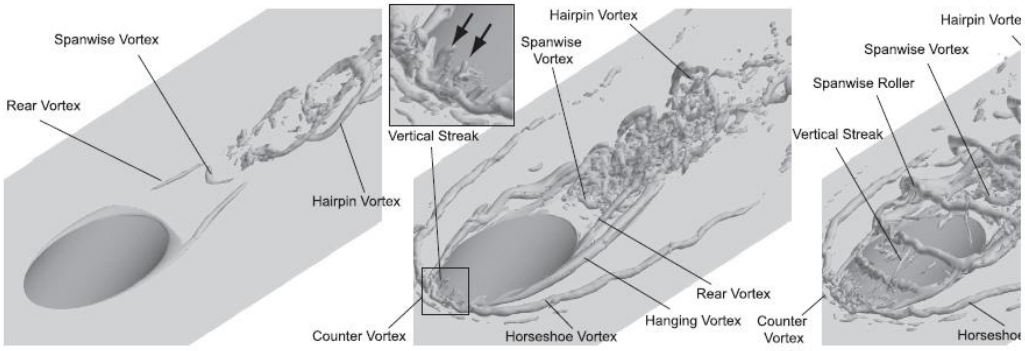

(*BR* = 0.1) **(*BR* = 0.7)** **(*BR* = 1.0)**

Figure 2-22 Comparison of the vortical structures around the nozzle exit for different values of *BR* [92]

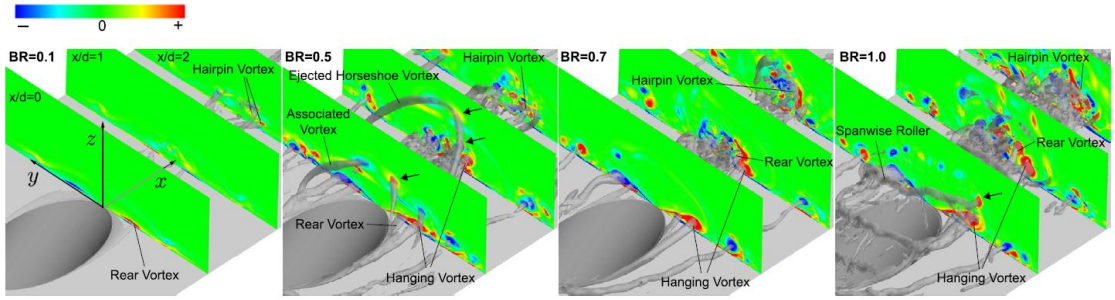

(a)

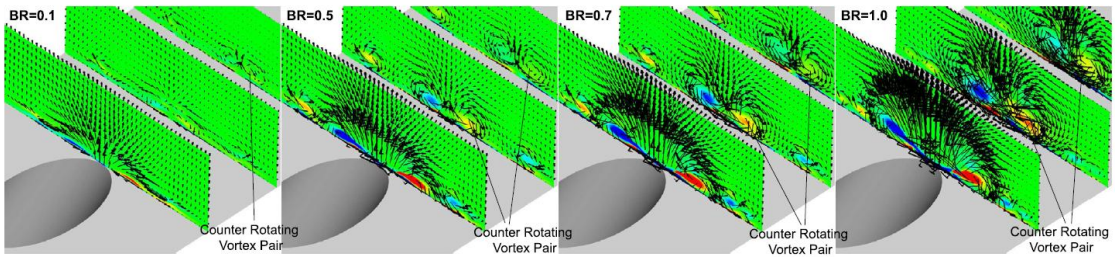

(b)

Figure 2-23 (a) Instantaneous and **(b)** time-averaged views of streamwise vorticity (ω_x) for *BR* = 0.1, 0.5, 0.7, and 1.0 [92]

Understanding the mixing process in non-isothermal JICFs is often complicated because of the different properties of the jet and the cross-flow fluid, such as density. Esmaeili et al. [127] studied the turbulent mixing process in isothermal and non-isothermal JICFs using the LES filtered mass density function (FMDF), and their results showed that with a decrease in the temperature ratio, the CRVP moves away from the wall and the jet may subsequently penetrate deeper into the cross-flow. In addition, the spreading rate, mixing, and entrainment are remarkably enhanced as the jet-to-cross-flow temperature ratio decreases.

Dai et al. [22] conducted a numerical study on the flow topologies and formation mechanisms of vortical structures associated with an inclined jet in a cross-flow at relatively lower Reynolds numbers and velocity ratios (r = 0.5–2.0), and then compared their results with experimental LIF and PIV measurements. Since there is agreement that the RANS models have poor predictive ability for the anisotropy JICF problem and that DNS has the limitation of an enormous computational cost, the LES was applied for Dai et al.'s [22] numerical work.

Comparison of the simulation and experimental results shows that LES can well capture the evolution of the CRVP. It is also clear that the flow patterns drastically change with the velocity ratio (see Figures 2-24 and 2-25). From their research, the hairpin vortices mainly dominates the JICF when r = 0.5, while the fundamental flow topologies recover and time-averaged CRVP originates mostly from the coherent structures within the jet nozzle when r = 2.0. The LES results presented in the study by Dai et al. [22] clarified that for the inclined JICF problem, the vortical structures formed in the jet nozzle may play a significant role in the formation of the hairpin vortex.

More recently, Uyanwaththa et al. [82] numerically studied the mixing process of a JICF through approximating the jet stream as a passive scalar and by use of the LES method with three dynamic SGS stress models to simulate the turbulent velocity field. The open-source CFD code OpenFOAM was also applied for the simulation. The DSM, dynamic mixed model (DMM), and dynamic one-equation model (DOEM) were validated with experimental measurements of the Reynolds stress field and the mean velocity field results of the test case by Cárdenas et al. [76] and Galeazzo et al. [107,108]. All the mentioned SGS stress models presented acceptable agreement with experimental data in predicting the Reynolds stress and mean velocity fields. Furthermore, comparison of the simulation results and experimental data of both fields showed that the influence of the CRVP can be seen in the form of a kidney-shaped distribution, and the CRVP conserves the passive scalar concentration at its core due to the highest concentration being observed there.

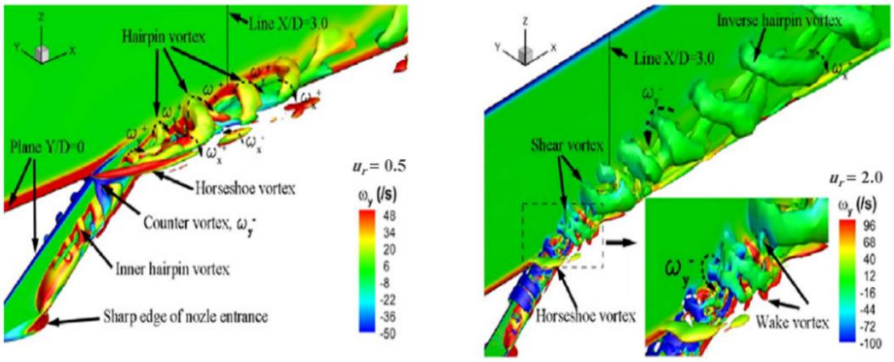

(a) **(b)**

Figure 2-24 Spanwise vorticity (ω_y) on iso-surfaces of: **(a)** $\nabla 2P/\rho$ = 100/s2 for r = 0.5 and **(b)** $\nabla 2P/\rho$= 50/s2 for r = 2.0 [22]

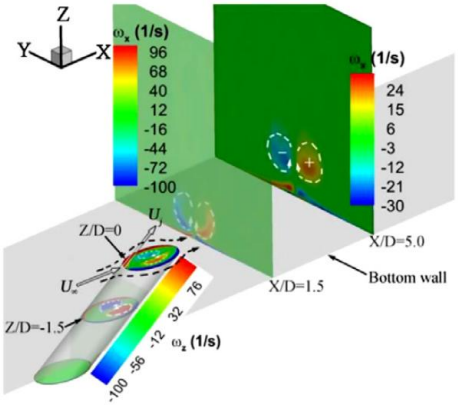

Figure 2-25 Time-averaged vorticity contours within the jet nozzle and the vertical planes [22]

It is worthwhile to mention that less attention has been given in the literature to CFD simulations of buoyant JICF mixing applications involving dilution. To the authors' knowledge, the only systematic CFD study in which the effects of flowing ambient cross-flow ($0.2 < u_r F < 1.6$) on plume trajectory and dilution predictions were examined to date was done by Baum and Gibbes [40]. Using RANS equations with a k-ω turbulence closure scheme, they successfully modeled the discharge behavior of inclined multiport diffusers in the Gold Coast desalination plant in Australia. A threshold value of $u_r F \sim 0.8$ was also identified for the distinct variations between the current-dominated and dense-jet-dominated regimes. Therefore, following the advancements in available CFD methods, it can be stated that more research efforts should be devoted to the application of this simulation tool in predicting the mixing behaviors of buoyant jets issuing into cross-flows.

2.9 Future Research Needs

The flow structures resulting from the interaction of jets and cross-flows and the impacts of flowing current on mixing and transport behaviors have been the main focuses in studies on buoyant JICFs to date. Although some improvements have been achieved in the existing knowledge of buoyant JICF behaviors by using state-of-the-art experimental techniques such as LIF and PIV systems as well as practical CFD tools, there are still key deficiencies in understanding that should be further addressed.

These knowledge gaps include but are not limited to the following research areas:

- Most of the previous studies aimed at understanding the formation and evolution of vortical structures have been carried out by using buoyant JICF applications involving film cooling, and the influence of vortical structures on the mixing behaviors of dilution applications has been less studied.
- Research efforts aimed at understanding CRVP origination as the most significant mixing structure in JICFs under different velocity ratios and working conditions should be intensified.
- Further use of a combination of LIF and PIV flow imaging will help provide a fundamental understanding of both the vortical structures and jet trajectories and properties when dealing with complex interactions of buoyant jets and cross-flows.
- The existence of neighboring boundaries such as the bed and shallow water surface can certainly affect the jet spreading behavior, and therefore, the mixing behaviors of JICFs become more complex, which needs further investigation.
- The paucity of knowledge regarding the interplay between port spacing and cross-flow effects restricts our ability to achieve optimal designs for multiport diffuser configurations and requires further research.
- Since applying marine outfall discharges in deep water environments has been one of the main interests in their field applications, the influence of flow depth on jet mixing behaviors should be studied in more detail.
- Investigating the mixing and dilution behaviors of marine outfall discharges into wave-forcing conditions as the dominant representation of mixing mechanisms in coastal environments remains largely unexplored. However, the data obtained from discharges

into uniform cross-flow ambient conditions, although conservative, can be considered as relevant results.

- In both the experimental and CFD studies, little attention has been spent on jet mixing behaviors beyond the plume's impact (i.e., intermediate- and far-field regions), where the jet is mainly affected by laterally spreading current and ambient turbulence and diffusion.
- Despite significant advancements in the applications of CFD methods for the simulation of buoyant JICFs, special attention should be given to the complexity of CFD models' setup and validation, difficulties in CFD mesh generation and the stability of turbulence models, and CFD computational costs for complex jet configurations.
- Opportunities exist to assess the CFD simulation of buoyant JICF mixing applications involving dilution by applying various turbulence modeling approaches such as RANS and LES.
- Applying instantaneous CFD analysis should be further investigated due to the turbulent nature of flow behaviors resulting from buoyant jet interactions with ambient cross-flow conditions.
- Artificial intelligence (AI) techniques have recently shown great potential for modeling and solving complex nonlinear water and marine engineering problems [128–136]. Thus, extensive and promising datasets obtained from experimental and CFD research efforts on buoyant JICFs can be employed in future AI studies.

2.10 Conclusions

Optimizing the design of marine outfall discharges for the purpose of minimizing environmental impacts is an important issue in order to adhere to regulatory demands. Since the receiving environment is rarely stationary, the influence of ambient cross-flows on the mixing process of jet discharges needs to be well understood. Interactions between jets and cross-flows may generate highly complex, unsteady, and nonlinear flow structures, and as a result, the application of buoyant JICFs has gained considerable attention in many experimental and numerical studies in fluid mechanics. Recent advances in experimental techniques such as LIF and PIV systems, as well as the availability of practical CFD tools, have helped scientists to draw better conclusions regarding the performance of buoyant JICFs. The literature review shows that several experimental studies are generally available on buoyant JICFs in

comparison with numerical studies. Thus, numerical models in this field still require further progress and investigation.

In terms of the formation and evolution of vortical structures as significant structures in the mixture and entrainment between jets and cross-flows, most of the previous experimental and numerical studies have been done in the field of buoyant JICF film-cooling applications. These studies have demonstrated that CRVPs and horseshoe vortices are properties of the mean flow field in contrast to shear-layer and wake vortices, which are instantaneous and temporal and can be removed by time-averaging. In addition, the origin of CRVPs is still a subject of much debate, despite it being generally considered as the most significant mixing structure in a JICF. Currently, the jet shear-layer has been generally identified as the main origin of CRVP formation, but investigations of different velocity ratios and working conditions will provide a better picture of the complex vortical structures in buoyant JICFs.

The value of $u_r F$ for the case of single-port discharges, and the values of $u_r F$ and $\frac{L_p}{DF}$ for the case of multi-port discharges into ambient cross-flow conditions, play the key roles in determining a jet's dilution properties and trajectory. Studies on multiport discharges compared to the singular ones have shown that small changes in diffuser design can lead to significant changes in the flow field and therefore dilution. Accordingly, in complex situations, the difficulty in predicting these effects may result in the need for physical models. That is why little attention has been spent on the multiport configurations in the outfall discharge research in comparison with the singular ones.

The literature review shows that integral jet models may not capture some key aspects of the mixing behavior of JICFs due to simplifying assumptions. Numerical CFD methods, however, have shown significant capabilities for overcoming the deficiencies of integral models and resolving most of the complex behaviors of outfall discharges. The review shows that steady-state RANS simulations provide a reasonable agreement with the experimental data when the flow is statistically stationary. Conversely, when the flow is not statistically stationary (i.e., when the effect of large-scale coherent structures becomes noteworthy), the Reynolds-averaged values do not converge to their time-averages. As coherent structures are not turbulent in nature, their effects on the mean flow are not capable of being modeled by turbulence models. Hence, to attain trustworthy and reliable results for all variables, time-dependent simulations are compulsory, which significantly rises the computational cost. Fortunately, the rise in the computational cost of these simulations may translate into higher precision and

validity, particularly for turbulent mixing problems. Research has also confirmed advancements in CFD simulations from the Reynolds-averaged approach to large-eddy and hybrid approaches.

Although the main features of buoyant JICFs are reasonably well understood, there remain many intriguing fundamental research questions. Lastly, this paper helps provide a fundamental understanding of the performance of JICFs, and presents a critical review of relevant modeling and experimental studies in order to advance the academic research and engineering applications of buoyant JICFs.

Author Contributions: Both authors were involved in the literature review, discussion, and interpretation. M.T. prepared the original draft, and A.M. reviewed and edited the manuscript. Authors have read and agreed to the published version of the manuscript.

Funding: This research received no external funding.

Acknowledgments: The first author, M.T., is a recipient of a scholarship from the Ontario Trillium Scholarship (OTS) program.

Conflicts of Interest: The authors declare no conflict of interest.

Nomenclature

Abbreviation	
3DLIF	Three-dimensional laser-induced fluorescence
BDFF	Buoyancy Dominated Far-Field
BDNF	Buoyancy Dominated Near-Field
CFD	Computational fluid dynamics
CRVP	Counter-rotating vortex pair
DMM	Dynamic mixed model
DNS	Direct numerical simulation
DOEM	Dynamic one-equation model
DSM	Dynamic Smagorinsky model
FMDF	Filtered mass density function
JICF	Jet in cross-flow
LA	Light attenuation
LES	Large eddy simulation
LIF	Laser-induced fluorescence

LRR	Launder-Reece-Rodi
MDFF	Momentum Dominated Far-Field
MDNF	Momentum Dominated Near-Field
NS	Navier-Stokes
PIV	Particle image velocimetry
PTV	Particle tracking velocimetry
RANS	Reynolds-averaged Navier-Stokes
SGS	Sub-grid scale
URANS	Unsteady Reynolds-averaged Navier-Stokes

Mathematical Symbols

B_0	Discharge buoyancy flux
BR	Blowing Ratio
c	Local fluid conductivity
c_0	Initial jet fluid conductivity
c_a	Ambient fluid conductivity
D	Jet discharge diameter
F	Jet-densimetric Froude Number
g	Acceleration due to gravity
g'	Modified acceleration due to gravity
g'_0	Initial modified acceleration due to gravity
H	Flow depth
J	Jet to cross-flow momentum flux ratio
l_b	Plume-to-cross-flow (Buoyancy) Length Scale
l_m	Jet-to-cross-flow Length Scale
l_M	Jet-to-plume Length Scale
L_p	port-spacing
l_Q	Discharge Length Scale
M_0	Discharge momentum flux
P	Pressure
Q_0	Discharge volume flux
r	Jet to cross-flow velocity ratio
Re	Reynolds numbers
Re_0	Jet Reynolds Number

S	Jet dilution properties
S_i	Centerline peak dilution
S_t	Impact dilution
U	Mean velocity component
U_0	Jet discharge velocity
U_a	Ambient flow velocity
U_c	Velocity scale
u_r	Ambient cross-flow to jet velocity ratio
$u_r F$	Cross-flow based Froude number
$\overline{u'u'}$	Specific Reynolds stress component
x	Horizontal distance
x_i	Horizontal distance to jet impact point
x_t	Horizontal distance to jet terminal rise height
y	Lateral distance
z	Vertical distance
z_0	Jet port height
z_t	Maximum centerline height of jet trajectory
z_{tm}	Maximum terminal height of jet trajectory
Greek symbols	
δ	Boundary layer thickness
ζ	Geometric scales of the flow
θ	Jet discharge angle relative to the horizontal
v_0	Kinematic viscosity of jet flow discharge
ρ_0	Jet discharge density
ρ_a	Ambient flow density
ϕ	Angle of cross-flow relative to the discharge propagation at the source
ω_x	Streamwise vorticity
ω_y	Spanwise vorticity

2.11 References

[1] J. Kucera, Desalination: water from water, 2nd Edition, John Wiley and Sons Inc., 2019. https://doi.org/10.1002/9781119407874.

[2] T.M. Missimer, B. Jones, R.G. Maliva, Intakes and Outfalls for Seawater Reverse-Osmosis Desalination Facilities: Innovations and Environmental Impacts, Springer, New York, 2015. https://doi.org/10.1007/978-3-319-13203-7.

[3] X. Yan, A. Mohammadian, Numerical Modeling of Vertical Buoyant Jets Subjected to Lateral Confinement, Journal of Hydraulic Engineering 143 (2017) 04017016. https://doi.org/10.1061/(asce)hy.1943-7900.0001307.

[4] M. Ben Meftah, M. Mossa, Turbulence measurement of vertical dense jets in crossflow, Water (Basel) 10 (2018) 286. https://doi.org/10.3390/w10030286.

[5] G.R. Jones, J.D. Nash, R.L. Doneker, G.H. Jirka, Buoyant surface discharges into water bodies. I: Flow classification and prediction methodology, Journal of Hydraulic Engineering 133 (2007) 1010–1020. https://doi.org/10.1061/(ASCE)0733-9429(2007)133:9(1010).

[6] J. Andreopoulos, W. Rodi, Experimental investigation of jets in a crossflow, J Fluid Mech 138 (1984) 93–127. https://doi.org/10.1017/S0022112084000057.

[7] R. Gu, H.G. Stefan, Stratification dynamics in wastewater stabilization ponds, Water Res 29 (1995) 1909–1923. https://doi.org/10.1016/0043-1354(95)00011-9.

[8] G.H. Jirka, Improved discharge configurations for brine effluents from desalination plants, Journal of Hydraulic Engineering 134 (2008) 116–120. https://doi.org/10.1061/(ASCE)0733-9429(2008)134:1(116).

[9] C. Marugán-Cruz, J. Rodríguez-Rodríguez, C. Martínez-Bazán, Negatively buoyant starting jets, Physics of Fluids 21 (2009) 1–14. https://doi.org/10.1063/1.3253690.

[10] M. Mossa, M. Ben Meftah, F. De Serio, H.M. Nepf, How vegetation in flows modifies the turbulent mixing and spreading of jets, Sci Rep 7 (2017) 1–14. https://doi.org/10.1038/s41598-017-05881-1.

[11] S. Jenkins, J. Paduan, P.J.W. Roberts, D. Schlenk, J. Weis, Management of brine discharges to coastal waters recommendations of a science advisory panel (Tech. Report No. 694), Southern California Coastal Water Research Project, Costa Mesa, CA, USA, 2012.

[12] O. Abessi, P.J.W. Roberts, Dense jet discharges in shallow water, Journal of Hydraulic Engineering 142 (2016) 1–13. https://doi.org/10.1061/(ASCE)HY.1943-7900.0001057.

[13] M.A. Zeitoun, W.F. McIlhenny, R.O. Reid, C.-M. Wong, W.F. Savage, W.W. Rinne, C.L. Gransee, Conceptual designs of outfall systems for desalting plants, Research and Development Progress Rep. 550, Office of Saline Water, Washington DC, USA, 1970.

[14] R. Bashitialshaaer, M. Larson, K.M. Persson, An Experimental Investigation on Inclined Negatively Buoyant Jets, Water (Basel) 4 (2012) 720–738. https://doi.org/10.3390/w4030720.

[15] A. Cipollina, A. Brucato, F. Grisafi, S. Nicosia, Bench-Scale Investigation of Inclined Dense Jets, Journal of Hydraulic Engineering 131 (2005) 1017–1022. https://doi.org/10.1061/(asce)0733-9429(2005)131:11(1017).

[16] G.A. Kikkert, M.J. Davidson, R.I. Nokes, Inclined Negatively Buoyant Discharges, Journal of Hydraulic Engineering 133 (2007) 545–554. https://doi.org/10.1061/(asce)0733-9429(2007)133:5(545).

[17] C.C.K. Lai, J.H.W. Lee, Mixing of inclined dense jets in stationary ambient, Journal of Hydro-Environment Research 6 (2012) 9–28. https://doi.org/10.1016/j.jher.2011.08.003.

[18] C.J. Oliver, M.J. Davidson, R.I. Nokes, Predicting the near-field mixing of desalination discharges in a stationary environment, Desalination 309 (2013) 148–155. https://doi.org/10.1016/j.desal.2012.09.031.

[19] I.G. Papakonstantis, G.C. Christodoulou, P.N. Papanicolaou, Inclined negatively buoyant jets 1: Geometrical characteristics, Journal of Hydraulic Research 49 (2011) 3–12. https://doi.org/10.1080/00221686.2010.537153.

[20] I.G. Papakonstantis, G.C. Christodoulou, P.N. Papanicolaou, Inclined negatively buoyant jets 2: Concentration measurements, Journal of Hydraulic Research 49 (2011) 13–22. https://doi.org/10.1080/00221686.2010.542617.

[21] D. Shao, A.W.-K. Law, Mixing and boundary interactions of 30° and 45° inclined dense jets, Environmental Fluid Mechanics 10 (2010) 521–553. https://doi.org/10.1007/s10652-010-9171-2.

[22] C. Dai, L. Jia, J. Zhang, Z. Shu, J. Mi, On the flow structure of an inclined jet in crossflow at low velocity ratios, Int J Heat Fluid Flow 58 (2016) 11–18. https://doi.org/10.1016/j.ijheatfluidflow.2015.12.001.

[23] P.J.W. Roberts, G. Toms, Inclined Dense Jets in Flowing Current, Journal of Hydraulic Engineering 113 (1987) 323–340. https://doi.org/10.1061/(asce)0733-9429(1987)113:3(323).

[24] C.C.K. Lai, J.H.W. Lee, Initial mixing of inclined dense jet in perpendicular crossflow, Environmental Fluid Mechanics 14 (2014) 25–49. https://doi.org/10.1007/s10652-013-9290-7.

[25] K.W. Choi, C.C.K. Lai, J.H.W. Lee, Mixing in the Intermediate Field of Dense Jets in Cross Currents, Journal of Hydraulic Engineering 142 (2016) 04015041. https://doi.org/10.1061/(asce)hy.1943-7900.0001060.

[26] O. Abessi, P.J.W. Roberts, Rosette diffusers for dense effluents in flowing currents, Journal of Hydraulic Engineering 144 (2018) 1–7. https://doi.org/10.1061/(ASCE)HY.1943-7900.0001403.

[27] J. Chang, Y. Du, X. Shao, Y. Zhao, S. Zheng, Investigation and analysis of vortex and application of jet in crossflow, Case Studies in Thermal Engineering 14 (2019) 0–6. https://doi.org/10.1016/j.csite.2019.100459.

[28] K. Mahesh, The interaction of jets with crossflow, Annu Rev Fluid Mech 45 (2013) 379–407. https://doi.org/10.1146/annurev-fluid-120710-101115.

[29] A.C.H. Lai, D. Yu, J.H.W. Lee, Mixing of a Rosette Jet Group in a Crossflow, Journal of Hydraulic Engineering 137 (2011) 787–803. https://doi.org/10.1061/(ASCE)HY.1943-7900.0000359.

[30] A.R. Karagozian, The jet in crossflow, Physics of Fluids 26 (2014). https://doi.org/10.1063/1.4895900.

[31] A. Coussement, O. Gicquel, G. Degrez, Large eddy simulation of a pulsed jet in cross-flow, J Fluid Mech 695 (2012) 1–34. https://doi.org/10.1017/jfm.2011.539.

[32] L. Cortelezzi, A.R. Karagozian, On the formation of the counter-rotating vortex pair in transverse jets, J Fluid Mech 446 (2001) 347–373. https://doi.org/10.1017/s0022112001005894.

[33] R.J. Margason, R. J., Fifty years of jet in cross flow research, in: In Computational and Experimental Assessment of Jets in Cross Flow, AGARD-CP-534, Winchester, UK, 1993.

[34] D.A. Botelho, O. Abessi, D.A. Botelho, B. Miller, P. Roberts, O. Obessi, M. Mohammadian, M. Wood, D.D. Shao, J. Bradley, R. Morelissen, A.W.K. Law, Marine Outfall Systems: Current Trends, Research and Challenges, International Water Association, London, UK, 2016.

[35] A.R. Karagozian, Transverse jets and their control, Prog Energy Combust Sci 36 (2010) 531–553. https://doi.org/10.1016/j.pecs.2010.01.001.

[36] M. Ni, H. Zhu, Y. Qiu, D. Xu, S. Liu, Review of aero-turbine blade cooling technologies, Gas Turbine Technol 18 (2005) 25–33.

[37] M. Ben Meftah, D. Malcangio, F. De Serio, M. Mossa, Vertical dense jet in flowing current, Environmental Fluid Mechanics 18 (2018) 75–96. https://doi.org/10.1007/s10652-017-9515-2.

[38] A. Cipollina, A. Bonfiglio, G. Micale, A. Brucato, Dense jet modelling applied to the design of dense effluent diffusers, Desalination 167 (2004) 459–468. https://doi.org/10.1016/j.desal.2004.06.161.

[39] E. Gungor, P.J.W. Roberts, Experimental studies on vertical dense jets in a flowing current, Journal of Hydraulic Engineering 135 (2009) 935–948. https://doi.org/10.1061/(ASCE)HY.1943-7900.0000106.

[40] M.J. Baum, B. Gibbes, Field-Scale Numerical Modeling of a Dense Multiport Diffuser Outfall in Crossflow, Journal of Hydraulic Engineering 146 (2020) 1–16. https://doi.org/10.1061/(ASCE)HY.1943-7900.0001635.

[41] A. Gharavi, A. Mohammadian, I. Nistor, E. Peña, J. Anta, Experimental study of surface buoyant jets in crossflow, Environmental Fluid Mechanics 20 (2020) 1007–1030. https://doi.org/10.1007/s10652-020-09737-7.

[42] A. Pincince, E. List, Disposal of brine into an estuary, J Water Pollut Control Fed 45 (1973) 2335–2344.

[43] H.B. Fischer, E.J. List, R.C.Y. Koh, J. Imberger, N.H. Brooks, Mixing in Inland and Coastal Waters, Elsevier Inc., New York: Academic Press, 1979. https://doi.org/10.1016/C2009-0-22051-4.

[44] P.J.W. Roberts, A. Ferrier, G. Daviero, Mixing in Inclined Dense Jets, Journal of Hydraulic Engineering 123 (1997) 693–699. https://doi.org/10.1061/(asce)0733-9429(1997)123:8(693).

[45] O. Abessi, M. Saeedi, M. Davidson, N.H. Zaker, Flow classification of negatively buoyant surface discharge in an ambient current, J Coast Res 28 (2012) 148–155. https://doi.org/10.2112/JCOASTRES-D-10-00131.1.

[46] S.J. Wright, Mean Behavior of Buoyant Jets in a Crossflow, Journal of the Hydraulics Division 103 (1977).

[47] O. Abessi, P.J.W. Roberts, 45 degree dense jet in low ambient flow by Ozeair Abessi and Philip Roberts - YouTube, (2014). https://www.youtube.com/watch?v=Lh9JD7he0os (accessed November 4, 2020).

[48] O. Abessi, P.J.W. Roberts, 45 degree dense jet in low ambient counter flow by Ozeair Abessi and Philip Roberts - YouTube, (2014). https://www.youtube.com/watch?v=vhgnS48KTUg (accessed November 4, 2020).

[49] P. Palomar, I. Losada, Impacts of brine discharge on the marine environment. Modelling as a predictive tool, in: Michael Schorr (Ed.), Desalination: Trends and Technologies, IntechOpen, 2010.

[50] J. Anderson, F. Parker, B. Benedict, Negatively Buoyant Jets in a Cross-Flow, in: International Symposium on Stratified Flows, Washington DC, USA, 1973.

[51] O. Abessi, P.J.W. Roberts, Multiport diffusers for dense discharge in flowing ambient water, Journal of Hydraulic Engineering 143 (2017). https://doi.org/10.1061/(ASCE)HY.1943-7900.0001279.

[52] A. Mohammadian, H. Kheirkhah Gildeh, I. Nistor, CFD Modeling of Effluent Discharges: A Review of Past Numerical Studies, Water (Basel) 12 (2020) 856. https://doi.org/10.3390/w12030856.

[53] O. Abessi, Brine Disposal and Management-Planning, Design, and Implementation, in: Sustainable Desalination Handbook: Plant Selection, Design and Implementation, Elsevier Inc., 2018: pp. 259–303. https://doi.org/10.1016/B978-0-12-809240-8.00007-1.

[54] W.E. Frick, Visual Plumes mixing zone modeling software, Environmental Modelling and Software 19 (2004) 645–654. https://doi.org/10.1016/j.envsoft.2003.08.018.

[55] J.H.W. Lee, V. Cheung, Generalized Lagrangian Model for Buoyant Jets in Current, Journal of Environmental Engineering 116 (1990) 1085–1106. https://doi.org/10.1061/(asce)0733-9372(1990)116:6(1085).

[56] J.H.W. Lee, V. Chu, Turbulent jets and plumes: a Lagrangian approach, Kluwer Academic Publishers, Massachusetts, USA, 2003.

[57] G.H. Jirka, Integral Model for Turbulent Buoyant Jets in Unbounded Stratified Flows. Part I: Single Round Jet, Environmental Fluid Mechanics 4 (2004) 1–56. https://doi.org/10.1023/A:1025583110842.

[58] P. Palomar, J.L. Lara, I.J. Losada, Near field brine discharge modeling part 2: Validation of commercial tools, Desalination 290 (2012) 28–42. https://doi.org/10.1016/j.desal.2011.10.021.

[59] H.S. Tang, J. Paik, F. Sotiropoulos, T. Khangaonkar, Three-Dimensional Numerical Modeling of Initial Mixing of Thermal Discharges at Real-Life Configurations, Journal of Hydraulic Engineering 134 (2008) 1210–1224. https://doi.org/10.1061/(asce)0733-9429(2008)134:9(1210).

[60] S. Zhang, B. Jiang, A.W.-K. Law, B. Zhao, Large eddy simulations of 45° inclined dense jets, Environmental Fluid Mechanics 16 (2016) 101–121. https://doi.org/10.1007/s10652- 015-9415-2.

[61] P. Vafeiadou, I. Papakonstantis, G. Christodoulou, Numerical simulation of inclined negatively buoyant jets, in: Proceedings of the 9th International Conference on Environmental Science and Technology, Rhodes Island, Greece, 2005: pp. A1537–A1542.

[62] C. Oliver, M. Davidson, R. Nokes, k-ε Predictions of the initial mixing of desalination discharges, Environmental Fluid Mechanics 8 (2008) 617–625. https://doi.org/10.1007/s10652-008-9108-1.

[63] X. Yan, A. Mohammadian, X. Chen, Three-Dimensional Numerical Simulations of Buoyant Jets Discharged from a Rosette-Type Multiport Diffuser, J Mar Sci Eng 7 (2019) 409. https://doi.org/10.3390/jmse7110409.

[64] X. Yan, A. Mohammadian, X. Chen, Numerical modeling of inclined plane jets in a linearly stratified environment, Alexandria Engineering Journal 59 (2020) 1857–1867. https://doi.org/10.1016/j.aej.2020.05.023.

[65] X. Yan, B. Ghodoosipour, A. Mohammadian, Three-Dimensional Numerical Study of Multiple Vertical Buoyant Jets in Stationary Ambient Water, Journal of Hydraulic Engineering 146 (2020) 04020049. https://doi.org/10.1061/(asce)hy.1943-7900.0001768.

[66] G. Seil, Q. Zhang, CFD modeling of desalination plant brine discharge systems, Journal of the Australian Water Association 37 (2010) 79–83.

[67] H. Kheirkhah Gildeh, A. Mohammadian, I. Nistor, H. Qiblawey, Numerical modeling of turbulent buoyant wall jets in stationary ambient water, Journal of Hydraulic Engineering 140 (2014). https://doi.org/10.1061/(ASCE)HY.1943-7900.0000871.

[68] H. Kheirkhah Gildeh, A. Mohammadian, I. Nistor, H. Qiblawey, Numerical modeling of 30◦ and 45◦ inclined dense turbulent jets in stationary ambient, Environmental Fluid Mechanics 15 (2015) 537–562. https://doi.org/10.1007/s10652-014-9372-1.

[69] H. Kheirkhah Gildeh, A. Mohammadian, I. Nistor, H. Qiblawey, X. Yan, CFD modeling and analysis of the behavior of 30° and 45° inclined dense jets-new numerical insights, Journal of Applied Water Engineering and Research 4 (2016) 112–127. https://doi.org/10.1080/23249676.2015.1090351.

[70] D. Robinson, M. Wood, M. Piggott, G. Gorman, CFD modelling of marine discharge mixing and dispersion, Journal of Applied Water Engineering and Research 4 (2016) 152–162. https://doi.org/10.1080/23249676.2015.1105157.

[71] B.R. Plum, Modelling of Desalination Plant Outfalls, Final Thesis Report, University of New South Wales: Sydney, Australia

[72] H. Alfaifi, A. Mohammadian, H. Kheirkhah Gildeh, A. Gharavi, Experimental and numerical study of the characteristics of thermal and nonthermal offset buoyant jets discharged into stagnant water, Desalination Water Treat 141 (2019) 171–186. https://doi.org/10.5004/dwt.2019.23477.

[73] X. Yan, A. Mohammadian, Numerical Modeling of Multiple Inclined Dense Jets Discharged from Moderately Spaced Ports, Water (Basel) 11 (2019) 2077. https://doi.org/10.3390/w11102077.

[74] S. Zhang, A.W.K. Law, M. Jiang, Large eddy simulations of 45° and 60° inclined dense jets with bottom impact, Journal of Hydro-Environment Research 15 (2017) 54–66. https://doi.org/10.1016/j.jher.2017.02.001.

[75] M. Jiang, A.W.K. Law, A.C.H. Lai, Turbulence characteristics of 45° inclined dense jets, Environmental Fluid Mechanics 19 (2019) 27–54. https://doi.org/10.1007/s10652-018-9614-8.

[76] C. Cárdenas, R. Suntz, J.A. Denev, H. Bockhorn, Two-dimensional estimation of Reynolds-fluxes and -stresses in a Jet-in-Crossflow arrangement by simultaneous 2D-LIF and PIV, Appl Phys B 88 (2007) 581–591. https://doi.org/10.1007/s00340-007-2734-3.

[77] T.F. Fric, A. Roshko, Vortical Structure in the Wake of a Transverse Jet, J Fluid Mech 279 (1994) 1–47. https://doi.org/10.1017/S0022112094003800.

[78] R. Fearn, R.P. Weston, Vorticity associated with a jet in a cross flow, AIAA Journal 12 (1974) 1666–1671. https://doi.org/10.2514/3.49576.

[79] S. Muppidi, K. Mahesh, Direct numerical simulation of round turbulent jets in crossflow, J Fluid Mech 574 (2007) 59–84. https://doi.org/10.1017/S0022112006004034.

[80] R.M. Kelso, T.T. Lim, A.E. Perry, An experimental study of round jets in cross-flow, J Fluid Mech 306 (1996) 111–144. https://doi.org/10.1017/S0022112096001255.

[81] S. Muppidi, K. Mahesh, Study of trajectories of jets in crossflow using direct numerical simulations, J Fluid Mech 530 (2005) 81–100. https://doi.org/10.1017/S0022112005003514.

[82] A. Uyanwaththa, W. Malalasekera, G. Hargrave, M. Dubal, Large eddy simulation of scalar mixing in jet in a cross-flow, J Eng Gas Turbine Power 141 (2019) 1–13. https://doi.org/10.1115/1.4042089.

[83] S.H. Smith, M.G. Mungal, Mixing, structure and scaling of the jet in crossflow, J Fluid Mech 357 (1998) 83–122. https://doi.org/10.1017/S0022112097007891.

[84] J.E. Broadwell, R.E. Breidenthalt, Structure and Mixing of a Transverse Jet in Incompressible Flow, J Fluid Mech 148 (1984) 405. https://doi.org/10.1017/S0022112084002408.

[85] T. Fric, Structure in the near field of the transverse jet, PhD Thesis, California Institute of Technology, 1990.

[86] L.L. Yuan, R. Street, J.H. Ferziger, Large-eddy simulations of a round jet in crossflow, J. Fluid Mech 379 (1999) 71–104. https://doi.org/10.1007/978-3-642-15748-6_25.

[87] T.T. Lim, T.H. New, S.C. Luo, On the development of large-scale structures of a jet normal to a cross flow, Physics of Fluids 13 (2001) 770–775. https://doi.org/10.1063/1.1347960.

[88] Y.M. Marzouk, A.F. Ghoniem, Vorticity structure and evolution in a transverse jet, J Fluid Mech 575 (2007) 267–305. https://doi.org/10.1017/S0022112006004411.

[89] M. Tyagi, S. Acharya, Large eddy simulation of film cooling flow from an inclined cylindrical jet, J Turbomach 125 (2003) 734–742. https://doi.org/10.1115/1.1625397.

[90] X. Guo, W. Schröder, M. Meinke, Large-eddy simulations of film cooling flows, Comput Fluids 35 (2006) 587–606. https://doi.org/10.1016/j.compfluid.2005.02.007.

[91] R.J. Fawcett, A.P.S. Wheeler, L. He, R. Taylor, Experimental investigation into the impact of crossflow on the coherent unsteadiness within film cooling flows, Int J Heat Fluid Flow 40 (2013) 32–42. https://doi.org/10.1016/j.ijheatfluidflow.2013.01.001.

[92] E. Sakai, T. Takahashi, H. Watanabe, Large-eddy simulation of an inclined round jet issuing into a crossflow, Int J Heat Mass Transf 69 (2014) 300–311. https://doi.org/10.1016/j.ijheatmasstransfer.2013.10.027.

[93] R.M. Kelso, A.J. Smits, Horseshoe vortex systems resulting from the interaction between a laminar boundary layer and a transverse jet, Physics of Fluids 7 (1995) 153–158. https://doi.org/10.1063/1.868736.

[94] A. Krothapalli, L. Lourencof, J.M. Buchlini, Separated Flow Upstream of a Jet in a Crossflow, AIAA JOURNAL 28 (1990) 414–420. https://doi.org/10.2514/3.10408.

[95] M.S. Acarlar, C.R. Smith, A study of hairpin vortices in a laminar boundary layer. Part 2. Hairpin vortices generated by fluid injection, J Fluid Mech 175 (1987) 43–83. https://doi.org/10.1017/S0022112087000284.

[96] R. Sau, K. Mahesh, Dynamics and mixing of vortex rings in crossflow, J Fluid Mech 604 (2008) 389–409. https://doi.org/10.1017/S0022112008001328.

[97] D.G. Kim, H.Y. Cho, Modeling the buoyant flow of heated water discharged from surface and submerged side outfalls in shallow and deep water with a cross flow, Environmental Fluid Mechanics 6 (2006) 501–518. https://doi.org/10.1007/s10652-006-9006-3.

[98] A. Coussement, O. Gicquel, G. Degrez, Large eddy simulation of a pulsed jet in cross-flow, J Fluid Mech 695 (2012) 1–34. https://doi.org/10.1017/jfm.2011.539.

[99] Z.M. Moussa, J.W. Trischka, S. Eskinazi, The near field in the mixing of a round jet with a cross-stream, J Fluid Mech 80 (1977) 49–80. https://doi.org/10.1017/S0022112077001530.

[100] E.T. Curran, Scramjet engines: The first forty years, J Propuls Power 17 (2001) 1138–1148. https://doi.org/10.2514/2.5875.

[101] T. Cambonie, N. Gautier, J.L. Aider, Experimental study of counter-rotating vortex pair trajectories induced by a round jet in cross-flow at low velocity ratios, Exp Fluids 54 (2013). https://doi.org/10.1007/s00348-013-1475-9.

[102] B.D. Pratte, W.D. Baines, Profiles of the round turbulent jet in a cross flow, Journal of the Hydraulics Division 93 (1967) 53–64.

[103] J.W. Ramsey, R.J. Goldstein, Interaction of a heated jet with a deflecting stream, J Heat Transfer 93 (1971) 365–372. https://doi.org/10.1115/1.3449832.

[104] Y. Kamotani, I. Greber, Experiments on a turbulent jet in a cross flow, AIAA Journal 10 (1972) 1425–1429. https://doi.org/10.2514/3.50386.

[105] S.H. Smith, A. Lozano, M.G. Mungal, R.K. Hanson, Scalar mixing in the subsonic jet in crossflow, in: AGARD's Jet in Cross Flow Symposium, Winchester, United Kingdom, 1993.

[106] L.K. Su, M.G. Mungal, Simultaneous measurements of scalar and velocity field evolution in turbulent crossflowing jets, J Fluid Mech 513 (2004) 1–45. https://doi.org/10.1017/S0022112004009401.

[107] F.C.C. Galeazzo, G. Donnert, P. Habisreuther, N. Zarzalis, R.J. Valdes, W. Krebs, Measurement and simulation of turbulent mixing in a jet in crossflow, J Eng Gas Turbine Power 133 (2011). https://doi.org/10.1115/1.4002319.

[108] F.C. Galeazzo, Simulation of Turbulent Flows with and without Combustion with Emphasis on the Impact of Coherent Structures on the Turbulent Mixing, PhD Thesis, KIT Scientific Publishing; Karlsruhe (Germany), 2013.

[109] E.M. Ivanova, B.E. Noll, M. Aigner, Computational modeling of turbulent mixing of a transverse jet, J Eng Gas Turbine Power 133 (2011). https://doi.org/10.1115/1.4002015.

[110] E.M. Ivanova, B.E. Noll, M. Aigner, A numerical study on the turbulent Schmidt numbers in a jet in crossflow, J Eng Gas Turbine Power 135 (2013). https://doi.org/10.1115/1.4007374.

[111] F. Coletti, M.J. Benson, J. Ling, C.J. Elkins, J.K. Eaton, Turbulent transport in an inclined jet in crossflow, Int J Heat Fluid Flow 43 (2013) 149–160. https://doi.org/10.1016/j.ijheatfluidflow.2013.06.001.

[112] P.J.W. Roberts, O. Abessi, Optimization of desalination diffusers using three-dimensional laser-induced fluorescence: Report No. 167, United States Bureau of Reclamation, School of Civil and Environmental Engineering, Atlanta, Georgia, USA, 2014.

[113] M. Jiang, A.W.K. Law, S. Zhang, Mixing behavior of 45° inclined dense jets in currents, Journal of Hydro-Environment Research 18 (2018) 37–48. https://doi.org/10.1016/j.jher.2017.10.008.

[114] O. Abessi, P.J.W. Roberts, Multiport Diffusers for Dense Discharges, Journal of Hydraulic Engineering 140 (2014) 04014032. https://doi.org/10.1061/(asce)hy.1943-7900.0000882.

[115] L.-N. Fan, Turbulent buoyant jets into stratified or flowing ambient fluids: Report No. KH-R-15, W. M. Keck Laboratory of Hydraulics and Water Resources, Division of Engineering and Applied Science, California Institute of Technology, Pasadena, California, 1967.

[116] G. Abraham, The flow of round buoyant jets issuing vertically into ambient fluid flowing in a horizontal direction, in: 5th International Water Pollution Research Conference, San Francisco, USA, 1970.

[117] S.S. Tong, K.D. Stolzenbaeh, Submerged Discharges of Dense Effluent: Report No. 243, Massachusetts Institute of Technology, Cambridge, Massachussetts, USA, 1979.

[118] C.C.K. Lai, Mixing of inclined dense jets, Master Thesis, The University of Hong Kong, Pokfulam, Hong Kong, 2009.

[119] S. V. Patankar, D.K. Basu, S.A. Alpay, Prediction of the three-dimensional velocity field of a deflected turbulent jet, Journal of Fluids Engineering, Transactions of the ASME 99 (1977) 758–762. https://doi.org/10.1115/1.3448902.

[120] J. Alvarez, W. Jones, R. Seoud, Predictions of momentum and scalar fields in a jet in cross-flow using first and second order turbulence closures, in: Computational and Experimental Assessment of Jets in Cross Flow, Vol. 1, AGARD Conference Proceedings, Winchester, UK, 1993.

[121] W.P. Jones, M. Wille, Large-eddy simulation of a plane jet in a cross-flow, Int J Heat Fluid Flow 17 (1996) 296–306. https://doi.org/10.1016/0142-727X(96)00045-8.

[122] K.S. Chen, J.Y. Hwangt, Experimental Study on the Mixing of One-and Dual-Line Heated Jets with a Cold Crossflow in a Confined Channel, AIAA Journal 29 (1990) 353–360. https://doi.org/10.2514/3.10586.

[123] S.A. Sherif, R.H. Fletcher, Measurements of the flow and turbulence characteristics of round jets in crossfiow, Journal of Fluids Engineering, Transactions of the ASME 111 (1989) 165–171. https://doi.org/10.1115/1.3243618.

[124] J.U. Schlüter, T. Schönfeld, LES of jets in cross flow and its application to a gas turbine burner, Flow Turbul Combust 65 (2000) 177–203. https://doi.org/10.1023/A:1011412810639.

[125] P. Majander, T. Siikonen, Large-eddy simulation of a round jet in a cross-flow, Int J Heat Fluid Flow 27 (2006) 402–415. https://doi.org/10.1016/j.ijheatfluidflow.2006.01.004.

[126] F.C.C. Galeazzo, G. Donnert, C. Cárdenas, J. Sedlmaier, P. Habisreuther, N. Zarzalis, C. Beck, W. Krebs, Computational modeling of turbulent mixing in a jet in crossflow, Int J Heat Fluid Flow 41 (2013) 55–65. https://doi.org/10.1016/j.ijheatfluidflow.2013.03.012.

[127] M. Esmaeili, A. Afshari, F.A. Jaberi, Turbulent mixing in non-isothermal jet in crossflow, Int J Heat Mass Transf 89 (2015) 1239–1257. https://doi.org/10.1016/j.ijheatmasstransfer.2015.05.055.

[128] X. Yan, A. Mohammadian, Multigene Genetic-Programming-Based Models for Initial Dilution of Laterally Confined Vertical Buoyant Jets, J Mar Sci Eng 7 (2019) 246. https://doi.org/10.3390/jmse7080246.

[129] X. Yan, A. Mohammadian, Evolutionary prediction of multiple vertical buoyant jets in stationary ambient water, Desalination Water Treat 178 (2020) 41–52. https://doi.org/10.5004/dwt.2020.24938.

[130] X. Yan, A. Mohammadian, Prediction of a rosette dense jet group in crossflow ambient conditions using multi-gene genetic programming, Desalination Water Treat 190 (2020) 440–448. https://doi.org/10.5004/dwt.2020.25746.

[131] A. Danandeh Mehr, V. Nourani, E. Kahya, B. Hrnjica, A.M.A. Sattar, Z.M. Yaseen, Genetic programming in water resources engineering: A state-of-the-art review, J Hydrol (Amst) 566 (2018) 643–667. https://doi.org/10.1016/j.jhydrol.2018.09.043.

[132] M. Jahandideh-Tehrani, O. Bozorg-Haddad, H.A. Loáiciga, Application of particle swarm optimization to water management: an introduction and overview, Springer (n.d.). https://doi.org/10.1007/s10661-020-8228-z.

[133] A. Hipni, A. El-shafie, A. Najah, O.A. Karim, A. Hussain, M. Mukhlisin, Daily Forecasting of Dam Water Levels: Comparing a Support Vector Machine (SVM) Model With Adaptive Neuro Fuzzy Inference System (ANFIS), Water Resources Management 27 (2013) 3803–3823. https://doi.org/10.1007/s11269-013-0382-4.

[134] F. Rezaei, H.R. Safavi, A. Mirchi, K. Madani, f-MOPSO: An alternative multi-objective PSO algorithm for conjunctive water use management, Journal of Hydro-Environment Research 14 (2017) 1–18. https://doi.org/10.1016/j.jher.2016.05.007.

[135] A.H. Zaji, H. Bonakdari, B. Gharabaghi, Developing an AI-based method for river discharge forecasting using satellite signals, Theor Appl Climatol 138 (2019) 347–362. https://doi.org/10.1007/s00704-019-02833-9.

[136] M. Sit, B.Z. Demiray, Z. Xiang, G.J. Ewing, Y. Sermet, I. Demir, A comprehensive review of deep learning applications in hydrology and water resources, Water Science and Technology (2020). https://doi.org/10.2166/wst.2020.369.

3 Laboratory Study on Inclined Desalination Discharges in Perpendicular Cross-flow[2]

Abstract

To mitigate the ecological impact of dense effluents discharged from diffusers, understanding the influence of ambient currents and discharge characteristics on desalination outfall performance is crucial. For this purpose, a series of laser-induced fluorescence (LIF) experimental tests were conducted to address the combined effects of the flowing current strength and nozzle inclination in the discharge region for dense jets issuing into a plane perpendicular to the cross-flows. Various nozzle discharge angles (30°, 45°, and 60°) and cross-flow Froude numbers ($u_rF = \frac{u_a}{u_0} \times \frac{u_0}{\sqrt{g_0' D}}$) are studied to assess 3D jet trajectory and concentration distribution. Empirical equations describing the dilution and geometrical characteristics of the jets are also derived. The findings indicate that deploying the 60° jet can achieve dilutions of over 50% and 20% compared to the 30° and 45° jets, respectively, due to its longer trajectory and greater expansion. Thus, the previously reported insensitivity of dilution to the nozzle angles in the range of 40°-70° for stationary ambient water is questioned herein when dealing with flowing currents. Moreover, the 60° jet is more sensitive to the changes in u_rF compared to the two other shallower angles. The presented outcomes provide valuable insights for safeguarding coastal water bodies through the efficient design of inclined dense outfall discharges.

Keywords: Inclined desalination discharges; Jet in cross-flow; Submerged dense jets; Laser-induced fluorescence; Dilution performance

[2] This chapter has been published as: Taherian, M., Saeidi Hosseini, S. A. R., Mohammadian, A., Ferrari, S., Roberts, P. J. (2024). Laboratory study on inclined desalination discharges in perpendicular cross-flow. Desalination, 583, 117719.

3.1 Introduction

Freshwater scarcity and security, which can be ascribed to population and economic growth, alteration of socioeconomic consumption patterns and living standards, and enlargement of irrigated agricultural industries, are becoming critical concerns worldwide [1,2]. As a sustainable supply remedy for clean water, the capacity of seawater reverse osmosis (SWRO) desalination technologies needs to expand [3–6]. This, however, results in the disposal of hypersaline by-products into source oceanic environments. The SWRO brine effluents, being denser than the receiving ambient waters, sink to the seafloor, thus diminishing the quality of water and endangering the endemic benthic biota [7–11]. Therefore, strict regulatory criteria must be considered, particularly in terms of salinity limit and its impact distance from the brine disposal point, to reduce the relevant marine ecological detriment [2,9,12].

A widely accepted approach for safely discharging brine effluents is to employ offshore diffusers. These diffusers should be designed such that the brine effluents can quickly become diluted to near-background levels, minimizing their environmental effects. This can be obtained by discharging effluents through submerged turbulent buoyant jets at upward angles and high velocities containing both buoyancy and momentum fluxes [13–15]. For the optimal design of turbulent buoyant jets, the influence of several factors should be investigated, including the jet discharge configuration and ambient hydrodynamic forcing functions [12,16].

Regarding the discharge configuration, buoyant jets can be employed in the form of inclined jets at an angle range of 0° to 90°, i.e., covering orientations from horizontal to vertical. In most situations, inclined jets are preferred due to their horizontal momentum components [2,13,17,18]. Specifically, in the case of release into shallow waters close to shoreline regions, inclined dense jets are desirable to prevent impacting the water surface and thereby impairing dilution [19]. Regarding ambient hydrodynamic characteristics, buoyant jets can be released into stationary and dynamic waters. Coastal settings which are representative of realistic conditions are rarely stationary and are mainly predominated by flowing currents, turbulence, and shear [20]. This interplay with the ambient non-stationary environment not only highlights the importance of predicting jet flow behavior but also amplifies the associated challenges.

Several studies have targeted discharges into stationary water bodies as the basis for the design of dense outfalls. In one of the earliest attempts, Zeitoun et al. [21] examined dilution for different inclinations using a point-based conductivity technique and recommended a 60° angle as the best option in terms of having the longest trajectory and highest dilution compared

with 30°, 45°, and 90° angles. Roberts et al. [13] further studied the 60° discharge and provided more detailed dilution measurements. Kikkert et al. [22] also investigated the nozzle inclination effects on the behavior of dense jets using a light attenuation (LA) technique. They reported that the dilution performance at the terminal point of the jet trajectory was almost similar for angles ranging from 15°-60° while the return point dilution was slightly higher for 60°. Later, Jirka [23] questioned the de facto standard of a 60° discharge angle by conducting a theoretical study and stated that the 45° dense jet had a slightly higher terminal rise dilution. Papakonstantis et al. [24,25] and Lai and Lee [26] argued that the dilution performance was insensitive to the discharge angle over the range of 45°-75° using a conductivity technique and 38°-60° using a laser-induced fluorescence (LIF) technique, respectively. Oliver et al. [27] challenged the results of Jirka's study [23] and found a significant effect of the discharge angle on the return point dilution with approximately two-fold dilution for 60° compared to 30°. Abessi and Roberts [17] applied LIF techniques and found a narrow variation in the dilution performance for nozzle angles of 45°-65°.

In comparison, very few studies have been conducted on inclined dense discharges into flowing water bodies, although this scenario is more representative of the coastal environment [20,28]. Flowing currents add further complexity to the investigation of outfall discharges, particularly leading to the alteration of the initial mixing behavior of dense outfalls; accordingly, it is worthwhile to study. Based on the interplay of flowing current direction and jet trajectory, the descriptions of co-/counter-flow and cross-flow are used in the literature. The terms of co-/counter-flow denote the scenarios where the jet discharge aligns with or opposes the direction of the ambient current, respectively, resulting in 2D jet flow trajectories.

On the other hand, the scenario in which the ambient current is perpendicular to the plane of the jet discharge is known as a buoyant jet in cross-flow (JICF). As a result of the interaction between the buoyant jet and cross-flow, the jet is deflected along the ambient water [29]. In addition to this cross-flow influence, the interplay between the discharge momentum and buoyancy forces determines the jet trajectory [30]. Thus, a complex 3D jet flow trajectory is expected. A sketch of the definition of a dense jet issuing into a cross-flow, including the key flow parameters of interest, is shown in Figure 3-1. A jet with an angle θ to the horizontal *x*-*z* plane discharges dense effluents with a concentration, density, and velocity of C_0, ρ_0, and u_0, respectively, into receiving waters through a round nozzle with a diameter of *D*. A uniform ambient current, with a concentration and density of C_a and ρ_a, respectively, flows with a velocity of u_a parallel to the *x*-*y* plane and a water depth of H_a above the center of the nozzle

tip (the reference point). This current makes an angle of ϕ = 90° relative to the discharge propagation plane at the source.

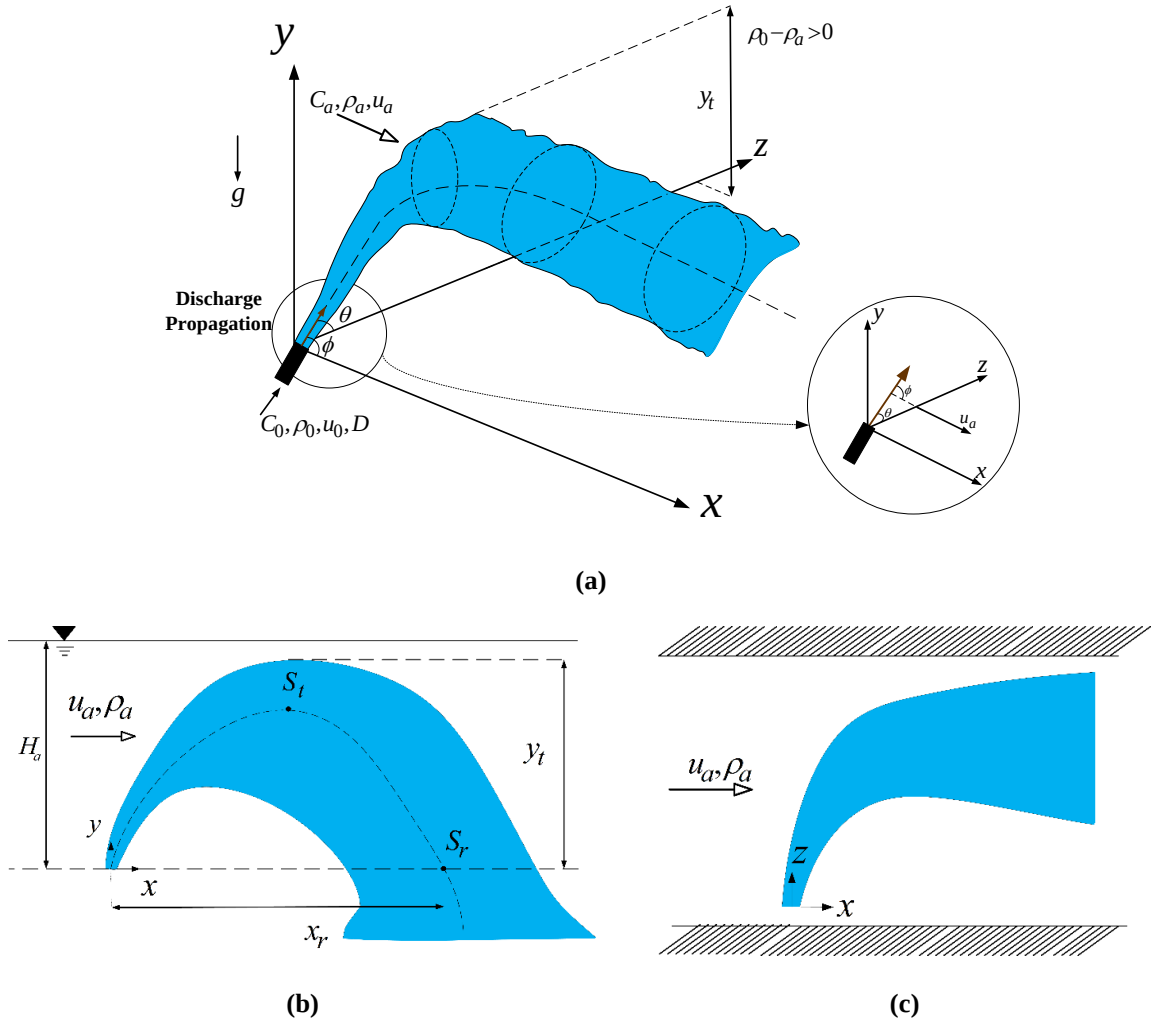

Figure 3-1 Schematic definition of inclined dense jet flow influenced by perpendicular cross-flow **(a)** 3D trajectory, **(b)** front view, and **(c)** top view

(where *S* and *g* are the dilution and gravity acceleration, respectively; indexes *0* and *a* represent the discharge and ambient characteristics, respectively; and indexes *t* and *r* denote the terminal and return point characteristics, respectively.)

Among the few works focused on dense discharge in flowing water, Tong and Stolzenbach [31] investigated the dilution performance of 60° and vertical heated saline effluent jets using temperature as a tracer and a photogrammetry technique. They found that a relatively insensitive dilution amount to the discharge source inclination for the condition tested. Roberts and Toms [32] extensively examined 60° inclined and vertical dense jets for different co-flow and counter-flow cases, as well as five tests for perpendicular cross-flow using photogrammetry and suction sampling techniques. They showed that there is a dependency of

dilution and geometrical characteristics on a cross-flow Froude number defined as $u_r F = \frac{u_a}{u_0} \times \frac{u_0}{\sqrt{g_0' D}}$ (where F is the jet-densimetric Froude number and g_0' is the modified acceleration due to gravity), and the 60° discharge jets outperformed the vertical jets in most cases. Furthermore, comparing dilution data revealed an increasing trend with the angle of current relative to the discharge propagation at the source (ϕ). The lowest dilution occurred for the jet directly opposing the ambient current (counter-flow, ϕ = 0°), while the highest dilution was associated with the jet flowing in the same direction as the ambient current (co-flow, ϕ = 180°). In another study, Lindberg [33] identified three different flow regimes based on the definition of $u_r F$ (namely negligible cross-flow, weak cross-flow, and strong cross-flow) and reported geometrical parameters of the jet flow using the experimental tests of inclined negatively buoyant jets in a water tow tank.

Later, Gungor and Roberts [14] examined the concentration flow field of vertical dense jets with a 2D trajectory using a LIF technique over the cross-flow range of $0.21 < u_r F < 0.92$ in a quiescent tow tank. The increase in the dilution of terminal rise height and impact point was observed with the increase of current speed for the experimental condition tested. Moreover, they generally argued that as a result of the interaction between cross-flow currents and vertical dense jets, different jet flow behaviors could be experienced according to the values of cross-flow parameter, $u_r F$. For zero current speed, the jet falls back on itself, reducing dilution. For $u_r F \approx 0.2$, there is a slight deflection in the jet flow with an intrusion of the upstream wedge against the current, while for $u_r F \approx 0.5$ no upstream wedge is available and almost maximum rise height occurs. With a further increase of current speed $u_r F \approx 1$, the jet is considerably bent over, and it nearly becomes horizontal when $u_r F$ exceeds approximately 2. Another study by Ben Meftah et al. [34,35] also discussed vertical dense jets issuing into ambient currents, focusing on only $u_r F$ values of 1.0 and 1.1.

Lai and Lee [36] studied the concentration flow field using LIF for a 60° dense jet influenced by a perpendicular cross-flow with a 3D trajectory. Only terminal rise data including dilution and location were reported in the field of view considered in their study. They concluded that the jet trajectory and its mixing behavior were predominantly influenced by the ambient current characteristics for $u_r F \geq 0.8$, and detrainment (i.e., the peeling off of dense fluid from the main jet) had a negligible impact on the jet behavior for $u_r F \geq 2.0$. More recently, the mixing of a 45° dense jet discharging into co-flow and counter-flow currents in a quiescent water tow tank was investigated using the LIF approach by Jiang et al. [37]. Based on their results, the

source discharge characteristics could mainly affect the flow behavior within the range of $u_r F < 1.0$ (i.e., jet-dominated regime); however, the ambient currents could play key roles in the mixing behavior of dense jets outside of this range (i.e., current-dominated regime).

The literature discussed above is mainly concerned with inclined dense jets discharging into co- or counter-flows or with vertical jets discharging into cross-flow currents, resulting in 2D trajectories. Previous studies have employed a towing system to simulate the flowing ambient, leading to some differences in the jet discharge behavior compared to releasing in a real flowing environment. In addition, the majority of collected data were within the jet-dominated regime or within the strong cross-flow regime, where the jets become nearly horizontal and have minimal impact on the seabed because they move quickly into the far-field region (i.e., the outfall signature is considerably eliminated) [14]. However, as a representation of realistic site conditions that may occur, investigations on the mixing behavior of perpendicular cross-flow currents within the range of $1.0 \sim < u_r F < \sim 1.6$, regular cross-flow dictated regime [30], should be further intensified. In addition, there is little information on different nozzle discharge angles issuing into flowing waters. A study of different inclined dense jet configurations can be used as a basis for outfall designs, particularly when diffusers are close to the shoreline regions and may have interaction with the water surface.

This study presents the first attempt to experimentally simulate dense discharges with different source inclinations issuing into perpendicular cross-flow currents with 3D trajectories using the LIF imaging approach. By applying dimensional analysis, it is shown that the dense jet flow behavior mainly depends on the cross-flow Froude number and discharge angle. Accordingly, the main objectives of this study are to reduce the negative impacts of dense discharges into marine environments by addressing the effects of discharge angles along with the flowing current strength in the discharge regions. The major flow features of inclined dense JICFs are compared, and design instructions are provided. The analysis of the results includes instantaneous and time-averaged flow visualizations, jet trajectories, geometrical and dilution characteristics of jet flow, jet growth, and concentration variance. To protect receiving water bodies and improve the management of outfall discharges, such information is of significant importance.

The remainder of this paper is organized as follows. Section 3.2 presents a dimensional analysis of the inclined dense JICFs and the experimental procedure. The results and discussion are presented in Section 3.3. General observations of the flow behaviors and jet trajectories are discussed in Sections 3.3.1, and 3.3.2, respectively. Section 3.3.3 presents the effect of $u_r F$

and discharge angles on the main flow parameters, and empirical equations for the dilution and geometrical characteristics of the jets are presented. Jet widening and variance of concentration are explained in Sections 3.3.4, and 3.3.5, respectively. Finally, Section 3.4 has some concluding remarks.

3.2 Methodology and Experimental Conditions

3.2.1 Dimensional Analysis

To simplify the presentation of the dimensional analysis, a constant discharge angle of 90°, resulting in a 2D trajectory, is first assumed (see Figure 3-2). Subsequently, the analysis is developed for the inclined discharge angles, which are the focus of this study. Two fundamental assumptions underlie the application of dimensional analysis to the case of dense jets. The discharges are fully turbulent, with no viscosity effects. Besides, the Boussinesq approximation, $(\rho_0 - \rho_a) \ll \rho_a$, is valid [38].

The jet initially reaches its terminal rise height of y_t (i.e., the vertical distance between the center of the nozzle tip and the maximum height of the flow) with a dilution of S_t (i.e., dilution at the terminal rise point). Then, it descends because of the downward buoyancy forces and travels a horizontal distance of x_r (i.e., the horizontal distance between the center of the nozzle tip and the return point of the flow) with dilution of S_r (i.e., dilution at the return point). These main flow parameters, including the geometrical and dilution characteristics, can be described as a function of the ambient cross-flow properties and initial source conditions (see Eq. (3-11)) [32,35].

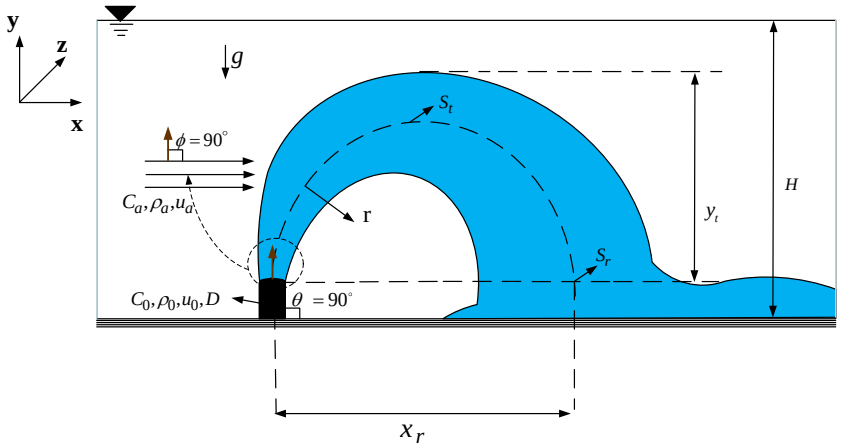

Figure 3-2 A schematic definition of major flow parameters including geometrical and dilution characteristics for a dense jet vertically discharged into ambient cross-flow (where *r* represents the radial distance from the centreline)

$$x_r, y_t, S_r, S_t = f(Q_0, B_0, M_0, u_a, \phi) \tag{3-1}$$

where Q_0 is the discharge volume flux, $B_0 (= g_0' Q_0)$ is the discharge buoyancy flux (where $g_0' = g(\rho_0 - \rho_a)/\rho_a$), M_0 $(= u_0 Q_0)$ is the discharge momentum flux. Velocity and length scales, which are relevant to the fluxes of discharge volume, discharge buoyancy, and discharge momentum, can be defined as [14,20,32]:

$$u_c = {B_0^{1/2}}\Big/{M_0^{1/4}} \tag{3-2}$$

$$l_M = {M_0^{3/4}}\Big/{B_0^{1/2}} \tag{3-3}$$

$$l_Q = {Q_0}\Big/{M_0^{1/2}} \tag{3-4}$$

where u_c is the velocity scale, l_M is the jet-to-plume length scale, and l_Q is the discharge length scale. Following the dimensional analysis and considering that the jet dilution properties can be expressed as $S = g'/g_0' = (\rho - \rho_a)/(\rho_0 - \rho_a)$ (where ρ is the local fluid density) due to the validity of Boussinesq assumption [20], Eq. (3-1) can be rewritten as below for the geometric scales of flow trajectory and dilution properties [32]:

$$\frac{x_r}{l_M} or \frac{y_t}{l_M};\ S_r \frac{l_Q}{l_M} or\ S_t \frac{l_Q}{l_M} = f(\frac{l_M}{l_Q}, \frac{u_a}{u_c}, \phi) \tag{3-5}$$

The right-hand side of the above relationship can be replaced by some equivalencies for a round turbulent buoyant jet with a source diameter of *D* which are presented as follows [20,32]:

$$l_M = (\frac{\pi}{4})^{1/4} DF;\ \frac{l_M}{l_Q} = (\frac{\pi}{4})^{-1/4} F;\ \frac{u_a}{u_c} = (\frac{\pi}{4})^{-1/4} u_r F \tag{3-6}$$

where u_r is the ratio of ambient cross-flow to jet velocity ($u_r = u_a/u_0$). Thus, Eq. (3-5) can be stated as [32]:

$$\frac{x_r}{DF} or \frac{y_t}{DF};\ \frac{S_r}{F} or \frac{S_t}{F} = f(F, u_r F, \phi) \tag{3-7}$$

where the parameter $u_r F$ is a cross-flow Froude number. This definition indicates the relative strength of ambient flow speed to buoyancy [39]. According to the Eq. (3-7), it can be inferred that the jet dilution properties scale with *F*, while the geometric parameters scale with *DF*.

In the case of $F(or\frac{l_M}{l_Q}) \gg 1$, the jet-densimetric Froude number can be eliminated as an individual term in the list of independent parameters, or in other words, the influence of the source volumetric flux is insignificant [14,32]. This statement will be also discussed later in Section 3.3.3. Based on these assumptions and for the case of having a perpendicular angle between cross-flow and the discharge propagation at the source ($\phi = 90°$), Eq. (3-7) becomes:

$$\frac{x_r}{DF} or \frac{y_t}{DF}; \frac{S_r}{F} or \frac{S_t}{F} = f(u_r F) \tag{3-8}$$

Along with $u_r F$, the present study considers the discharge angle θ as an effective parameter that can considerably change the flow behavior. Thus, Eq. (3-8) can be modified as below:

$$\frac{x_r}{DF} or \frac{y_t}{DF}; \frac{S_r}{F} or \frac{S_t}{F} = f(u_r F, \theta) \tag{3-9}$$

Hence, the combined impacts of $u_r F$ and θ play key roles in determining the jet's dilution properties and trajectory for the targeted case of inclined dense JICF.

3.2.2 Experimental Setup and Procedures

In this study, experimental investigations of submerged dense jet discharge into a flowing ambient environment were conducted using LIF, which can capture the flow structure evolution as well as measure the jet trajectory and concentration distribution of the discharge system. The experimental tests were conducted at the Hydraulics Laboratory of the University of Cagliari, Sardinia, Italy. The flume used in these experiments was 6 m long, 0.4 m wide, and 0.5 m deep. A reservoir tank was set in the proximity of the flume for water supply. The experimental flume was made of glass to enable an appropriate flow visualization. The flow rate in the flume was controlled by a ball valve close to the entrance tank. An adjustable weir placed downstream was used to control the flow head. The experimental setup is shown in Figure 3-3.

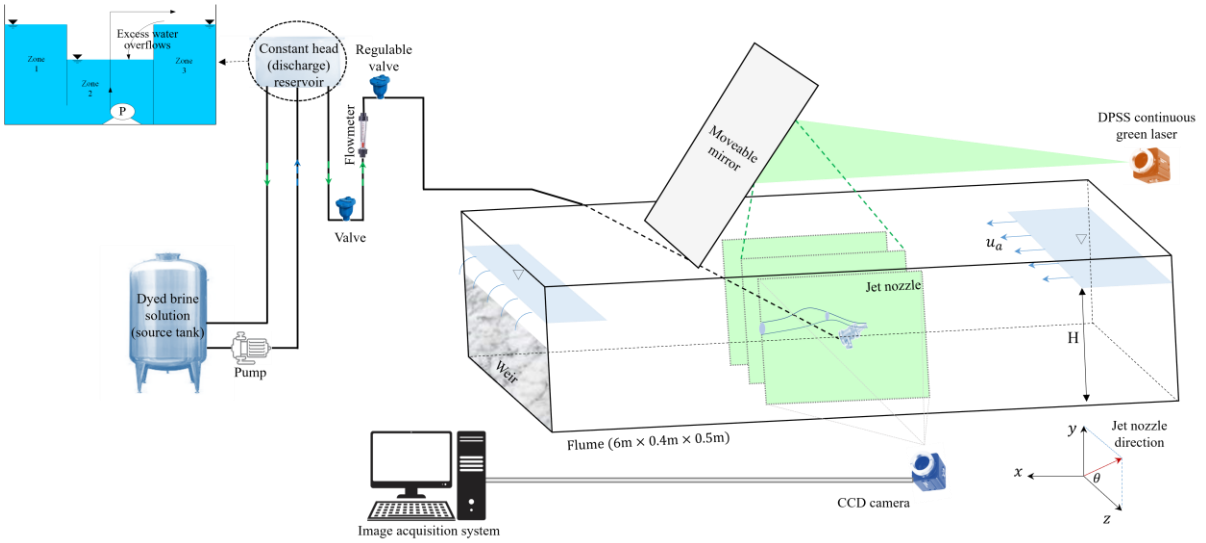

Figure 3-3 Schematic depiction of the experimental setup

The nozzle was located in the middle of the flume length, 3 m from the flume entrance, and 3 m from the weir, ensuring a fully developed and stable ambient flow. The distances between the nozzle tip and the back and front walls were on average 5 cm and 35 cm, respectively. The front wall had a minimal effect on the jet dynamics as the flume was wide enough (40 cm), such that at least 12 cm was maintained between the jet and the front wall in all experiments. The 5 cm gap between the nozzle tip and back wall was sufficient to ensure a limited back wall effect on the jet dynamics because the jets were discharging perpendicular to and immediately moving away from the back wall.

Discharged brine was obtained from a constant-head closed hydraulic circuit. Three separate zones were considered in the discharging reservoir, as shown in Figure 3-3. Zone 1 was used to reduce the chaos of inflow from the source tank to the reservoir. Zone 2 provided a constant water level in Zone 3 through the use of a submersible pump, and Zone 3 was connected to the discharge nozzle while keeping a stable discharge rate in the flume. The discharge rate from the nozzle was measured using a flowmeter. The nozzle was a round pipe with an inner diameter of 3.2 mm, and the length of the nozzle pipe before the outlet was sufficiently long to ensure that the discharge flow regime was fully developed. In the present study, nozzles with discharge angles (θ) of 30°, 45°, and 60° to the horizontal were applied. The distance between the center of the nozzle tip and the flume bottom was on average 0.1 m.

Fresh tap water was used as the ambient water and saline water was used as the discharged effluent. To prepare saline water as a source of negative buoyancy, different predetermined amounts of table salt (NaCl) were dissolved in fresh tap water in the source tank, which

established different discharged effluent densities. The density of the effluent was then measured and controlled using a handheld bubble density meter. The discharge densities ranged from 1030 to 1065 kg/m^3. The temperatures of both the source discharge and ambient water were maintained at 25 $\pm$ 1 °C. To do this, the discharging reservoir was equipped with a device, Corio CD Heating Immersion & Bridge Mounted Circulator, which facilitated precise temperature regulation with an accuracy of approximately $\pm$ 0.03 °C. This device was used to ensure that the temperature within the discharging reservoir remained constant during the experiments. For the main reservoir tank, which served as a source of water supply in the flume, following each refill, a full day was allowed to reach room temperature and stay in the range of 25 $\pm$ 1 °C before running the experiments. Additionally, two digital thermometers at the upstream and downstream of the flume were also used to continuously monitor the water temperature in the flume.

The brine jet was discharged into the flume for a while to achieve a steady state flow condition. Due to the lower density of ambient water compared to the effluent discharge density, a negatively buoyant discharge (NBJ) was generated. It should be mentioned that the main reservoir tank was continuously washed at a very low flow rate with fresh tap water during each run to minimize the possible salt concentration buildup effect during the experiments. After each of three series of runs which had their specific density, the tank was also refilled completely with fresh water and then allowed to reach room temperature. Table 3-1 presents the experimental conditions.

Table 3-1 Experimental Conditions

Run	Discharge Angles, θ (°)	Effluent Density, ρ_0 (kg/m^3)	Jet-densimetric Froude Number, F	Discharge Buoyancy Flux ($B_0(m^4/s^3) = g'_0 Q_0$)	Jet-to-plume Length Scale ($l_M(m) = M_0^{3/4} / B_0^{1/2}$)	Plume-to-cross-flow (Buoyancy) Length Scale ($l_b(m) = B_0 / U_a^3$)	$u_r F$	g'_0 (m/s^2)
R1	30	1030	33.7	2.4693E-06	0.1014	0.0199	1.62	0.2963
R2	45	1030	33.7	2.4693E-06	0.1014	0.0199	1.62	0.2963
R3	60	1030	33.7	2.4693E-06	0.1014	0.0199	1.62	0.2963
R4	30	1035	31.2	2.8782E-06	0.0939	0.0232	1.50	0.3454
R5	45	1035	31.2	2.8782E-06	0.0939	0.0232	1.50	0.3454

R6	60	1035	31.2	2.8782E-06	0.0939	0.0232	1.50	0.3454
R7	30	1040	29.2	3.287E-06	0.0879	0.0265	1.40	0.3944
R8	45	1040	29.2	3.287E-06	0.0879	0.0265	1.40	0.3944
R9	60	1040	29.2	3.287E-06	0.0879	0.0265	1.40	0.3944
R10	30	1045	27.5	3.6958E-06	0.0829	0.0298	1.32	0.4435
R11	45	1045	27.5	3.6958E-06	0.0829	0.0298	1.32	0.4435
R12	60	1045	27.5	3.6958E-06	0.0829	0.0298	1.32	0.4435
R13	30	1050	26.1	4.1047E-06	0.0787	0.0331	1.26	0.4926
R14	45	1050	26.1	4.1047E-06	0.0787	0.0331	1.26	0.4926
R15	60	1050	26.1	4.1047E-06	0.0787	0.0331	1.26	0.4926
R16	30	1055	24.9	4.5135E-06	0.075	0.0364	1.20	0.5416
R17	45	1055	24.9	4.5135E-06	0.075	0.0364	1.20	0.5416
R18	60	1055	24.9	4.5135E-06	0.075	0.0364	1.20	0.5416
R19	30	1060	23.8	4.9223E-06	0.0718	0.0397	1.15	0.5907
R20	45	1060	23.8	4.9223E-06	0.0718	0.0397	1.15	0.5907
R21	60	1060	23.8	4.9223E-06	0.0718	0.0397	1.15	0.5907
R22	30	1065	22.9	5.3312E-06	0.069	0.043	1.10	0.6397
R23	45	1065	22.9	5.3312E-06	0.069	0.043	1.10	0.6397
R24	60	1065	22.9	5.3312E-06	0.069	0.043	1.10	0.6397

T_{ave} = 25 $\pm$ 1 °C, Discharge volume flux (Q_0) = 8.33E-06 (m^3/s), Discharge momentum flux ($M_0 = U_0 Q_0$) = 8.64E-06 (m^4/s^2), Jet-to-cross-flow length scale ($l_m = {M_0^{1/2}}/{U_a}$) = 0.0589 (m), Discharge length scale ($l_Q = {Q_0}/{M_0^{1/2}}$) = 0.0028 (m), H_a = 0.28 m

A small amount of fluorescent titanium dioxide dye was added to the source discharge tank containing saline water as a tracer, which emits a longer wavelength of incident light. A diode-pumped solid-state (DPSS) continuous green laser with an output power of 5 W and wavelength of 532 nm caused the dye to fluoresce. The fluoresced light was captured by a high-speed charge-coupled device (CCD) camera (Mikrotron EoSens 4CXP CoaXPres) at 50 frames per second (to ensure that the flow fields on two consecutive frames were uncorrelated) with a resolution of 2336 × 1728 pixels. The acquisition was continuous, and the exposure time was 1/4000 second. The captured images were stored at a Mono8 bit resolution, i.e., 256 grayscale

levels. Thus, the recorded images displayed a jet flow with bright color on a dark background, where the light intensity level of each pixel could have 256 values ranging from pure black to pure white. The brine concentration was linearly correlated to the light intensity [16].

An F-mount 50 mm lens with f/1.4 was used to increase the coverage area. An orange filter was installed on the camera to cut off the light below 550 nm and filter out the scattered light from the green laser. Consequently, the quality and contrast of the obtained images were enhanced. The camera was connected to a computer using the PCI frame grabber with four CameraLink cables. Laser reflections from the bottom and side walls of the flume were prevented during the experimental tests using black non-reflective materials.

Before discharging the jets, a series of approximately 100 images of only the background, without the presence of NBJs, were recorded and time-averaged to eliminate unwanted light that did not correspond to the jet fluid concentration. After the flow stabilized, a series of more than 3,000 images were recorded. The background image was then subtracted from the resulting images with the jet to remove the background light.

To obtain the jet trajectory and concentration distribution contours, the captured images required further post-processing using a MATLAB code developed for the specific purposes of the present experiments. This code computes the tracer concentrations of each pixel in grayscale images and converts them into color-coded versions. A statistical analysis, including the time-averaged images and their variance, was also performed using the program by considering the instantaneous frames. Subsequently, the concentration distribution fields and contours based on the non-dimensionalized C/C_0 parameter (where C_0 is the discharge concentration) were generated, showing the mean concentration reduction (dilution level) compared to the initial concentration.

The flow field visualization was obtained by sequentially moving the position of the vertical laser sheet emission through the width of the flume such that eight different slices spaced approximately 25 mm apart were achieved. By placing the obtained frames together using ParaView visualization software tools, 2D and 3D depictions of flow fields were eventually formed. To obtain the return point location and dilution, the camera was located above the flume, and images were captured using a horizontal laser sheet placed at the level of the nozzle. Figure 3-4 illustrates the image processing procedure.

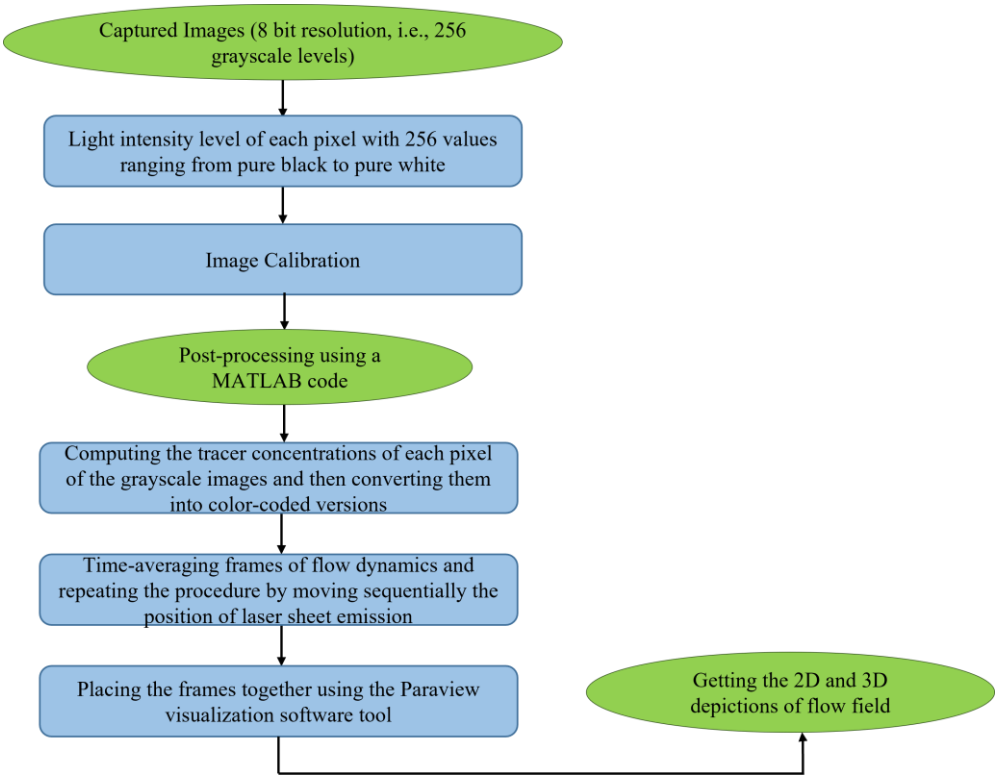

Figure 3-4 Workflow for post-processing the LIF images

3.3 Results and Discussion

3.3.1 General Observation

3.3.1.1 Instantaneous Visualization

Figure 3-5 shows 3D instantaneous concentration flow fields corresponding to the discharge angles of 30°, 45°, and 60° and two different u_rF values, denoted by experimental case numbers R7-9 and R19-21. These visual representations offer valuable insights into the mixing mechanisms contributing to the jet flow dilution. The general flow behavior of an inclined jet unfolds in two distinct phases. During the ascending phase, a well-defined flow structure initially forms due to the jet momentum. However, as the jet movement reverses, the main jet flow begins to disperse. Groups of tracer fluid gradually break apart from the main jet flow as the negative buoyancy predominates [15,35].

Two notable flow features occur at the upper and lower edges of the flow following the jet descending arm. The rotating bundle of tracers along the upper edge, indicated by orange rectangles, facilitates entrainment of the ambient flow into the main jet flow. This reflects the prevailing effect of large-scale eddy motion on this border. In addition, the detrainment of the fluid mass from the primary jet flow, indicated by the blue rectangles, appears along the lower

edge. This occurs because of the unstable density gradient that is available along this edge, where the jet flow with higher density sits atop the lighter ambient environment. This phenomenon is known as buoyancy-induced instability [15,36].

A comparison of the impact of different discharge inclinations on the jet flow behavior shows that the buoyant instabilities are less prominent for shallower discharge angles due to their higher z-direction momentum component. This results in a longer preservation of the form of the initial jet primary flow. Furthermore, a comparison of the flow fields for the series of experiments with higher $u_r F = 1.4$ (R7-9) with the ones with lower $u_r F = 1.15$ (R19-21) can reveal less confinement and greater spread of the jet flow within the ambient environment when applying higher cross-flow Froude numbers. This observation will be also discussed later in Section 3.3.4.

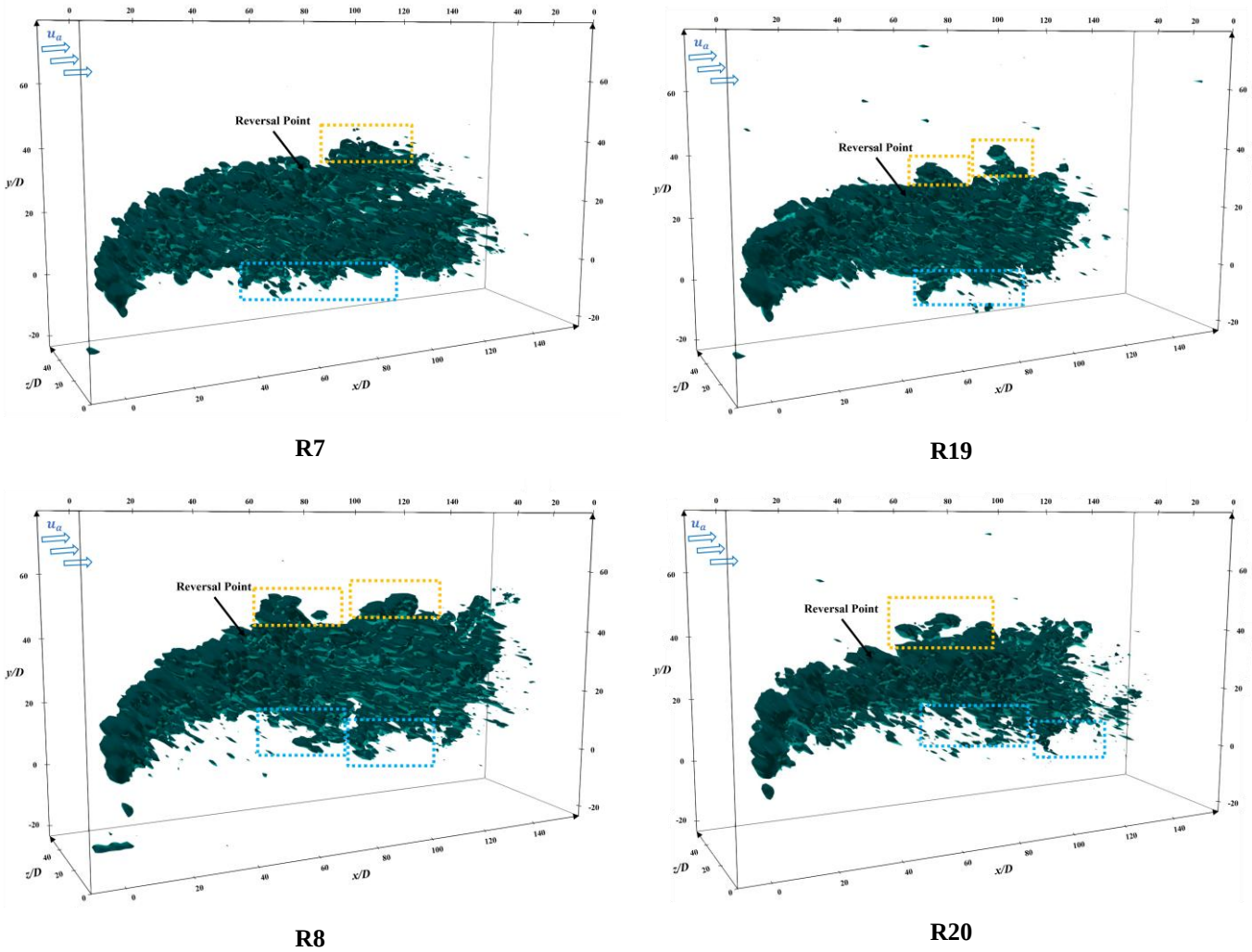

R7 **R19**

R8 **R20**

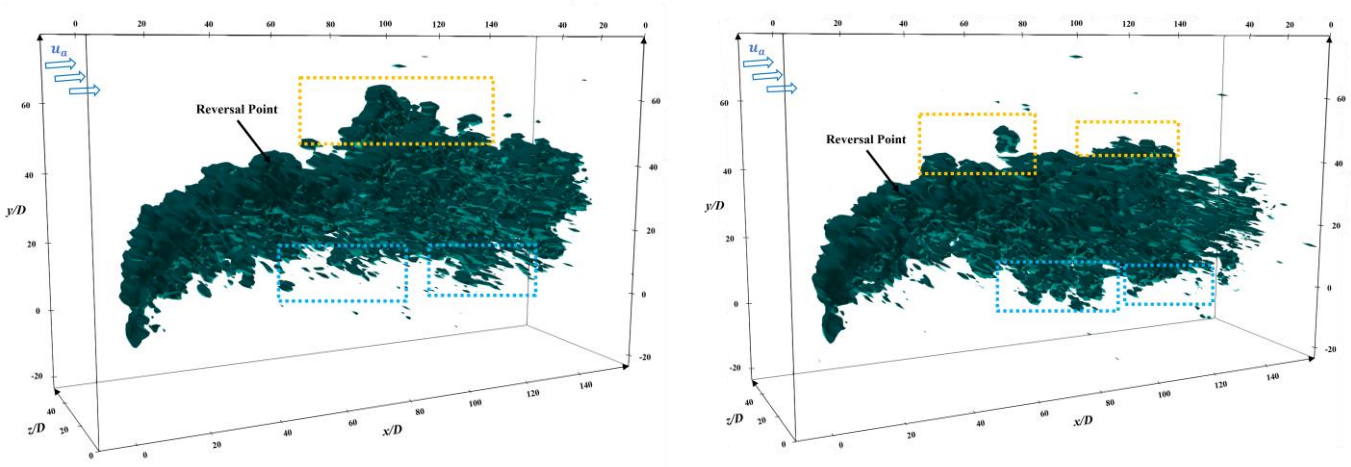

R9

(a)

R21

(b)

Figure 3-5 Instantaneous concentration flow fields for cases **(a)** R7-9 and **(b)** R19-21 (iso-surface C/C_0 = 0.03)

3.3.1.2 Timed-averaged Visualization

The time-averaged 3D flow depictions were obtained using the ParaView software tool, as shown in Figure 3-6. First, jet rising movement occurs as the momentum force is dominant. The body of the jet then starts bending along the longitudinal direction of the flume as a result of the cross-flow current. The momentum force then reduces continuously and becomes equal to the buoyant force where the maximum height of the jet occurs. Subsequently, the buoyant force overcomes the momentum of the jet discharge, and the jet falling stage occurs [20,28,34]. A comparison of the impact of the discharge angles on the flow movement can also be highlighted by the following statements:

- For the case of 30°, the movement of the brine flow along the flume width was more progressive than for the other discharge angles. This is mainly because of the higher z-direction momentum component of this angle.
- The terminal rise point of the 60° discharge was higher than that of the other two angles because of its higher y-direction momentum component.
- For the case of 60°, the longest jet trajectory was obtained, providing more time for the jet to interact with the ambient flow.

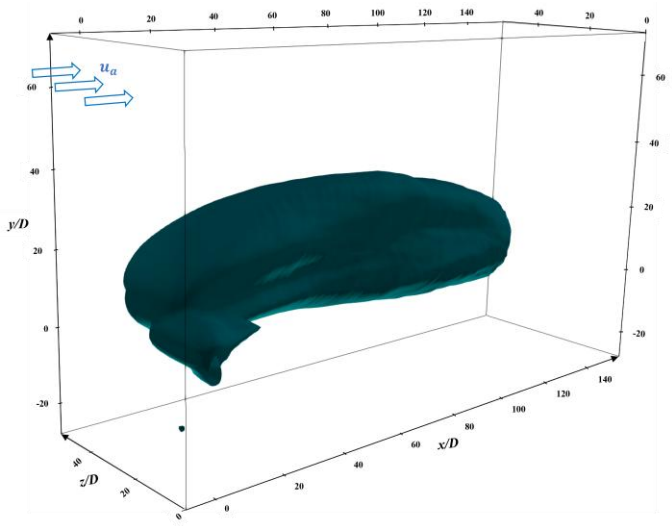

(a)

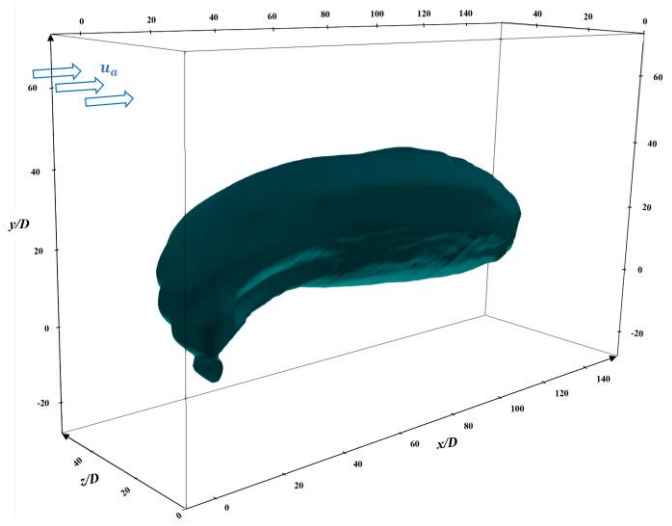

(b)

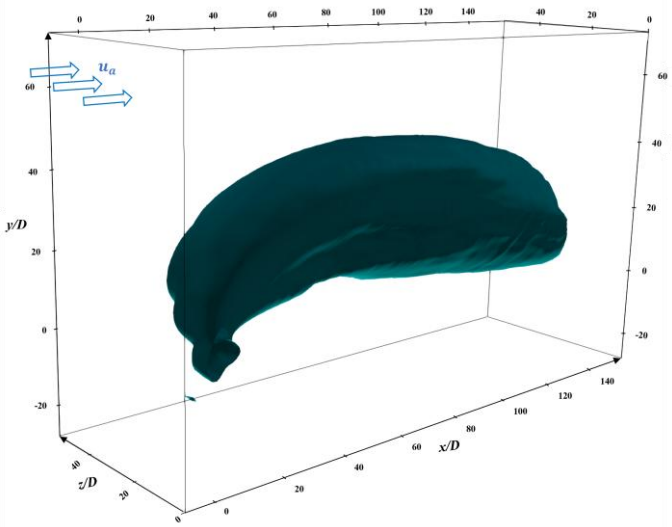

(c)

Figure 3-6 Timed-averaged 3D visualization of the jet discharge flow field for cases **(a)** R19: θ = 30°, **(b)** R20: θ = 45°, and **(c)** R21: θ = 60° (iso-surface C/C_0 = 0.03)

Figure 3-7 illustrates the time-averaged 2D concentration profiles at three different cross-sections for cases R19 and R21 with discharge angles of 30° and 60°, respectively. A comparison of the concentration fields of the 30° and 60° jets at a similar distance from the discharge point shows that the steeper inclination leads to higher dilutions. The dispersion of jet flow in ambient water for the discharge angle of 60° is also higher than that for the 30° jet, which can be evidence of the better dilution performance of the jet with a 60° angle in the dynamic environment. The development of the concentration flow field along the flume width reveals that the 30° jet first attempts to form an almost C-shaped concentration distribution with distinguishable upper and lower edges, e.g., Figure 3-7 (b), and gradually becomes more uniform as the jet moves farther from the discharge point, e.g., Figure 3-7 (c). However, for the 60° jet, the jet forms a concentration distribution with only a noticeable upper edge of high concentration in the proximity of the discharge source, e.g., Figure 3-7 (d), and then a uniform distribution begins to appear immediately, e.g., Figure 3-7 (e), which is closer to the discharge point compared to the 30° jet.

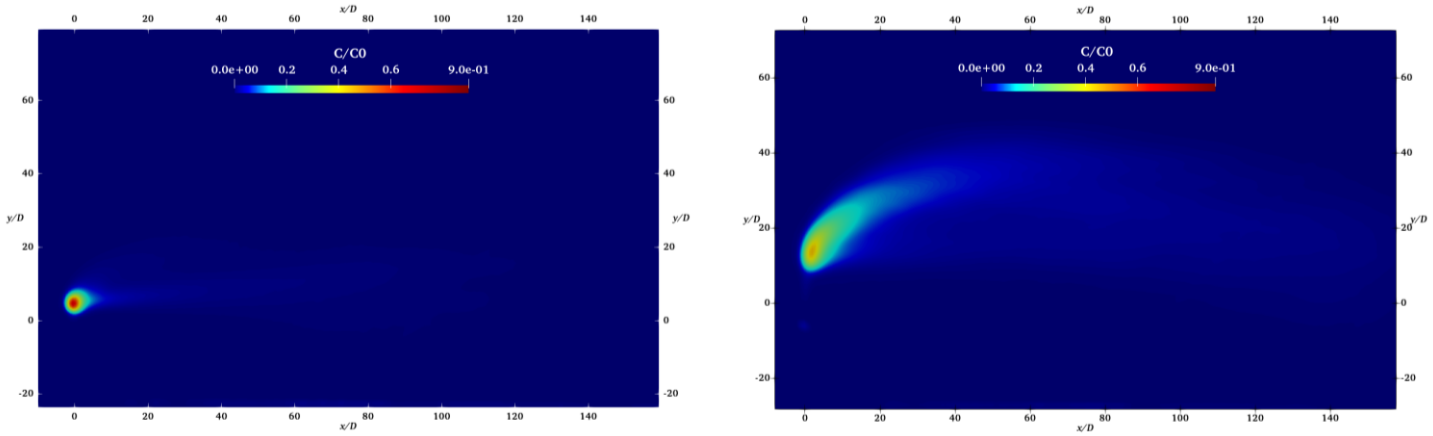

(a) **(d)**

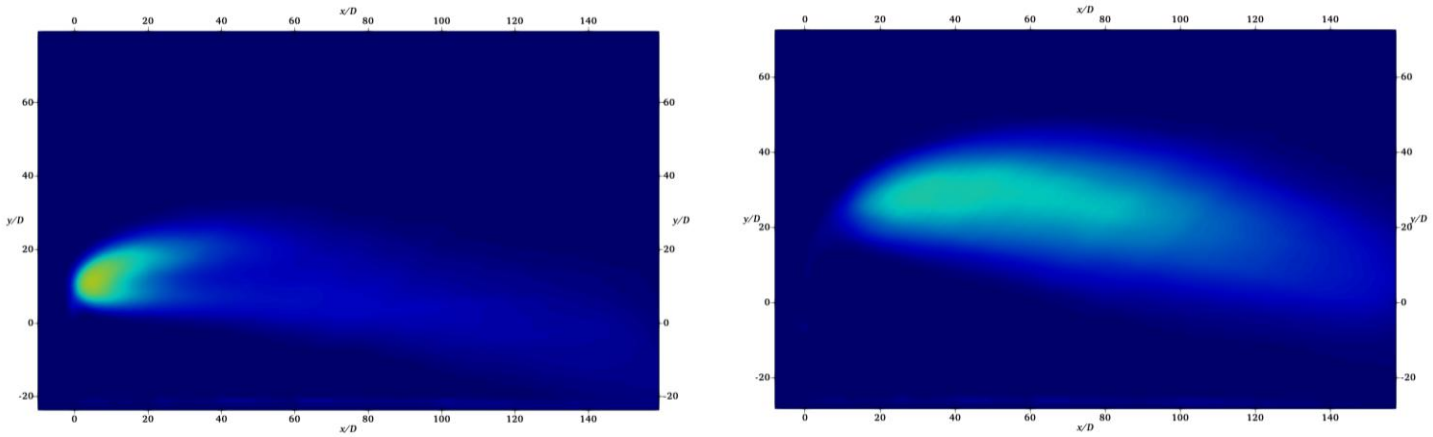

(b) **(e)**

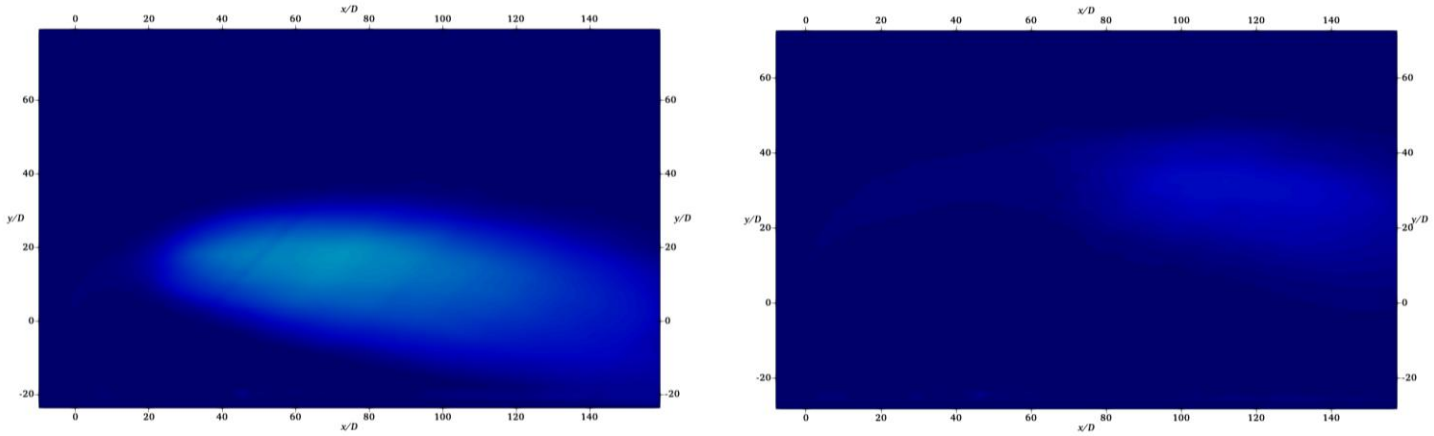

Figure 3-7 Timed-averaged 2D visualization of the concentration flow field for case **(a-c)** R19 at the cross-sections of *z/DF* = 0.33, 0.98, and 1.97, respectively, and for case **(d-f)** R21 at the cross-sections *z/DF* = 0.33, 0.98, and 1.97, respectively.

3.3.2 Jet Trajectory

The jet trajectory can be defined as the locus of maximum concentration, as shown in Figure 3-8, from two different front and top views. Accordingly, the following conclusions can be drawn.

- The 60° discharge angle leads to a higher increase in height compared to the other two angles.
- Rapid ascending and gradual descending phases can be observed for all the jet flows.
- Jet flow penetration along the width of the flume increases with a reduction in the discharge angle from 60° to 30°, due to the higher momentum component in the z-direction for shallower angles.
- The jet at 60° deflects more sharply along the longitudinal direction of the flume due to the influence of the cross-flow current and lower momentum component in the z-direction compared to the other two angles.
- From both the top and front views, the longest trajectory occurs for the discharge angle of 60°.

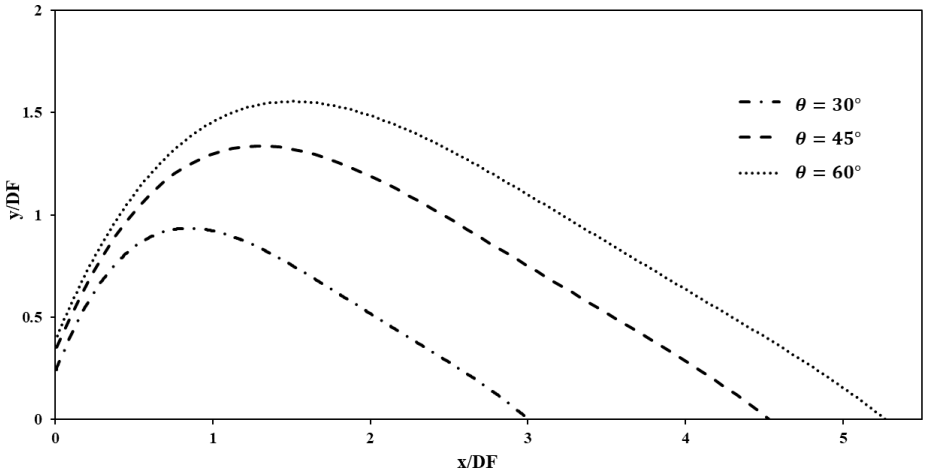

(a)

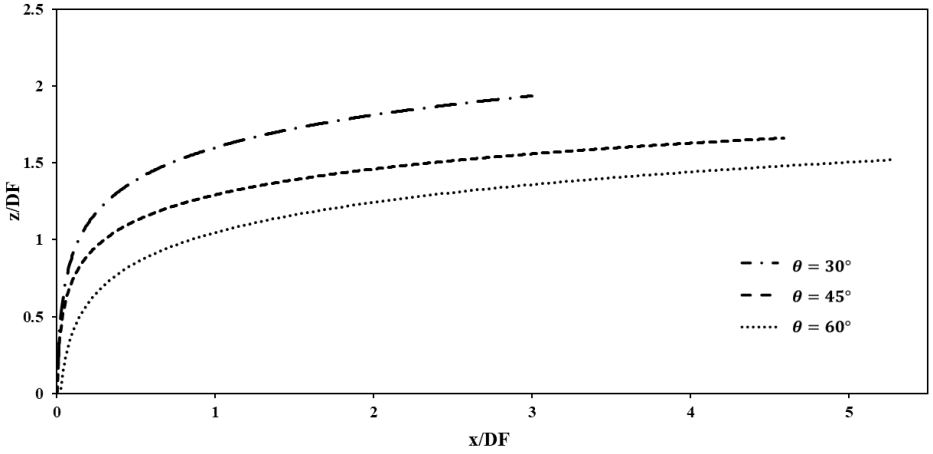

(b)

Figure 3-8 Jet centerline trajectories based on the **(a)** front view and **(b)** top view for the experimental cases of R7-9

3.3.3 Effects of $u_r F$ and Discharge Angle

3.3.3.1 Geometrical Characteristics

An important factor in the study of brine jet discharges is the jet terminal rise height. This is particularly important when dealing with discharges in shallow water. The jet terminal rise heights were obtained based on 10% of the transverse maximum concentration at the location of the maximum jet height [17]. In Figure 3-9, $\frac{y_t}{DF}$ as a function of $u_r F$ for the three tested inclined angles is presented. The mean absolute deviation (MAD) of the data for the discharge angles of 30°, 45°, and 60° are 0.08, 0.10, and 0.12, respectively, which shows an acceptable degree of variability in the data. Data from a few available studies for the jet of 60° with a 3D

trajectory in the range of u_rF covered herein is also shown in Figure 3-9 for comparison [31,32,36]. Accordingly, measurements for the terminal rise height of 60° jets are consistent with the previous studies.

In the region of u_rF studied in our experimental tests, which is out of the jet-dominated zone, the terminal rise height tends to decrease with increasing u_rF for all the inclined angles. Higher values of cross-flow Froude numbers deflect the jet toward the direction of ambient current at closer distances to the nozzles. This result is in accordance with the one obtained in the related studies [31,32,36] and the one for vertical dense jets in a cross-flow [14,35]. However, the notable decrease in the terminal rise points with the increase of u_rF has not been extensively reported in the studies conducted in the range of $u_rF < \sim 1.0$, i.e., jet-dominated zone [31,32,36]. This discrepancy suggests differing jet discharge behaviors between regimes dominated by jets and those dominated by currents. Therefore, relying on data from the literature within the range of $u_rF < \sim 1.0$ for predicting the mixing behavior of jets discharging into current-dominated flows may not be applicable. A comparison of different discharge angles impact on the terminal rise height reveals that this parameter is about, on average, 10% and 36% higher than for the jet of 60° compared to the 45° and 30°, respectively. The semi-empirical power-law dependencies of jet terminal rise height to cross-flow Froude numbers for the tested discharge angles are also proposed in Table 3-2 with their R^2 goodness-of-fit values.

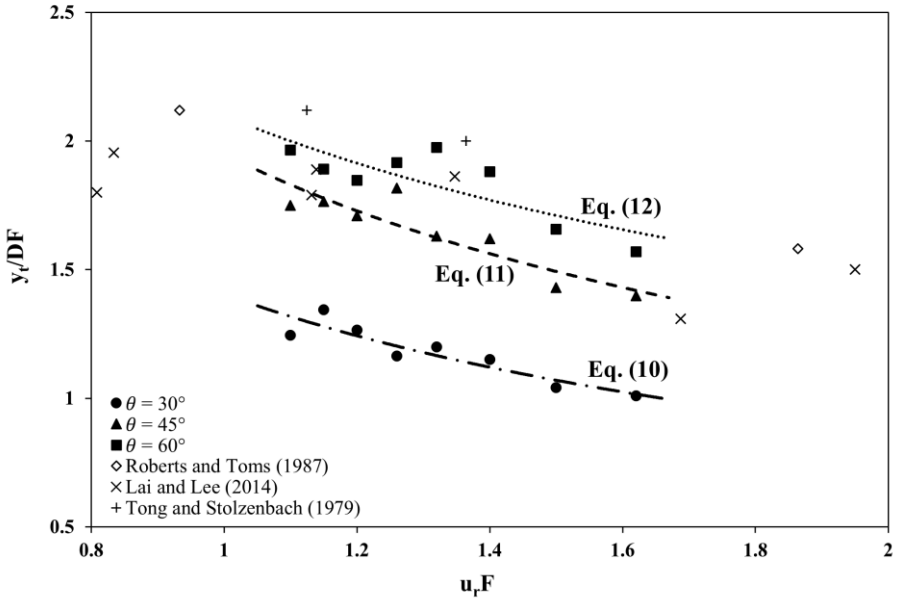

Figure 3-9 Terminal rise height for the discharge angle of 30°, 45°, and 60°

Table 3-2 Semi-empirical equations corresponding to the jet terminal rise height

θ (°)	$y_t/DF = a\,(u_rF)^b$		R^2	Eq.
	a	**b**		
30	1.4	- 0.67	0.87	(3-10)
45	1.95	- 0.65	0.84	(3-11)
60	2.1	- 0.5	0.73	(3-12)

Another important geometrical characteristic is the horizontal location of the jet impact point or return point. Attention should be given to the small difference between these two definitions, although both want to determine the length of the trajectory of the flow path and show how the near-field region is influenced by the initial mixing. The jet return point distance (x_r) indicates the horizontal distance from the discharge point to the location where the jet returns to the level of the nozzle tip and addresses the point where the jet impacts benthic organisms which may be environmentally important [38].

The $\frac{x_r}{DF}$ changes based on the u_rF are shown in Figure 3-10. The MAD of the data for the 30°, 45°, and 60° jets are 0.12, 0.15, and 0.09, respectively, which shows an acceptable variability in the dataset. There is a lack of available horizontal location data for $u_rF > 1.0$ in the literature. Thus, the results of this work can elucidate how this parameter changes within the critical range of u_rF between 1 and 2, i.e., out of the jet-dominated zone. With the increase of u_rF, there is a small alteration in the $\frac{x_r}{DF}$ parameter for our cases studied. However, with the rise of u_rF up to 1, the $\frac{x_r}{DF}$ parameter increased for the vertical dense jets according to the literature [14]. This result reveals that the difference in the jet-dominated and ambient cross-flow dominated zones should not be ignored regarding their effects on the jet return point. Additionally, the jet return points resulting from the discharge angle of 60° are higher than the two other angles. So that its corresponding results are about, on average, 16% and 41% higher than that of 45° and 30°, respectively. Table 3-3 presents the semi-empirical power-law dependencies of the jet return point to cross-flow Froude numbers for the 30°, 45°, and 60° discharge angles with their R^2 goodness-of-fit values.

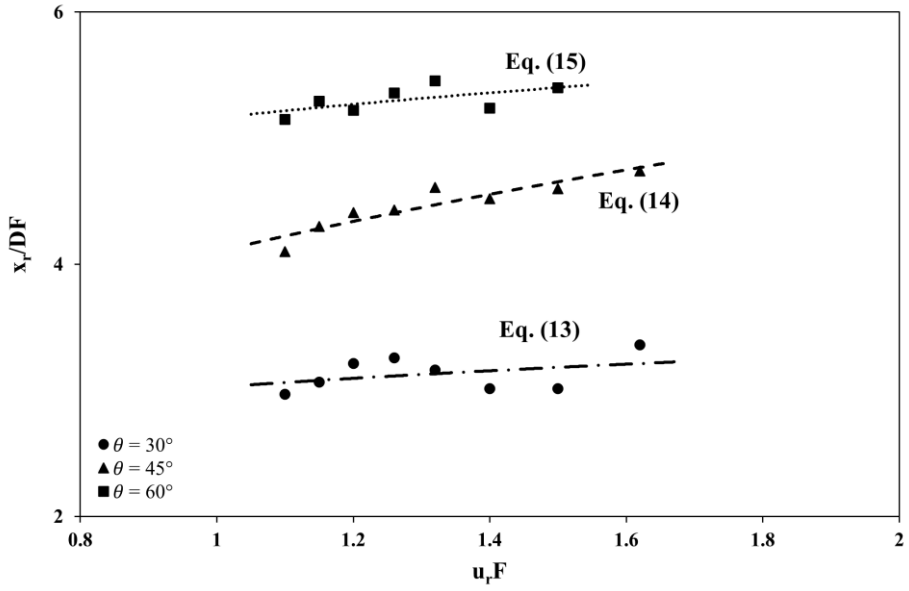

Figure 3-10 Horizontal return point location for the discharge angle of 30°, 45°, and 60° (data for the $u_rF = 1.62$ is not identified)

Table 3-3 Semi-empirical equations corresponding to the horizontal jet return point distance

θ (°)	$x_r/DF = c\,(u_rF)^d$		R^2	Eq.
	c	d		
30	3.03	0.12	0.66	(3-13)
45	4.1	0.31	0.85	(3-14)
60	5.16	0.11	0.78	(3-15)

3.3.3.2 Dilution Characteristics

For environmental impact assessment, dilution at specific points along the jet trajectory, such as the centerline peak point, is of utmost importance. In Figure 3-11, the variation of $\frac{S_t}{F}$ parameter with u_rF for the different discharge angles of 30°, 45°, and 60° are shown, and their corresponding semi-empirical equations are determined accordingly (see Table 3-4). The MAD of the data for the 30°, 45°, and 60° jets are 0.04, 0.06, and 0.16, respectively, which shows an appropriate variability in the dataset. Data from previous studies for the jet of 60° with a 3D trajectory in the range of u_rF covered herein are also presented for comparison. The obtained results are in close agreement with the previous measurements [31,32,36].

Accordingly, the dilution at the jet terminal rise height increases with the increase of u_rF in the tested range, showing a direct relationship between the cross-flow Froude number and the

mixing level. The jet with an angle of 60° leads to higher dilutions. This increase in dilution at the terminal point is about, on average, 39% and 55% compared to the 45° and 30° angles, respectively. In addition, the semi-empirical equations indicate more sensitivity of $\frac{S_t}{F}$ to $u_r F$ for a discharge angle of 60°. Hence, these results confirm the better mixing of dense jets at 60° compared to the two other angles.

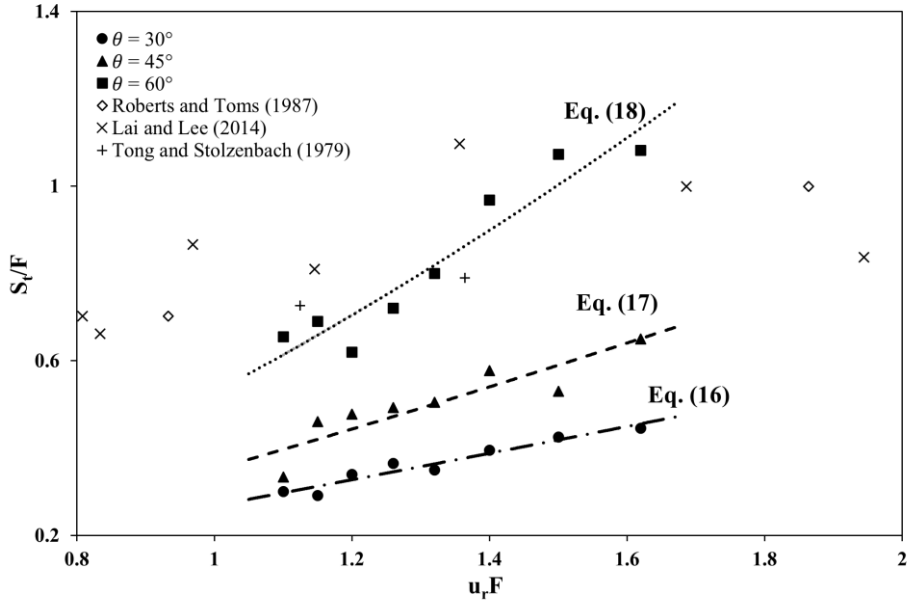

Figure 3-11 Dilution at the terminal rise height for the discharge angles of 30°, 45°, and 60°

Table 3-4 Semi-empirical equations corresponding to the dilution at the terminal rise height

θ (°)	$S_t/F = a\,(u_r F)^b$		R^2	Eq.
	a	**b**		
30	0.26	1.1	0.95	(3-16)
45	0.35	1.28	0.85	(3-17)
60	0.54	1.58	0.91	(3-18)

Return point dilution is defined as the minimum dilution at the return of the jet trajectory to the source discharge location. From the perspective of optimal outfall design, the maximum amount of jet desalination should be achieved in the near-field region. This parameter is key for benthic impact management as it represents the maximum substrate concentration [30]. Consequently, the study of the dilution amount at the jet return point is of particular interest for the design, operation, and regulation of desalination outfall applications. In Figure 3-12,

the changes in $\frac{S_r}{F}$ according to $u_r F$ for our test cases are compared. The MAD of the data for the discharge angles of 30°, 45°, and 60° are 0.09, 0.15, and 0.19, respectively, which shows an acceptable degree of variability in the data. The semi-empirical power-law dependencies of the minimum dilution at the jet return point to the cross-flow Froude numbers are also proposed in Table 3-5 with their R^2 goodness-of-fit values.

The dilution at the jet return point increases with the cross-flow magnitude. $\frac{S_r}{F}$ results are almost, on average, 20% higher for the inclined angle of 60° in comparison with the ones for the case of 45°, and the return point dilution for the 60° jet is more than twice that for the 30° jet. The obtained dilution results can be ascribed to the longer flow path trajectory for the 60° jet. This provides a higher surface available for entrainment of the external fluids into the jet and therefore more dilutions. These outputs highlight the importance of leveraging changes in the source discharge inclination and the cross-flow Froude number to enhance dilution.

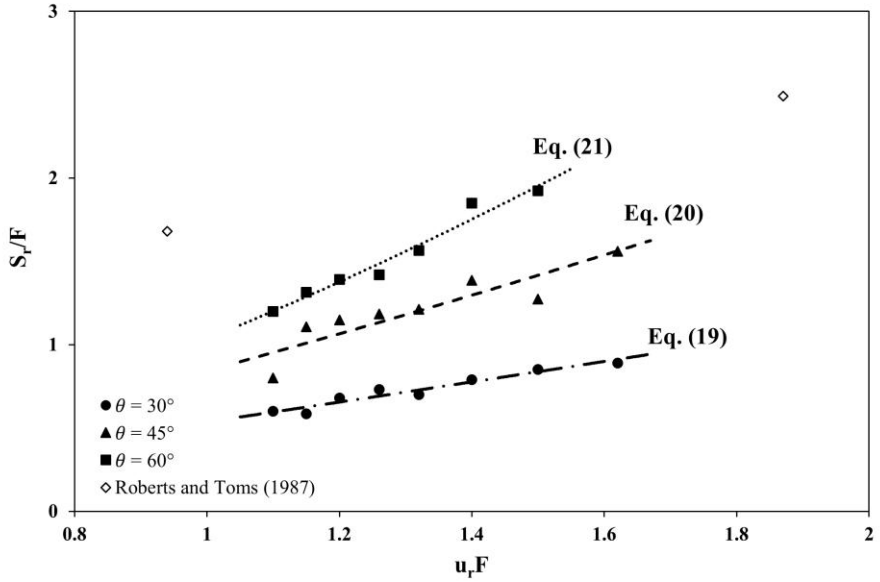

Figure 3-12 Dilution at the jet return point for the discharge angle of 30°, 45°, and 60°

Table 3-5 Semi-empirical equations corresponding to the dilution at the jet return point

θ (°)	$S_r/F = c\,(u_r F)^d$		R^2	Eq.
	c	**d**		
30	0.53	1.1	0.94	(3-19)
45	0.84	1.27	0.86	(3-20)
60	1.03	1.56	0.97	(3-21)

According to Tables 3-2 to 3-5, significant R^2 values for equations delineating the correlation between $u_r F$ and dilution properties are obtained, underscoring their power-law relationship nature. Conversely, for some equations linked to geometrical properties, R^2 values are comparatively lower. Additionally, the obtained empirical equations show that the sensitivity of both the jet terminal rise height and return dilutions to $u_r F$ increases with the discharge angle. However, this trend is not observed for geometrical properties. The return point distance for the 45° jet is more sensitive to $u_r F$ than that for two other angles. The terminal rise height shows the same sensitivity to $u_r F$ for the 30° and 45° jets and higher sensitivity to that for the 60° jet.

Moreover, following the statement of *F*-independency in the case of $F \gg 1$ as outlined in Section 3.2.1, we investigated the variation of geometrical and dilution properties as a function of *F* for the 30°, 45°, and 60° jets. However, the plots are not presented here for the sake of brevity. Analysis of the findings revealed that the geometrical properties for the three tested inclined angles approached an almost constant within the range of *F* tested in our study. However, the behavior of dilution properties as a function of *F* differed somewhat for the three discharge angles. Notably, S_t/F for the 60° jet showed significant sensitivity to the changes of *F* than other shallower angles and approached a constant for about $F > 29$. Similarly, S_t/F for the 45° approached a constant for about $F > 25$. The same behavior was also observed for S_r/F parameter.

3.3.4 Jet Widening

Studying the growth of the jet along its trajectory can highlight the jet development and the role of the discharge angle on the mixing and dilution performance. The normalized concentration profiles at different downstream cross-sections orthogonal to the central trajectory of the jet for the three discharge angles are presented in Figure 3-13. b_c represents the distance between the jet centerline and the location where the concentration is $e^{-1}C_{max}$, where C_{max} is the local centerline tracer concentration. Comparing the widening of the jets with different inclinations at a constant cross-section, Figure 3-13 (a), shows that the concentration profile is a little wider for the 30° than the other discharge angles near the jet release point. This can be attributed to the higher initial momentum component of the jet with a shallower angle in the z-direction (across the flume width). However, this component vanishes for all cases farther from the nozzle. The 60° jet has taken a longer path up to a section far from the nozzle compared to the other jets. It provides a longer time for interacting with the

external fluid and entraining ambient flow. Accordingly, the corresponding widening would be higher for the jet of 60° at farther cross-sections.

As shown in Figure 3-13 (b) (which demonstrates how the inner and outer edges of the jets behave along the trajectory), the inner half for the discharge angle of 60° spreads wider than the outer half. For the angles of 30° and 45°, the outer half is wider than the inner half. It has roots in the higher momentum values in the z-direction for the two shallower inclinations. Moreover, the comparison of jet widening for the discharge angle of 60° with two different values of $u_r F$, Figure 3-13 (c), reveals that applying lower $u_r F$ values lead to a more confined jet, showing the limited available surface for interacting with ambient flows and a lower level of dilution accordingly [40]. Hence, the study of the jet widening results confirms the data from the analysis of discharge angle and $u_r F$ impacts on the dilution rate.

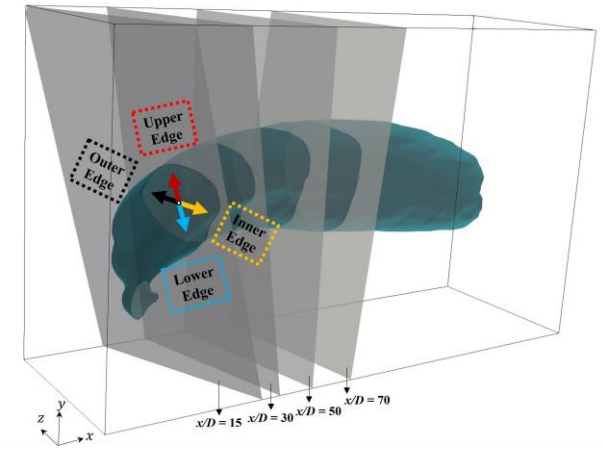

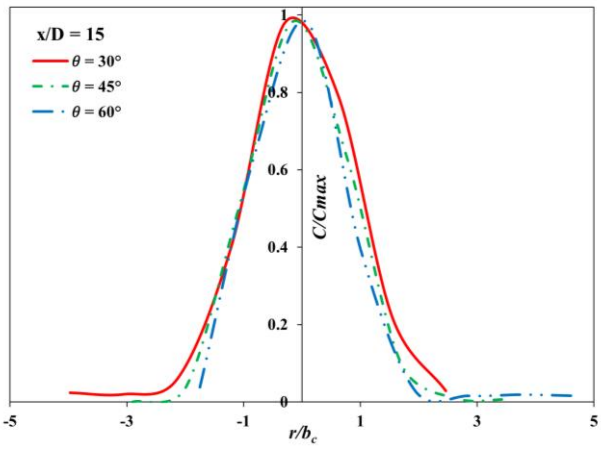

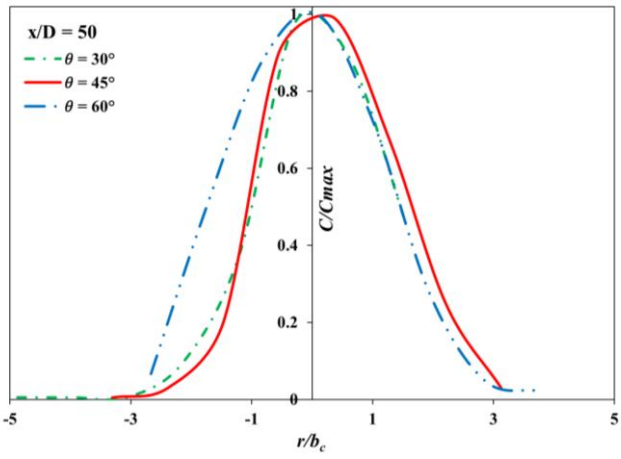

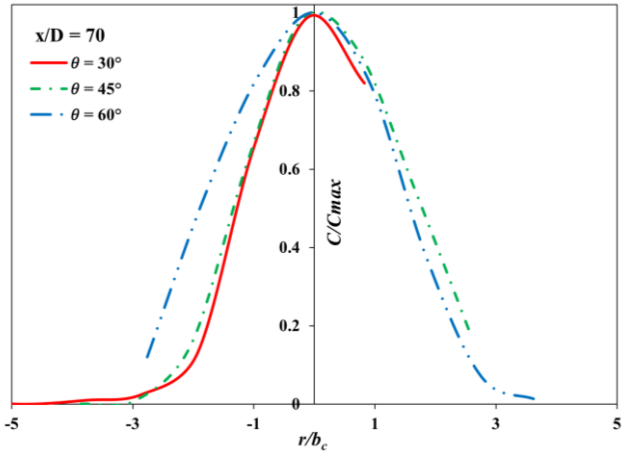
x/D = 70
θ = 30°
θ = 45°
θ = 60°
C/Cmax
r/b_c

(a)

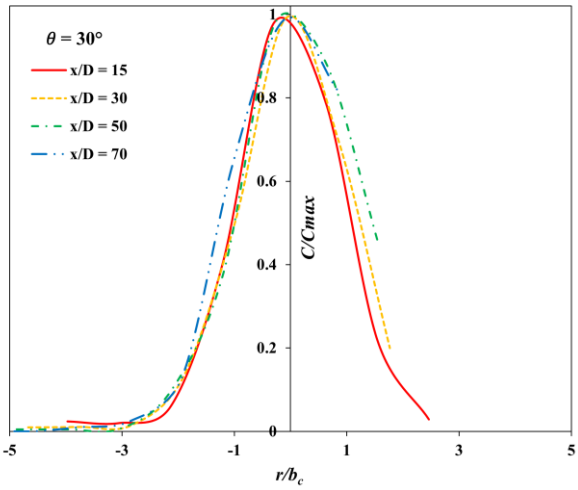
θ = 30°
x/D = 15
x/D = 30
x/D = 50
x/D = 70
C/Cmax
r/b_c

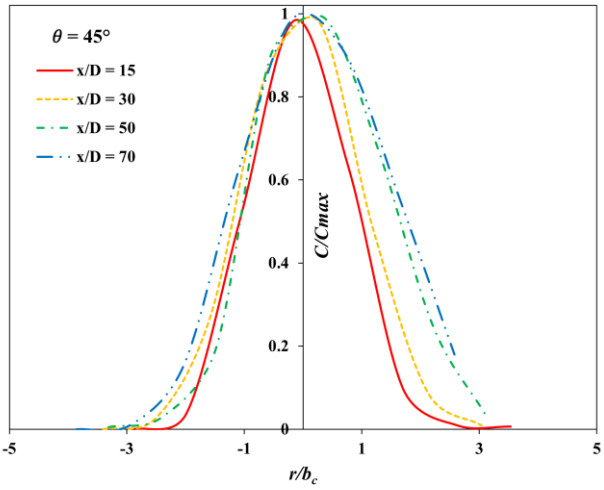
θ = 45°
x/D = 15
x/D = 30
x/D = 50
x/D = 70
C/Cmax
r/b_c

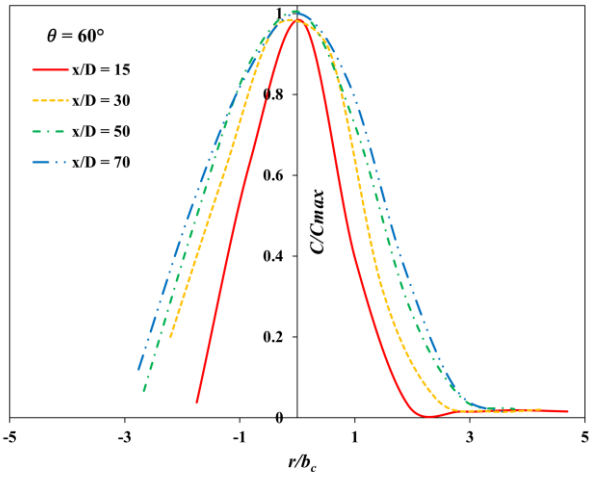
θ = 60°
x/D = 15
x/D = 30
x/D = 50
x/D = 70
C/Cmax
r/b_c

(b)

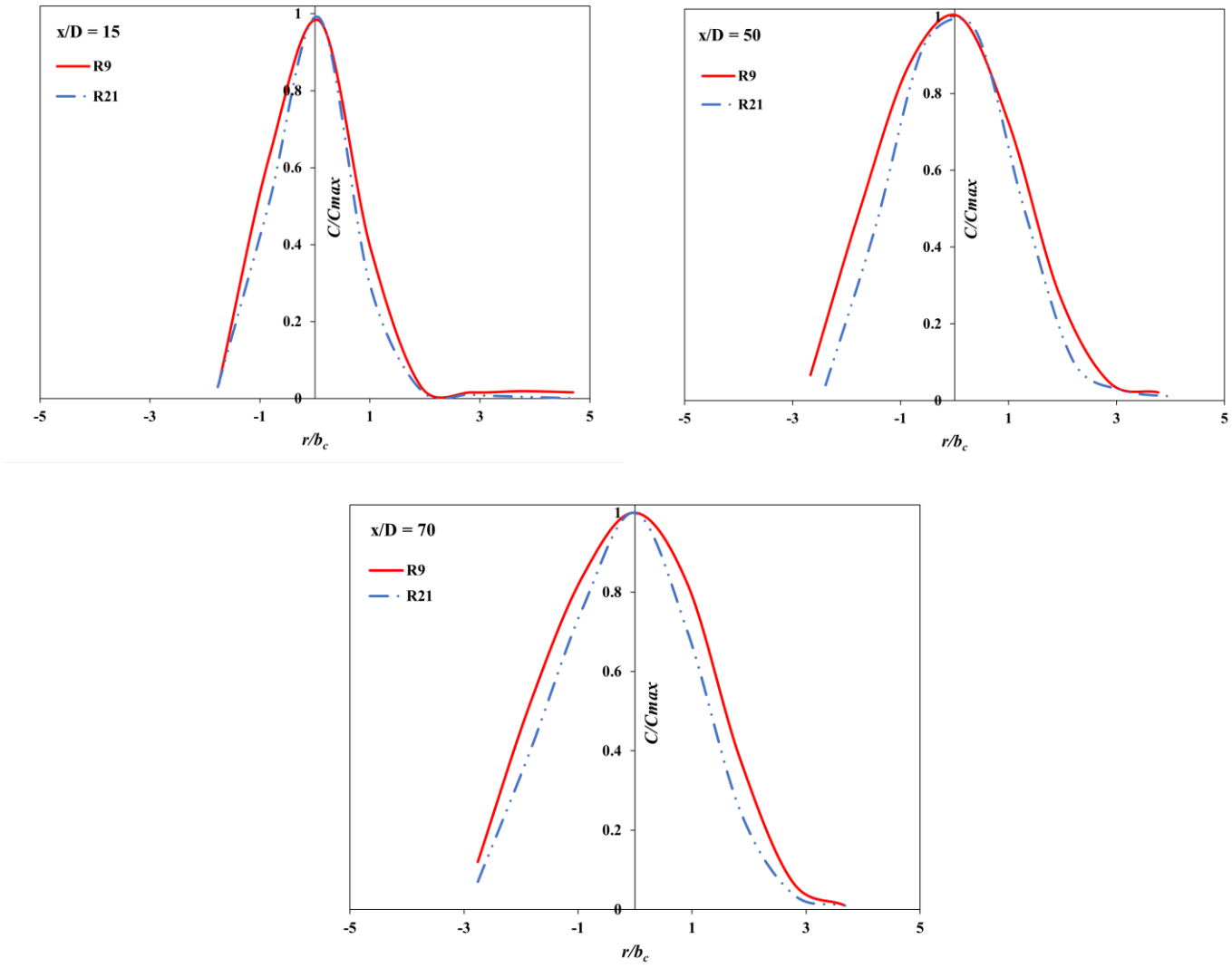

(c)

Figure 3-13 Jet widening profile over the line covering the jet flow width, inner and outer edges, for cases R7-9 **(a)** different angles and constant cross-section, **(b)** different cross-sections and constant angle, and comparison of R9 and R21 **(c)** at three different cross-sections

3.3.5 Variance of Concentration

Examining the concentration fluctuations can highlight the different natures of mixing in the interaction regions between the jet and ambient flows. The non-dimensional variance of concentrations (σ^2/C_{max}^2, where σ is the concentration standard deviation) at different downstream cross-sections orthogonal to the central jet trajectory are presented in Figure 3-14 for cases R7, R9, R19, and R21. According to the obtained results, a bimodal distribution can be observed in the variance profiles with a minimum on the jet centerline. The variance profiles show that the jet core is less involved in mixing. In comparison, two peaks in the variance profiles are observed: one in the upper and one in the lower edge. The upper edge peak is higher

than in all cases compared to the lower edge peak, resulting from the formation and break of Kelvin-Helmholtz (KH) instability structures [40,41]. At the upper edge, the downward buoyancy hinders the upward development of KH waves and rapidly breaks them, resulting in sudden changes in light intensity at a fixed point and therefore a high variance.

As moving along the trajectory, the bimodal distribution becomes smoother and finally collapses into one line. Close to the nozzle, e.g., *x/D* = 15, 30, and 50, two well-defined peaks are observed because of the intense interaction of jets with the ambient water, resulting from the perpendicular intrusion of high-velocity jets into the ambient water. However, at farther distances, e.g., *x/D* = 120, the profiles are smoother because the jet direction is already aligned with the ambient flow direction, and the jet initial momentum significantly decreases. Moreover, comparisons of Figures 3-14 (a) and (b) show that the variance level is higher when the jet is influenced by the ambient current with higher $u_r F$, revealing more variation of concentration and thus more signs of jet and ambient water interactions.

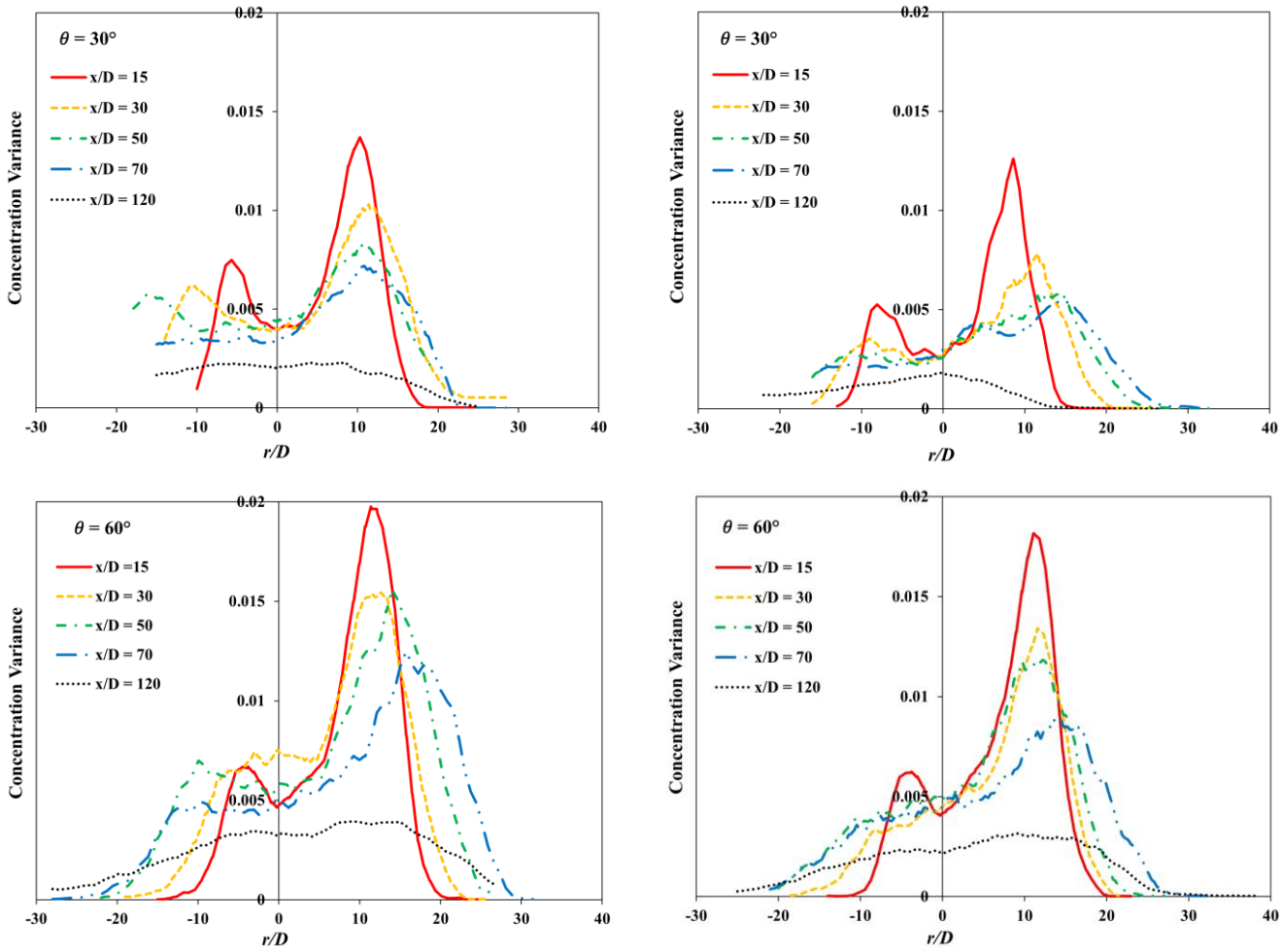

(a) **(b)**

Figure 3-14 Variance profiles over the line presented in Figure 3-13, upper and lower edges, at different downstream cross-sections orthogonal to the central jet trajectory for cases **(a)** R7 and R9 and **(b)** R19 and R21

3.3.6 Design Implications

One of the critical aspects of designing desalination outfalls involves deciding whether to orient the diffuser ports for co-, counter-, or cross-flows. This decision depends on various factors such as the local current patterns, the diffuser's specific objectives, and compliance with environmental regulations [32]. Figure 3-15 compares dilution at the terminal rise height (S_t/F), and at the jet return (S_r/F) /impact (S_i/F) point for the jet discharges at a 60° angle while interacting with different current directions. According to the literature [30], in the presence of a co-flowing current (ϕ = 180°), the jet deflects downstream, with both impact distance and dilution increasing as u_rF increases. This result is in accordance with the targeted case in the present study, where the 60° jet issuing into perpendicular cross-flow. Conversely, for a counter-flowing current (ϕ = 0°), impact distance and dilution decrease until u_rF reaches a specific value, where the jet falls back on itself. This value was determined around 0.2 and 0.67 based on the conditions tested in the studies on single 60° inclined jets [32] and multiport jets at 60° [30], respectively. The jet trajectory reverses with a further increase in u_rF, leading it to impact downstream of the diffuser.

The analysis of Figure 3-15 shows significant discrepancies in the performance comparison between co- and counter-flowing discharges as documented in the literature. Notably, Roberts and Toms [32] and Choi et al. [39] studies focusing on the single 60° dense jets showed outperformance of co-flowing over counter-flowing orientations. However, Baum and Gibbes [30] challenged this assumption and argued that for multiport jets at 60° and $u_rF > 1.2$, counter-flowing orientations may yield greater dilution compared to co-flowing ones. From a design-oriented perspective, both co- and counter-flow discharges may show fluctuations in expected dilution due to the presence of tidal currents, which change direction according to lunar cycles. This change can result in transitions between co-flow and counter-flow orientations, potentially diminishing the overall mixing performance of outfall discharge. However, a design featuring perpendicular cross-flow may remain unaffected by these shifts in the current direction. This underscores the importance of investigating the dilution of JICF and the mixing performance of outfalls under such conditions.

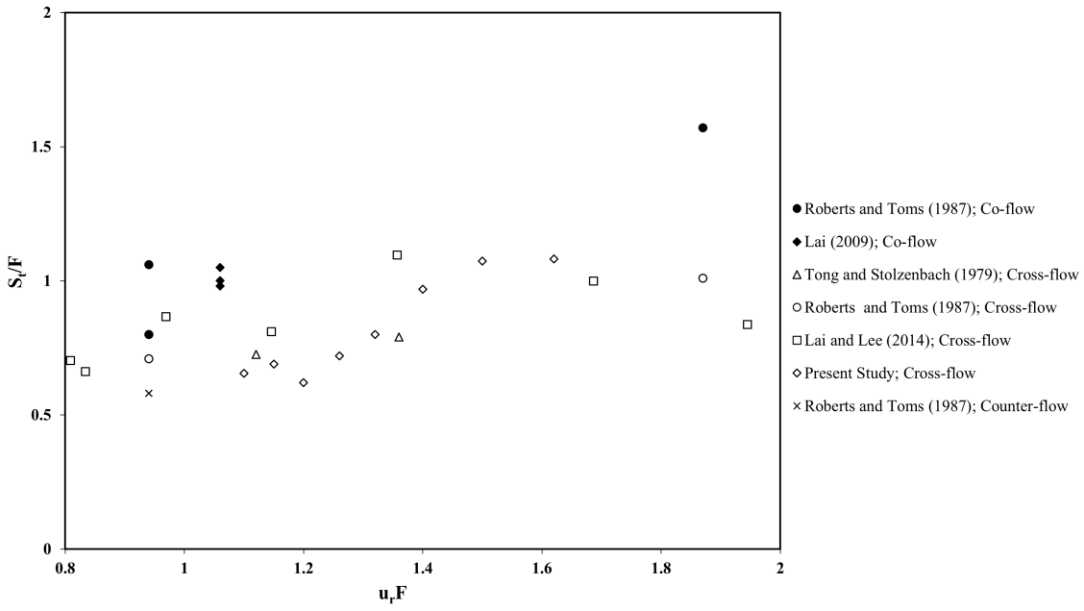

(a)

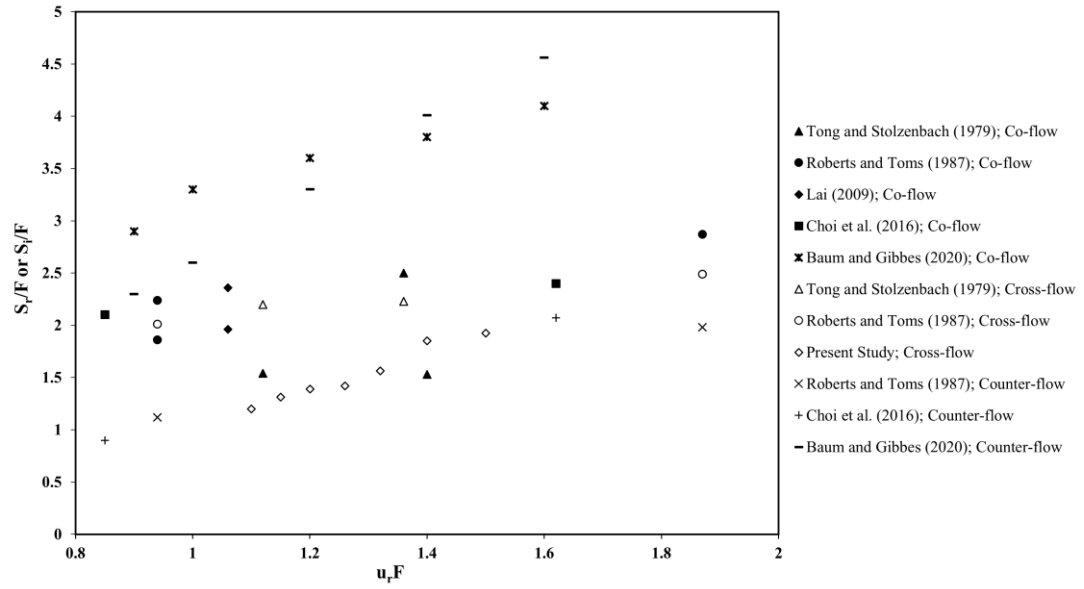

(b)

Figure 3-15 Dilution at **(a)** the terminal rise height and **(b)** the jet return/impact point for the 60° jet discharges into different current orientations (It should be mentioned that the data in our study were measured at the jet return point; The data were adapted from [30–32,36,39,42] for comparison)

3.4 Conclusions

For an efficient design of desalination diffusers, understanding the role of factors affecting the flow discharge and mixing behaviors is critical. This study addressed the combined impacts of

different flowing current strengths and discharge inclinations on outfall performance. For this purpose, the mixing processes and concentration distribution of inclined dense discharges (including 30°, 45°, and 60°) issuing into a perpendicular current with 3D trajectories were investigated using the LIF experimental technique. The $u_r F$ parameter was selected in a way to stand in a critical range between about 1 and 2 in which the jets are considerably bent over.

Instantaneous and time-averaged flow visualizations were obtained using LIF experimentation. The major flow parameters (such as the terminal rise height, downstream position of the jet return point, and dilution at the terminal and jet return points) were quantified. Their Empirical equations were derived, which can have further implications for the design of SWRO outfalls. The results revealed that almost all major flow parameters, except for terminal rise height, increased with increasing values of the cross-flow Froude number within the range tested. In addition, with an increase in the discharge angle from 30° to 45° and then to 60°, the geometrical parameters, including the downstream position of the return point and terminal rise height and the associated dilution levels, were increased.

While horizontal location data for the range of $u_r F > 1$ is notably scarce in the literature, this study aimed to fill this gap by obtaining the variations of this parameter within the range of $1 < u_r F < 2$. So that the parameter of $\frac{x_r}{DF}$ for the 60° jet was about, on average, 40% and 16% higher than that for the 30° and 45° jets, respectively. $\frac{y_t}{DF}$ also increased by an average of 36% and 10% when applying the 60° inclination in comparison with the 30° and 45°, respectively. More than two-fold improvement of dilution at the terminal and return points was achieved by the increase of inclination from 30° to 60°. This enhancement in the dilutions was on average 39% and 20% for the terminal and return points, respectively, with the changes of discharge angle from 45° to 60°.

Studying the jet growth results showed that the larger $u_r F$ values and steeper inclinations resulted in more dispersed jets. It led to the higher available surface for interacting with ambient flows and thus higher dilution rates. The variance of concentration also demonstrated a higher variance level when dealing with the jet discharge in the ambient current with a larger $u_r F$ magnitudes. This revealed more signs of jet and ambient water interactions and more entrainment of ambient water into the jet.

Hence, it is recommended to discharge dense effluents by applying a high cross-flow Froude number for efficient release if the regular current regime is dictated. This can be achieved with the increase of the jet-densimetric Froude number (F) and/or ambient cross-flow to jet velocity

ratio (u_r). Deploying the jet of 60° compared to the 45° and 30° is also preferable in terms of better mixing in the dynamic waters. The findings of this investigation can be useful for the application of outfalls in shoreline regions where lower discharge inclinations are required. Finally, by applying the detailed laboratory experiments, this study attempted to provide valuable insights into the efficient design of buoyant discharges of brine effluents into dynamic ambient environments for increasing dilution. The results will also be of importance to the development of mathematical models of dense jet dynamics.

Author Contributions: Mostafa Taherian: Conceptualization, Methodology, Software, Validation, Formal analysis, Investigation, Resources, Data curation, Writing – original draft, Visualization. **Seyed Ahmad Reza Saeidi Hosseini:** Methodology, Software, Validation, Investigation, Resources, Data curation, Writing – review & editing, Visualization. **Abdolmajid Mohammadian:** Conceptualization, Methodology, Software, Data curation, Writing – review & editing, Supervision, Project administration, Funding acquisition. **Simone Ferrari:** Methodology, Software, Investigation, Resources, Data curation, Writing – review & editing, Supervision. **Philip J.W. Roberts:** Data curation, Writing – review & editing.

Funding: This research received no external funding.

Acknowledgments: This research was funded by the Natural Sciences and Engineering Research Council of Canada (NSERC).

Conflicts of Interest: The authors declare no conflict of interest.

3.5 References

[1] J. Kucera, Desalination: water from water, 2nd Edition, John Wiley and Sons Inc., 2019. https://doi.org/10.1002/9781119407874.

[2] T.M. Missimer, B. Jones, R.G. Maliva, Intakes and Outfalls for Seawater Reverse-Osmosis Desalination Facilities: Innovations and Environmental Impacts, Springer, New York, 2015. https://doi.org/10.1007/978-3-319-13203-7.

[3] U. Caldera, C. Breyer, Learning curve for seawater reverse osmosis desalination plants: capital cost trend of the past, present, and future, Water Resources Research. 53 (2017) 10523–10538. https://doi.org/10.1002/2017WR021402.

[4] S. Lattemann, M.D. Kennedy, J.C. Schippers, G. Amy, Chapter 2 Global Desalination Situation, Sustainability Science and Engineering. 2 (2010) 7–39. https://doi.org/10.1016/S1871-2711(09)00202-5.

[5] M.J. Baum, B. Gibbes, A. Grinham, S. Albert, P. Fisher, D. Gale, Near-Field Observations of an Offshore Multiport Brine Diffuser under Various Operating

Conditions, Journal of Hydraulic Engineering. 144 (2018) 05018007. https://doi.org/10.1061/(ASCE)HY.1943-7900.0001524.

[6] M.T. Flavin, J. Fernandes, R. AlQabandi, E. Adams, J. Han, B. Al-Anzi, Numerical modeling of plunging jets of brine: Mass transport and implications for desalination plant outfalls, Desalination. 568 (2023) 116996. https://doi.org/10.1016/j.desal.2023.116996.

[7] P. Palomar, I.J. Losada, Desalination in Spain: Recent developments and recommendations, Desalination. 255 (2010) 97–106. https://doi.org/10.1016/J.DESAL.2010.01.008.

[8] R. Einav, F. Lokiec, Environmental aspects of a desalination plant in Ashkelon, Desalination. 156 (2003) 79–85. https://doi.org/10.1016/S0011-9164(03)00328-X.

[9] M. Taherian, S.A.R. Saeidi Hosseini, A. Mohammadian, Overview of Outfall Discharge Modeling with a Focus on Turbulence Modeling Approaches, in: Advances in Fluid Mechanics: Modeling and Simulation, Springer Nature, Singapore, 2022, pp. 139–177. https://doi.org/10.1007/978-981-19-1438-6_4.

[10] P. Palomar, J.L. Lara, I.J. Losada, Near field brine discharge modeling part 2: Validation of commercial tools, Desalination. 290 (2012) 28–42. https://doi.org/10.1016/j.desal.2011.10.021.

[11] S.A.R. Saeidi Hossieni, A. Mohammadian, P.J.W. Roberts, O. Abessi, Numerical Study on the Effect of Port Orientation on Multiple Inclined Dense Jets, Journal of Marine Science and Engineering. 10 (2022) 590. https://doi.org/10.3390/jmse10050590.

[12] S. Jenkins, J. Paduan, P.J.W. Roberts, D. Schlenk, J. Weis, Management of brine discharges to coastal waters recommendations of a science advisory panel (Tech. Report No. 694), Southern California Coastal Water Research Project, Costa Mesa, CA, USA, 2012.

[13] P.J.W. Roberts, A. Ferrier, G. Daviero, Mixing in Inclined Dense Jets, Journal of Hydraulic Engineering. 123 (1997) 693–699. https://doi.org/10.1061/(asce)0733-9429(1997)123:8(693).

[14] E. Gungor, P.J.W. Roberts, Experimental studies on vertical dense jets in a flowing current, Journal of Hydraulic Engineering. 135 (2009) 935–948. https://doi.org/10.1061/(ASCE)HY.1943-7900.0000106.

[15] A. Ramakanth, M.J. Davidson, R.I. Nokes, Laboratory study to quantify lower boundary influences on desalination discharges, Desalination. 529 (2022) 115641. https://doi.org/10.1016/j.desal.2022.115641.

[16] S.A.R. Saeidi Hosseini, M. Taherian, A. Mohammadian, S. Ferrari, P.J.W. Roberts, Mixing behavior of multiport diffusers with non-uniform port orientation, Desalination. 567 (2023) 116962. https://doi.org/10.1016/j.desal.2023.116962.

[17] O. Abessi, P.J.W. Roberts, Effect of Nozzle Orientation on Dense Jets in Stagnant Environments, Journal of Hydraulic Engineering. 141 (2015) 06015009. https://doi.org/10.1061/(asce)hy.1943-7900.0001032.

[18] I.G. Papakonstantis, E.I. Tsatsara, Mixing Characteristics of Inclined Turbulent Dense Jets, Environmental Processes. 6 (2019) 525–541. https://doi.org/10.1007/s40710-019-00359-w.

[19] H. Kheirkhah Gildeh, A. Mohammadian, I. Nistor, Inclined dense effluent discharge modelling in shallow waters, Environmental Fluid Mechanics. 21 (2021) 955–987. https://doi.org/10.1007/s10652-021-09805-6.

[20] M. Taherian, A. Mohammadian, Buoyant jets in cross-flows: Review, developments, and applications, J Mar Sci Eng. 9 (2021) 61. https://doi.org/10.3390/jmse9010061.

[21] M.A. Zeitoun, W.F. McIlhenny, R.O. Reid, C.-M. Wong, W.F. Savage, W.W. Rinne, C.L. Gransee, Conceptual designs of outfall systems for desalting plants, Research and Development Progress Rep. 550, Office of Saline Water, Washington DC, USA, 1970.

[22] G.A. Kikkert, M.J. Davidson, R.I. Nokes, Inclined Negatively Buoyant Discharges, Journal of Hydraulic Engineering. 133 (2007) 545–554. https://doi.org/10.1061/(asce)0733-9429(2007)133:5(545).

[23] G.H. Jirka, Improved discharge configurations for brine effluents from desalination plants, Journal of Hydraulic Engineering. 134 (2008) 116–120. https://doi.org/10.1061/(ASCE)0733-9429(2008)134:1(116).

[24] I.G. Papakonstantis, G.C. Christodoulou, P.N. Papanicolaou, Inclined negatively buoyant jets 1: Geometrical characteristics, Journal of Hydraulic Research. 49 (2011) 3–12. https://doi.org/10.1080/00221686.2010.537153.

[25] I.G. Papakonstantis, G.C. Christodoulou, P.N. Papanicolaou, Inclined negatively buoyant jets 2: Concentration measurements, Journal of Hydraulic Research. 49 (2011) 13–22. https://doi.org/10.1080/00221686.2010.542617.

[26] C.C.K. Lai, J.H.W. Lee, Mixing of inclined dense jets in stationary ambient, Journal of Hydro-Environment Research. 6 (2012) 9–28. https://doi.org/10.1016/j.jher.2011.08.003.

[27] C.J. Oliver, M.J. Davidson, R.I. Nokes, Predicting the near-field mixing of desalination discharges in a stationary environment, Desalination. 309 (2013) 148–155. https://doi.org/10.1016/j.desal.2012.09.031.

[28] S. Ferrari, M.G. Badas, G. Querzoli, On the effect of regular waves on inclined negatively buoyant jets, Water (Switzerland). 10 (2018) 726. https://doi.org/10.3390/w10060726.

[29] J. Chang, Y. Du, X. Shao, Y. Zhao, S. Zheng, Investigation and analysis of vortex and application of jet in crossflow, Case Studies in Thermal Engineering. 14 (2019) 0–6. https://doi.org/10.1016/j.csite.2019.100459.

[30] M.J. Baum, B. Gibbes, Field-Scale Numerical Modeling of a Dense Multiport Diffuser Outfall in Crossflow, Journal of Hydraulic Engineering. 146 (2020) 1–16. https://doi.org/10.1061/(ASCE)HY.1943-7900.0001635.

[31] S.S. Tong, K.D. Stolzenbaeh, Submerged Discharges of Dense Effluent: Report No. 243, Massachusetts Institute of Technology, Cambridge, Massachussetts, USA, 1979.

[32] P.J.W. Roberts, G. Toms, Inclined Dense Jets in Flowing Current, Journal of Hydraulic Engineering. 113 (1987) 323–340. https://doi.org/10.1061/(asce)0733-9429(1987)113:3(323).

[33] W.R. Lindberg, Experiments on Negatively Buoyant Jets, with and without Cross-Flow, in: Recent Research Advances in the Fluid Mechanics of Turbulent Jets and Plumes. Kluwer, Dordrecht, The Netherland, 255 (1994) pp. 131–145. https://doi.org/10.1007/978-94-011-0918-5_8.

[34] M. Ben Meftah, M. Mossa, Turbulence measurement of vertical dense jets in crossflow, Water (Switzerland). 10 (2018) 286. https://doi.org/10.3390/w10030286.

[35] M. Ben Meftah, D. Malcangio, F. De Serio, M. Mossa, Vertical dense jet in flowing current, Environmental Fluid Mechanics. 18 (2018) 75–96. https://doi.org/10.1007/s10652-017-9515-2.

[36] C.C.K. Lai, J.H.W. Lee, Initial mixing of inclined dense jet in perpendicular crossflow, Environmental Fluid Mechanics. 14 (2014) 25–49. https://doi.org/10.1007/s10652-013-9290-7.

[37] M. Jiang, A.W.K. Law, S. Zhang, Mixing behavior of 45° inclined dense jets in currents, Journal of Hydro-Environment Research. 18 (2018) 37–48. https://doi.org/10.1016/j.jher.2017.10.008.

[38] M.J. Baum, Dense jet behaviour in dynamic receiving environments, The University of Queensland, 2019. https://doi.org/10.14264/UQL.2019.247.

[39] K.W. Choi, C.C.K. Lai, J.H.W. Lee, Mixing in the Intermediate Field of Dense Jets in Cross Currents, Journal of Hydraulic Engineering. 142 (2016) 04015041. https://doi.org/10.1061/(asce)hy.1943-7900.0001060.

[40] L.A. Besalduch, M.G. Badas, S. Ferrari, G. Querzoli, On the near field behavior of inclined negatively buoyant jets, EPJ Web Conf. 67 (2014) 02007. https://doi.org/10.1051/EPJCONF/20146702007.

[41] S. Ferrari, G. Querzoli, Mixing and re-entrainment in a negatively buoyant jet, Journal of Hydraulic Research. 48 (2010) 632–640. https://doi.org/10.1080/00221686.2010.512778.

[42] C.C.K. Lai, Mixing of inclined dense jets, Master's Thesis, The University of Hong Kong, Hong Kong, China, 2009.

4 CFD Numerical Simulation of Submerged Dense Jets in Cross-flows[3]

Abstract

The positive environmental impacts obtained through the use of submerged outfall discharges of dense effluents have recently gained considerable attention from both regulatory agencies and research groups. Since the ambient water bodies are rarely stationary, investigating the buoyant outfall discharge performance while issuing into cross-flow, which has been known as the buoyant jet in cross-flow (JICF), is of significant importance. Therefore, a deeper understanding and more accurate design guidelines for this type of outfall are required. A numerical study was presented herein by using the computational codes developed with OpenFOAM which is based on the finite volume technique. The accuracy of the model was verified by the comparison of the simulation results and experimental data obtained from the literature. Moreover, the jet trajectory and dilution behavior of dense jets were numerically investigated by employing four different Reynolds-averaged Navier-Stokes (RANS) modeling approaches, namely standard $k-\varepsilon$, realizable $k-\varepsilon$, $k-\omega$ shear stress transport (SST), and Launder-Reece-Rodi (LRR). Based on the findings of this study, the presented realizable $k-\varepsilon$ and LRR schemes compared to the other approaches showed quite well potential to simulate the flow behavior and dilution performance of densely buoyant JICFs. In addition, the evolution of time-averaged counter-rotating vortex pair (CRVP) was successfully visualized along the jet trajectory based on the applied modeling approach.

Keywords: Outfall discharge; Densely buoyant jets in cross-flows; OpenFOAM simulation; Reynolds-averaged Navier-Stokes approaches

[3] This chapter has been published as: Taherian, M., Saeidi Hosseini, S. A. R., Mohammadian, A. (2022). CFD Numerical Simulation of Submerged Dense Jets in Cross-flows. In Proceedings of the 39th IAHR World Congress, Granada, Spain.

4.1 Introduction

Direct discharges of dense effluents, which can be a by-product of desalination plants, into the receiving water bodies can cause severe environmental issues such as water quality damage and marine life disruption [1]. Thus, they need to be discharged in the form of turbulent buoyant jets (involving both momentum and buoyancy fluxes) to make progress in dispersion and mixing of them into ambient waters, thereby minimizing their adverse environmental effects [2].

The ambient receiving environment that typifies the realistic oceanic conditions is often characterized by the flowing currents and turbulence. An ambient environment with flowing currents, compared to a stationary environment, can provide a higher dilution for brine effluent discharges [3-5]. It is mainly due to the vortical structures, such as significant time-averaged counter-rotating vortex pairs (CRVPs), established as the jet extends downstream in this scenario [6]. Therefore, when dealing with the discharges of brine outfalls into ambient water, the impacts of flowing currents on their flow behavior should not be underestimated. These types of brine outfall discharge are known as buoyant jet in cross-flows (JICFs).

In addition, discharges of buoyant JICFs can generally happen either as a surface or submerged jet. Among them, submerged discharges are more favorable due to the higher level of mixing and dilution compared to the surface ones as a consequence of the entrainment of surrounding fluid into the jet in all directions [7].

Considering the mentioned benefits for the submerged discharges of dense jets issuing into cross-flows, a number of experimental studies have been conducted on mixing applications involving dilution of this type of outfalls [3, 8-12]. For example, the jet trajectory and dilution behavior of vertical dense jets under the influence of ambient flowing currents were investigated using the laser-induced fluorescence (LIF) method in a study by Gungor and Roberts [12]. The results of their work demonstrated the importance of cross-flow based Froude number ($u_r F$, in which u_r is the ratio of ambient to jet velocity and F is the jet-densimetric Froude number) on the terminal rise height and the jet impact distance and dilution. A kidney-shaped concentration distribution was also observed in their study because of the formation of two counter-rotating vortices, thereby entraining more ambient flow into the jet flow and enhancing the dilution amount. Moreover, the salinity concentration and velocity flow fields resulting from the interactions of a vertical dense jet and ambient cross-flow ($u_r F \sim 1.0$) were experimentally examined in studies by Ben Meftah et al. [10,11]. The velocity fields

showed that dense buoyant JICFs can be characterized by two different phases, including jet- and plume-like mixing. The formation of CRVP within the cross-section of jet trajectory was confirmed and a strong amount of dilution within the initial rise phase was also reported.

Compared to the experimental works, less attention has been devoted to the application of computational fluid dynamics (CFD) on submerged dense jets in cross-flows. And most of the previous CFD studies have been focused on the discharges into stationary receiving environments. Although interactions between the cross-flows and the buoyant jets make the prediction of flow behaviors and trajectories highly complex, improvements in computational resources and techniques over the last decades have allowed CFD numerical modeling to be introduced as an efficient approach for the outfall discharge modeling. In critical reviews by Taherian et al. [2,13], Reynolds-averaged Navier Stokes (RANS) modeling approaches were shown as practical and easy-to-implement methods which can reasonably reproduce the flow field and dilution performance of outfall discharges. Most recently, Baum and Gibbes [14] successfully demonstrated the applicability of RANS equations with a $k-\omega$ turbulence closure scheme for the modeling of ambient cross-flow impacts on the jet dilution and the plume trajectory within the range of $0.2 < u_r F < 1.6$. It was one of the limited attempts for analyzing the feasibility of RANS approaches in predictions of dense buoyant JICFs. Accordingly, the performance of various RANS closure schemes is worthwhile to be studied further.

To the best of the authors' knowledge, this is one of the first studies comparing the applicability of commonly RANS turbulence modeling approaches including standard $k-\varepsilon$, realizable $k-\varepsilon$, $k-\omega$ shear stress transport (SST), and Launder-Reece-Rodi (LRR) for the simulation of trajectory and mixing processes in submerged buoyant JICFs. The capability of each model in the prediction of flow discharge behavior was assessed by comparing the numerical results with experimental data. Subsequently, the applied modeling approach with reasonable accuracy was further investigated for the study of time-averaged CRVP structure along the jet trajectory and its role in enhancing the dilution level.

4.2 Methodology

4.2.1 Analysis of the Flow Discharge Behavior of a Submerged Dense Buoyant JICF

The performance of a buoyant jet is mainly determined by the geometrical characteristics of the near-field region, which is located in the vicinity of the discharge point. Thus, obtaining

information about the jet characteristics like impact point location and maximum terminal rise height is of significant importance when dealing with the optimal design of outfall discharges.

Figure 4-1 presents a definition schematic of a submerged dense jet vertically discharged into ambient cross-flow. In this case, a dense effluent with a concentration, density, and velocity of C_0, ρ_0, and U_0, respectively, is discharged into the ambient cross-flow environment with a concentration, density, uniform velocity, and flow depth of C_a, ρ_a, U_a, and H, respectively, through a vertical nozzle ($\theta = 90°$) with a diameter of D. The movement of the jet is influenced by the interplay between momentum and buoyancy forces. The jet initially peaks its maximum centerline (y_c) and terminal rise height (y_t) at a horizontal distance of x_t with a centerline peak dilution of S_c and subsequently falls and impacts the bottom because of the downward buoyancy forces at a horizontal distance of x_i. After the jet impacts the bottom, a lateral density current is formed.

4.2.2 Governing Equations

The governing equations for CFD numerical modeling of fluid flow behaviors in outfall discharges include a set of partial differential equations (PDEs) of continuity and momentum, which are known as Navier-Stokes (NS) equations. Due to the turbulent nature of the flow in outfalls, turbulence modeling approaches are needed to be applied to numerically closing this system of equations. To achieve this, RANS modeling approaches can be used in which NS equations are time-averaged before being numerically solved.

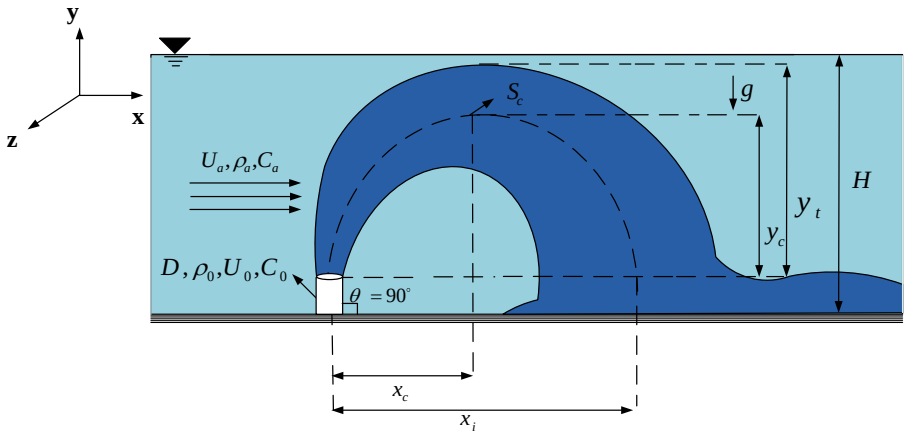

Figure 4-1 Schematic of flow discharge behavior for a vertical dense jet issued into a cross-flow

Time-averaged format of NS equations for continuity, momentum, and scalar transport can be expressed as follows, respectively [14,15]:

$$\frac{\partial \rho}{\partial t} + \frac{\partial}{\partial x_i}(\bar{\rho}\bar{u}_i) = 0 \tag{4-1}$$

$$\frac{\partial (\bar{\rho}\bar{u}_i)}{\partial t} + \frac{\partial}{\partial x_j}\left(\bar{\rho}\bar{u}_i\bar{u}_j\right) = \frac{\partial \bar{p}}{\partial x_i} + \frac{\partial}{\partial x_j}\left(\mu\frac{\partial \bar{u}_i}{\partial x_j}\right) - \frac{\partial \tau_{ij}}{\partial x_j} + \bar{\rho}g_i \tag{4-2}$$

$$\frac{\partial (\bar{\rho}\bar{u}_i)}{\partial t} + \frac{\partial}{\partial x_j}\left(\bar{\rho}\bar{c}\bar{u}_j\right) = \frac{\partial}{\partial x_j}\left(\Gamma\frac{\partial \bar{c}}{\partial x_j}\right) - \frac{\partial q_j}{\partial x_j} \tag{4-3}$$

where i, j, and k subscription denote direction; the overbar represents time-averaged variables; ρ is the fluid density, u is the fluid velocity; μ the dynamic viscosity of the fluid, p is pressure; g is the gravitational acceleration; Γ is the scalar diffusivity; c is the scalar concentration; q is the turbulent scalar flux; and τ denotes the Reynolds stresses.

In the present study, four common closure schemes including standard $k-\varepsilon$, realizable $k-\varepsilon$, $k-\omega$ SST as a subcategory of eddy viscosity model (EVM) and LRR as a subcategory of Reynolds stress model (RSM) were adopted to close the system of equations. The ones under EVM consider the Reynolds stresses to be in proportion to the mean rates of deformation, while the one under RSM deploys the Reynolds stress transport equations to derive the Reynolds stress tensor. More details about the mentioned turbulence modeling approaches can be found in [15,16].

4.2.3 Modeling Setup and Mesh Configuration

After the determination of governing equations, the equations were solved using the finite volume method. For this purpose, OpenFOAM was used as the CFD tool for the simulations of targeted dense buoyant JICFs. The laboratory test conditions considered by Ben Meftah et al. [10,11] were selected as a basis for analyzing the performance of the four RANS closure schemes. The simulation parameters for the studied scenarios are presented in Table 4-1.

Table 4-1 Simulation parameters

Run*	U_0 **(m/s)**	U_a **(m/s)**	F	u_rF	ρ_0 **(kg/m^3)**	ρ_a **(kg/m^3)**	H **(m)**	**Initial** k **(m^2/s^2)**	**Initial** ε **(m^2/s^3)**	**Initial** ω **(1/s)**
R1	0.32	0.0419	7.9	1.0	1013.5	998.9	0.36	0.0061	0.1966	32
R2	0.38	0.0419	9.8	1.1	1012.5	998.9	0.36	0.0086	0.3292	38

* Vertical nozzle with a diameter of D = 0.01 m

The dimensions of the simulation domain were set to have 80 cm length, 60 cm width, and 36 cm height, and it was discretized with a structured mesh while considering 920,000 computational cells. It is worthwhile mentioning that the cell sizes were set to be much fine at the discharge point and along the jet trajectory to better capture the flow properties. Figure 4-2 shows the geometry of the computational domain, mesh structures, and boundary conditions.

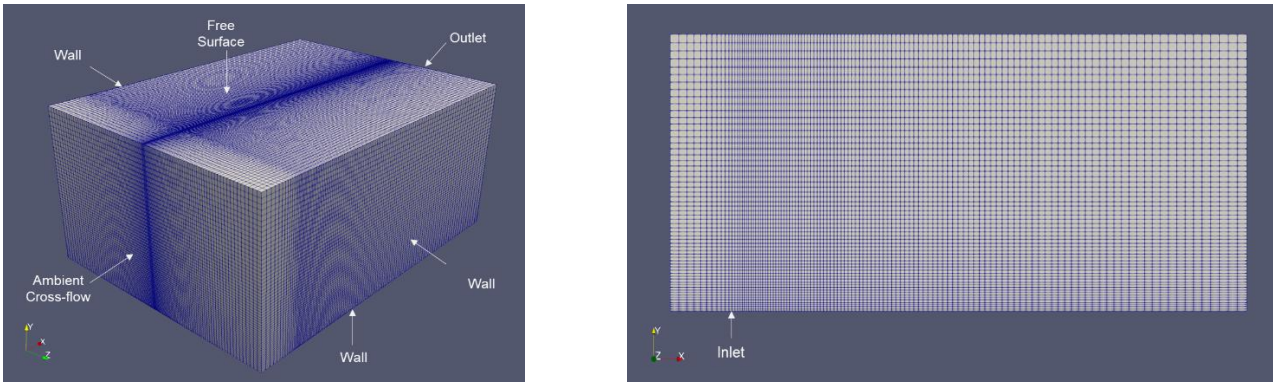

Figure 4-2 Model geometry, mesh structures, and boundary conditions

The solver used in this study was the twoLiquidMixingFoam, which is a transient solver for incompressible flows. The applicability of this solver for outfall discharge modeling has been widely approved in previous studies [16-18]. For the discretization of the temporal term as well as the gradient and Laplacian terms, Euler and Gauss linear schemes were applied, respectively. In addition, Gauss upwind, Gauss linear, and Gauss vanLeer were used for the discretization of the divergence terms. The initial time step was 0.01 s and was set to be adjusted during the simulation runs to ensure that the maximum Courant number could not exceed 0.5 and thereby making the simulation run stable. The duration of each simulation was considered 100s. Then, the results were time-averaged over the course of 60 s to 100 s to ensure a fully-developed flow and stable outputs. The computational domain was also decomposed into 16 regions to speed up the simulation process. It should be noted that all the computations were conducted on the national research computing platform of Compute Canada.

4.3 Results and Discussion

4.3.1 Evaluation of Different RANS Schemes

The prediction capability of the four different RANS schemes was evaluated by comparing the difference between the numerical and experimental results, as demonstrated in Table 4-2. Results showed that the applied realizable $k-\varepsilon$, LRR, and standard $k-\varepsilon$ could reproduce the

geometrical characteristics of the studied cases with an acceptable average percentage error of below 11%.

In addition, the values of peak dilution for the studied cases were compared, as presented in Figure 4-3. In this comparison, the peak dilution values were obtained from the experimental tests conducted by Ben Meftah et al. [10], the present simulation results, and an empirical equation. The empirical equation, as defined in Eq. (4-4), was presented by Gungor and Roberts [12] for the prediction of S_c value in dense JICFs' scenarios using a large experimental dataset.

$$\frac{S_c}{F} = 0.87(u_r F)^{1/2} \tag{4-4}$$

From Figure 4-3, it can be generally concluded that with the increase of $u_r F$ the jet dilution increases, as confirmed by Gungor and Roberts [12]. It is mainly due to the enhancement of ambient flow impacts on the flow discharge behavior. Thus, the key important role of $u_r F$ should be emphasized when dealing with the design of dense JICFs. By the comparison of numerical results with the empirical equation achieved from a large experimental dataset, the error percentages of (3.63%, 5.44%), (10.36%, 8.98%), (21.80%, 19.79%), and (17.36%, 23.16%) were obtained for LRR, realizable $k-\varepsilon$, standard $k-\varepsilon$, and $k-\omega$ approach, respectively, for the cases of (R1, R2).

Table 4-2 Comparison of simulation results with experimental data [10,11] for the prediction of geometrical characteristics of the studied cases

Run	**RANS Schemes/ Experimental Data**	**Geometrical Characteristics**			
		x_i **(cm)**	y_c **(cm)**	y_t **(cm)**	**Averaged Percentage Error (%)**
R1	LRR	25.11	11.90	13.26	8.62
	Standard $k-\varepsilon$	32.55	10.71	12.68	4.02
	Realizable $k-\varepsilon$	31.70	10.82	12.95	2.82
	$k-\omega$ SST	30.88	6.95	11.17	19.32
	Experimental Data	32.03	11.62	13.01	------
R2	LRR	33.98	13.30	17.92	9.18
	Standard $k-\varepsilon$	45.28	13.63	15.52	8.91
	Realizable $k-\varepsilon$	45.99	13.03	15.50	10.93
	$k-\omega$ SST	39.95	8.32	13.31	21.36
	Experimental Data	39.89	14.31	16.95	------

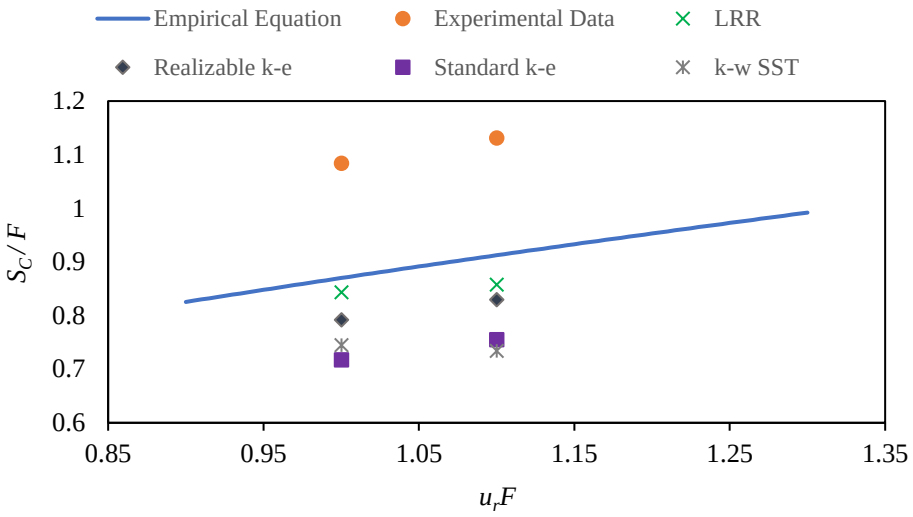

Figure 4-3 Comparing the amounts of peak dilution based on the experimental data [10], the empirical equation [12], and the four various RANS schemes

Hence, among the schemes investigated herein, the realizable $k-\varepsilon$ and LRR approaches led to the most precise results for the prediction of both ascending and descending phases of the jet discharge behavior as well as the estimation of dilution amount. The reason behind this can be mainly attributed to the realizability assumption in the realizable $k-\varepsilon$ scheme. This assumption overcomes the limitation of other EVMs, where the character of eddy viscosity is considered to be isotropic [15]. Using this scheme can also assure the Reynolds stresses to be physically realistic even in the regions of high shear such as in the close proximity of jet discharge [19]. Moreover, the LRR scheme can be considered as a reliable approach since it resolves the Reynolds stresses by employing the Reynolds stress transport equations. These results were in agreement with the interpretation discussed on the applications of RANS approaches for outfall discharge modeling in the literature [19,20].

In contrast, $k-\omega$ SST approach was not successful particularly in capturing the jet trajectory of simulated cases compared to the other schemes, and generally underestimated the geometrical parameters of the flow field. It should be noted that the application of this scheme was priorly shown to be suitable for the simulation of the dense jets discharging into the stationary water where the impact of wall boundary conditions becomes important [15,16].

4.3.2 General Observation

Figure 4-4 illustrates the side views of the concentration fields and contours (C/C_0, in which C is the local concentration and C_0 is the initial concentration) obtained from the realizable $k-\varepsilon$ approach, which was successful in predicting both the trajectory and dilution amount. Based

on Figure 4-4, a rapid rise phase, jet-like mixing, and a gradual fall phase, plume-like mixing, were observed along the jet trajectory. During the initial ascending region, the jet's salinity was significantly reduced, and as moving forward along the jet trajectory, the jet's flow field was widened due to the entrainment of more ambient flow [10].

According to the literature [2], there are four fundamental vortical structures available in a JICF, including the horseshoe, jet shear-layer, wake vortices, and CRVP. Among them, the CRVP has been introduced as a significant time-averaged structure. The evolution of CRVP structure resulting from the interactions of jet and ambient flow is illustrated in Figure 4-5 at different non-dimensional (x/D) distances from the discharge point. As the presented sections in this figure were extracted based on a time-averaged simulation, and the CRVP structure was observed in all sections, the current simulation also confirmed the time-averaged feature of the CRVP.

Figure 4-5 (a) shows the section in the ascending phase of the jet trajectory, in which the CRVP was not fully-formed. As moving forward in the descending phase of the jet trajectory (Figures 4-5 (b) to 4-5 (d)), a kidney shape characteristic of CRVP was gradually developed. Besides, more ambient flow could be entrained into the jet due to the existence of CRVP structure, and therefore higher level of dilution was observed in these sections. Following the impact of jet to the bottom (Figures 4-5 (e) and 4-5 (f)), the existence of CRVP structure led to the flow bifurcation resulting in additional dilution and mixing. These results were in agreement with the study by Gungor and Roberts [12].

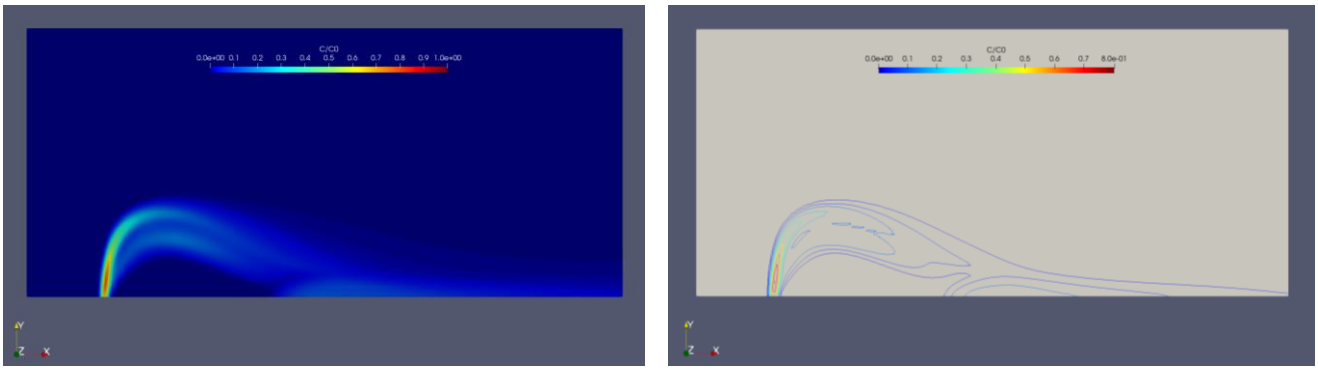

(a) **(b)**

Figure 4-4 Time-averaged concentration distribution **(a)** profiles and **(b)** contours at the center plane using the applied realizable $k-\varepsilon$ scheme

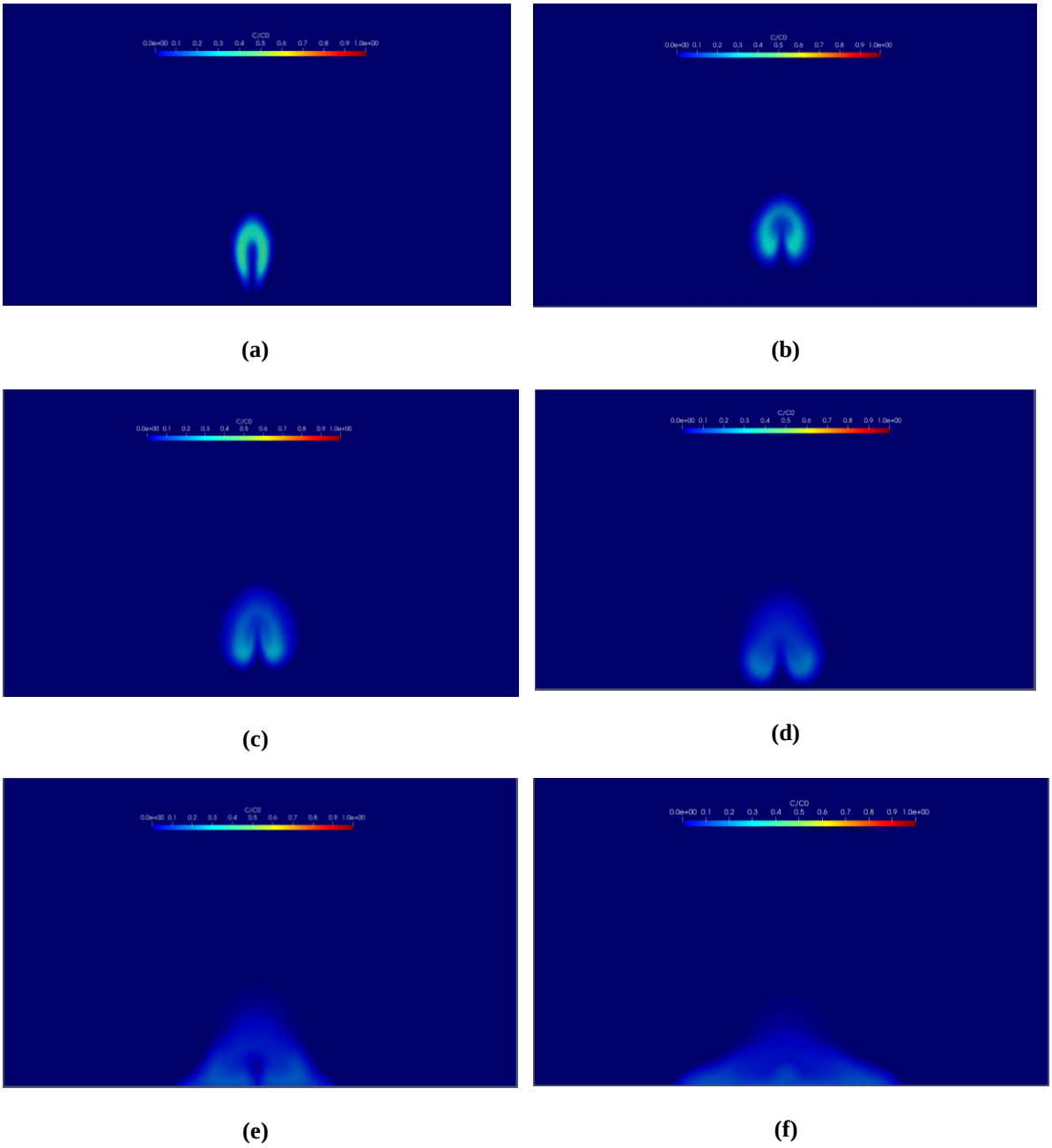

Figure 4-5 Visualization of CRVP evolution along the jet trajectory at different non-dimensional distances from the discharge point **(a)** $x/D = 13$, **(b)** $x/D = 18$, **(c)** $x/D = 24$, **(d)** $x/D = 30$, **(e)** $x/D = 35$, and **(f)** $x/D = 40$

4.4 Conclusions

The applications of brine outfall discharges are significant particularly in arid and semi-arid regions and this, in turn, raises the importance of more investigation on the submerged discharge responses to the dynamic environments (i.e., submerged buoyant JICFs) for obtaining the optimal design of these outfalls. To this end, a CFD numerical modeling was proposed herein. The performance of four different RANS closure schemes (including

realizable $k-\varepsilon$, standard $k-\varepsilon$, LRR, and $k-\omega$ SST) was accordingly analyzed for the simulation of dense jet discharges impacted by the ambient flowing currents. Among them, the realizable $k-\varepsilon$ and LRR schemes resulted in the most accurate solution for resolving both rising and falling phases of the jet discharge behavior as well as predicting of dilution amount. In addition, the formation of a time-averaged CRVP structure for this type of outfall discharge into cross-flow was approved. The bifurcation of the downstream flow field because of the CRVP structure also provided additional dilution and mixing after the dense jet impacted to the bottom. Hence, considering the great promise in the application of proposed CFD modeling approaches for the successful simulation of these outfall discharges, its further use is recommended.

Acknowledgment

The authors would like to acknowledge the advanced research computing (ARC) center of Compute Canada (a not-for-profit-organization) for providing the computational resources used in this work. The research of A.M. was supported by the Natural Sciences and Engineering Research Council of Canada (NSERC).

4.5 References

[1] T.M. Missimer, B. Jones, R.G. Maliva, Intakes and Outfalls for Seawater Reverse-Osmosis Desalination Facilities: Innovations and Environmental Impacts, Springer, New York, 2015. https://doi.org/10.1007/978-3-319-13203-7.

[2] M. Taherian, A. Mohammadian, Buoyant jets in cross-flows: Review, developments, and applications, J Mar Sci Eng 9 (2021). https://doi.org/10.3390/jmse9010061.

[3] C.C.K. Lai, J.H.W. Lee, Initial mixing of inclined dense jet in perpendicular crossflow, Environmental Fluid Mechanics 14 (2014) 25–49. https://doi.org/10.1007/s10652-013-9290-7.

[4] P.J.W. Roberts, G. Toms, Inclined Dense Jets in Flowing Current, Journal of Hydraulic Engineering 113 (1987) 323–340. https://doi.org/10.1061/(asce)0733-9429(1987)113:3(323).

[5] O. Abessi, P.J.W. Roberts, Rosette diffusers for dense effluents in flowing currents, Journal of Hydraulic Engineering 144 (2018) 1–7. https://doi.org/10.1061/(ASCE)HY.1943-7900.0001403.

[6] K. Mahesh, The interaction of jets with crossflow, Annu Rev Fluid Mech 45 (2013) 379–407. https://doi.org/10.1146/annurev-fluid-120710-101115.

[7] A. Gharavi, A. Mohammadian, I. Nistor, E. Peña, J. Anta, Experimental study of surface buoyant jets in crossflow, Environmental Fluid Mechanics 20 (2020) 1007–1030. https://doi.org/10.1007/s10652-020-09737-7.

[8] O. Abessi, P.J.W. Roberts, Multiport diffusers for dense discharge in flowing ambient water, Journal of Hydraulic Engineering 143 (2017). https://doi.org/10.1061/(ASCE)HY.1943-7900.0001279.

[9] M. Jiang, A.W.K. Law, S. Zhang, Mixing behavior of 45° inclined dense jets in currents, Journal of Hydro-Environment Research 18 (2018) 37–48. https://doi.org/10.1016/j.jher.2017.10.008.

[10] M. Ben Meftah, D. Malcangio, F. De Serio, M. Mossa, Vertical dense jet in flowing current, Environmental Fluid Mechanics 18 (2018) 75–96. https://doi.org/10.1007/s10652-017-9515-2.

[11] M. Ben Meftah, M. Mossa, Turbulence measurement of vertical dense jets in crossflow, Water (Basel) 10 (2018) 286. https://doi.org/10.3390/w10030286.

[12] E. Gungor, P.J.W. Roberts, Experimental studies on vertical dense jets in a flowing current, Journal of Hydraulic Engineering 135 (2009) 935–948. https://doi.org/10.1061/(ASCE)HY.1943-7900.0000106.

[13] M. Taherian, S.A.R. Saeidi Hosseini, A. Mohammadian, Overview of Outfall Discharge Modeling with a Focus on Turbulence Modeling Approaches, in: D. Zeidan, L. Zhang, E.G. Da Silva, J. Merker (Eds.), Advances in Fluid Mechanics: Modeling and Simulation, Springer Nature, Accepted, Singapore, 2022.

[14] M.J. Baum, B. Gibbes, Field-Scale Numerical Modeling of a Dense Multiport Diffuser Outfall in Crossflow, Journal of Hydraulic Engineering 146 (2020) 1–16. https://doi.org/10.1061/(ASCE)HY.1943-7900.0001635.

[15] H. Kheirkhah Gildeh, A. Mohammadian, I. Nistor, Inclined dense effluent discharge modelling in shallow waters, Environmental Fluid Mechanics 21 (2021) 955–987. https://doi.org/10.1007/s10652-021-09805-6.

[16] X. Wang, A. Mohammadian, C.D. Rennie, Influence of Negatively Buoyant Jets on a Strongly Curved Open-Channel Flow Using RANS Models with Experimental Data, Water (Basel) 14 (2022) 347. https://doi.org/10.3390/w14030347.

[17] X. Yan, B. Ghodoosipour, A. Mohammadian, Three-Dimensional Numerical Study of Multiple Vertical Buoyant Jets in Stationary Ambient Water, Journal of Hydraulic Engineering 146 (2020) 04020049. https://doi.org/10.1061/(asce)hy.1943-7900.0001768.

[18] S. Zhang, B. Jiang, A.W.-K. Law, B. Zhao, Large eddy simulations of 45° inclined dense jets, Environmental Fluid Mechanics 16 (2016) 101–121. https://doi.org/10.1007/s10652- 015-9415-2.

[19] H. Kheirkhah Gildeh, A. Mohammadian, I. Nistor, H. Qiblawey, Numerical modeling of turbulent buoyant wall jets in stationary ambient water, Journal of Hydraulic Engineering 140 (2014). https://doi.org/10.1061/(ASCE)HY.1943-7900.0000871.

[20] H. Kheirkhah Gildeh, A. Mohammadian, I. Nistor, H. Qiblawey, Numerical modeling of 30◦ and 45◦ inclined dense turbulent jets in stationary ambient, Environmental Fluid Mechanics 15 (2015) 537–562. https://doi.org/10.1007/s10652-014-9372-1.

5 Large Eddy Simulation Study on the Mixing Behavior of Inclined Dense Jets in Cross-flow[4]

Abstract

Outfall desalination discharge technology offers a practical solution for enhancing mixing and dispersion in receiving waters, thereby ensuring both compliance and environmental sustainability. The hydrodynamic effects of non-stationary environments, which more accurately represent real oceanic conditions, pose challenges for predicting the mixing behavior of these types of discharges. Accordingly, this subject requires greater focus to improve the modeling accuracy. This study presents the first investigation into the behavior of inclined dense jets in cross-flow (JICF) conditions, utilizing Large Eddy Simulation (LES) implemented through OpenFOAM software. The simulations replicate and expand upon previous experimental study by Taherian et al. (2024), demonstrating the enhanced mixing efficiency of 60° inclined dense jets. Results are validated against experimental data and further extended to explore a wide range of cross-flow Froude numbers ($0.6 < u_r F < 2.6$) to capture the transition between three distinct flow regimes: jet-dominated, regular cross-flow, and strong cross-flow dominated. The results demonstrate that LES accurately predicts key flow characteristics, including jet trajectory and dilution performance, with mean absolute percentage error (MAPE) values remaining below 10%. The findings provide new insights into the design and optimization of desalination outfalls, helping to mitigate environmental impacts in dynamic coastal settings. The research also highlights the potential of the LES approach for capturing complex flow dynamics more effectively than traditional modeling techniques.

Keywords: Outfall desalination discharge; Dense jets in cross-flows; Mixing Behavior; OpenFOAM simulation; Large Eddy Simulation (LES) approach

[4] This chapter will be submitted to the Desalination Journal as a continuation of the previous experimental study published in the same journal: Taherian, M., Mohammadian, A., Goodarzi, D., Saeidi Hosseini, S. A. R. Large Eddy Simulation Study on the Mixing Behavior of Inclined Dense Jets in Cross-flow.

5.1 Introduction

Discharging dense effluents, often produced by desalination plants, directly into coastal water bodies can lead to significant environmental problems, including the deterioration of water quality and disruption of marine ecosystems [1–5]. To mitigate these negative impacts, it is essential to release dense effluents through outfall diffusers as turbulent buoyant jets, which combine momentum and buoyancy forces to enhance their dispersion and mixing with the surrounding water as well as their dilution levels [6–8]. This approach can help to reduce harmful environmental consequences. However, the interaction of multiple factors, including jet discharge configurations and hydrodynamic forces in the surrounding environment, strongly influences the effective mixing behavior of discharges [9,10]. Thus, accurately predicting the mixing of jets under different operational conditions is crucial for designing systems that satisfy regulatory requirements.

Buoyant jet configurations can include both surface and submerged jets, with submerged jets generally being more desirable because of their enhanced mixing and dilution capabilities [6]. This is because the submerged jets draw in the surrounding fluid from all directions, leading to better dispersion [11]. Additionally, these jets can be discharged at various angles, ranging from horizontal (0°) to vertical (90°). Inclined jets are particularly favored for most applications because of their horizontal momentum components, which are particularly beneficial when releasing dense effluents into shallow waters near shorelines [12–14]. This inclination helps prevent jets from reaching the water surface, thereby improving dilution and minimizing environmental impact [15].

Moreover, buoyant jets can be discharged into both stationary and dynamic water environments; however, oceanic and coastal settings, which reflect real-world conditions, are rarely stationary [16]. The dynamic and turbulent nature of non-stationary environments adds complexity to the prediction of jet behavior [6]. Depending on the orientation of the discharge relative to the ambient current, three scenarios can occur: co-flow, counter-flow, and cross-flow. In a co-flow, the jet discharge aligns with the current, while in a counter-flow, it opposes the current; both create a two-dimensional flow path [17]. However, when the current is perpendicular to the jet discharge, known as a buoyant jet in cross-flow (JICF), the jet is deflected by ambient water, leading to a complex three-dimensional trajectory for inclined discharges [6,18]. This complexity underscores the need to understand fluid interactions and the initial mixing behavior to effectively manage and control dense discharges.

The literature review reveals that most research on the design of dense outfalls has focused on discharges into stationary environments. In contrast, discharges into flowing water bodies, which better represent real-world conditions, have been studied less extensively. Additionally, studies on the mixing behavior of dense jets influenced by flowing currents have primarily relied on experimental approaches. For example, Roberts and Toms [19] studied 60° inclined and vertical dense jets under various co-flow and counter-flow conditions, along with five tests involving perpendicular cross-flow. Their results showed that 60° inclined jets generally performed better than vertical jets in most scenarios. Using photogrammetry and suction sampling techniques, they found that jet dilution and geometry depend on a parameter called the cross-flow Froude number, defined as $u_r F$, where u_r is the ratio of ambient cross-flow to jet velocity, and *F* is the jet-densimetric Froude number. Gungor and Roberts [8] used a laser-induced fluorescence (LIF) technique to study the concentration flow field of vertical dense jets with a 2D trajectory. They found that as the current speed increased (within a cross-flow range of $0.21 < u_r F < 0.92$), both the dilution at the terminal rise height and the impact point also increased.

Later, Lai and Lee [18] found that the dilution and location of the terminal rise point for a 60° dense jet in a perpendicular cross-flow were primarily influenced by ambient currents when $u_r F \geq 0.8$, with detrainment being negligible for $u_r F \geq 2.0$. Jiang et al. [17] also showed that for a 45° dense jet, the source discharge characteristics dominated the flow behavior when $u_r F < 1.0$, while ambient currents became more significant in the mixing process when $u_r F$ was higher. Ben Meftah et al. [20,21] conducted studies on vertical dense jets in ambient cross-flow currents, focusing on $u_r F$ of around 1.0 and 1.1. They experimentally examined the resulting salinity concentration and velocity flow fields and identified two distinct mixing phases: jet-like and plume-like. Their findings confirmed the formation of counter-rotating vortex pairs (CRVPs) within the jet trajectory, which led to significant dilution during the initial rise phase.

Recently, Taherian et al. [7] investigated the impact of ambient currents and discharge angles on the performance of desalination outfall discharges when issuing into perpendicular cross-flow currents with 3D trajectories. Using LIF experiments, they examined the effects of various nozzle angles (30°, 45°, 60°) and cross-flow Froude numbers ($1.1 \leq u_r F \leq 1.62$) on dense jet trajectories and dilution. They showed that a 60° jet enhanced dilution by more than 50%, on average, compared to a 30° jet and by 20%, on average, compared to a 45° jet. Their results also indicated that using steeper inclinations and larger $u_r F$ values within the tested

range significantly improved the mixing efficiency due to the longer trajectory and greater expansion achieved.

Although experimental studies have greatly advanced our understanding of discharge into flowing water bodies, they are often costly and time-consuming. However, these experimental results are invaluable for developing mathematical models of dense jet dynamics, which offers a more efficient alternative. Supplementary approaches, such as jet integral models and jet flow modeling using computational fluid dynamics (CFD) techniques, are particularly appealing because they can leverage experimental data to enhance accuracy while reducing the need for extensive physical testing [2,6,22]. Jet integral models are commonly used by designers to evaluate jet mixing behavior and form the basis of commercial tools, such as JetLag [23,24], CoreJet [25], and Visual Plumes [26]. These models simplify the governing mass and momentum conservation equations by assuming Gaussian and axisymmetric velocity profiles, without radial changes [1]. Palomar et al. [27] compared the applications of various commercial jet integral tools (such as JetLag, UM3, and CoreJet) and highlighted their limitations by showing substantial discrepancies, up to approximately 50% underestimation, in the prediction of terminal rise height and dilution at the impact point when these models are applied to inclined dense jets in dynamic ambient environments. These findings suggest that while jet integral models are valuable, their simplified assumptions restrict their effectiveness in capturing complex jet-ambient interactions, making them less reliable for certain applications, especially buoyant JICF scenarios.

CFD techniques have demonstrated significant potential in addressing the limitations of integral models and effectively capturing and resolving the complex dynamics associated with outfall discharges. Despite being more computationally intensive, CFD offers a promising approach for simulating desalination outfalls because it relies on fewer assumptions [28]. This approach has become even more viable with advancements in computational resources and CFD tools [29]. In CFD simulations, the momentum and continuity equations, known as Navier–Stokes (NS) equations, are numerically solved using turbulence closure models to simplify the complex nature of turbulence and make computations more feasible. Among the various turbulence modeling approaches available for simulating outfall discharges, Reynolds-Averaged Navier–Stokes (RANS) and Large Eddy Simulation (LES) are the most widely used [1,29]. RANS models, which include closures, such as k-ε, k-ω, and Launder–Reece–Rodi (LRR), rely on time-averaging techniques. On the other hand, LES models, including the standard Smagorinsky and dynamic Smagorinsky models (DSM), use filtering methods to

capture the effects of turbulence by directly simulating large eddies while modeling smaller scales.

Several CFD studies have been conducted to resolve inclined buoyant jet discharges in stagnant environments, with a particular focus on the RANS modeling approach [30–33]. Zhang [34,35] and Jiang [36] employed the LES technique to model inclined dense jet discharges in similar stagnant settings. These LES studies have shown significant advancements in accurately predicting jet trajectory and dilution, outperforming the integral jet models used by Palomar et al [27]. The improved accuracy of the LES approach is primarily due to its ability to capture coherent eddy structures along the jet trajectory, offering a more detailed and accurate representation of the flow dynamics. Recent studies, including a review by Mohammadian et al. [29], have confirmed the progress of CFD simulations from the RANS approach to LES, and hybrid approaches for the design of buoyant jets.

Despite these advancements, the application of CFD to modeling inclined dense JICFs remains relatively underexplored. To the best of the authors' knowledge, the only CFD study that has investigated the influence of varying flowing current strengths ($0.2 < u_rF < 1.6$) on jet trajectory and dilution was conducted by Baum and Gibbes [28]. They employed RANS equations with a k-ω turbulence closure model to effectively simulate the discharge behavior of inclined multiport diffusers at the Gold Coast desalination plant in Australia. Their findings revealed a critical u_rF value of approximately 0.8, highlighting a significant shift between the regimes dominated by ambient currents and those dominated by dense jets. This study, along with recent advancements in CFD techniques, indicates that further research should focus on using CFD to predict the complicated mixing behaviors of dense jet discharges while interacting with ambient cross-flow conditions.

The literature review underscores the absence of a comprehensive LES study on dense JICFs, despite its potential as an effective turbulence closure system for capturing complex flow dynamics. Moreover, insights from the referenced experimental studies highlight the key role of the u_rF parameter in determining the mixing performance of dense discharges into flowing water bodies. Variations in this parameter are expected to result in different mixing flow regimes. Accordingly, this study focuses on evaluating the capability of the LES approach in the simulation of the inclined dense JICFs and assessing their mixing performance across a wide range of cross-flow Froude numbers.

To the best of the authors' knowledge, this study represents one of the first attempts to simulate dense jet discharges into cross-flow currents using the LES approach. The LES technique, implemented using the OpenFOAM software, is employed to replicate the experimental results from Taherian et al. [7] for 60° dense jets in a perpendicular cross-flow, which showed an enhanced mixing efficiency. The ability of the model to predict key flow parameters is initially validated against the experimental data, before extending the simulations across a wider range of cross-flow Froude numbers. This analysis reveals three distinct regimes: jet-dominated, regular cross-flow, and strong cross-flow dominated. These findings provide valuable insights into optimizing the design of inclined desalination outfalls in dynamic environments to achieve better dilution.

5.2 Methodology

5.2.1 Analysis of Inclined Dense Jets in Cross-flow Currents

Figure 5-1 provides a schematic representation of the key flow parameters, including both the geometrical and dilution characteristics, for an inclined dense jet discharged into a perpendicular cross-flow current. In this scenario, a dense effluent with an initial concentration (C_0), density (ρ_0), and velocity (u_0) is discharged into an ambient cross-flow environment, characterized by a concentration (C_a), density (ρ_a), uniform velocity (u_a) parallel to the *x*-*y* plane, and flow depth (H), through an inclined nozzle at an angle to the horizontal *x*-*z* plane ($\theta = 60°$) with a diameter (D). The uniform ambient current forms an angle of $\emptyset = 90°$ with respect to the plane of discharge propagation at the source. The movement of the jet is governed by the interaction between momentum and buoyancy forces. Initially, the jet reaches its terminal rise height (y_t), the maximum vertical distance between the nozzle tip and the peak of the flow, with a dilution of S_t. After reaching this peak, the jet descends due to downward buoyancy forces, traveling a horizontal distance (x_r) from the nozzle tip to the return point of the flow, where the dilution is S_r.

Two key assumptions are made for the dimensional analysis of dense JICFs. First, the flow is assumed to be fully turbulent, neglecting the effects of viscosity. Second, the Boussinesq approximation is applied, meaning that the density difference between the effluent and the ambient fluid, ($\rho_a - \rho_0$), is considered small compared to the ambient density (ρ_a), allowing buoyancy effects to drive the flow [16]. The interaction of dense jets with ambient cross-flows has been extensively investigated in the literature [7,18,19,28]. Accordingly, for a fixed

discharge inclination angle and perpendicular cross-flow current ($\emptyset = 90°$), the major flow parameters, including the geometrical and dilution characteristics of the jet, can be described as:

$$\frac{x_r}{DF} or \frac{y_t}{DF}; \frac{S_r}{F} or \frac{S_t}{F} = f(u_r F) \tag{5-1}$$

Thus, the parameter $u_r F$, which represents the relative strength of the ambient flow speed to buoyancy, is critical in defining the dilution characteristics and trajectory of inclined dense JICFs in the scenario under consideration.

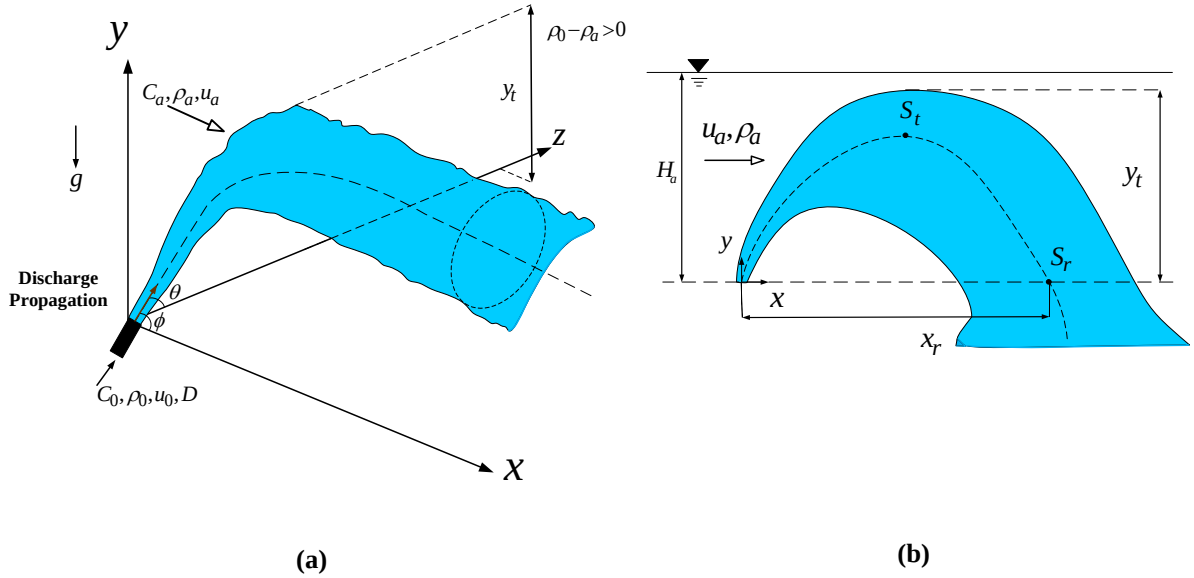

(a) **(b)**

Figure 5-1 Schematic representation of the flow behavior of an inclined dense jet affected by a perpendicular cross-flow **(a)** 3D trajectory and **(b)** Front view plan

5.2.2 Governing Equations

In the LES approach, unlike RANS models, which only provide mean flow data by modeling all turbulence, turbulent eddies are categorized based on their size relative to the local grid resolution. The LES method directly computes large eddies by solving the instantaneous NS equations, while smaller eddies are modeled using subgrid-scale (SGS) models [6].

In this paper, momentum and mass transport were governed by dimensionless incompressible NS equations, coupled with an advection-diffusion equation for scalar transport. To directly resolve large-scale flow features while filtering out small-scale features, the LES method with implicit filtering was employed. Because the density difference between the dense jet and ambient fluid was less than 10%, the Boussinesq approximation was used to

model the coupling between the momentum and buoyancy forces. The non-dimensional governing equations were formulated as follows [37,38]:

$$\frac{\partial \widetilde{u_\iota}}{\partial \widetilde{x_\iota}} = 0 \tag{5-2}$$

$$\frac{\partial \widetilde{u_\iota}}{\partial \tilde{t}} + \frac{\partial \widetilde{u_\iota}\widetilde{u_J}}{\partial \widetilde{x_J}} = -\frac{\partial \tilde{p}}{\partial \widetilde{x_\iota}} + \frac{1}{Re}\frac{\partial^2 \widetilde{u_\iota}}{\partial \widetilde{x_J}\,\partial \widetilde{x_J}} - \frac{\partial \widetilde{\tau_{\iota J}}}{\partial \widetilde{x_J}} + e_i^g \frac{1}{Fr^2}\tilde{c} \tag{5-3}$$

$$\frac{\partial \tilde{c}}{\partial \tilde{t}} + \frac{\partial \widetilde{u_\iota}\tilde{c}}{\partial \widetilde{x_\iota}} = \frac{1}{ReSc}\frac{\partial^2 \tilde{c}}{\partial \widetilde{x_\iota}\,\partial \widetilde{x_\iota}} - \frac{\partial \widetilde{\tau_\iota^c}}{\partial \widetilde{x_\iota}} z \tag{5-4}$$

Here, the indices $(i, j = 1, 2, 3)$ represent the spatial dimensions, $(\widetilde{u_\iota})$ denotes the (i)-th component of the dimensionless velocity, and $(\tilde{p})$ represents the pressure. The kinematic viscosity is denoted by (ν), and $(\tilde{t})$ shows the time. The SGS stress tensor is expressed as $(\widetilde{\tau_{\iota J}})$. Gravitational acceleration acts in the direction of the unit vector $e_i^g = (0, -1, 0)$, and $(\tilde{c})$ represents dimensionless salinity concentration. Throughout this study, variables with tilde $(\tilde{\ })$ are dimensionless and filtered. Dimensionless variables were derived using the characteristic scales for length, velocity, and time, as detailed in Table 5-1.

Table 5-1 Definition of the nondimensionalizations used in the simulation

Parameter	Nondimensionalization
Length	$\widetilde{x_\iota} = x_i/d_0$
Velocity	$\widetilde{u_\iota} = u_i/U_0$
Time	$\tilde{t} = (U_0/d_0)t$
Pressure	$\tilde{p} = (d_0/\rho_a U_0^2)p$
Salinity	$\tilde{c} = c/C_0$

In this study, the Wall-Adapting Local Eddy-viscosity (WALE) model was adopted for SGS. For more detailed information, readers are referred to [37,38]. The stress tensor τ_{ij}, which accounts for both viscous and SGS contributions, is defined as:

$$\tau_{ij} = 2\nu S_{ij} + \tau_{ij}^{sgs} \tag{5-5}$$

where the S_{ij} denotes the resolved velocity strain rate tensor, and the SGS stress tensor τ_{ij}^{sgs} are specified by

$$\overline{S_{ij}} = \frac{1}{2}\left(\frac{\partial \overline{u_i}}{\partial x_j} + \frac{\partial \overline{u_j}}{\partial x_i}\right) \tag{5-6}$$

$$\tau_{ij}^{sgs} = 2\nu_{sgs}S_{ij} + \frac{1}{3}\tau_{kk}^{sgs}\delta_{ij} \tag{5-7}$$

The eddy viscosity ν_{sgs} in the WALE model is calculated using:

$$\nu_{sgs} = (C_w\Delta)^2 \frac{\left(S_{ij}^d S_{ij}^d\right)^{3/2}}{\left(S_{ij}S_{ij}\right)^{5/2} + \left(S_{ij}^d S_{ij}^d\right)^{5/4}} \tag{5-8}$$

where C_w is the model constant, Δ is the filter width, and S_{ij}^d is the deviatoric part of the strain rate tensor. An in-depth discussion of this formulation is provided in [37,38].

5.2.3 Mesh Configuration and Computational Setup

The objective of this study was to evaluate the accuracy of the LES approach in predicting the behavior of inclined dense JICFs and to investigate the effects of varying the current strength on mixing performance. The first step involved validating the LES model by simulating experiments conducted by Taherian et al. [7], which examined a 60° discharge angle and cross-flow Froude numbers in the range of $1.1 \leq u_r F \leq 1.62$. This study was selected for validation because of its detailed three-dimensional concentration field measurements using LIF and its comprehensive dataset on inclined dense effluents. The simulation results were compared with experimental data to ensure the accuracy of the model. Once validated, the model was used to analyze a broader range of $u_r F$ values and their impact on the mixing behavior of dense jets.

The governing equations were solved using the finite-volume method with OpenFOAM as the CFD tool for simulating the targeted dense JICFs. The simulation parameters for the study are outlined in Table 5-2, encompassing 12 cases. Cases C1, C2, C3, and C4 were used for the model validation, directly matching the experimental scenarios from Taherian et al. [7]. Additional cases (R1-R8) extended the simulations beyond the experimental scope.

A customized version of the standard OpenFOAM solver *pimpleFoam* was used for the simulations. This solver, designed for incompressible flow, was coupled with an advection-diffusion equation to account for the buoyancy effects, modeled through the Boussinesq approximation. To enhance the stability, the *pimple* algorithm, a hybrid of the PISO and SIMPLE algorithms, was employed to resolve the pressure-velocity coupling in the NS equations. For all simulations, a Courant-Friedrichs-Lewy (CFL) number below 0.5 was maintained, with automatic time step control to ensure accuracy. For further information on the *pimple* algorithm and OpenFOAM, readers can refer to [39,40].

To achieve second-order accuracy, the time derivative terms were discretized using the backward differencing scheme, while the gradient terms were handled using the Gauss linear method. The divergence terms were discretized using the Gauss-limitedLinear scheme, viscous terms using the Gauss-linear scheme, and Laplacian terms using the Gauss linear uncorrected scheme [41–43]. Each simulation was run until a statistically steady state was reached, and the flow quantities were averaged over 40,000 non-dimensional time units to ensure robust results.

The computational domain was discretized into a mesh comprising 19 million hexahedral cells, as shown in Figure 5-2. The mesh was generated using the open-source tool Gmsh, which applies a multi-level refinement strategy to enhance the resolution in critical regions of interest [44]. The use of hexahedral cells ensured high computational accuracy and smooth transitions across the domain.

Table 5-2 Characteristics of numerical cases

Run	Jet-densimetric Froude Number, F	Ratio of ambient cross-flow to jet velocity, u_r	$u_r F$
C1	23.8	0.05	1.15
C2	26.1	0.05	1.26
C3	29.2	0.05	1.4
C4	31.2	0.05	1.50
R1	23.3	0.03	0.70
R2	26.7	0.03	0.80
R3	30.0	0.03	0.90
R4	33.3	0.03	1.00
R5	23.3	0.075	1.75
R6	26.7	0.075	2.00
R7	30.0	0.075	2.25
R8	33.3	0.075	2.50

Nozzle diameter (D) = 0.0032 m; discharge angle (θ) = 60°

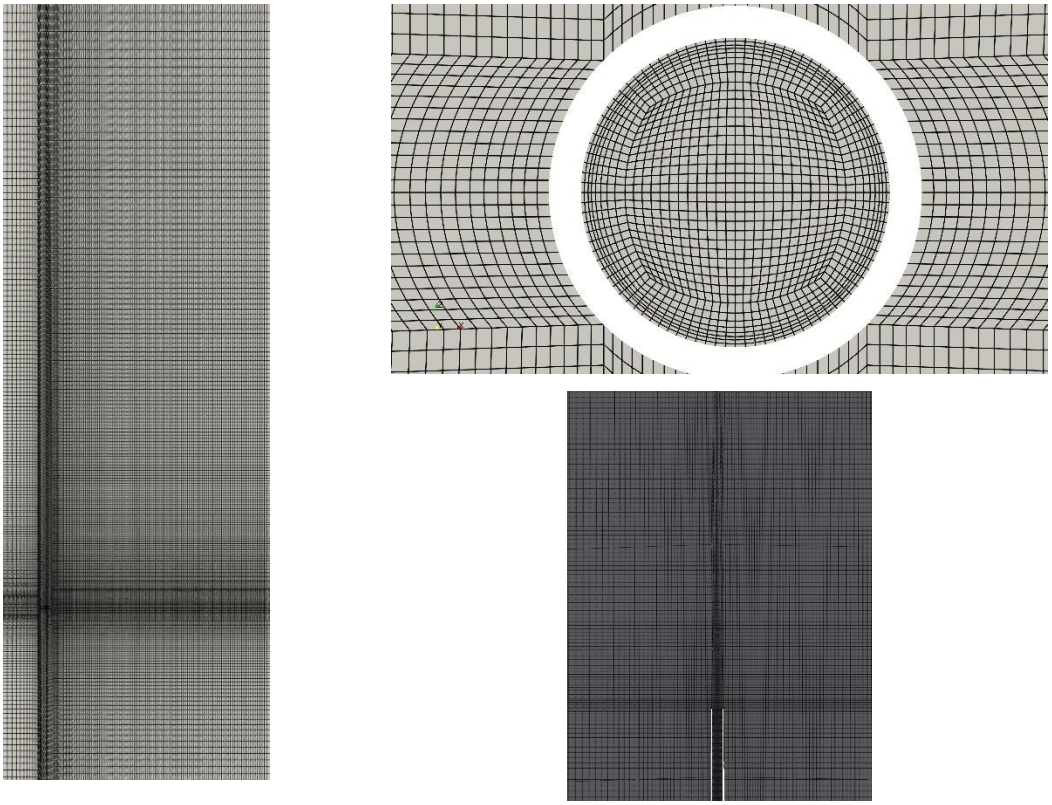

Figure 5-2 The visualization of the computational mesh used in the simulation highlights the hexahedral cell structure, with refined mesh regions strategically placed around critical areas for enhanced resolution and accuracy.

5.3 Results and Discussion

5.3.1 Model Validation

Four cases, C1 through C4, with a $u_r F$ range between 1.15 and 1.5, were simulated using the LES model. The model's predictions for the terminal rise height, corresponding dilution, and the horizontal location of the return point, along with its dilution, were then compared to the experimental measurements conducted by Taherian et al. [7]. Table 5-3 presents a comparison of the experimental and numerical data for the major flow parameters of C1-C4. In addition, the prediction of the model accuracy for each flow parameter is quantified using the mean absolute percentage error (MAPE), following the approach used in [2,45]. As shown in the table, the model predictions for all major flow parameters closely align with the experimental measurements, with MAPE values remaining below 10%. This indicates that the LES method accurately replicates the experimental results, and can be considered a reliable approach for practical applications.

Table 5-3 Model validation of major flow parameters

Parameters	x_r/DF			y_t/DF			S_t/F			S_r/F		
	Exp.*	Pred.**	Error (%)	Exp.	Pred.	Error (%)	Exp.	Pred.	Error (%)	Exp.	Pred.	Error (%)
C1	5.29	4.79	-9.52	1.89	1.76	-6.67	0.69	0.78	12.77	1.31	1.45	10.34
C2	5.36	4.98	-7.07	1.92	1.72	-10	0.72	0.8	10.86	1.42	1.56	10.2
C3	5.24	5.65	7.86	1.88	1.68	-10.75	0.97	0.98	1.06	1.85	2.01	8.93
C4	5.4	5.45	0.9	1.66	1.54	-7.32	1.07	0.94	-11.9	1.92	2.07	7.7
MAPE (%)	6.34			8.68			9.15			9.3		

* Experimental data

** Predicted data

5.3.2 General Flow Behavior

The general flow behavior of the 60° inclined jet in cross-flow currents can be divided into two distinct phases: rising and falling. In the initial rising phase, the jet momentum dominates, propelling the jet upward. As the jet rises, it begins to bend along the longitudinal direction of the flume due to the influence of the cross-flow current. The jet momentum gradually decreases until it becomes equal to the buoyant force, marking the point at which the jet reaches its maximum height. At this stage, the buoyant force surpasses the momentum of the jet, initiating the falling phase, in which the jet descends toward the bed [6,20,46]. As shown in Figure 5-3, along the trajectory of the jet, continuous dilution occurs, which is driven by both jet spread and water entrainment.

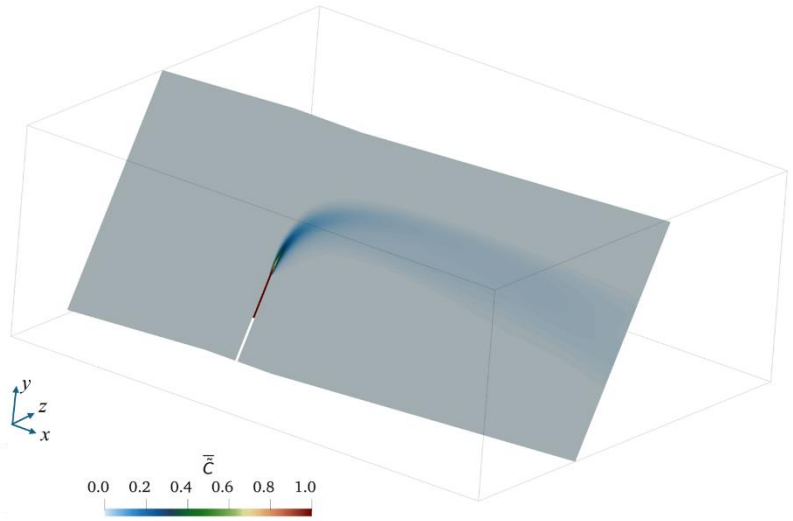

Figure 5-3 The time-averaged dimensionless concentration of the jet is shown on a slice with a 60-degree inclination in the x-y plane, aligned with the jet pipe center, and slightly inclined in the x-z plane to follow the direction of the jet flow.

In addition, a comparison of flow behavior based on variations in the parameter $u_r F$ reveals that the interaction between cross-flow currents and 60° dense jets leads to three distinct flow regimes: jet-dominated, regular cross-flow, and strong cross-flow-dominated, see Figure 5-4. In the jet-dominated regime ($u_r F < 1.0$), the jet experiences minimal deflection, with almost similar rising and falling flows as discharges into stagnant ambient waters. Mixing in this regime is primarily driven by the momentum of the jet. As the current speed increases to $1.0 < u_r F < 2.0$, the jet rises to lower levels and deflects more rapidly in the direction of the ambient flow due to the stronger current. Meanwhile, the descent phase becomes more gradual, causing the jet to impact further downstream. This regime is characterized by a regular cross-flow influence. Finally, when $u_r F$ exceeds approximately 2.0, the jet is nearly horizontal and heavily influenced by the cross-flow. In this strong cross-flow-dominated regime, the jet is rapidly dispersed by ambient turbulence and may enter the far-field or become trapped by ambient density stratification. This interpretation is in agreement with the discussion of Gungor and Roberts [8] on the flow behavior of a 90° dense jet influenced by perpendicular cross-flow currents.

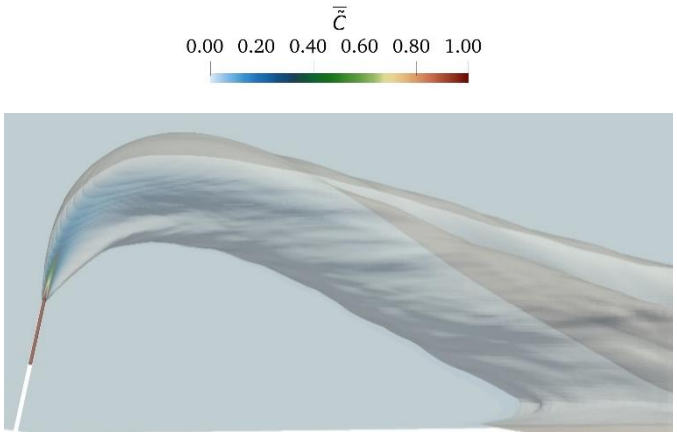

(a)

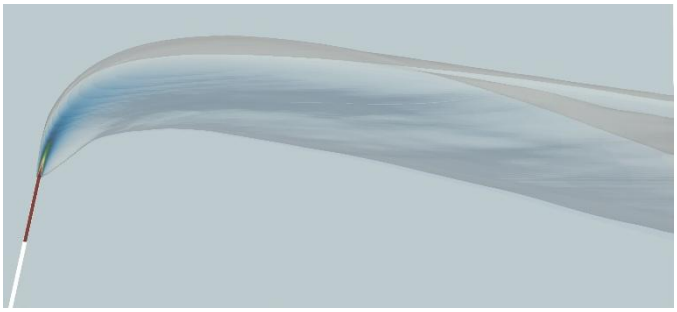

(b)

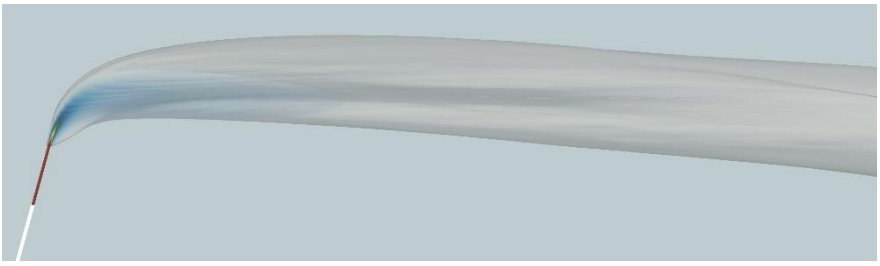

(c)

Figure 5-4 General flow characteristics for different cross-flow parameter values: **(a)** jet-dominated regime ($u_r F < 1.0$), R1; **(b)** regular cross-flow regime ($1.0 < u_r F < 2.0$), C2; and **(c)** strong cross-flow regime ($u_r F > 2.0$), R7.

Figure 5-5 illustrates the development of CRVP along the jet trajectory. As the jet progresses through the descending phase, the CRVP gradually forms a distinctive kidney-shaped structure. This vortex formation enhances ambient flow entrainment into the jet, contributing to increased dilution in these regions. Upon reaching the return point of the jet, the CRVP structure further promotes flow bifurcation, leading to additional dilution and mixing. These findings are consistent with the observations of [8,21].

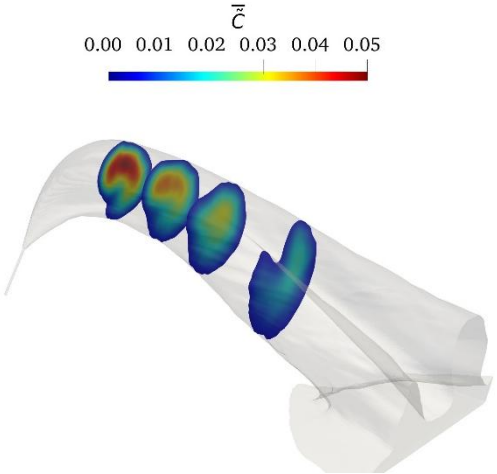

Figure 5-5 Visualization of the CRVP evolution along the jet trajectory for simulation case R1

5.3.3 Terminal Rise Height and its Dilution

The terminal rise height (y_t) refers to the maximum height a jet reaches in the time-averaged concentration field, where the vertical component of the momentum diminishes and approaches zero. The jet terminal rise height is a critical parameter in the study of brine jet discharges, particularly in shallow waters, as it significantly influences the discharge behavior and environmental impact. There is no consensus in the literature regarding the definition of this

height. Roberts et al. [47] described y_t as the location at which the concentration is 10% of the transverse maximum concentration at the peak height of the jet. Similarly, Abessi and Roberts [47] used this 10% threshold to define y_t in their experiments. On the other hand, Lai and Lee [48] suggested using the 25% concentration contour to establish the visual boundary, while the integral model CORJET [25] employed cut-off levels of 3% and 25% for this purpose. Shao et al. [49] adopted a 3% cut-off level.

In this study, the terminal rise height was determined using a 10% threshold, which is consistent with the experimental data of Taherian et al. [7]. The results of the normalized terminal rise height (y_t/DF) versus u_rF are shown in Figure 5-6. Accordingly, the terminal rise height is almost constant and independent of the changes in the u_rF parameter in the jet-dominated regime, where $u_rF < 1.0$. However, the dimensionless terminal rise height decreases as $\sim(u_rF)^{-0.62}$ in the cross-flow-dominated regime, $u_rF > 1.0$. This behavior can be attributed to the deflection of the jet along the longitudinal axis of the flume under the influence of the cross-flow current. The semi-empirical relationships between the terminal rise height of the jet and cross-flow Froude number are presented in Eqs. (5-9) and (5-10), with both equations demonstrating strong goodness-of-fit values of approximately R^2 = 0.97.

$$\frac{y_t}{DF} = 1.75 \qquad for\ u_rF < 1.0 \tag{5-9}$$

$$\frac{y_t}{DF} = 2.0(u_rF)^{-0.62} \qquad for\ u_rF > 1.0 \tag{5-10}$$

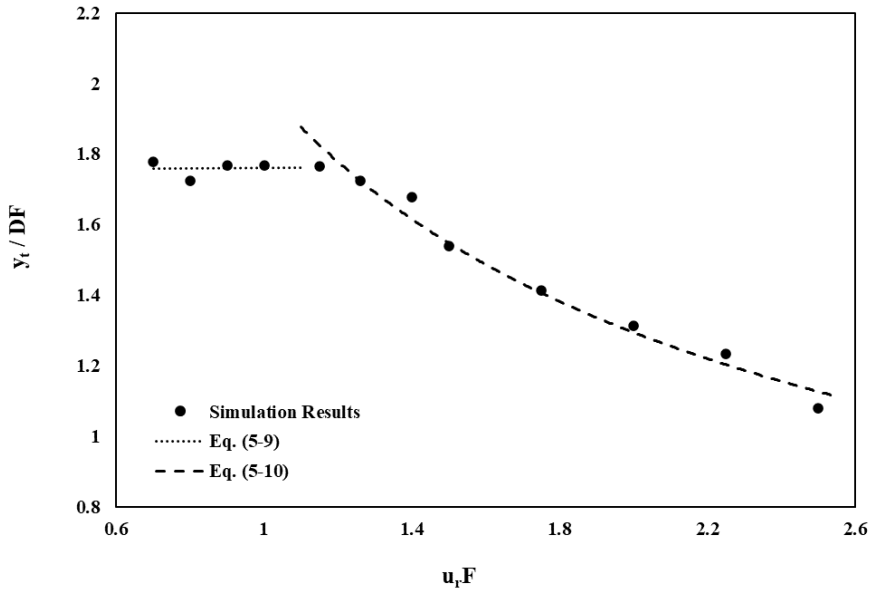

Figure 5-6 Jet terminal rise height

Figure 5-7 illustrates the variation of the S_t/F parameter with u_rF, with the corresponding semi-empirical equation yielding an R^2 goodness-of-fit value of 0.92, see Eq. (5-11). The dilution at the jet's terminal rise height increases with u_rF, following a relationship of $\sim(u_rF)^{1/3}$, indicating a direct correlation between the cross-flow Froude number and mixing efficiency. In the jet-dominated region, where the jet momentum is the controlling factor, the increase in dilution with increasing u_rF is less pronounced than in regions where the flow is dominated by the cross-flow current.

$$\frac{S_t}{F} = 0.8(u_rF)^{0.39} \tag{5-11}$$

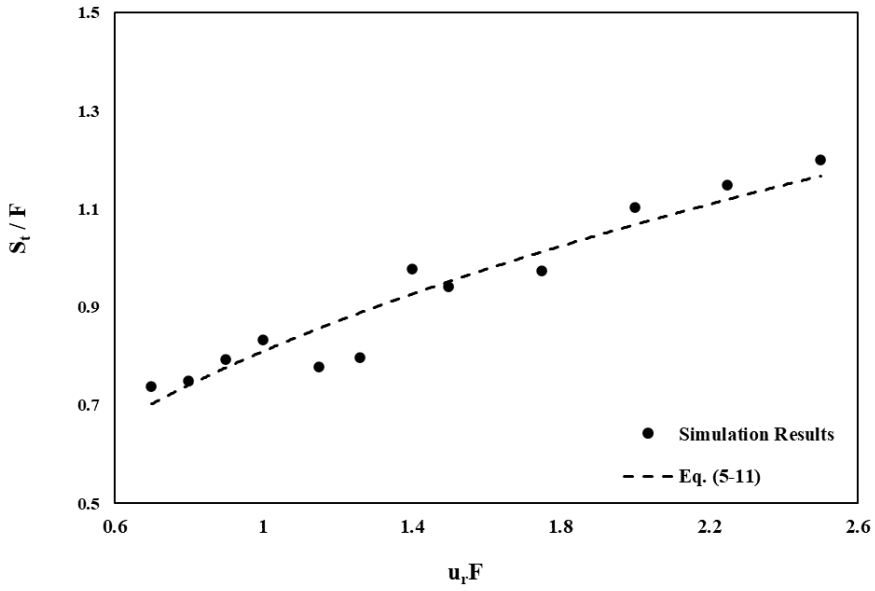

Figure 5-7 Dilution at terminal rise height

5.3.4 Horizontal Location of the Jet Return Point and its Dilution

Another major jet flow parameter is the horizontal location of the jet return point (x_r), which represents the distance from the discharge point to thee point where the jet returns to the level of the nozzle tip during its descending phase. This point is important as it indicates where the jet impacts the seabed, potentially affecting benthic organisms, and where minimum dilution occurs along the lower boundary of the plume. The distance to the jet return point (x_r/DF) varies with the ambient cross-flow parameter (u_rF), as shown in Figure 5-8. The semi-empirical power-law relationship between the jet return point and the cross-flow Froude number is given by Eq. (5-12), demonstrating a strong fit with an R^2 value of 0.98. Accordingly, the distance to the jet return point increases with u_rF, following a relationship of $\sim(u_rF)^{0.6}$.

$$\frac{x_r}{DF} = 4.3(u_r F)^{0.64} \tag{5-12}$$

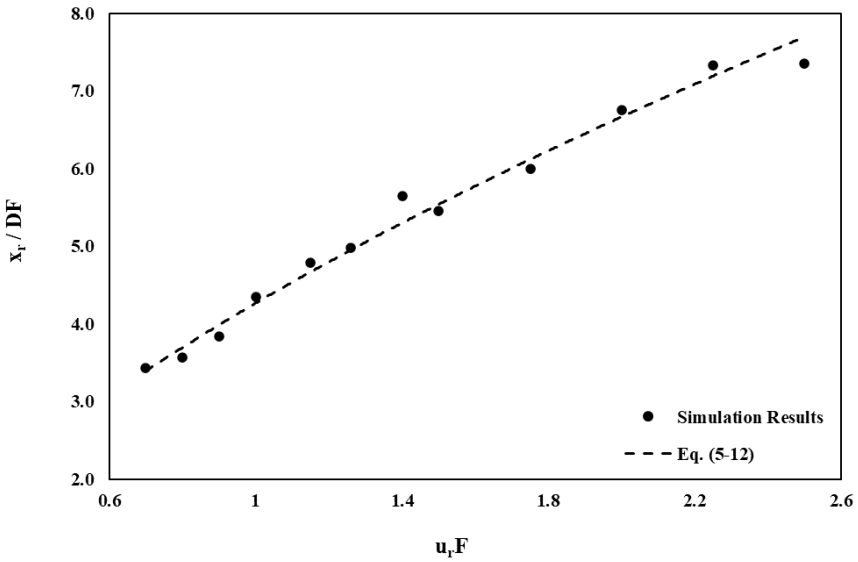

Figure 5-8 Horizontal return point location

Figure 5-9 illustrates the variation of S_r/F as a function of $u_r F$. The semi-empirical power-law relationship between the minimum dilution at the jet return point and cross-flow Froude number is expressed by Eq. (5-13), with a goodness-of-fit R^2 value of 0.86. As the cross-flow magnitude increases, the dilution at the jet return point increases following a $\sim(u_r F)^{0.4}$ dependency. This increase in dilution can be attributed to the extended flow trajectory, which allows a greater surface area for external fluid entrainment and provides more time for the jet to interact with the ambient flow, leading to enhanced dilution.

$$\frac{S_r}{F} = 1.6(u_r F)^{0.42} \tag{5-13}$$

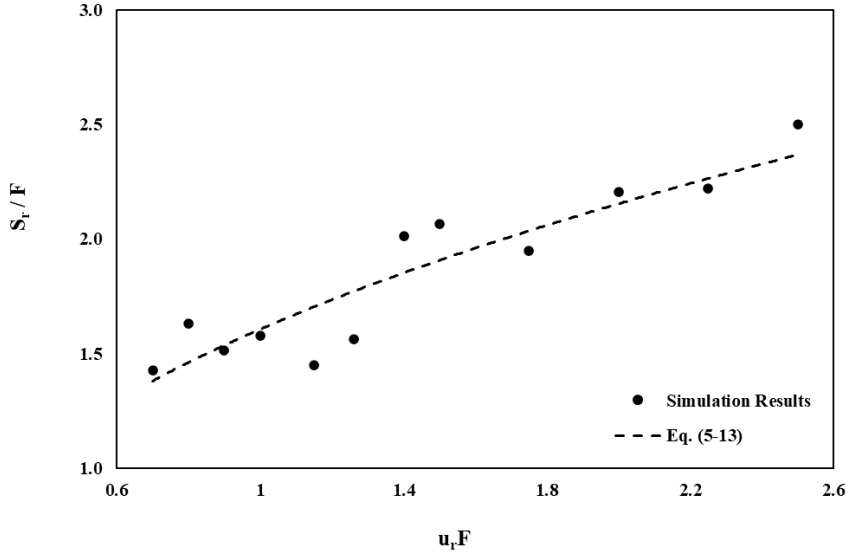

Figure 5-9 Dilution at the jet return point

5.4 Conclusions

This study investigated the behavior of inclined JICFs through the application of LES to simulate and assess their mixing performance across a range of cross-flow Froude numbers ($0.6 < u_r F < 2.6$). By validating the LES approach against experimental data, the accuracy and reliability of the method were approved for predicting key flow parameters, such as terminal rise height, return point, and dilution characteristics. The model predictions of the major flow parameters demonstrated excellent agreement with the experimental measurements, with a MAPE of less than 10%, confirming the accuracy of the model in the reproduction of dense jet dynamic behavior. The LES model also successfully captured the complex flow structures associated with JICFs, including the development of the CRVP and distinctive flow regimes that emerge with varying ambient current strengths.

The findings confirmed the existence of three distinct flow regimes: jet-dominated, regular cross-flow, and strong cross-flow-dominated, which are defined by the relative strength of the cross-flow current. In the jet-dominated regime, the jet momentum plays a central role, whereas the influence of the cross-flow becomes progressively more dominant in regular and strong cross-flow regimes. As the cross-flow Froude number increases, the jet trajectory flattens, leading to greater horizontal displacement, reduced terminal rise height, and enhanced mixing due to more extensive ambient entrainment.

Semi-empirical relationships were developed to describe the dependence of the terminal rise height, return point, and dilution on the cross-flow Froude number. According to the obtained equations, the terminal rise height is almost constant for the range of $u_r F < 1.0$, and then follows a dependency of $\sim(u_r F)^{-0.62}$ for the range of $u_r F > 1.0$. Moreover, the dilution at the terminal rise height, horizontal location of the jet return point, and its corresponding dilution follow a dependency of $\sim(u_r F)^{1/3}$, $\sim(u_r F)^{0.6}$, and $\sim(u_r F)^{0.4}$, respectively, within the tested range of $u_r F$. These relationships offer practical insights into the behavior of inclined dense jets in cross-flows, which is crucial for optimizing the design of submerged offshore outfall diffusers, especially in desalination applications where the environmental impact is a key concern. In particular, the results showed that dilution at both the terminal rise height and return point increases with the cross-flow Froude number, indicating that stronger ambient currents promote greater mixing efficiency and minimize the potential environmental risks associated with brine discharge.

Overall, this study enhances the understanding of dense JICFs and provides valuable data for improving outfall design and environmental impact assessments. Future research could further extend the analysis to include a broader range of discharge inclinations and ambient current conditions, as well as explore more complex stratified environments. The robustness of the LES method in accurately predicting the complicated flow behavior and mixing performance of dense JICFs is clearly demonstrated in this study. LES effectively resolved the large-scale turbulence structures that govern the jet trajectory and mixing, while accounting for the intricate interaction between buoyancy and cross-flow currents. Its ability to replicate experimental results with a high degree of accuracy, particularly in complex flow regimes, underscores the suitability of LES as a powerful tool for modeling and optimizing real-world environmental engineering problems, such as the design of submerged diffusers in dynamic marine environments.

5.5 References

[1] M. Taherian, S.A.R. Saeidi Hosseini, A. Mohammadian, Overview of Outfall Discharge Modeling with a Focus on Turbulence Modeling Approaches, in: Forum for Interdisciplinary Mathematics, Springer, 2022: pp. 139–177. https://doi.org/10.1007/978-981-19-1438-6_4.

[2] S.A.R. Saeidi Hossieni, A. Mohammadian, P.J.W. Roberts, O. Abessi, Numerical Study on the Effect of Port Orientation on Multiple Inclined Dense Jets, J Mar Sci Eng 10 (2022). https://doi.org/10.3390/jmse10050590.

[3] P. Palomar, I.J. Losada, Desalination in Spain: Recent developments and recommendations, Desalination 255 (2010) 97–106. https://doi.org/10.1016/J.DESAL.2010.01.008.

[4] R. Einav, F. Lokiec, Environmental aspects of a desalination plant in Ashkelon, Desalination 156 (2003) 79–85. https://doi.org/10.1016/S0011-9164(03)00328-X.

[5] A. Ramakanth, M.J. Davidson, R.I. Nokes, Laboratory study to quantify lower boundary influences on desalination discharges, Desalination 529 (2022). https://doi.org/10.1016/j.desal.2022.115641.

[6] M. Taherian, A. Mohammadian, Buoyant jets in cross-flows: Review, developments, and applications, J Mar Sci Eng 9 (2021). https://doi.org/10.3390/jmse9010061.

[7] M. Taherian, S.A.R. Saeidi Hosseini, A. Mohammadian, S. Ferrari, P.J.W. Roberts, Laboratory study on inclined desalination discharges in perpendicular cross-flow, Desalination 583 (2024) 117719. https://doi.org/10.1016/J.DESAL.2024.117719.

[8] E. Gungor, P.J.W. Roberts, Experimental studies on vertical dense jets in a flowing current, Journal of Hydraulic Engineering 135 (2009) 935–948. https://doi.org/10.1061/(ASCE)HY.1943-7900.0000106.

[9] S.A.R. Saeidi Hosseini, M. Taherian, A. Mohammadian, S. Ferrari, P.J.W. Roberts, Mixing behavior of multiport diffusers with non-uniform port orientation, Desalination 567 (2023). https://doi.org/10.1016/j.desal.2023.116962.

[10] S. Jenkins, J. Paduan, P.J.W. Roberts, D. Schlenk, J. Weis, Management of brine discharges to coastal waters recommendations of a science advisory panel (Tech. Report No. 694), Southern California Coastal Water Research Project, Costa Mesa, CA, USA, 2012.

[11] A. Gharavi, A. Mohammadian, I. Nistor, E. Peña, J. Anta, Experimental study of surface buoyant jets in crossflow, Environmental Fluid Mechanics 20 (2020) 1007–1030. https://doi.org/10.1007/s10652-020-09737-7.

[12] T.M. Missimer, B. Jones, R.G. Maliva, Intakes and Outfalls for Seawater Reverse-Osmosis Desalination Facilities: Innovations and Environmental Impacts, Springer, New York, 2015. https://doi.org/10.1007/978-3-319-13203-7.

[13] P.J.W. Roberts, A. Ferrier, G. Daviero, Mixing in Inclined Dense Jets, Journal of Hydraulic Engineering 123 (1997) 693–699. https://doi.org/10.1061/(asce)0733-9429(1997)123:8(693).

[14] I.G. Papakonstantis, E.I. Tsatsara, Mixing Characteristics of Inclined Turbulent Dense Jets, Environmental Processes 6 (2019) 525–541. https://doi.org/10.1007/s40710-019-00359-w.

[15] H. Kheirkhah Gildeh, A. Mohammadian, I. Nistor, Inclined dense effluent discharge modelling in shallow waters, Environmental Fluid Mechanics 21 (2021) 955–987. https://doi.org/10.1007/s10652-021-09805-6.

[16] Baum, M. Jeffrey, Dense jet behaviour in dynamic receiving environments, The University of Queensland, 2019. https://doi.org/10.14264/UQL.2019.247.

[17] M. Jiang, A.W.K. Law, S. Zhang, Mixing behavior of 45° inclined dense jets in currents, Journal of Hydro-Environment Research 18 (2018) 37–48. https://doi.org/10.1016/j.jher.2017.10.008.

[18] C.C.K. Lai, J.H.W. Lee, Initial mixing of inclined dense jet in perpendicular crossflow, Environmental Fluid Mechanics 14 (2014) 25–49. https://doi.org/10.1007/s10652-013-9290-7.

[19] P.J.W. Roberts, G. Toms, Inclined Dense Jets in Flowing Current, Journal of Hydraulic Engineering 113 (1987) 323–340. https://doi.org/10.1061/(asce)0733-9429(1987)113:3(323).

[20] M. Ben Meftah, M. Mossa, Turbulence measurement of vertical dense jets in crossflow, Water (Basel) 10 (2018) 286. https://doi.org/10.3390/w10030286.

[21] M. Ben Meftah, D. Malcangio, F. De Serio, M. Mossa, Vertical dense jet in flowing current, Environmental Fluid Mechanics 18 (2018) 75–96. https://doi.org/10.1007/s10652-017-9515-2.

[22] M. Taherian, S.A.R. Saeidi Hosseini, A. Mohammadian, Overview of Outfall Discharge Modeling with a Focus on Turbulence Modeling Approaches, in: D. Zeidan, L. Zhang,

E.G. Da Silva, J. Merker (Eds.), Advances in Fluid Mechanics: Modeling and Simulation, Springer Nature, Accepted, Singapore, 2022.

[23] J.H.W. Lee, V. Chu, Turbulent jets and plumes: a Lagrangian approach, Kluwer Academic Publishers, Massachusetts, USA, 2003.

[24] J.H.W. Lee, V. Cheung, Generalized Lagrangian Model for Buoyant Jets in Current, Journal of Environmental Engineering 116 (1990) 1085–1106. https://doi.org/10.1061/(asce)0733-9372(1990)116:6(1085).

[25] G.H. Jirka, Integral Model for Turbulent Buoyant Jets in Unbounded Stratified Flows. Part I: Single Round Jet, Environmental Fluid Mechanics 4 (2004) 1–56. https://doi.org/10.1023/A:1025583110842.

[26] W.E. Frick, Visual Plumes mixing zone modeling software, Environmental Modelling and Software 19 (2004) 645–654. https://doi.org/10.1016/j.envsoft.2003.08.018.

[27] P. Palomar, J.L. Lara, I.J. Losada, Near field brine discharge modeling part 2: Validation of commercial tools, Desalination 290 (2012) 28–42. https://doi.org/10.1016/j.desal.2011.10.021.

[28] M.J. Baum, B. Gibbes, Field-Scale Numerical Modeling of a Dense Multiport Diffuser Outfall in Crossflow, Journal of Hydraulic Engineering 146 (2020) 1–16. https://doi.org/10.1061/(ASCE)HY.1943-7900.0001635.

[29] A. Mohammadian, H. Kheirkhah Gildeh, I. Nistor, CFD Modeling of Effluent Discharges: A Review of Past Numerical Studies, Water (Basel) 12 (2020) 856. https://doi.org/10.3390/w12030856.

[30] P. Vafeiadou, I. Papakonstantis, G. Christodoulou, Numerical simulation of inclined negatively buoyant jets, in: Proceedings of the 9th International Conference on Environmental Science and Technology, Rhodes Island, Greece, 2005: pp. A1537–A1542.

[31] C. Oliver, M. Davidson, R. Nokes, k-ε Predictions of the initial mixing of desalination discharges, Environmental Fluid Mechanics 8 (2008) 617–625. https://doi.org/10.1007/s10652-008-9108-1.

[32] H. Kheirkhah Gildeh, A. Mohammadian, I. Nistor, H. Qiblawey, Numerical modeling of 30∘ and 45∘ inclined dense turbulent jets in stationary ambient, Environmental Fluid Mechanics 15 (2015) 537–562. https://doi.org/10.1007/s10652-014-9372-1.

[33] H. Kheirkhah Gildeh, A. Mohammadian, I. Nistor, H. Qiblawey, X. Yan, CFD modeling and analysis of the behavior of 30° and 45° inclined dense jets-new numerical insights, Journal of Applied Water Engineering and Research 4 (2016) 112–127. https://doi.org/10.1080/23249676.2015.1090351.

[34] S. Zhang, A.W.K. Law, M. Jiang, Large eddy simulations of 45° and 60° inclined dense jets with bottom impact, Journal of Hydro-Environment Research 15 (2017) 54–66. https://doi.org/10.1016/j.jher.2017.02.001.

[35] S. Zhang, B. Jiang, A.W.-K. Law, B. Zhao, Large eddy simulations of 45° inclined dense jets, Environmental Fluid Mechanics 16 (2016) 101–121. https://doi.org/10.1007/s10652- 015-9415-2.

[36] M. Jiang, A.W.K. Law, A.C.H. Lai, Turbulence characteristics of 45° inclined dense jets, Environmental Fluid Mechanics 19 (2019) 27–54. https://doi.org/10.1007/s10652-018-9614-8.

[37] F. Nicoud, F. Ducros, Subgrid-scale stress modelling based on the square of the velocity gradient tensor, Flow Turbul Combust 62 (1999) 183–200. https://doi.org/10.1023/A:1009995426001/METRICS.

[38] P. Sagaut, Large Eddy Simulation for Incompressible Flows: An Introduction, Springer Science & Business Media, 2004.

[39] T. Holzmann, 2016, Mathematics, numerics, derivations and OpenFOAM®, in: Loeben, Holzmann CFD, Germany. https://doi.org/10.13140/RG.2.2.27193.36960.

[40] F. Moukalled, L. Mangani, M. Darwish, The finite volume method, Fluid Mechanics and Its Applications 113 (2016) 103–135. https://doi.org/10.1007/978-3-319-16874-6_5/FIGURES/22.

[41] H. Jasak, Error analysis and estimation in the Finite Volume method with applications to fluid flows, (1996).

[42] J. Martínez, F. Piscaglia, A. Montorfano, A. Onorati, S.M. Aithal, Influence of spatial discretization schemes on accuracy of explicit LES: Canonical problems to engine-like geometries, Comput Fluids 117 (2015) 62–78. https://doi.org/10.1016/J.COMPFLUID.2015.05.007.

[43] A.S. Epikhin, Numerical Schemes and Hybrid Approach for the Simulation of Unsteady Turbulent Flows, Mathematical Models and Computer Simulations 11 (2019) 1019–1031. https://doi.org/10.1134/S2070048219060024/FIGURES/19.

[44] C. Geuzaine, J.-F. Remacle, An introduction to geometrical modelling and mesh generation with Gmsh, (2008).

[45] X. Yan, A. Mohammadian, Numerical Modeling of Multiple Inclined Dense Jets Discharged from Moderately Spaced Ports, Water (Basel) 11 (2019) 2077. https://doi.org/10.3390/w11102077.

[46] S. Ferrari, M.G. Badas, G. Querzoli, On the effect of regularwaves on inclined negatively buoyant jets, Water (Switzerland) 10 (2018). https://doi.org/10.3390/w10060726.

[47] O. Abessi, P.J.W. Roberts, Multiport Diffusers for Dense Discharges, Journal of Hydraulic Engineering 140 (2014) 04014032. https://doi.org/10.1061/(asce)hy.1943-7900.0000882.

[48] C.C.K. Lai, J.H.W. Lee, Mixing of inclined dense jets in stationary ambient, Journal of Hydro-Environment Research 6 (2012) 9–28. https://doi.org/10.1016/j.jher.2011.08.003.

[49] D. Shao, A.W.-K. Law, Mixing and boundary interactions of 30° and 45° inclined dense jets, Environmental Fluid Mechanics 10 (2010) 521–553. https://doi.org/10.1007/s10652-010-9171-2.

6 Summary, Concluding Remarks, and Recommendations

6.1 Summary and Concluding Remarks

Increasing global concern over freshwater scarcity and security has positioned seawater reverse osmosis (SWRO) desalination as a key solution for sustainable water supply. However, hypersaline effluents produced during this process pose environmental risks, including marine life disruption and water quality degradation. One effective strategy to mitigate these risks involves the use of submerged offshore diffusers, which promote the rapid dilution of these effluents to reduce environmental harm. Optimizing the diffuser design requires a thorough understanding of how ambient hydrodynamic forces and discharge characteristics affect their performance. Coastal environments, marked by dynamic currents, turbulence, and shear, complicate the mixing behavior of buoyant JICF. Through a comprehensive review of the literature, this study identified the challenges associated with dense JICFs that affect the mixing process and limit dilution. Accordingly, this research aims to enhance the accuracy of flow predictions and establish more precise design guidelines by investigating JICFs by combining both experimental and numerical approaches. This represents a pioneering effort to simulate dense discharges with various source inclinations in perpendicular cross-flow currents, offering valuable insights into improving the design and efficiency of dense outfall systems.

This study addresses these issues by conducting a comprehensive literature review, numerical analysis, and experimental investigation, all of which are explained below.

In chapter 2 of this thesis:

- A thorough explanation of the fundamental concepts related to outfall discharges into cross-flow currents and a critical review of the current state of the art in this domain are provided.
- Optimizing marine outfall discharges is crucial to minimize environmental impact and meet regulations.
- Cross-flow interactions create complex, unsteady flow structures that affect mixing and require detailed study.
- Advances in experimental techniques (LIF and PIV) and CFD tools have improved the understanding of buoyant JICFs.

- More experimental than numerical studies exist, highlighting the need for further numerical research.
- Vortical structures (e.g., CRVPs) are key to mixing; however, their origins and behaviors require further investigation.
- Key parameters like $u_r F$ influence jet dilution and trajectory of buoyant discharges.
- Integral models have limitations, while CFD methods provide more accurate predictions of complex flow behaviors.
- LES and hybrid CFD approaches offer better accuracy for dynamic, non-stationary flows but have higher computational costs.
- The review advances the understanding of JICFs, supporting future research and practical applications.
- The literature shows a scarcity of applications of both CFD and experimental techniques for understanding the interaction of varying cross-flow strengths and nozzle inclinations in the performance of dense JICFs.

In chapter 3 of this thesis:

- Efficient desalination diffuser design requires an understanding of factors affecting flow discharge and mixing behaviors.
- This study examined how different flowing current strengths and discharge inclinations (30°, 45°, and 60°) influence the outfall performance using LIF experiments.
- The critical range of $u_r F$ (between 1 and 2) was studied, where the jets experience significant bending.
- Key flow parameters (rise height, jet return point position, and dilution) were quantified using empirical equations derived to aid SWRO outfall design.
- The results showed that most flow parameters, except the terminal rise height, increased with higher cross-flow Froude numbers.
- Steeper discharge angles (60°) led to greater geometrical parameters (downstream return point, rise height, dilution) than shallower angles (30° and 45°).
- The 60° jet achieved approximately 40% and 16% longer return point positions and 36% and 10% higher rise heights than the 30° and 45° jets, respectively.
- Dilution at the terminal and return points improved significantly with increasing inclination, showing more than a two-fold increase between 30° and 60°.

- Higher $u_r F$ values and steeper angles produce more dispersed jets, increasing the interaction with ambient flows and leading to better dilution.
- Larger $u_r F$ values revealed more jet-ambient water interactions and higher entrainment of ambient water into the jet.
- High cross-flow Froude numbers and steeper jet inclinations (60°) are recommended for better dilution in dynamic water.
- This study provides insights for designing efficient outfalls in dynamic environments, particularly for shoreline regions with lower discharge inclinations.
- These results contribute to the development of mathematical models for dense jet dynamics and improve the design of brine effluent discharges.

In chapter 4 of this thesis:

- Submerged buoyant JICFs require further investigation to improve outfall design.
- A CFD numerical modeling approach was proposed to study submerged discharges under dynamic conditions.
- This study analyzed the performance of four RANS turbulence models: realizable k-ε, standard k-ε, LRR, and k-ω SST.
- The realizable k–ε and LRR schemes provided the most accurate results for capturing jet behavior during both the rising and falling phases and for predicting dilution.
- The realizable k–ε scheme is effective because of its realizability assumption, which addresses the limitations of other EVMs that assume isotropic eddy viscosity.
- This scheme ensures that the Reynolds stresses are physically realistic, particularly in high-shear regions near the jet discharges.
- The LRR scheme is also reliable, as it resolves the Reynolds stresses using Reynolds stress transport equations.
- The time-averaged CRVP structures were successfully modeled by realizable k–ε approach for outfall discharges into cross-flow environments.
- The CRVP structure caused bifurcation in the downstream flow field, enhancing the dilution and mixing after the dense jet reached the bottom.
- The success of the proposed CFD approaches demonstrates their potential for accurately simulating outfall discharges, warranting further investigation in future studies.

In chapter 5 of this thesis:

- The study aimed to investigate the behavior of inclined JICFs by simulating their mixing performance across various cross-flow Froude numbers ($0.6 < u_r F < 2.6$).
- The LES approach was validated against experimental data, demonstrating high accuracy in predicting major flow parameters.
- The model's predictions showed excellent agreement with experimental measurements, achieving a MAPE of less than 10%.
- The LES model effectively captured complex flow structures associated with JICFs, including the development of the CRVP and distinct flow regimes influenced by varying ambient current strengths.
- Three distinct flow regimes were confirmed as follows:
  - ✓ Jet-dominated: Jet momentum is predominant.
  - ✓ Regular cross-flow: A balance between jet momentum and cross-flow influence.
  - ✓ Strong cross-flow dominated: Cross-flow effects are significantly more dominant.
- As the cross-flow Froude number increases:
  - ✓ Jet trajectory flattens, leading to greater horizontal displacement.
  - ✓ Terminal rise height decreases.
  - ✓ Enhanced mixing occurs due to increased ambient entrainment.
- Relationships were developed to describe the dependencies of terminal rise height, return point, and dilution on the cross-flow Froude number, revealing:
  - o Terminal rise height remains constant for $u_r F < 1.0$ and decreases as $u_r F$ increases with a dependency of $\sim(u_r F)^{-0.62}$.
  - o Dilution at terminal rise height follows a dependency of $\sim(u_r F)^{1/3}$.
  - o Jet return point location and its corresponding dilution follow a dependency of $\sim(u_r F)^{0.6}$ and $\sim(u_r F)^{0.4}$, respectively.
- The study underscores the robustness of the LES method in accurately modeling the complicated flow behavior and mixing performance of dense JICFs, confirming its suitability for addressing real-world environmental engineering challenges.

6.2 Recommendations for Future Studies

The following recommendations are proposed for future studies on multiport diffusers with non-uniform port orientations.

- Although this study mainly focused on analyzing the mixing behavior up to the return point, it would be valuable to extend the investigation to compare the performance of outfall discharges at the end of the near-field or even into the far-field.
- Evaluating the prediction capabilities of integral and hybrid numerical models, such as detached-eddy simulations (DES), for dense JICFs and comparing their predictions with the applied closure models herein would be valuable and interesting.
- The experimental data presented in this study can be further used to validate the numerical models. Therefore, different turbulence models can be applied and their prediction capabilities can be evaluated against the outputs presented in this study.
- Extending the analysis to broader discharge inclinations and current conditions, and exploring more complex stratified environments are recommended.
- Since marine outfall discharges are frequently applied in deep-water environments, the impact of flow depth on jet mixing behavior requires more detailed investigation.
- The mixing and dilution behavior of marine outfall discharges under wave-forcing conditions, which are the dominant mixing mechanisms in coastal environments, remains largely unexplored. While data from discharges into uniform cross-flow conditions may be conservative, they still provide relevant insights for understanding these complex interactions.
- The presence of nearby boundaries, such as the seabed and shallow water surface, can significantly influence jet spreading behavior, adding complexity to the mixing dynamics of JICFs, which warrants further investigation.
- The limited understanding of the interaction between port spacing and cross-flow effects hinders the development of optimal designs for multiport diffuser systems, necessitating additional research.
- Artificial intelligence (AI) techniques have recently demonstrated significant potential in modeling and solving complex nonlinear problems in water and marine engineering. As a result, the extensive and valuable datasets generated from experimental and CFD studies on buoyant JICFs offer promising opportunities for future AI-driven research.

Appendix A: Overview of Outfall Discharge Modeling with a Focus on Turbulence Modeling Approaches[5]

Abstract

A comprehensive understanding of outfall discharge behavior can significantly benefit the optimal design of outfall systems while ensuring compliance with regulatory requirements. Advances in computational resources and techniques over the past two decades have paved the way for the introduction of numerical modeling as a promising approach for simulating outfall discharges and gathering comprehensive data for the entire outfall region. Thus, there is a growing need to explore numerical methods for modeling jet and plume-type flows in greater detail. Among the various numerical techniques available, the computational fluid dynamics (CFD) method stands out, as it can provide highly detailed insights into the flow patterns of outfall discharge systems without relying on some of the simplified assumptions found in length-scale and jet integral approaches. This chapter aims to offer an overview of the current state-of-the-art in outfall discharge modeling and a summary of the research endeavors undertaken in this field. Additionally, it explores different aspects concerning turbulence modeling approaches within the CFD technique, showcasing the applicability of both Reynolds-averaged Navier-Stokes (RANS) and large eddy simulation (LES) in the modeling of outfall discharges.

Keywords: environmental impacts; outfall discharge modeling; flow behavior; CFD technique; turbulence modeling approaches.

[5] This chapter has been published as a part of a book chapter as: Taherian, M., Saeidi Hosseini, S. A. R., & Mohammadian, A. (2022). Overview of outfall discharge modeling with a focus on turbulence modeling approaches. In Advances in Fluid Mechanics: Modelling and Simulations (pp. 139-177). Singapore: Springer Nature Singapore.

A.1 Introduction and Background

A.1.1 Environmental Impacts of Effluent Discharge

These days, the disposal of effluents from power plants, mining operations, and coastal desalination facilities into water bodies has become a serious global concern because of the subsequent public health-related and environmental problems (Missimer et al. 2015). These effluents, which can be in the form of brine or thermal discharges, may reduce the water quality, damage near-shore recreational sites, or even alter the marine ecosystems as a consequence of increasing turbidity, changing ambient temperature, etc.

In particular, regarding the brine discharges, since the effluent has a density higher than the ambient water, it sinks to the sea-bottom and creates a salty desert in the area of the outlet, which results in almost permanent adverse effects on marine habitats, such as the prevention of growth of marine species and the reduction of fish cultures (Einav and Lokiec 2003). Results have also shown that brine discharges from desalination plants are more likely to affect the local natural environment at the near-field of the discharge point (Einav and Lokiec 2003; Hashim and Hajjaj 2005). In addition, the direct discharge of thermal effluents makes the ambient flow environmentally unstable, which requires further dispersion facilities to protect the receiving water bodies. Thus, a quick dispersion and mixing of both types of effluent discharges is required to diminish the adverse marine environmental effects.

A.1.2 Environmental Regulations

The consideration of environmental standards and regulations, such as US Environmental Protection Agency (EPA) (EPA, 1994) and EU Water Framework Directive (WFD) (Chave, 2001), is vital during the design, implementation, and monitoring of outfall systems, irrespective of the type of discharge. The reason behind this is that without such regulations it is impossible to check if one discharge system is properly designed and capable of efficiently providing the required mixing at various distances. The requirements for wastewater and thermal discharges are being quite well developed. For instance, discharges into rivers, lakes, and coastal waters of the US are regulated via the National Pollutant Discharge Elimination System (NPDES) (T. Missimer et al., 2015). Some regulations for brine discharges and their compliance points are indicated in Table A-1. The international regulations are usually defined based on either the salinity increment or the absolute salinity at a specific distance from outfalls.

Table A-1 International brine discharge regulations (Missimer et al. 2015; Abessi 2018)

Region/Authority	Salinity increment limit (ppt)	Absolute salinity limit (ppt)	Compliance point (relative to discharge) (m)
Sydney, Australia	≤ 1	-	50-75
Gold Coast, Australia	≤ 2	-	120
Oman	≤ 2	-	300
US EPA	≤ 4	-	-
Okinawa, Japan	≤ 1	-	Mixing zone boundary
Huntington Beach, CA	-	≤ 40	304.8
Carlsbad, CA	-	≤ 40	304.8

A.1.3 Outfall Discharge System as a Solution

To minimize environmental impacts while agreeing with regulatory demands, the effluent needs to be discharged through an outfall discharge system in the form of turbulent buoyant jets from diffuser ports or nozzles (see Figure A-1), after a proper level of land-based treatment. These facilities can be introduced as a remedy for solving the limited mixing behavior issues as the effluents enter the receiving environments. The ambient fluid is quickly mixed with the buoyant jet by turbulent entrainment resulting from the velocity gradient between the surrounding water and the jet (Missimer et al. 2015). This buoyant jet also grows in size due to the entrainment, which results in the adequate dispersion of effluents.

Prior research has shown the effectiveness of outfall systems. For instance, the impact of diffuser installation on brine plume discharge from two desalination plants located in San Pedro del Pinatar, Murcia, SE Spain (2006-2011) was examined by Loya-Fernández et al. (2018). Field measurements indicated that the installation of the diffuser significantly improved the dispersion of the brine discharge, and the brine plume was completely diluted over a shorter distance from the discharge point. It was also found that the use of the diffuser increased the dilution rate of samples taken 1 Km away from the outfall by almost 17 times, which clearly shows the significant effect of a diffuser on brine dispersion.

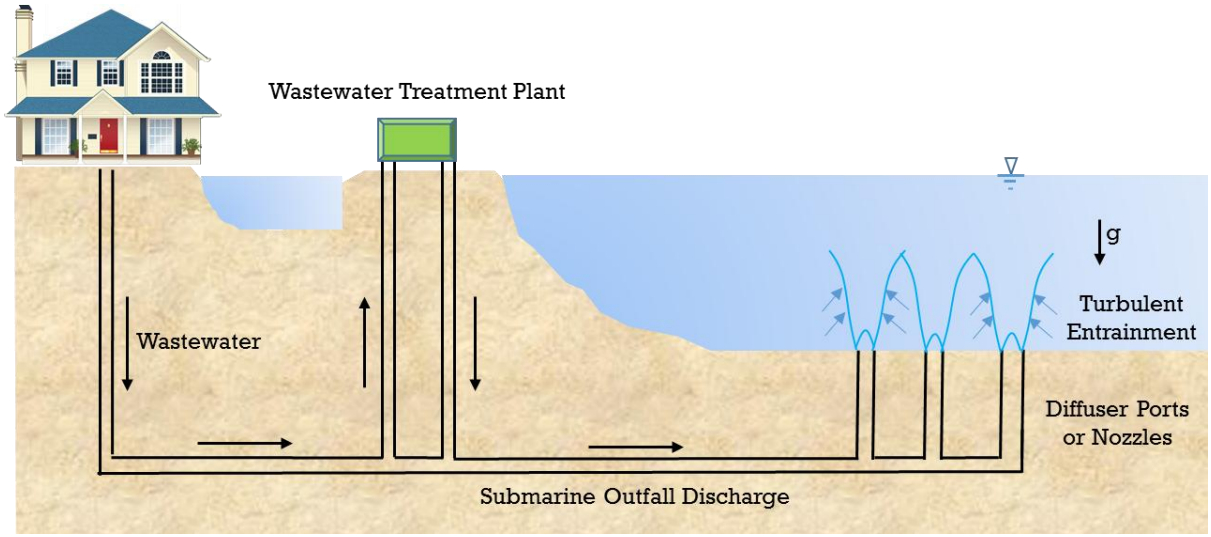

Figure A-1 Schematic of a tunneled marine outfall system

A.2 Outfall Discharge Mixing Behavior and Classification

A.2.1 Behavior of the Discharge: Near- and Far-Field Regions

The understanding of the behavior of discharges is closely related to the definitions and distinctions between different terms associated with outfall mixing. Table A-2 presents some common terminologies of outfall mixing.

Table A-2 Terminology for Outfall Mixing and Mixing Zones (Jenkins et al. 2012)

Term	Definition
Mixing Zone or Allocated Impact Zone (AIZ)	Refers to an area in which rapid mixing occurs and the numeric water quality criteria can go beyond what is allowed, although the intense toxic conditions have to be halted. Certain water quality provisions must be followed at the end of the AIZ.
Regulatory Mixing Zone or Legal Mixing Zone (LMZ)	As defined by the appropriate regulatory authority, can be a length, an area, or a volume of the receiving water bodies.
Near-Field or Hydrodynamic Mixing Zone	The zone where mixing is only induced by the processes resulting from the outfall. Near-field characteristics are closely dependent on the discharge parameters, and are under the control of the designer.
Far-Field	The ambient oceanic turbulence is the reason for the mixing processes in this region. Far-field mixing is not controlled by the engineer.
Initial Dilution	General terminology for the quick mixing occurring in the proximity of the outfall.

Zone of Initial Dilution (ZID)	Refers to a small zone in the immediate vicinity of the diffuser where dilution is mainly induced by both the momentum and buoyancy of the discharge.

Assume a jet discharge with an angle relative to the horizontal of θ_0, jet nozzle diameter of d_0, and port height of h_0 which releases an effluent with a density of ρ_0, concentration of C_0, and discharge velocity of U_0 into the stagnant receiving environment with an ambient density of ρ_a ($< \rho_0$), concentration of C_a, and flow depth of H_a. As shown in Figure A-2, the mixing process of this type of outfall discharge is typically divided into two regions.

The first region, which is located in the proximity of the discharge point, is named the near-field. This region is often characterized by its initial mixing, which significantly depends on the discharge configuration design and the effluent and ambient properties. Normally, a brine discharge system should be designed in such a way that maximum dilution can happen in the near-field region. In this region, the dilution rate is very high, and intense mixing occurs since mixing is a consequence of the initial buoyancy and momentum of the high-velocity discharge and their interaction with the ambient fluid. Furthermore, mixing and flow characteristics are dominated by small scales (~meters and ~minutes). According to (Roberts et al. 1997), the location where self-induced turbulence collapses under the effect of the induced density stratification is recognized as the end of the near-field, although it has not been uniquely defined.

The second region, which occurs beyond the near-field and further away from the discharge point or diffuser, is called the far-field, where the effluent moves along the bottom of the ocean as a density current. In this region, self-induced turbulence almost vanishes, mixing is predominantly caused by ambient turbulence, and the dilution rate is much lower compared to the near-field. Furthermore, mixing and flow features are dominated by large scales (~kilometers and ~hours) (Palomar and Losada 2011).

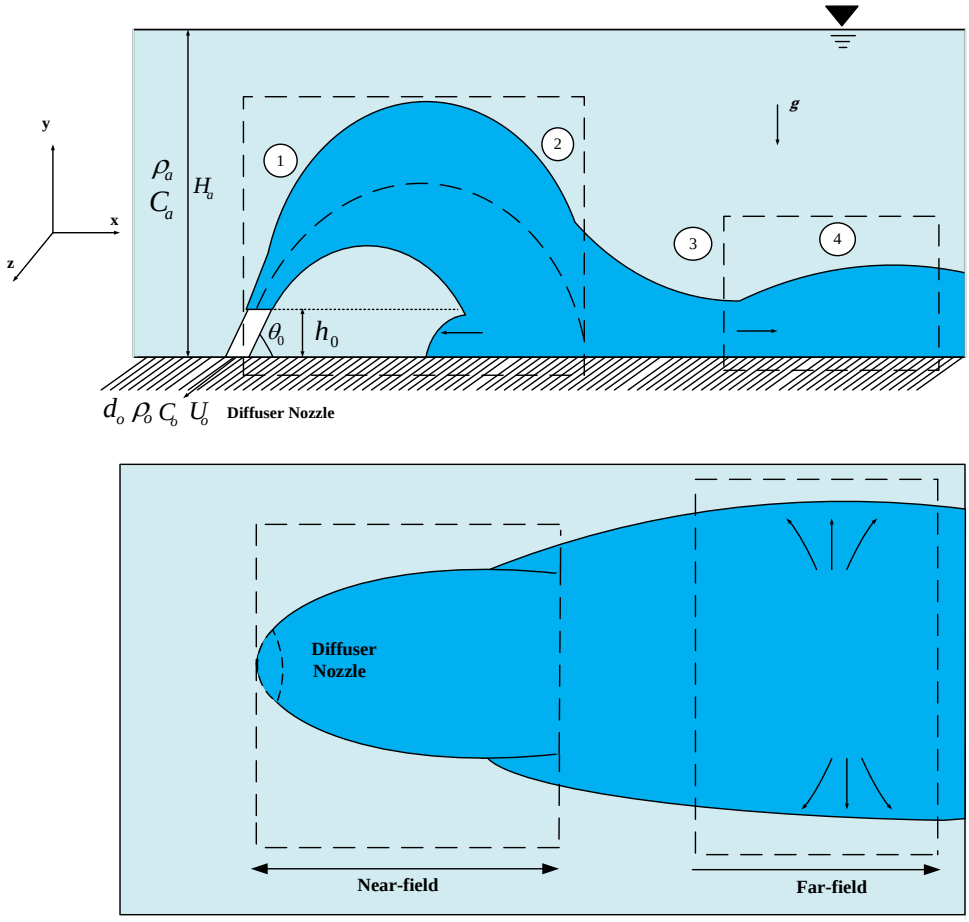

(Top view)

Figure A-2 Near- and far-field regions in a jet discharge

More precisely, the different flow behaviors of a brine jet discharge can be categorized into four regions (see Figure A-2), as specified by the following. In region (1), the momentum greatly impacts the ascending trajectory of the jet because of the inclined initial velocity. The momentum continuously decreases up to the point where the jet maximum height occurs; at this point, the momentum and buoyancy force are equal. In region (2), the buoyancy force is the predominant force, which leads the jet to descend until it reaches the seabed, where further dilution occurs as the effluent expands. Region (3) is called the transition zone and acts as a "spreading layer". This region covers the area between the impact point and the far-field region. Finally, in region (4), the far-field, the effluent acts as a density current (Palomar and Losada 2011).

A.2.2 Outfall Discharge Principles and Classification

The Froude number is an important non-dimensional parameter in fluid dynamics and is mainly related to the influence of gravity on fluid motion. It can be defined as:

$$F_r = \frac{u}{\sqrt{gl}} \tag{A-1}$$

where u is the characteristic flow velocity, g is the acceleration of the external field, and l is the characteristic length depending on the geometry of the flow channel.

However, when it comes to buoyant jets, the densimetric Froude number (F_0) is more common, which can be expressed as follows:

$$F_0 = \frac{U_0}{\sqrt{g'l}} \tag{A-2}$$

$$g' = \frac{\Delta\rho}{\rho_0} g \tag{A-3}$$

where g' is the modified gravitational buoyancy acceleration and $\Delta\rho$ is the density difference between the jet flow and the ambient fluid.

To design an ocean outfall system, it is essential to adopt the most efficient discharge form to reach rapid and efficient mixing. The classification of buoyant jets can vary depending on the different standards. Buoyant jets can be classified based on the discharge location, the jet density relative to the ambient water, or the discharge direction.

Regarding the discharge location, wastewaters may be discharged either as surface or submerged jets. Surface discharges do not achieve efficient mixing and rapidly change to density currents moving at the bottom of the surrounding water. However, the dilution rates for submerged jets are much higher compared to surface discharges since the surrounding fluid entrains into the jet in all directions. Previous studies confirm the idea that efficient mixing of the highly concentrated brine effluent can be reached by submerged discharge in an upwards direction as a high velocity turbulent jet (Roberts et al. 1997; Kheirkhah Gildeh et al. 2015; Loya-Fernández et al. 2018).

Considering the jet density compared to the surrounding water density, jets can be categorized into two main groups: positively and negatively buoyant jets, as shown in Figure A-3. A positively buoyant jet has a density less than the ambient fluid density ($\rho_0 < \rho_a$) so that both momentum and buoyancy affect the flow dynamics. Thermal discharges from power plants into colder ambient water and sewage discharges into denser ocean water can be the most applicable examples of positively buoyant jets. The effluent rises because of buoyancy forces until it reaches the water surface, and then spreads horizontally as plumes. However, the

effluent may not reach the water surface in a stratified ambient. In stratified receiving water, the effluent rises to a level where its density is the same as the ambient water, then spreads horizontally. In contrast, a negatively buoyant jet has a density higher than the ambient water ($\rho_0 > \rho_a$); as a result, its trajectory is completely different. Since the jet density is higher than the receiving water, the negative buoyancy causes the dense jet to reach a terminal rise height and then fall back to the lower boundary. Once the dense jet impacts the seabed, it spreads as a density current.

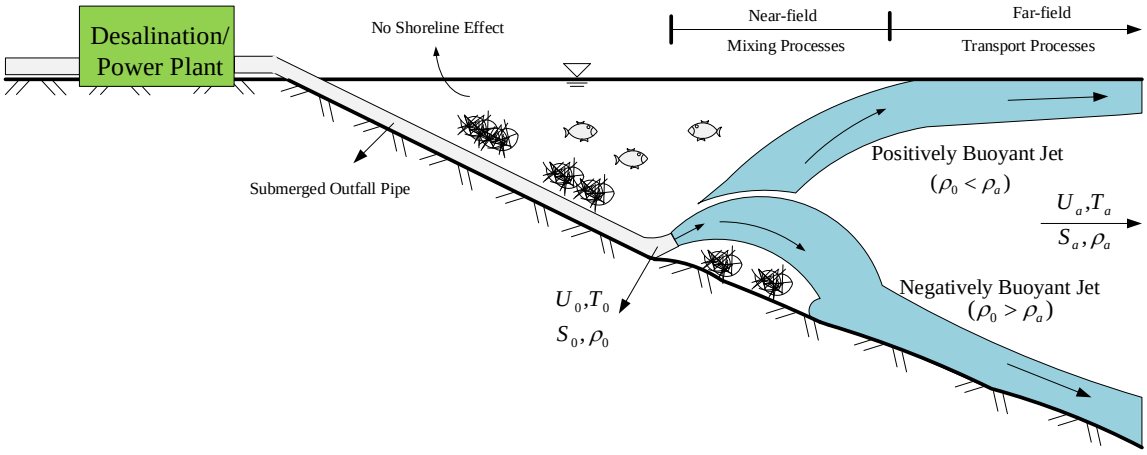

Figure A-3 Schematic of flow discharges in positively and negatively buoyant jets

(*U, T, S* denote the velocity, temperature, and salinity parameters, respectively; the subscripts *0* and *a* represent the jet and ambient characteristics, respectively.)

A buoyant jet can also be discharged horizontally (horizontal jet) or upwards, either vertically (vertical jet) or at some angle to the horizontal (inclined jet). The vertical dense jet in stagnant water tends to fall back on the source. This feature disturbs the dilution process and causes lower dilution, which may not be desirable in outfall discharge design (Missimer et al. 2015; Roberts et al. 1997; Fischer et al. 2013). In contrast, inclined jets can clear the effluent from the jet discharge site because of their horizontal component of momentum (Pincince and List 1973).

A.3 Outfall Discharge Modeling

A.3.1 Governing Equations

The mathematical representation of fluid flow processes in outfall discharges generally involves a set of partial differential equations (PDEs) of continuity and momentum, which are known as Navier-Stokes equations.

The conservation of mass is governed by the continuity equation, which can be written in the incompressible form (which means the pressure does not affect the density of fluid) as follows:

$$\frac{\partial u}{\partial x}+\frac{\partial v}{\partial y}+\frac{\partial w}{\partial z}=0 \tag{A-4}$$

where u, v, and w are the mean velocity in the *x*, *y*, and *z* directions, respectively.

The momentum equations for the three-dimensional incompressible fluids and in non-conservation form can also be expressed as:

$$\frac{Du}{Dt}=-\frac{1}{\rho}\frac{\partial p}{\partial x}+\frac{\partial}{\partial x}\left(\nu_{eff}\left(\frac{\partial u}{\partial x}\right)\right)+\frac{\partial}{\partial y}\left(\nu_{eff}\left(\frac{\partial u}{\partial y}\right)\right)+\frac{\partial}{\partial z}\left(\nu_{eff}\left(\frac{\partial u}{\partial z}\right)\right) \tag{A-5}$$

$$\frac{Dv}{Dt}=-\frac{1}{\rho}\frac{\partial p}{\partial y}+\frac{\partial}{\partial x}\left(\nu_{eff}\left(\frac{\partial v}{\partial x}\right)\right)+\frac{\partial}{\partial y}\left(\nu_{eff}\left(\frac{\partial v}{\partial y}\right)\right)+\frac{\partial}{\partial z}\left(\nu_{eff}\left(\frac{\partial v}{\partial z}\right)\right)-g\frac{\rho-\rho_0}{\rho} \tag{A-6}$$

$$\frac{Dw}{Dt}=-\frac{1}{\rho}\frac{\partial p}{\partial z}+\frac{\partial}{\partial x}\left(\nu_{eff}\left(\frac{\partial w}{\partial x}\right)\right)+\frac{\partial}{\partial y}\left(\nu_{eff}\left(\frac{\partial w}{\partial y}\right)\right)+\frac{\partial}{\partial z}\left(\nu_{eff}\left(\frac{\partial w}{\partial z}\right)\right) \tag{A-7}$$

where t is time, ν_{eff} is the effective kinematic viscosity ($\nu_{eff}=\nu+\nu_t$; ν_t is the turbulent kinematic viscosity), and *p* represents the fluid pressure.

It is worthwhile mentioning that to capture the variable density impacts, the buoyancy term $g\frac{\rho-\rho_0}{\rho}$ only exists in the momentum equation in the vertical direction (*y*-coordinate), and the term ρ exists in all momentum equations. For an incompressible fluid, the density can be calculated for both the surrounding fluid and the jet considering temperature (*T*) and salinity (*S*). In this regard, normally the empirical equation proposed by Millero and Poisson is applied (Millero et al. 1981):

$$\rho(T,S)=\rho_t+aS+bS^{3/2}+cS^2 \tag{A-8}$$

where empirical parameters ρ_t (the density of water changing with the temperature), *a*, *b*, and *c* can be defined as presented in Table A-3.

Along with the Navier-Stokes equations, the advection-diffusion equation governs the fluid concentration and temperature evolution over time in the system as follows:

Table A-3 Definition of empirical equation parameters used for the determination of density (Millero et al. 1981)

Empirical equation parameters (T [°C]): $\alpha + \beta T + \gamma T^2 + \delta T^3 + \theta T^4 + \varphi T^5$						
Empirical Parameters	**Coefficients**					
	α	β	γ	δ	θ	φ
ρ_t	999.842594	6.793952×10^{-2}	-9.09529×10^{-3}	1.001685×10^{-4}	-1.120083×10^{-6}	6.536332×10^{-9}
a	0.824493	-4.0899×10^{-3}	7.6438×10^{-5}	-8.2467×10^{-7}	5.3875×10^{-9}	-
b	-5.72466×10^{-3}	1.0227×10^{-4}	-1.6546×10^{-6}	-	-	-
c	4.8314×10^{-4}	-	-	-	-	-

$$\frac{DC}{Dt} = D\left(\frac{\partial^2 C}{\partial x^2} + \frac{\partial^2 C}{\partial y^2} + \frac{\partial^2 C}{\partial z^2}\right) \quad \text{(A-9)}$$

$$\frac{DT}{Dt} = k_{eff}\left(\frac{\partial^2 T}{\partial x^2} + \frac{\partial^2 T}{\partial y^2} + \frac{\partial^2 T}{\partial z^2}\right); \text{ with } k_{eff} = \frac{\nu_t}{Pr_t} + \frac{\nu}{Pr} \quad \text{(A-10)}$$

where C is the fluid concentration/salinity, D is the diffusion coefficient, T is the fluid temperature, k_{eff} is the heat transfer coefficient, Pr is the Prandtl number, and Pr_t is the turbulent Prandtl number.

Once the simplifying assumptions have been used, the governed PDEs are solved using available numerical techniques. It should be noted that the successful applications of these governing equations on outfall discharge modeling have been validated in prior research (Kheirkhah Gildeh et al. 2015; Kheirkhah Gildeh et al. 2014; Kheirkhah Gildeh et al. 2016; Yan et al. 2020b; Yan et al. 2019; Yan and Mohammadian 2019).

A.3.2 Solution Methods and Simulation Techniques for Discharge Modeling

There are three different solution approaches for the modeling of the behavior of outfall discharges, including length-scale models, jet integral models, and computational fluid dynamics (CFD) models (Taherian and Mohammadian 2021). Length-scale models, which are driven from the dimensional analysis of jet and plume mixing behavior, are a type of semi-empirical approach requiring large amounts of experimental and field data in order to generate a relatively accurate performance (see Sections A.4.1.1 and A.4.2.1 for details). As a result,

these models are obtained from highly simplified formulas for the flow characterization of outfall discharges and can only be reliable in obtaining general knowledge of their design. CORMIX and NRFIELD are among the common simulation tools being used based on the length-scale models.

Jet integral models solve the flow governing equations based on their integration over the cross-section and then these PDEs are transformed into a simple set of ordinary differential equations (ODEs) while using numerical solution methods such as the Runge Kutta formula. In these models, the velocity profile of jets is assumed to be axisymmetric and Gaussian, having no radial variations. The deficiency in comprehension of horizontal and lateral boundary effects, unsteady ambient flow situations, and unstable near-field conditions (re-entrainment of effluent into the jet as an example) may cause some limitations in the applications of jet integral models. JetLag of VISJET software, UM3 of Visual Plumes software, CoreJet of CORMIX software are among the available simulation tools being used based on the jet integral models.

The application of CFD modeling in the simulation of a large number of turbulent flows in nature, as well as engineering, has been increased recently (Jenkins et al. 2012). In CFD modeling, some turbulence closure assumptions are usually adopted to be able to numerically solve the equations of continuity and momentum; to review various CFD methods see (Sotiropoulos 2005). In general, two widely-used discretization methods are developed to address governing equations of the flow problems, namely finite difference method (FDM) and finite volume method (FVM). Different software packages and codes are being applied in the CFD numerical simulations such as ANSYS Fluent, OpenFOAM (OPEN Field Operation And Manipulation), and SU2 code.

With the recent advent of progressive CFD tools and robust computational resources, there is a great opportunity to overcome the deficiency of length-scale and jet integral models in the simulation of outfall discharge systems. CFD techniques can provide more detailed information on the flow fields of outfall discharges without considering some of the simplified assumptions of previous approaches. However, they require more sophisticated computational procedures to close the system of equations. Since most of the flow in outfalls are turbulent, the analysis of different applicable turbulence modeling approaches is important in order to accurately determine the discharge behaviors.

A.3.3 Turbulence Modeling

Turbulence modeling involves a large number of scale motions that need to be resolved or modeled. The three methods of Reynolds-averaged Navier-Stokes (RANS), large eddy simulation (LES), and direct numerical simulation (DNS) are the main numerical methods used to model turbulent flows. The application of DNS for the prediction of the mixing behavior of outfall discharges is limited since it requires a very high computational cost, although it can resolve all the turbulent flow problems. In this section, the two most practical modeling approaches of RANS and LES in outfall discharge modeling are described.

A.3.3.1 Reynolds-Averaged Navier-Stokes (RANS)

The focus of the RANS method is on the effects of turbulence on the mean flow field properties. In this approach, Navier-Stokes equations are usually time averaged before being numerically solved. More precisely, any instantaneous flow variable is decomposed into mean and fluctuating components. Afterward, they are replaced in the original equations, then the obtained equations are time-averaged (Versteeg and Malalasekera 2007; Moukalled et al. 2016). Figure A-4 represents fluctuating ($\emptyset'(t)$) and mean ($\overline{\emptyset}$) components of an instantaneous variable ($\emptyset(t)$). Each instantaneous variable ($\emptyset(t)$) can be demonstrated as in Eq. (A-11):

$$\emptyset(t) = \overline{\emptyset} + \emptyset'(t) \tag{A-11}$$

For instance, the instantaneous values of velocity (u) and pressure (p) can be decomposed as fluctuating components of u' and p', and mean values as $\bar{u}$ and $\bar{p}$:

$$u_i = \bar{u}_i + u_i' \tag{A-12}$$

$$p = \bar{p} + p' \tag{A-13}$$

The spread of the fluctuation component about the mean is usually represented by the variance $\overline{(\emptyset')^2}$:

$$\overline{(\emptyset')^2} = \frac{1}{\Delta t}\int_0^{\Delta t} (\emptyset')^2 dt \tag{A-14}$$

The velocity variances $\overline{(u_1')^2}$, $\overline{(u_2')^2}$, and $\overline{(u_3')^2}$ are employed to define the turbulent kinetic energy per mass (k) as Equation (2-8), where u_1', u_2' and u_3' are the fluctuations of the velocity components.

$$k = 0 \cdot 5\left(\overline{(u_1')^2} + \overline{(u_2')^2} + \overline{(u_3')^2}\right) \tag{A-15}$$

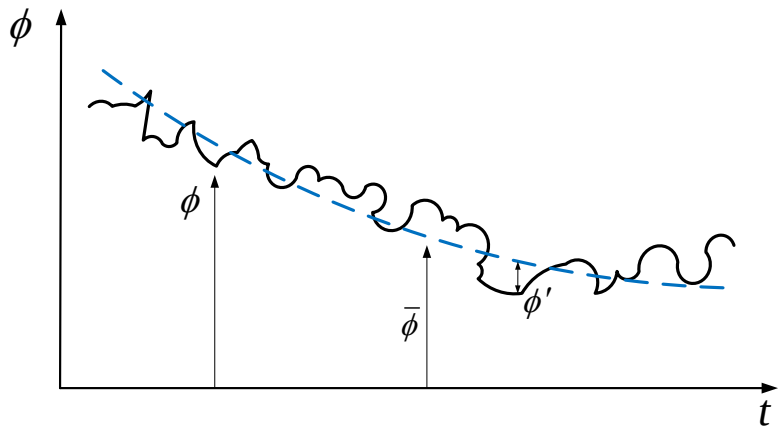

Figure A-4 An instantaneous variable and its mean and fluctuating components

Time averaging of Navier-Stokes equations leads to so-called RANS equations, which can be expressed as follows:

$$\frac{\partial \bar{u}_i}{\partial x_i} = 0 \tag{A-16}$$

$$\rho \frac{\partial \bar{u}_i}{\partial t} + \rho \bar{u}_j \frac{\partial \bar{u}_i}{\partial x_j} = -\frac{\partial p}{\partial x_i} + \frac{\partial}{\partial x_i}\left[\mu\left(\frac{\partial \bar{u}_i}{\partial x_j} + \frac{\partial \bar{u}_j}{\partial x_i}\right) - \rho \overline{u'}_i \overline{u'}_j\right] + \rho g \tag{A-17}$$

where μ is the dynamic viscosity of the fluid.

The process of time averaging results in the introduction of six extra unknowns of the Reynolds stress tensor ($-\rho \overline{u'}_i \overline{u'}_j$). These unknown terms must be estimated to be able to close the system of equations; otherwise, the closure problem emerges. Therefore, various turbulence models are developed to perform the estimations, which introduce additional transport equations in most cases. Turbulence models can be categorized based on the number of these extra transport equations into:

- Algebraic models (zero additional equation)

  In these models, eddy viscosity is computed based on an algebraic equation.
- Spalart-Allmaras models (one additional equation)

  In these models, one turbulent quantity is obtained based on a transport equation, and another turbulent quantity is acquired based on an algebraic expression.
- $k - \varepsilon$ and $k - \omega$ models (two additional equations)

These models are more complicated and apply two transport equations, which describe transport of two scalars. For instance, in the case of the $k-\varepsilon$ model, one transport equation is applied to describe transport of the turbulent kinetic energy and one for its dissipation.

- Reynold stress models (seven additional equations)

  These models consider six transport equations for the Reynolds tensor and one equation for the length scale of the turbulence.

From another point of view, the RANS turbulence models can be classified into Eddy viscosity model and Reynolds stress model (RSM), as discussed below.

A.3.3.1.1 Eddy Viscosity Model

This model has been proposed based on the Boussinesq assumption, which declares that Reynolds stresses are proportional to mean rates of deformation:

$$-\rho\overline{u'}_i\overline{u'}_j = \tau_{ij} = \mu_t\left(\frac{\partial\bar{u}_i}{\partial x_j}+\frac{\partial\bar{u}_j}{\partial x_i}\right)-\frac{2}{3}\rho k\delta_{ij} \tag{A-18}$$

where μ_t is the eddy viscosity and δ_{ij} is the Kronecker delta:

$$\begin{aligned}&\delta_{ij} = 1\ if\ i=j\\&\delta_{ij} = 0\ if\ i\neq j\end{aligned} \tag{A-19}$$

The Kronecker delta causes the correct answers for the normal Reynold stresses, where $i=j$. $k-\omega$, shear stress transport (SST) $k-\omega$, standard $k-\varepsilon$, re-normalization group (RNG) $k-\varepsilon$, and realizable $k-\varepsilon$ can be the best examples of the turbulence models based on the eddy viscosity model.

A.3.3.1.2 Reynolds Stress Model (RSM)

This model applies the Reynolds stress transport equations to obtain the Reynolds stress tensor. Accordingly, the direct effects of the Reynolds stress field can be achieved. This leads RSM to perform better compared to the Eddy viscosity model under the conditions where the flow fields are sophisticated (Versteeg & Malalasekera, 2007).

The Reynolds stress (R_{ij}) and the transport equation of R_{ij} are presented as Eqs. (A-20) and (A-21), respectively:

$$R_{ij} = -\frac{\tau_{ij}}{\rho} = \bar{u}_i\bar{u}_j - \overline{u_\iota u_J} \tag{A-20}$$

$$\frac{\partial R_{ij}}{\partial t} + u_j\frac{\partial R_{ij}}{\partial x_j} = P_{ij} + D_{ij} - \varepsilon_{ij} + \Pi_{ij} + \Omega_{ij} \tag{A-21}$$

where $\frac{\partial R_{ij}}{\partial t}$ is the rate of change of R_{ij}, $u_j\frac{\partial R_{ij}}{\partial x_j}$ is the transport term by convection, P_{ij} is the production rate of R_{ij}, D_{ij} is the transport term by diffusion, ε_{ij} is the dissipation rate of R_{ij}, Π_{ij} is the transport term by turbulent pressure-strain interactions, and Ω_{ij} is the transport term by rotation. In RSM, three terms: convection, production, and rotation maintain their exact forms, and the terms of diffusion, dissipation rate, and pressure-strain interactions need to be modeled; see (Launder et al., 1975) and (Rodi, 1984) for the required models.

A.3.3.2 Large Eddy Simulation (LES)

The LES approach was first proposed by Smagorinsky (1963). LES is a method in which the different behavior of large and small eddies is considered. The large eddies are almost anisotropic and their behavior is affected by external forces, the geometry of the domain, and boundary conditions, while the small eddies are almost isotropic and homogeneous (Versteeg and Malalasekera 2007; Zhiyin 2015). Furthermore, the large eddies are the reason for most of the momentum transfer, and incorporate most of the turbulence energy (Zhiyin 2015). Unlike the RANS models in which all eddies are modeled, in the LES approach, the unsteady nature of the large eddies is directly computed, and just small eddies are modeled using turbulence models.

LES employs the following steps to simulate the behavior of flows. The procedure of the LES approach is demonstrated in Figure A-5. At first, a spatial filter function and a filter size are determined to distinguish between the large and small eddies. Afterward, the filter is applied to the flow equations; the large eddies are resolved and the small eddies are eliminated. At the end, the small eddies are modeled using sub-grid scale (SGS) models. It is worth noting that the accuracy of LES strictly depends on the adopted SGS model (Mohammadian et al. 2020). The small eddies can be accurately modeled since they are independent of boundary conditions and the flow type (Moukalled et al. 2016)..

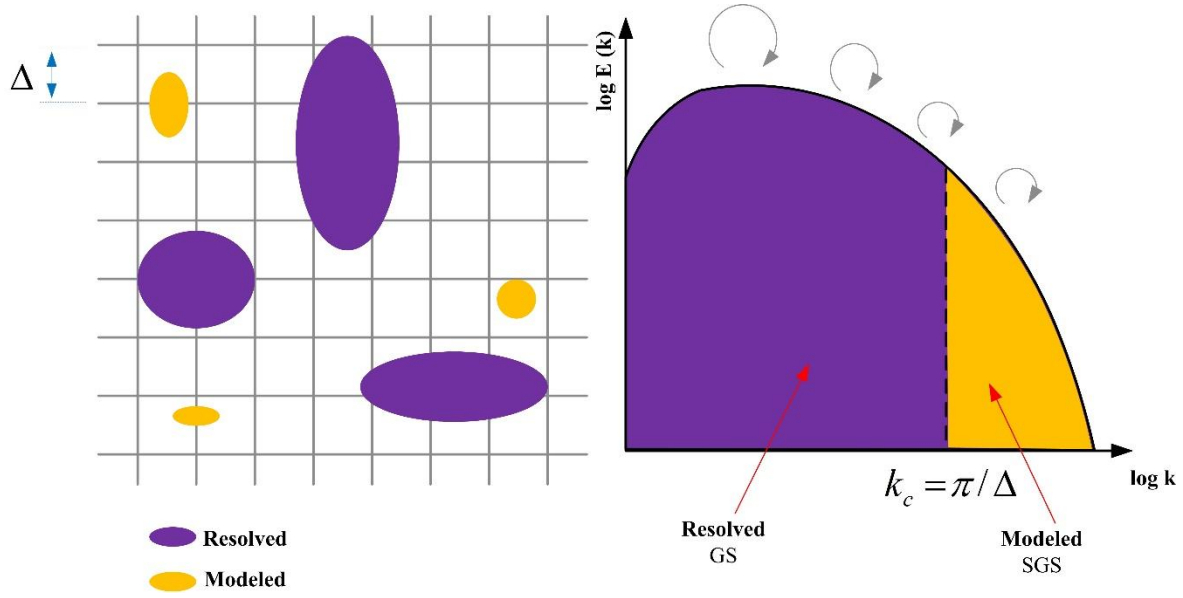

Figure A-5 Spatial filtering in the LES approach

The filtering operation in this method is defined as follows:

$$\bar{\varphi}(x.t) = \iiint_{-\infty}^{\infty} G(x.x'.\Delta)\varphi(x'.t)dx_1'dx_2'dx_3' \tag{A-22}$$

where $G(x.x'.\Delta)$ is the filtered function, Δ is the filter size, and $\varphi(x'.t)$ is the original function. Box filter, Gaussian filter, and spectral cutoff are the most common filtering functions in LES. The filter size (Δ) should not be smaller than the cell size. The truncation error can be almost eliminated when the filter size is larger than the cell size (Lund, 1997). It is usually considered to be the cube root of the cell volume (Versteeg & Malalasekera, 2007):

$$\Delta = \sqrt[3]{\Delta x \Delta y \Delta z} \tag{A-23}$$

where Δx, Δy, and Δz are the grid cell sizes in x, y, and z directions. The filtered Navier-Stokes equations including continuity and momentum equations can be presented for an incompressible fluid as Eqs. (A-24) and (A-25), respectively.

$$\frac{\partial(\bar{u}_i)}{\partial x_i} = 0 \tag{A-24}$$

$$\frac{\partial(\bar{u}_i)}{\partial t} + \frac{\partial(\bar{u}_i\bar{u}_j)}{\partial x_j} = -\frac{1}{\rho}\frac{\partial \bar{p}}{\partial x_i} + \nu\frac{\partial^2\bar{u}_i}{\partial x_j \partial x_j} - \frac{\partial \tau_{ij}}{\partial x_j} \tag{A-25}$$

where $\bar{u}_i$ is the filtered velocity, $\bar{p}$ is the filtered pressure field, and τ_{ij} indicates the SGS stresses.

The difference between the filtered velocity and the actual velocity is indicated in **Error! R eference source not found.**. The SGS stress can be defined as follows:

$$\tau_{ij} = \overline{u_i u_j} - \bar{u}_i \bar{u}_j \tag{A-26}$$

The SGS stresses in LES are somewhat like the Reynolds stresses in RANS, but they are created as a result of spatial filtering operation, not time averaging. Furthermore, like the Reynold stresses in RANS, they need to be modeled. They can be modeled either via standard or dynamic Smagorinsky methods.

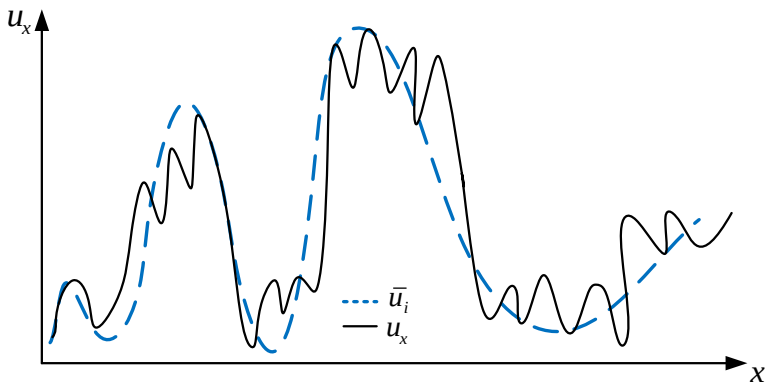

Figure A-6 Comparison of the filtered velocity and the actual velocity

A.3.3.3 Comparison of Turbulence Modeling Approaches

The relative advantages and disadvantages of applicable turbulence modeling approaches for the prediction of the mixing behavior of outfall systems can be explained by considering their conceptual differences.

RANS has some advantages over LES in simulating outfall discharges. The main relative advantages have to do with the computational cost and the validation. Time averaging and modeling all eddies allow RANS to have reasonable computational cost, which makes it quite favorable for industrial and full-scale simulations. When an engineer's focus is on the steady-state flow, simulation of detailed instantaneous flow is a waste of time and money. The computation of unsteady flow equations in LES leads it to require a much larger computational

expense compared to RANS. In addition to the fact that high computational time is undesirable for industrial applications, it may also lead to the unreliability of simulation results. The high computing times required for LES prevent performing multiple grid-dependency tests and sensitivity analysis in industrial studies, which may result in unreliable predictions (Gant 2010). Furthermore, the performance of RANS is validated by many studies, while there are fewer LES models, resulting in a lack of validation compared to the RANS method; therefore, the risk of applying LES models for field scale diffusers can be somewhat high. More precisely, to the authors' knowledge, there is no validated LES model for the simulation of multiport diffusers, even at the research stage. The limited studies on single port diffusers have mentioned the weakness of SGS models in dealing with low turbulence intensity (Zhang et al. 2015), the reproduction of the wall interaction processes (Zhang et al. 2017), and the convective mixing due to the buoyancy-induced instability (Zhang et al. 2016). In addition, a need for considering stratified effects in SGS models has been noted (Jiang et al. 2019). Due to the mentioned advantages, RANS has been the most widely used approach in industrial applications for turbulent flow simulations in recent decades (Moukalled et al. 2016).

On the other hand, LES has some unique features that distinguish it from RANS. The main superiority of LES over RANS is its accuracy and the detailed information that it can provide. Directly computing and capturing the large eddies which incorporate most of the turbulence energy has made LES a more accurate approach compared to RANS, in which all eddies are modeled. The dimensions of this difference may be even more highlighted for field-scale simulations. The accuracy of RANS has always been a concern in turbulent flow problems due to time averaging (Mohammadian et al. 2020). Furthermore, unlike RANS, LES is capable of providing statistics of the resolved fluctuations. With the recent advances in computational resources, more attention is given to these models, and the application of LES for industrial problems is becoming more promising (Moukalled et al. 2016; Mohammadian et al. 2020).

It should be noted that taking advantage of hybrid approaches such as detached eddy simulation (DES) has shown great potential in the simulation of turbulent flows, although it has not been adopted to simulate outfall discharges yet. For comparison, Table A-4 lists the differences between different turbulence modeling approaches.

Table A-4 Comparison between different applicable turbulence modeling approaches for outfall discharge modeling

Turbulence Models	Advantage	Limitations	Applications
DNS	1. Resolves NS equations with no turbulence approximation 2. Resolves all temporal and spatial turbulence scales	1. Extreme computational cost 2. Very fine meshes required to capture all the spatial scales	Simple flow or low Reynolds number flow/ less applicable to engineering problems
RANS	Most computationally inexpensive and easy to implement	Cannot be accurate within the entire flow field	Most suitable for steady flow
LES	1. High accuracy, as it directly computes large scale eddies 2. Much cheaper than DNS computationally due to modeling of only small scales	1. High computational cost 2. Small-scale turbulence theory still needs development for complex geometries	Unsteady flow with vortex and recirculation
DES	Combines the benefits of both RANS and LES	1. Difficult to couple RANS-LES interface 2. Unaffordable for large computational domains	Massively separated flow

A.4 Outfall Discharge Analysis and Design

A.4.1 Single Port Effluent Discharges

A.4.1.1 Dimensional Analysis

The primary flow parameters for a single brine jet in a stagnant ambient fluid are illustrated in Figure A-7. At first, due to the initial vertical momentum flux produced by the diffuser, the jet moves upwards. The buoyancy forces continuously decrease this momentum flux until it almost vanishes at the point where the jet reaches its maximum. Subsequently, the jet turns downwards and falls back to the sea bottom and develops as a gravity current.

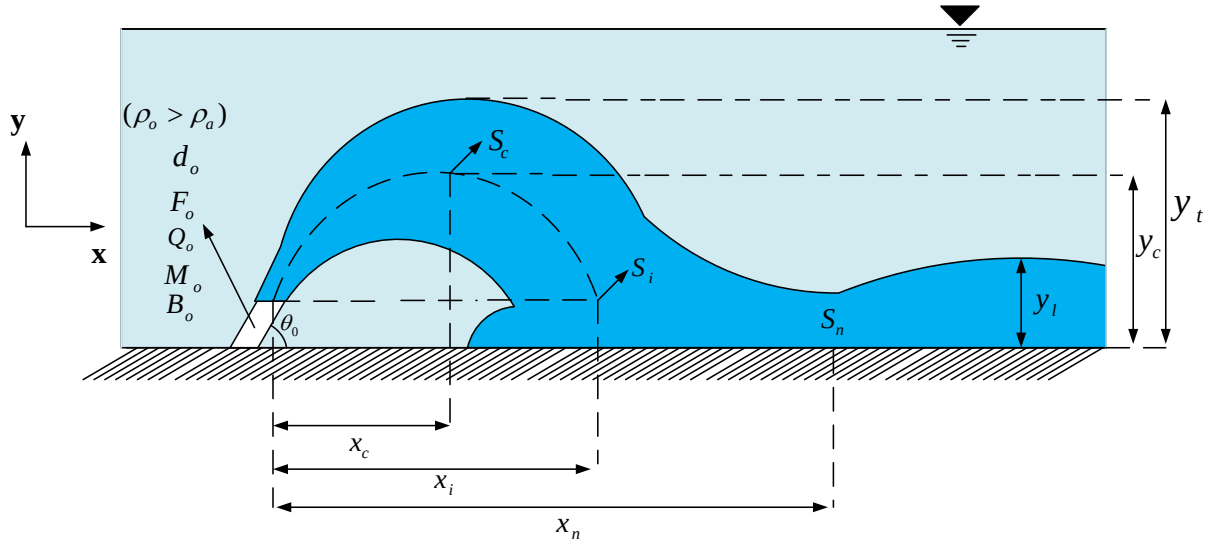

Figure A-7 Definition sketch for typical inclined jet parameters

Typically, jet-densimetric Froude number F_0, discharge volume flux Q_0, discharge momentum flux M_0, and discharge buoyancy flux B_0 determine the primary flow characteristics of the jet. These variables in the dimensional analysis are defined as follows:

$$Q_0 = \frac{\pi d_0^2}{4} U_0 \, , M_0 = \frac{\pi d_0^2}{4} U_0^2 = U_0 Q_0 , B_0 = \mathrm{g} \frac{\rho_0 - \rho_a}{\rho_a} Q_0 = \mathrm{g}_0' Q_0 \qquad \text{(A-27)}$$

where g_0' is the reduced gravitational buoyancy acceleration at the source. Furthermore, the flow characteristics mainly depend on some length scales derived from the volume, momentum, and buoyancy fluxes. These length scales are as below (P. J. W. Roberts & Toms, 1988):

$$l_M = \frac{M_0^{3/4}}{B_0^{1/2}} \;\; and \;\; l_Q = \frac{Q_0}{M_0^{1/2}} \qquad \text{(A-28)}$$

l_Q quantifies the distance over which the volume flux of the entrained ambient fluid becomes approximately equal to the initial volume flux. Therefore, for distances from the nozzle much larger than l_Q, the initial volume flux will not dynamically be of significance. l_M is a measure of the distance over which the buoyancy generates momentum approximately equal to the initial momentum. At distances from the nozzle much greater than l_M the effect of initial momentum flux becomes negligible and the buoyant jet has essentially become a plume (Wright 1984; Roberts et al. 1997; Doneker and Jirka 2007). It should be mentioned that since the direction of momentum and buoyancy are different in negatively buoyant jets, the initial momentum flux will always be an important parameter (Roberts et al. 1997)

Considering the assumption that states the flow is fully turbulent, any dependent variable, for example, the terminal rise height y_t, is a function of Q_0, M_0, and B_0 only:

$$y_t = f(Q_0, M_0, B_0) \tag{A-29}$$

The maximum rise height can be expressed in terms of the two length scales:

$$\frac{y_t}{l_M} = f\left(\frac{l_M}{l_Q}\right) \tag{A-30}$$

For $l_M >> l_Q$, the effect of the source volume flux becomes negligible, and Eq. (A-30) turns into:

$$\frac{y_t}{l_M} = K \tag{A-31}$$

where K is a constant. Eq. (A-31) can be rewritten as below for a round jet.

$$\frac{y_t}{d_0} = c_1 F_0 \tag{A-32}$$

where F_0 is the jet-densimetric Froude number and c_1 is a constant. Applying the same procedure, the other geometric jet parameters including the maximum centerline height y_c and its relevant horizontal location x_c, the thickness of the spreading layer y_l, the impact point location x_i, and the length of the near-field x_n can be similarly obtained, as Eq. (A-33). Moreover, the minimum dilution at the horizontal location x_c (S_c), the impact dilution S_i, and the ultimate dilution S_n are found to be constant as follows:

$$\frac{y_c}{d_0 F_0}, \frac{y_l}{d_0 F_0}, \frac{x_c}{d_0 F_0}, \frac{x_i}{d_0 F_0}, \frac{x_n}{d_0 F_0} = c_2, c_3, c_4, c_5, c_6 \quad \frac{S_c}{F_0}, \frac{S_i}{F_0}, \frac{S_n}{F_0} = c_7, c_8, c_9 \tag{A-33}$$

These constants (c_1 to c_9) are estimated by experiments and specify the trajectory of the jet and dilution rate at different points for the jet.

A.4.1.2 Numerical Studies

Generally, employing the proper discharge characteristics (like angle and configuration) and appropriate ambient water characteristics (like water depth and forcing currents) would be beneficial in obtaining an efficient mixing of effluent discharges into the receiving water bodies. Extensive studies have been conducted on the flow behavior of jets and plumes, taking into account the optimization of the discharge systems' performance as the main objective.

Among the conducted studies, the use of numerical simulations in comparison with the experimental works are less explored for the assessment of outfall discharge systems, although the numerical methods can be seen as an inexpensive and practical approach in this field.

Literature reviews show that improvements during the last two decades in the computational resources provide an ability to extract accurate numerical results for the entire field of outfall regions. Thus, the applications of numerical methods to jet and plume-type flows still need further attention. In the following paragraphs, a summary of numerical studies on single port effluent discharges is presented.

Hwang et al. (1995) numerically investigated the initial mixing of a vertical buoyant jet discharge into a density stratified cross-flow using the $k-\varepsilon$ turbulence model, which successfully shows the evolution of vortex pairs as a consequence of jet and ambient flow interactions. Blumberg et al. (1996) and Zhang and Adams (1999) employed the far-field CFD circulation models to predict the near-field plume characteristics of sewage outfalls. Vafeiadou et al. (2005) investigated the inclined negatively buoyant jets using the ANSYS CFX tool while applying the shear stress transport turbulence model to close the problem. This model is based on combining the $k-\omega$ and $k-\varepsilon$ models. They compared the results of the numerical model with the experimental works of Roberts et al. (1997) and Bloomfield and Kerr (2002), demonstrating relatively acceptable predictions for the terminal rise heights of the negatively buoyant jets studied. However, considerable discrepancies were observed for the forecast of the return point.

Furthermore, Kim and Cho (2006) numerically studied the mixing characteristics of both the surface and submerged heated flow discharges issuing into ambient cross-flow by applying the RNG $k-\varepsilon$ method as the turbulence closure method. The three-dimensional model was successfully built using the commercial CFD software package: Flow-3D. The effect of various levels of water depth (shallow and deep ambient water) was also investigated on the initial mixing of buoyant flows. Applying the ANSYS CFX model, Oliver et al. (2008) examined the geometrical and bulk flow parameters of inclined negatively buoyant jets. Two sets of $k-\varepsilon$ simulations, one based on the standard two-equation $k-\varepsilon$ turbulence approach and the other based on the calibration of turbulent Schmidt number in the tracer transport equation, were employed in this study. Although a comparison of the results from the standard and calibrated $k-\varepsilon$ approaches was more accurate than the analytical and integral model predictions, the implementation of these approaches could not provide a precise prediction for the bulk flow parameters at the centerline maximum height.

Papanicolaou et al. (2008) proposed Gaussian distribution and top-hat integral models for the prediction of concentration and velocity in negatively buoyant jets. In addition, different jet entrainment coefficient values were applied to measure the geometrical parameters and

dilution at the return point locations and the maximum centerline. Findings showed that the geometrical characteristics were underestimated, particularly when using the Gaussian formulation. HUAI et al. (2010) applied the realizable $k-\varepsilon$ turbulence closure model to predict the behavior of wall buoyant jets and then conducted a comparison between the numerical results (such as centerline trajectory, cling length, and dilutions) and the analytical and experimental data. A linear relationship between the dilutions of temperature and velocity and the distance from the nozzle was also suggested.

Christodoulou et al. (2010) proposed that the centerline trajectory and the upper boundary of inclined negatively buoyant jets with discharge angles in the range of 30° to 85° could be estimated in a non-dimensional form by a second degree polynomial. Palomar et al. (2012) studied the accuracy of different commercial software tools including VISJET, Visual Plumes, and CORMIX (CorJet) to model the behavior of brine jet discharges into both stagnant and dynamic receiving water environments. Results revealed that these commercial models underestimated the geometrical characteristics such as the terminal rise height of the jets. In addition, the dilution at the impact point was predicted with a deviation of 50% to 65%. Consequently, the commercial software models should be considered highly conservative when approximating the dilution levels. Oliver et al. (2013) presented a modified integral model for the simulation of a negatively buoyant jet's performance in the near-field region. According to the obtained results, it was claimed that the developed model could predict both the geometrical and dilution parameters with a higher accuracy than the previously introduced models by considering the influence of additional mixing in various initial conditions for submerged outfall discharges of brine effluents.

Kheirkhah Gildeh et al. (2014) numerically investigated the three-dimensional fields of velocity and temperature for both saline and thermal wall jets. The buoyancy modified solver was applied to simulate negatively buoyant jets in the OpenFOAM software. A modified version of PisoFoam solver was created that involves the density equation as a function of salinity and temperature. Seven turbulence models were used to evaluate the accuracy of RANS models for the simulation of jet discharges. The Launder-Reece-Rodi (LRR) turbulence models were introduced as the most reliable approach among those studied. Kheirkhah Gildeh et al. (2015) employed different turbulence models for the simulation of the inclined dense jet discharges (with the two angles of 30° and 45°) into the stationary shallow waters, demonstrating that the LRR and the realizable $k-\varepsilon$ models could predict this flow type more precisely than the other turbulence closure models examined.

Kheirkhah Gildeh et al. (2016) also applied the LRR and Realizable $k-\varepsilon$ turbulence models to investigate the geometrical and flow properties of 30° and 45° inclined negatively buoyant jets with a densimetric Froude number varying from 10 to 34. Moreover, the influence of buoyancy on the turbulence model was studied by modifying the standard $k-\varepsilon$ model using the standard Boussinesq gradient diffusion hypothesis (SGDH) and general gradient diffusion hypothesis (GGDH) approaches. Considering that the buoyancy term in the turbulence model resulted in a wider spread of dense jets on the inner half, this points out the more realistic results according to the physical experiments.

In addition, Zhang et al. (2016) presented a numerical simulation of a submerged negatively buoyant jet in the OpenFOAM software and applied the "twoLiquidMixingFoam" solver with both the Smagorinsky and dynamic Smagorinsky SGS models, then validated the obtained data with the experiments conducted. More recently, Ardalan and Vafaei (2019) numerically modeled 45° inclined thermal-saline effluent discharges into the stationary environment using the realizable $k-\varepsilon$ turbulence model. Experimental data were applied to calibrate the model results. The findings demonstrated an acceptable simulation performance for the prediction of geometrical characteristics in the thermal-saline jets studied.

A summary of some prominent numerical studies using the RANS approaches to simulate single jets is presented in Table A-5. These studies confirm the predictive capability of these models in simulating the mixing behavior of single jets. Among different RANS models, the realizable $k-\varepsilon$ and LRR models can be considered as the most reliable models for single jets and can be utilized when designing outfall systems. Furthermore, Table A-6 presents a summary of numerical studies using the LES models for the simulation of single jets.

Table A-5 Prominent numerical studies using the RANS modeling approaches for the simulation of single jets and their remarks

Ref.	Applied models	Jet type	Outcome/Remarks
(Plum et al., 2008)	Standard $k-\varepsilon$, realizable $k-\varepsilon$, standard $k-\omega$, and RSM	60° inclined dense jet	• The realizable k − ε model provided the most accurate predictions of the mixing in the negatively buoyant plume and the spreading bed layer. • The RSM models required unacceptable processing time for the level of accuracy required for the problem.

(Oliver et al., 2008)	Standard $k-\varepsilon$ and calibrated $k-\varepsilon$	Inclined dense jet	• A $k-\varepsilon$ model based on the calibration of the turbulent Schmidt number was proposed. • $k-\varepsilon$ models led to more accurate predictions of the behavior of inclined dense jets compared to integral models and analytical solutions. • Both models underestimated the flow spread and the centerline dilution at the maximum height. • There was no improvement in the quality of the predictions of bulk flow parameters at the centerline maximum height when using $k-\varepsilon$ models compared to analytical solutions.
(El-Amin et al., 2010)	Standard $k-\varepsilon$, realizable $k-\varepsilon$, RNG $k-\varepsilon$, and standard $k-\omega$	Heated and unheated confined vertical jets	• The realizable k − ε model provided the most accurate predictions of the jet characteristics. • The heated jet was a lazy plume. • The maximum velocity was theoretically predicted.
(Huai et al., 2010)	Realizable $k-\varepsilon$	Horizontal wall jet	• The realizable $k-\varepsilon$ model could successfully predict velocity distribution and temperature dilutions. • Velocity profile had a Gaussian form after the distance of $5d_0$ from the nozzle. • The distributions of velocity and temperature dilutions indicated a similarity along the axial direction at centerline in the near-field.
(Kheirkhah Gildeh et al., 2014b)	Standard $k-\varepsilon$, realizable $k-\varepsilon$, RNG $k-\varepsilon$, $k-\omega$ SST, LRR, and Launder-Gibson	Thermal and saline wall jet	• The LRR and realizable k − ε models led to the most accurate solutions for saline and thermal wall jets. • Stream-wise and span-wise profiles for velocity and temperature were self-similar after an initial distance from the nozzle. • The stream-wise temperature profiles had a general Gaussian pattern at various distances from the nozzle. • Bed slope shortened the cling length. • The bed roughness effect on the temperature field was less than on the velocity field.
(Gildeh et al., 2014)	Realizable $k-\varepsilon$ and LRR	60^o, 80^o, and 85^o inclined dense jets	• Brine discharges could be accurately modeled using the realizable $k-\varepsilon$ and LRR models.

			• The terminal rise height was underestimated by about 5% using both models. • The terminal rise height for 80° jets was higher than 85° jets. • The LRR model captured secondary flows and buoyancy-induced forces since it considers the effects of the stress anisotropy.
(Kheirkhah Gildeh et al., 2015b)	Realizable $k-\varepsilon$, RNG $k-\varepsilon$, nonlinear $k-\varepsilon$, LRR, and Launder-Gibson	30° and 45° inclined dense jet	• The LRR and realizable k − ε models resulted in more accurate solutions compared to the other models. • The nonlinear k − ε model led to the least accurate results. • The dilution was slightly underestimated by all models. • Port inclination did not have a significant effect on the dilution at the return point. • The cross-sectional velocity and concentration profiles of the outer half of the jet had an axisymmetric Gaussian pattern.
(Kheirkhah Gildeh et al., 2016b)	Realizable $k-\varepsilon$ and LRR	30° and 45° inclined dense jet	• The LRR model led to a slightly better prediction of the jet geometry and dilution characteristics since it could capture secondary flows and buoyancy-induced forces. • After the potential core region ($x/d_0 > 3$), the maximum velocity at the jet centerline decreased almost linearly. • Considering the density-induced term in the turbulence model caused the inner part of the jet to spread more widely.
(Ardalan & Vafaei, 2019)	Realizable $k-\varepsilon$	45° thermal-saline jet	• Thermal-saline discharges could be accurately modeled by the realizable $k-\varepsilon$ model. • The accuracy of the predictions decreased from the jet-like regions toward the plume-like region • The outer side boundary of the flow was predicted less accurately compared to the inner side boundary. • The salinity and temperature dilution ratios in thermal-saline jets were 93% and 89% for the return point and the centerline peak, respectively.

			• The combination of saline and thermal effluent could be a proper approach to optimize the mixing of effluent.
(Yan, Mohammadian, et al., 2020)	RNG $k-\varepsilon$	45^o inclined plane jet	• The accuracy of the RNG $k-\varepsilon$ model in simulating inclined jets in linearly stratified fluids was evaluated. • The prediction errors for the terminal rise height, the depth of the under-flow, and the spreading layer thickness were about 4%, 9%, and 9%, respectively. • A new length scale that characterizes the effects of ambient stratification was proposed.

Table A-6 Prominent numerical studies using the LES modeling approach for the simulation of single jets and their remarks

Ref.	**Jet type**	**Outcome/Remarks**
(R. Q. Wang et al., 2011)	Vertical downward jet	• Buoyancy flux had a positive effect on the penetration rate. • The penetrative distances driven by the initial buoyancy and momentum fluxes were independent. • The total penetration distance can be treated as a linear combination of the penetrative mechanisms driven by the initial buoyancy and momentum fluxes.
(Zhang et al., 2015)	Wall jet	• LES model, compared to standard $k-\varepsilon$ and $k-\omega$ models, led to more accurate results of both the kinematic and scalar mixing characteristics. • Standard $k-\varepsilon$ and $k-\omega$ models were unable to predict the strong anisotropic spreading of the wall jet near the boundary. • The weakness of the Smagorinsky SGS model in dealing with low turbulence intensity in regions far from the centerline led to faster reduction of spanwise turbulence intensity in those regions.
(Ghaisas et al., 2015)	Horizontal jet	• The velocity decay rate was dependent on the Richardson number. • The Richardson number had a significant positive effect on the vertical deflection. • The anisotropy increased when increasing the Richardson number. • The co-flow affected the jet trajectory and the radial half-widths, but not the turbulent energetics. • The Reynolds number, Re, had no effect on the total radial spread, the jet trajectory, and the turbulent fluctuations. • The ratio of scalar and velocity spreads was non-constant.

		• Coherent vortex rings were formed on the upper side of the jet, while intermittent coherent vortices and small-scale structures were produced on the lower part.
(Zhang et al., 2016)	45^{o} inclined jet	• The LES model was able to predict the geometric characteristics with a slight over-prediction of 10% and the return point dilution with an under-prediction of 20%. • The LES approach outperformed the integral models. • The jet spread widths were reasonably predicted in regions close to the nozzle, but not beyond the centerline peak. • Both the Smagorinsky and dynamic Smagorinsky SGS models were not fully able to capture the convective turbulence under the influence of buoyancy.
(Zhang et al., 2017)	45^{o} and 60^{o} inclined jets	• The LES model was able to simulate reasonably well the geometric characteristics. • The return point dilution was underestimated by 20%. • The LES model was able to reproduce the localized concentration build-up at the impact point.
(M. Jiang et al., 2019)	45^{o} inclined jet	• The LES model could reasonably reproduce the time-averaged first order mixing characteristics. • Turbulence kinetic energy spectrum decreased with the log slope of $-5/3$ at the frequency from 2 to 20 Hz near and beyond the centerline peak. • SGS models needed to be improved in such a way that incorporate the stratification effects.
(Tofighian et al., 2022)	15^{o}, 30^{o}, 45^{o}, 60^{o}, and 75^{o} inclined jets	• The model was able to reasonably predict the geometrical and mixing features; however, the flow features were still underestimated by up to 25%. • The model was able to reproduce the local concentration build-up near the impact point.

It is worthwhile mentioning the CFD modeling is also useful for the investigation of some real-world jet and plume applications that may encounter with multiphase flows. Discharging particulate matters in dredge disposal operations as well as sand and sediment during land reclamation can be the best examples of these applications, in which using predictive tools can shed light on their design development. In this regards, the successful use of multiphase CFD-based modeling to analyze the mixing and flow behaviors of single port sediment jet and plumes has been confirmed in previous studies (Azimi et al. 2012; Chan et al. 2020; Chan et al. 2014).

A.4.2 Multiport Effluent Discharges

A.4.2.1 Dimensional Analysis

Although the mixing of inclined dense single jets has been widely investigated for many years, the behavior of multiport diffusers has recently gained more attention. These diffusers have been applied in some areas around the world; the relevant instances include the Australian cities of Melbourne, Perth, and Sydney (Missimer et al. 2015). Results demonstrated that discharges from a multiport diffuser can achieve a higher dilution in comparison with an equivalent single port discharge (Fischer et al. 2013; Lee and Chu 2003). Marine outfalls may be designed as a diffuser with multiple ports (multiport diffuser). There are different designs depending on the site-specific conditions. For example, nozzles can be aligned uni-directionally in the offshore direction to decrease impacts on the sensitive receivers (Lai and Lee 2012). Jirka (2006) reported a summary of other types of diffuser designs.

In modern outfall designs, the wastewater is typically discharged through a number of risers mounted on the outfall; each riser is fitted circumferentially with 2-8 horizontal nozzles (Lai and Lee 2012). Figure A-8 shows the perspective view of these risers with a 6-nozzle configuration. With this type of nozzle arrangement, experiments have shown that the diffuser length can be minimized (Isaacson et al. 1983), resulting in a cost-effective construction.

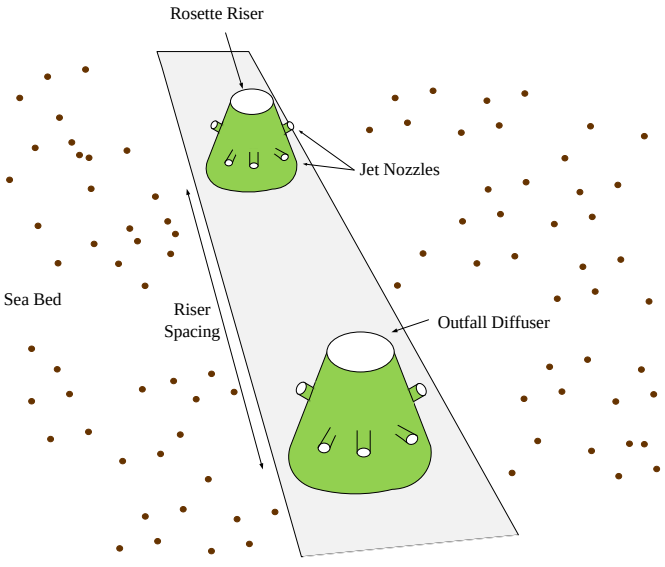

Figure A-8 Perspective view of multiport rosette diffuser on a submarine outfall

(the obtained jet flow is shaped like a rose, and is called a rosette jet group)

Considering the multiport diffuser illustrated in Figure A-9 (with discharge either from one or both sides) whose port spacing is L_p, the constants on the right-hand side of Eq. (A-33) then become functions of $\frac{L_p}{d_0F_0}$ (Missimer et al. 2015):

$$\frac{y_t}{d_0F_0} = f\left(\frac{L_p}{d_0F_0}\right); \frac{x_i}{d_0F_0} = f\left(\frac{L_p}{d_0F_0}\right); \frac{x_n}{d_0F_0} = f\left(\frac{L_p}{d_0F_0}\right); \\ \frac{S_i}{F_0} = f\left(\frac{L_p}{d_0F_0}\right); \frac{S_n}{F_0} = f\left(\frac{L_p}{d_0F_0}\right) \tag{A-34}$$

Therefore, the effect of the port spacing is completely encapsulated in the dimensionless parameter $\frac{L_p}{d_0F_0}$ (Missimer et al. 2015).

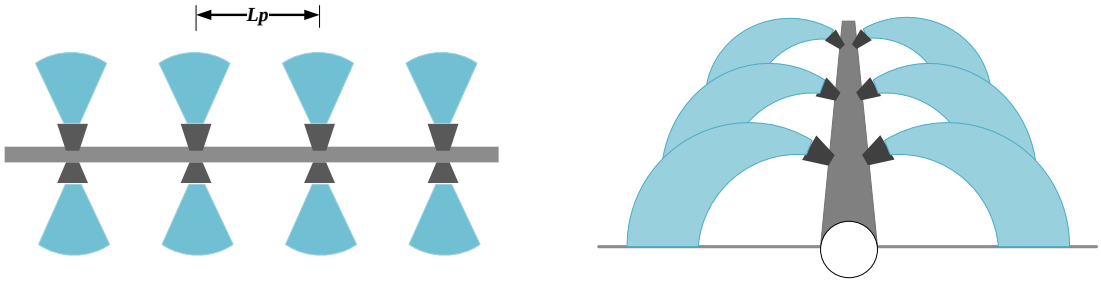

Figure A-9 Definition diagram for the multiport dense jet

When the jets are adequately far from each other ($\frac{L_p}{d_0F_0} \gg 1$), the jets do not have any interactions and behave as single jets, and Eq. (A-33) can be applied for the multiport instead of Eq. (A-34). On the other hand, when the ports are close together $\frac{L_p}{d_0F_0} \ll 1$, they are considered as if they are discharged from a line. Thus, the jet parameters are introduced per unit diffuser length rather than the individual jet parameters. The discharge volume, momentum, and buoyancy fluxes per unit length can be introduced as q_0, m_0, and b_0, respectively:

$$q_0 = \frac{Q_T}{L}; m_0 = U_0q_0; \; b_0 = g_0'q_0 \tag{A-35}$$

where Q_T is the total discharge from the diffuser and L is the diffuser length. The terminal rise height for a line source is as follows, instead of Eq. (A-29):

$$y_t = f(q_0, m_0, b_0) \tag{A-36}$$

which following a dimensional analysis becomes:

$$\frac{y_t b^{2/3}}{m_0} = Constant \tag{A-37}$$

For a long diffuser, b_0 and m_0 can be expressed as B_0/L_p and M_0/L_p, respectively. Considering the concept of the Froude number, Eq. (A-37) can be expressed as (Missimer et al. 2015):

$$\frac{y_t}{d_0 F_0} = c_{10}\left(\frac{L_p}{d_0 F_0}\right)^{-1/3} \tag{A-38}$$

The other geometrical parameters can be presented using the same procedure and for dilution (Missimer et al. 2015):

$$\frac{S_t}{F_0} = c_{11}\left(\frac{L_p}{d_0 F_0}\right)^{1/3} \tag{A-39}$$

where c_{10} and c_{11} are experimental constants. Eqs. (A-38) and (A-39) show the negative effect of the port spacing on the terminal rise height and the positive effect of it on the dilution (Missimer et al. 2015).

A.4.2.2 Numerical Studies

There are a number of studies using CFD to investigate the jet interaction in multiport diffuser discharges. Anderson and Spall (2001) studied twin parallel plane momentum jet discharges using CFD and compared them with their experimental observations. A recirculation region was successfully simulated, which was also observed in experiments. Law et al. (2002) reported the first CFD computation of rosette jet groups with 20 8-port risers, which required a run time of four days. Kuang et al. (2006) carried out a numerical study to investigate the plume interaction above an alternating diffuser. The negative cavity pressure was confirmed by the computation. The merging process between neighboring jets was found. The dependency of the degree of interaction on nozzle spacing was also observed. The computation was however performed with an assumed infinite water depth, which is somewhat different from the actual situation. Xiao et al. (2006) conducted a numerical study of four tandem jets in a cross-flow. The sheltering influence observed in the experiments was well reproduced. Jet trajectories were in agreement with experimental data. Rear jets were deflected to a similar degree by the ambient cross-flow. The induced velocity and pressure field, which are difficult to determine comprehensively in an experiment, were also obtained. The flow field showed a decrease in the effective cross-flow velocity after being sheltered by the front jet.

Lai and Lee (2012) also presented a general semi-analytical model for the dynamic interaction of multiple buoyant jets in a stagnant environment. Results showed that jet merging and mixing can be remarkably influenced by jet interactions. Model predictions of the jet trajectories, merging height, the centerline velocity, and concentration of the buoyant jet group are corroborated by the experimental findings.

Some of the prominent studies on the modeling of multiport jets are presented in Table A-7. The prediction capabilities of the RANS models for rosette buoyant, multiple inclined, and multiple vertical jets have been indicated in recent studies. These studies show that multiple jets can be simulated using the RANS models with reasonable error. Regarding the previous studies focusing on the different turbulence closures, the RNG $k-\varepsilon$ model led to more accurate results compared to the other RANS models for various multiple jet types. Thus, this model can be applied as a reliable model to predict the mixing behavior of multiport diffusers. Although the effect of port spacing on the mixing behavior of multiple jets has been well studied, the effect of port inclination on the mixing process has not been well recognized. Furthermore, to the authors' knowledge, multiple jets have not yet been simulated using the LES models. The reason may be the high computational cost and complexity when it comes to the simulation of the complex geometry of multiport discharges.

Table A-7 Prominent numerical studies on the simulation of multiple jets and their remarks

Ref.	Method	Applied models	Multiple jet type	Outcome/Remarks
(Anderson & Spall, 2001)	Numerical	Differential Reynolds stress (RSM) and standard $k-\varepsilon$	Dual, parallel planar jets	• A numerical model
(H. J. Wang & Davidson, 2003a)	Theoretical	-	Uni-directional multiple jets	• A theoretical model • Individual jets asymmetrically spread during jet merging. • Models that employed the summation of velocity and tracer distributions underestimated centerline dilutions.
(P. C. Yannopoulos & Noutsopoulos, 2006)	Entrainment restriction	-	Uni-directional multiple jets	• A theoretical model • The merging effect became significant on the centerline velocities and concentrations after about double the

				distance where the nearby optical jet boundaries intersected.
(Tang et al., 2008)	Numerical	Eddy viscosity	Multiple inclined jets	• A numerical model • Unlike empirical mixing zone models, the complex interplay of the ambient flow and thermal jets and jets interactions could be properly resolved via the CFD model.
(A. C. H. Lai & Lee, 2012)	Semi-analytical	-	Rosette buoyant jets	• A Semi-analytical model • Jet interactions significantly affected mixing behavior. • Dynamic interactions between the jet groups were negatively affected by ambient cross-flow.
(Yan et al., 2019)	Numerical	Standard $k-\varepsilon$ and RNG $k-\varepsilon$	Rosette buoyant jets with upward and downward 30°, 45°, and 60° inclined ports	• A numerical model • The port inclination affected mixing behavior. • The RNG $k-\varepsilon$ outperformed the standard $k-\varepsilon$. • Jets became less diluted in the cases with greater angles. • The better performance of the RNG $k-\varepsilon$ was due to the consideration of the influence of the Reynolds number on the effective turbulence transport, incorporating a new term in the ε, and determination of the inverse effective Prandtl numbers.
(Yan & Mohammadian, 2019)	Numerical	Standard $k-\varepsilon$ and RNG $k-\varepsilon$	Multiple 60° inclined jets	• A numerical model • The port spacing significantly impacted mixing behavior. • The RNG $k-\varepsilon$ model outperformed the standard $k-\varepsilon$. • Both the standard and RNG $k-\varepsilon$ models could provide results of terminal rise height and impact dilution with errors smaller than 15%.

(Yan & Mohammadian, 2020a)	Artificial intelligence (AI)	Single-gene genetic programming (SGGP) and multigene genetic programming (MGGP)	Multiple 60° inclined jets	• AI-based models • The MGGP models outperformed the SGGP models and the existing regression-based empirical models.
(Yan & Mohammadian, 2020b)	AI	MGGP	Multiple vertical jets	• AI-based models • The non-dimensional vertical displacement of the merging point and concentration where the jets were well mixed became more sensitive to port spacing than to the Froude number. • The non-dimensional centerline concentration was more sensitive to the Froude number than to port spacing. • There was no clear trend regarding the sensitivity of the non-dimensional vertical displacement of the merging point versus the Froude number.
(M. J. Baum & Gibbes, 2020)	Numerical	$k-\omega$ (SST)	Multiple 60° inclined jets	• A numerical model • Cross-flow conditions significantly affected mixing behavior. • Quasi-quiescent conditions produced the largest areal extent across the salinity spectrum. • Cross-flow decreased the salinity footprint. • Impact distances and dilutions were about 10% lower for the logarithmic cross-flow regime compared to the equivalent uniform velocity regime.
(Yan et al., 2020)	Numerical	Standard $k-\varepsilon$, RNG $k-\varepsilon$, standard $k-\omega$, and $k-\omega$ (SST)	Multiple vertical jets	• A numerical model • The port spacing significantly influenced the mixing behavior. • The RNG $k-\varepsilon$ outperformed other RANS models.

	• The port spacing positively affected the characteristic jet width in the streamwise direction. • The jets with larger port spacing merged at locations farther from the nozzle. • A new formula for centerline concentration profiles considering the effect of port spacing was proposed.

A.5 Knowledge Gaps

According to the literature review on outfall discharge modeling, there are some main gaps in the existing numerical modeling that need to be considered. Addressing these deficiencies can lead to more realistic predictions of outfall discharge behavior via modeling. The major knowledge gaps can be expressed as follows:

- The effect of neighboring boundaries including the bottom layer roughness, the bed slope, and shallow water surface on the mixing behavior of jets requires further research.
- With the advancements in computational resources, more attention should be given to hybrid simulation approaches.
- To capture precisely the coherence structures and turbulence behavior of discharge flow, the use of instantaneous CFD analysis instead of time averaging should be further explored.
- Simulation difficulties such as mesh generation deficiencies and instability of models for outfall discharge modeling, particularly for complex multiport diffuser configuration, need to be considered.
- One of the most important challenges in applicability of CFD methods is to define the appropriate mesh and boundary conditions in a way that provide stable results. The definition of high mesh resolutions required for the accurate and stable solution can be translated into high computational cost. Meshfree CFD methods such as smoothed particle hydrodynamics (SPH), which have been recently studied in fluid mechanics problems (Aristodemo et al. 2015; Hu and Adams 2015; Tran-Duc et al. 2017; Liu et

al. 2021; Meister et al. 2017) with the idea of replacing the mesh with a set of arbitrarily distributed particles, can overcome the conventional CFD methods' deficiencies. This method as the next-generation of CFD approach should be investigated further for the modeling of outfall discharges.

- The applications of lattice Boltzmann method in the modeling of fluid flow within the complex outfall geometries are worthwhile to examine.
- A more realistic scenario involving ambient flow and wave currents representative of a coastal situation should be studied in future research.
- Dynamic of ambient stratification in CFD analysis of outfall discharge requires further investigation.
- Investigating the flow discharge behavior beyond the impact point, intermediate and far-field regions, in CFD studies should be conducted in detail.
- Modifications to turbulence models, such as the incorporation of buoyancy terms, have demonstrated an effective way to enhance the prediction of jet characteristics and should be further explored.
- As AI techniques have been introduced as promising approaches in the prediction of mixing behavior in recent years, collecting rich data based on experiments and CFD simulations can be a valuable basis for future AI studies.

A.6 Concluding Remarks

Outfall systems have been introduced as a solution for the adverse environmental impacts on marine life resulting from the disposal of effluents in oceans and seas. Outfall discharges protect marine habitats by providing rapid mixing, which leads to a drop in salinity and thermal levels. Modeling of outfall discharge empowers engineers to predict the mixing behavior of discharges and design proper discharges that meet water quality standards at the point of compliance. This chapter provided a comprehensive description of the basic concepts involved in outfall discharge modeling and a critical review on the current state-of-the-art in this field.

Thanks to the advancements in computational resources over the past two decades, the application of CFD modeling in the prediction of jet-mixing behavior has been dramatically increased. It was shown that numerical modeling is a promising tool for simulating both outfall single and multiple discharges, and it can be predicted that, in the near future, CFD modeling

will be widely applied in engineering designs to decrease experimental and field costs. Considering the pros and cons of different turbulence modeling approaches, the LES approach provides more accurate results compared to the RANS approach, although it requires higher computational cost. Therefore, as computational resources improve, more attention should be given to the application of the LES for outfall discharge simulation, compared to the RANS. Regarding different turbulence closures adopted in the RANS approach, realizable $k-\varepsilon$ and RNG $k-\varepsilon$ models have shown better performance in the simulation of single and multiple jets, respectively. These comparisons would provide valuable insight into the efficient modeling of outfalls for engineering applications. Finally, by the identification of knowledge gaps and research directions, this study can be addressed as a reference for future researchers conducting numerical assessments on the outfall discharges.

Nomenclature

Abbreviation

AI	Artificial Intelligence
AIZ	Allocated Impact Zone
CFD	Computational Fluid Dynamics
DES	Detached Eddy Simulation
DNS	Direct Numerical Simulation
EPA	Environmental Protection Agency
FDM	Finite Difference Method
FVM	Finite Volume Method
GGDH	General Gradient Diffusion Hypothesis
LES	Large Eddy Simulation
LMZ	Legal Mixing Zone
LRR	Launder-Reece-Rodi
MGGP	Multigene Genetic Programming
NPDES	National Pollutant Discharge Elimination System
ODE	Ordinary Differential Equation
OpenFOAM	OPEN Field Operation And Manipulation
PDE	Partial Differential Equations
RANS	Reynolds-Averaged Navier-Stokes
RNG	Re-Normalization Group
RSM	Reynolds Stress Model

SGDH	Standard Gradient Diffusion Hypothesis
SGGP	Single-Gene Genetic Programming
SGS	Sub-Grid Scale
SPH	Smoothed Particle Hydrodynamics
SST	Shear Stress Transport
WFD	Water Framework Directive
ZID	Zone of Initial Dilution

Mathematical Symbols

a, b, and c	Empirical parameters in Millero and Poisson equation
B_0	Discharge buoyancy flux
b_0	Discharge buoyancy flux per unit length
C	Fluid concentration
C_0	Initial jet fluid concentration
C_a	Ambient fluid concentration
c_1 to c_{11}	Constants in dimensional analysis
D	Diffusion coefficient
D_{ij}	Transport term by diffusion
d_0	Jet nozzle diameter
F_0	Jet-densimetric Froude number
g	Acceleration due to gravity
g'	Modified acceleration due to gravity
g'_0	Initial modified acceleration due to gravity
H_a	Ambient flow depth
h_0	Port height
k	Turbulent kinetic energy per mass
k_{eff}	Heat transfer coefficient
L	Diffuser length
l_M	Jet-to-plume Length Scale
L_p	Port-spacing
l_Q	Discharge Length Scale
M_0	Discharge momentum flux
m_0	Discharge momentum flux per unit length
p	Fluid pressure

p'	Fluctuating component of pressure
$\bar{p}$	Mean/ filtered component of pressure
P_{ij}	production rate of R_{ij}
Pr	Prandtl number
Pr_t	Turbulent Prandtl number
Q_0	Discharge volume flux
q_0	Discharge volume flux per unit length
R_{ij}	Reynolds stress
Re	Reynolds numbers
Re_0	Jet Reynolds Number
S	Salinity
S_0	Jet discharge dilution
S_c	Centerline peak dilution
S_i	Impact dilution
S_n	Ultimate dilution
S_t	Terminal peak dilution
T	Temperature
T_0	Jet discharge temperature
T_a	Ambient fluid temperature
t	Time
U_0	Jet discharge velocity
U_a	Ambient flow velocity
u'	Fluctuating component of velocity
$\bar{u}$	Mean/ filtered component of velocity
u, v, and w	Mean velocity in the *x*, *y*, and *z* directions
x_c	Horizontal distance to jet terminal rise height
x_i	Horizontal distance to jet impact point
x_n	Horizontal distance to near-field location
y_c	Maximum centerline height
y_l	Thickness of the spreading layer
y_t	Maximum terminal rise height

Greek symbols

Δ	Filter size

Δx, Δy, and Δz	Grid cell sizes in x, y, and z directions
$\Delta\rho$	Density difference between the jet flow and the ambient fluid
δ_{ij}	Kronecker delta
ε_{ij}	Dissipation rate of R_{ij}
θ_0	Jet discharge angle relative to the horizontal
μ	Dynamic viscosity of the fluid
μ_t	Eddy viscosity
ν	kinematic viscosity
ν_{eff}	Effective kinematic viscosity
ν_t	Turbulent kinematic viscosity
Π_{ij}	Transport term by turbulent pressure-strain interactions
ρ_0	Jet discharge density
ρ_a	Ambient flow density
ρ_t	Density of water changing with the temperature in Millero and Poisson empirical equation
τ_{ij}	Sub-grid scale stresses
$\emptyset(t)$	Instantaneous variable
$\emptyset'$	Fluctuating component of an instantaneous variable
$\overline{\emptyset}$	Mean component of an instantaneous variable
Ω_{ij}	Transport term by rotation

A.7 References

[1] T. Missimer, B. Jones, R. Maliva, Intakes and Outfalls for Seawater Reverse-Osmosis Desalination Facilities: Innovations and Environmental Impacts, 2015.

[2] R. Einav, F. Lokiec, Environmental aspects of a desalination plant in Ashkelon, Desalination 156 (2003) 79–85. https://doi.org/10.1016/S0011-9164(03)00328-X.

[3] A. Hashim, M. Hajjaj, Impact of desalination plants fluid effluents on the integrity of seawater, with the Arabian Gulf in perspective, Desalination 182 (2005) 373–393. https://doi.org/10.1016/j.desal.2005.04.020.

[4] U. EPA, Water Quality Standards Handbook, 2nd ed., Washington, DC, USA, 1994.

[5] P. Chave, The EU water framework directive, IWA Publishing, 2001.

[6] O. Abessi, Brine Disposal and Management—Planning, Design, and Implementation, in: Sustainable Desalination Handbook: Plant Selection, Design and Implementation, Elsevier Inc., Amsterdam, 2018: pp. 259–303.

[7] Á. Loya-Fernández, L.M. Ferrero-Vicente, C. Marco-Méndez, E. Martínez-García, J.J. Zubcoff Vallejo, J.L. Sánchez-Lizaso, Quantifying the efficiency of a mono-port diffuser in the dispersion of brine discharges, Desalination 431 (2018) 27–34. https://doi.org/10.1016/j.desal.2017.11.014.

[8] S. Jenkins, J. Paduan, P. Roberts, D. Schlenk, J. Weis, Management of brine discharges to coastal waters: Recommendations of a Science Advisory Panel: Submitted at the request of the California Water Resources, (2012).

[9] P.J.W. Roberts, A. Ferrier, G. Daviero, Mixing in inclined dense jets, Journal of Hydraulic Engineering 123 (1997) 693–699. https://doi.org/10.1061/(ASCE)0733-9429(1997)123:8(693).

[10] P. Palomar, I. Losada, Impacts of brine discharge on the marine environment. Modelling as a predictive tool, in: In Desalination: Trends and Technologies; Michael, S., Ed., IntechOpen, London, UK, 2011.

[11] H. Kheirkhah Gildeh, A. Mohammadian, I. Nistor, H. Qiblawey, Numerical modeling of 30◦ and 45◦ inclined dense turbulent jets in stationary ambient, Environmental Fluid Mechanics 15 (2015) 537–562. https://doi.org/10.1007/s10652-014-9372-1.

[12] H. Fischer, J. List, C. Koh, J. Imberger, N. Brooks, Mixing in inland and coastal waters, Elsevier Inc., San Diego, CA, USA, 2013.

[13] A.B. Pincince, E.J. List, Disposal of brine into an estuary, Water Pollution Control Federation 45 (1973) 2335–2344.

[14] F. Millero, A.P.-D.S.R.P.A. Oceanographic, U. 1981, International one-atmosphere equation of state of seawater, J. of Deep-Sea Res.1 28 (1981) 625–629. https://doi.org/10.1016/0198-0149(81)90122-9.

[15] H. Kheirkhah Gildeh, A. Mohammadian, I. Nistor, H. Qiblawey, Numerical modeling of turbulent buoyant wall jets in stationary ambient water, Journal of Hydraulic Engineering 140 (2014). https://doi.org/10.1061/(ASCE)HY.1943-7900.0000871.

[16] H. Kheirkhah Gildeh, A. Mohammadian, I. Nistor, H. Qiblawey, X. Yan, CFD modeling and analysis of the behavior of 30° and 45° inclined dense jets - New numerical insights, Journal of Applied Water Engineering and Research 4 (2016) 112–127. https://doi.org/10.1080/23249676.2015.1090351.

[17] X. Yan, A. Mohammadian, X. Chen, Numerical modeling of inclined plane jets in a linearly stratified environment, Alexandria Engineering Journal 59 (2020) 1857–1867. https://doi.org/10.1016/j.aej.2020.05.023.

[18] X. Yan, A. Mohammadian, X. Chen, Three-dimensional numerical simulations of Buoyant Jets discharged from a Rosette-type multiport diffuser, J Mar Sci Eng 7 (2019) 1–15. https://doi.org/10.3390/jmse7110409.

[19] X. Yan, A. Mohammadian, Numerical modeling of multiple inclined dense jets discharged from moderately spaced ports, Water (Switzerland) 11 (2019) 14–16. https://doi.org/10.3390/w11102077.

[20] M. Taherian, A. Mohammadian, Buoyant Jets in Cross-Flows: Review, Developments, and Applications, J Mar Sci Eng 9 (2021) 61. https://doi.org/10.3390/jmse9010061.

[21] F. Sotiropoulos, Introduction to statistical turbulence modelling for hydraulic engineering flows, in: In Computational Fluid Dynamics. Applications in Environmental Hydraulics, John Wiley & Sons, Chichester, UK, 2005.

[22] H.K. Versteeg, W. Malalasekera, An introduction to computational fluid dynamics: the finite volume method, 2nd ed., Pearson education, 2007.

[23] F. Moukalled, L. Mangani, M. Darwish, Fluid Mechanics and Its Applications The Finite Volume Method in Computational Fluid Dynamics, Springer, 2016.

[24] B. Launder, G. Reece, W. Rodi, Progress in the development of a Reynolds-stress turbulence closure, Journal of Fluid Mechanics 68 (1975) 537–566. https://doi.org/10.1017/S0022112075001814.

[25] W. Rodi, Turbulence models and their applications in hydraulics-a state-of-the-art review, Delft, The Netherlands, 1984.

[26] J. Smagorinsky, General circulation experiments with the primitive equations: I. The basic experiment, Mon Weather Rev 91 (1963) 99–164. https://doi.org/10.1175/1520-0493(1963)091<0099:GCEWTP>2.3.CO;2.

[27] Y. Zhiyin, Large-eddy simulation: Past, present and the future, Chinese Journal of Aeronautics 28 (2015) 11–24. https://doi.org/10.1016/j.cja.2014.12.007.

[28] A. Mohammadian, H.K. Gildeh, I. Nistor, CFD modeling of effluent discharges: A review of past numerical studies, Water (Switzerland) 12 (2020) 856. https://doi.org/10.3390/w12030856.

[29] T. Lund, On the use of discrete filters for large eddy simulation, Annual Res. Briefs (1997) 83–95.

[30] S. Gant, Reliability Issues of LES-Related Approaches in an Industrial Context, Flow Turbulence Combust 84 (2010) 325–335. https://doi.org/10.1007/s10494-009-9237-8.

[31] S. Zhang, A.W.K. Law, B. Zhao, Large eddy simulations of turbulent circular wall jets, Int J Heat Mass Transf 80 (2015) 72–84. https://doi.org/10.1016/j.ijheatmasstransfer.2014.08.082.

[32] S. Zhang, A.W.K. Law, M. Jiang, Large eddy simulations of 45° and 60° inclined dense jets with bottom impact, Journal of Hydro-Environment Research 15 (2017) 54–66. https://doi.org/10.1016/j.jher.2017.02.001.

[33] S. Zhang, B. Jiang, A.W.K. Law, B. Zhao, Large eddy simulations of 45° inclined dense jets, Environmental Fluid Mechanics 16 (2016) 101–121. https://doi.org/10.1007/s10652-015-9415-2.

[34] M. Jiang, A.W.K. Law, A.C.H. Lai, Turbulence characteristics of 45° inclined dense jets, Environmental Fluid Mechanics 19 (2019) 27–54. https://doi.org/10.1007/s10652-018-9614-8.

[35] P.J.W. Roberts, G. Toms, Ocean outfall system for dense and buoyant effluents, Journal of Environmental Engineering 114 (1988) 1175–1191.

[36] S.J. Wright, Buoyant jets in density-stratified crossflow, Journal of Hydraulic Engineering 110 (1984) 643–656.

[37] R.L. Doneker, G.H. Jirka, Cormix User Manual 6.0E: A Hydrodynamic Mixing Zone Model and Decision Support System for Pollutant Discharges into Surface Waters, U.S. Environmental Protection Agency, Washington DC, 2007.

[38] R.R. Hwang, T.P. Chiang, W.C. Yang, Effect of Ambient Stratification on Buoyant Jets in Cross-Flow, J Eng Mech 121 (1995) 865–872. https://doi.org/10.1061/(asce)0733-9399(1995)121:8(865).

[39] A.F. Blumberg, Z.-G. Ji, C.K. Ziegler, Modeling Outfall Plume Behavior Using Far Field Circulation Model, Journal of Hydraulic Engineering 122 (1996) 610–616. https://doi.org/10.1061/(asce)0733-9429(1996)122:11(610).

[40] X.-Y. Zhang, E.E. Adams, Prediction of Near Field Plume Characteristics Using Far Field Circulation Model, Journal of Hydraulic Engineering 125 (1999) 233–241. https://doi.org/10.1061/(asce)0733-9429(1999)125:3(233).

[41] P. Vafeiadou, I. Papakonstantis, G. Christodoulou, Numerical simulation of inclined negatively buoyant jets, in: In Proceedings of the 9th International Conference on Environmental Science and Technology, Rhodes Islands, Greece, 2005: pp. A1537–A1542.

[42] L. Bloomfield, R. Kerr, Inclined turbulent fountains, J Fluid Mech 451 (2002) 283–294. https://doi.org/0.1017/S002211200100652.

[43] D.G. Kim, H.Y. Cho, Modeling the buoyant flow of heated water discharged from surface and submerged side outfalls in shallow and deep water with a cross flow, Environmental Fluid Mechanics 6 (2006) 501–518. https://doi.org/10.1007/s10652-006-9006-3.

[44] C.J. Oliver, M.J. Davidson, R.I. Nokes, k-ε Predictions of the initial mixing of desalination discharges, Environmental Fluid Mechanics 8 (2008) 617–625. https://doi.org/10.1007/s10652-008-9108-1.

[45] P. Papanicolaou, I. Papakonstantis, G. Christodoulou, On the entrainment coefficient in negatively buoyant jets, J Fluid Mech 614 (2008) 447–470. https://doi.org/10.1017/S002211200800350.

[46] W. xin HUAI, Z. wei LI, Z. dong QIAN, Y. hong ZENG, J. HAN, W. qi PENG, Numerical simulation of horizontal buoyant wall jet, Journal of Hydrodynamics 22 (2010) 58–65. https://doi.org/10.1016/S1001-6058(09)60028-7.

[47] G. Christodoulou, I.P.-E. Hydraulics, U. 2010, Simplified estimates of trajectory of inclined negatively buoyant jets, in: In Christodoulou GC, Stamou AI (Eds.)

Environmental Hydraulics- Proceedings of the 6th International Symposium on Environmental Hydraulics, Taylor & Francis, Milton Park, Didcot, 2010: pp. 165–170.

[48] P. Palomar, J. Lara, I. Losada, Near field brine discharge modeling part 2: Validation of commercial tools, Desalination 290 (2012) 28–42.

[49] C.J. Oliver, M.J. Davidson, R.I. Nokes, Predicting the near-field mixing of desalination discharges in a stationary environment, Desalination 309 (2013) 148–155. https://doi.org/10.1016/j.desal.2012.09.031.

[50] H. Ardalan, F. Vafaei, CFD and Experimental Study of 45° Inclined Thermal-Saline Reversible Buoyant Jets in Stationary Ambient, Environmental Processes 6 (2019) 219–239. https://doi.org/10.1007/s40710-019-00356-z.

[51] B. Plum, T. Webb, J. Young, Modelling of Desalination Plant Outfalls, 2008.

[52] M.F. El-Amin, S. Sun, W. Heidemann, H. Müller-Steinhagen, Analysis of a turbulent buoyant confined jet modeled using realizable k-ε model, Heat and Mass Transfer/Waerme- Und Stoffuebertragung 46 (2010) 943–960. https://doi.org/10.1007/s00231-010-0625-3.

[53] H.K. Gildeh, A. Mohammadian, I. Nistor, H. Qiblawey, Numerical Modelling of Brine Discharges Using OpenFOAM, in: Proceedings of the International Conference on New Trends in Transport Phenomena, Ottawa, ON, Canada, 2014: p. 51.

[54] R.Q. Wang, A.W.K. Law, E.E. Adams, O.B. Fringer, Large-eddy simulation of starting buoyant jets, Environmental Fluid Mechanics 11 (2011) 591–609. https://doi.org/10.1007/s10652-010-9201-0.

[55] N.S. Ghaisas, D.A. Shetty, S.H. Frankel, Large eddy simulation of turbulent horizontal buoyant jets, Journal of Turbulence 16 (2015) 772–808. https://doi.org/10.1080/14685248.2015.1008007.

[56] A. Azimi, D. Zhu, N. Rajaratnam, Computational investigation of vertical slurry jets in water, International Journal of Multiphase Flow 47 (2012) 94–114. https://doi.org/10.1016/j.ijmultiphaseflow.2012.07.002.

[57] S.N. Chan, A.C.H. Lai, A.W.K. Law, E. Eric Adams, Two-Phase CFD Modeling of Sediment Plumes for Dredge Disposal in Stagnant Water, in: Estuaries and Coastal Zones in Times of Global Change, Springer, Singapore, 2020: pp. 409–423. https://doi.org/10.1007/978-981-15-2081-5_24.

[58] S.N. Chan, K.W.Y. Lee, J.H.W. Lee, · K W Y Lee, J.H.W. Lee, Numerical modelling of horizontal sediment-laden jets, Environmental Fluid Mechanics 14 (2014) 173–200. https://doi.org/10.1007/s10652-013-9287-2.

[59] J. Lee, V. Chu, urbulent Jets and Plumes: A Lagrangian Approach, Kluwer Academic Publishers, Hingham, MA, USA, 2003.

[60] A.C.H. Lai, J.H.W. Lee, Dynamic interaction of multiple buoyant jets, J Fluid Mech 708 (2012) 539–575. https://doi.org/10.1017/jfm.2012.332.

[61] G.H. Jirka, Integral model for turbulent buoyant jets in unbounded stratified flows part 2: Plane jet dynamics resulting from multiport diffuser jets, Environmental Fluid Mechanics 6 (2006) 43–100. https://doi.org/10.1007/s10652-005-4656-0.

[62] M.S. Isaacson, R.C.Y. Koh, N.H. Brooks, Plume Dilution for Diffusers With Multiport Risers, Journal of Hydraulic Engineering 109 (1983) 199–220. https://doi.org/10.1061/(asce)0733-9429(1983)109:2(199).

[63] E.A. Anderson, R.E. Spall, Experimental and numerical investigation of two-dimensional parallel jets, Journal of Fluids Engineering, Transactions of the ASME 123 (2001) 401–406. https://doi.org/10.1115/1.1363701.

[64] A. Law, C. Lee, Y. Qi, CFD modeling of a multiport diffuser in an oblique current, in: In Proceedings of the Marine Waste Water Discharges, MWWD, Istanbul, Turkey, 2002.

[65] C. Kuang, J. Lee, S. Liu, J. Gu, Numerical study on plume interaction above an alternating diffuser in stagnant water, China Ocean Eng. 20 (2006) 289–302.

[66] Y. Xiao, J. Lee, H. Tang, D. Yu, Three-dimensional computations of multiple tandem jets in crossflow, China Ocean Eng. 20 (2006) 99–112.

[67] H.J. Wang, M.J. Davidson, Jet Interaction in a Still Ambient Fluid, Journal of Hydraulic Engineering 129 (2003) 349–357. https://doi.org/10.1061/(asce)0733-9429(2003)129:5(349).

[68] P.C. Yannopoulos, G.C. Noutsopoulos, Interaction of vertical round turbulent buoyant jets - Part I: Entrainment restriction approach, Journal of Hydraulic Research 44 (2006) 218–232. https://doi.org/10.1080/00221686.2006.9521677.

[69] H.S. Tang, J. Paik, F. Sotiropoulos, T. Khangaonkar, Three-Dimensional Numerical Modeling of Initial Mixing of Thermal Discharges at Real-Life Configurations, Journal of Hydraulic Engineering 134 (2008) 1210–1224. https://doi.org/10.1061/(asce)0733-9429(2008)134:9(1210).

[70] X. Yan, A. Mohammadian, Evolutionary Modeling of Inclined Dense Jets Discharged from Multiport Diffusers, Journal of Coastal Research 36 (2020) 362–371. https://doi.org/10.2112/JCOASTRES-D-19-00057.1.

[71] X. Yan, A. Mohammadian, Evolutionary prediction of multiple vertical buoyant jets in stationary ambient water, Desalination and Water Treatment 178 (2020) 41–52. https://doi.org/10.5004/dwt.2020.24938.

[72] M.J. Baum, B. Gibbes, Field-Scale Numerical Modeling of a Dense Multiport Diffuser Outfall in Crossflow, Journal of Hydraulic Engineering 146 (2020) 05019006. https://doi.org/10.1061/(asce)hy.1943-7900.0001635.

[73] X. Yan, B. Ghodoosipour, A. Mohammadian, Three-Dimensional Numerical Study of Multiple Vertical Buoyant Jets in Stationary Ambient Water, Journal of Hydraulic Engineering 146 (2020) 04020049. https://doi.org/10.1061/(asce)hy.1943-7900.0001768.

[74] F. Aristodemo, S. Marrone, I. Federico, SPH modeling of plane jets into water bodies through an inflow/outflow algorithm, Ocean Eng. 105 (2015) 160–175. https://doi.org/10.1016/j.oceaneng.2015.06.018.

[75] X.Y. Hu, N.A. Adams, A SPH model for incompressible turbulence, Procedia IUTAM 18 (2015) 66–75. https://doi.org/10.1016/j.piutam.2015.11.007.

[76] T. Tran-Duc, N. Phan-Thien, B.C. Khoo, A smoothed particle hydrodynamics (SPH) study of sediment dispersion on the seafloor, Physics of Fluids 29 (2017) 083302. https://doi.org/10.1063/1.4993474.

[77] S. Liu, X. Wang, X. Ban, Y. Xu, J. Zhou, J. Kosinka, A.C. Telea, Turbulent Details Simulation for SPH Fluids via Vorticity Refinement, COMPUTER GRAPHICS Forum 40 (2021) 54–67. https://doi.org/10.1111/cgf.14095.

[78] M. Meister, D. Winkler, M. Rezavand, W. Rauch, Integrating hydrodynamics and biokinetics in wastewater treatment modelling by using smoothed particle hydrodynamics, Computers & Chemical Eng. 99 (2017) 1–12. https://doi.org/10.1016/j.compchemeng.2016.12.020.

Appendix B: Test Setup and Equipment Employed in this Research

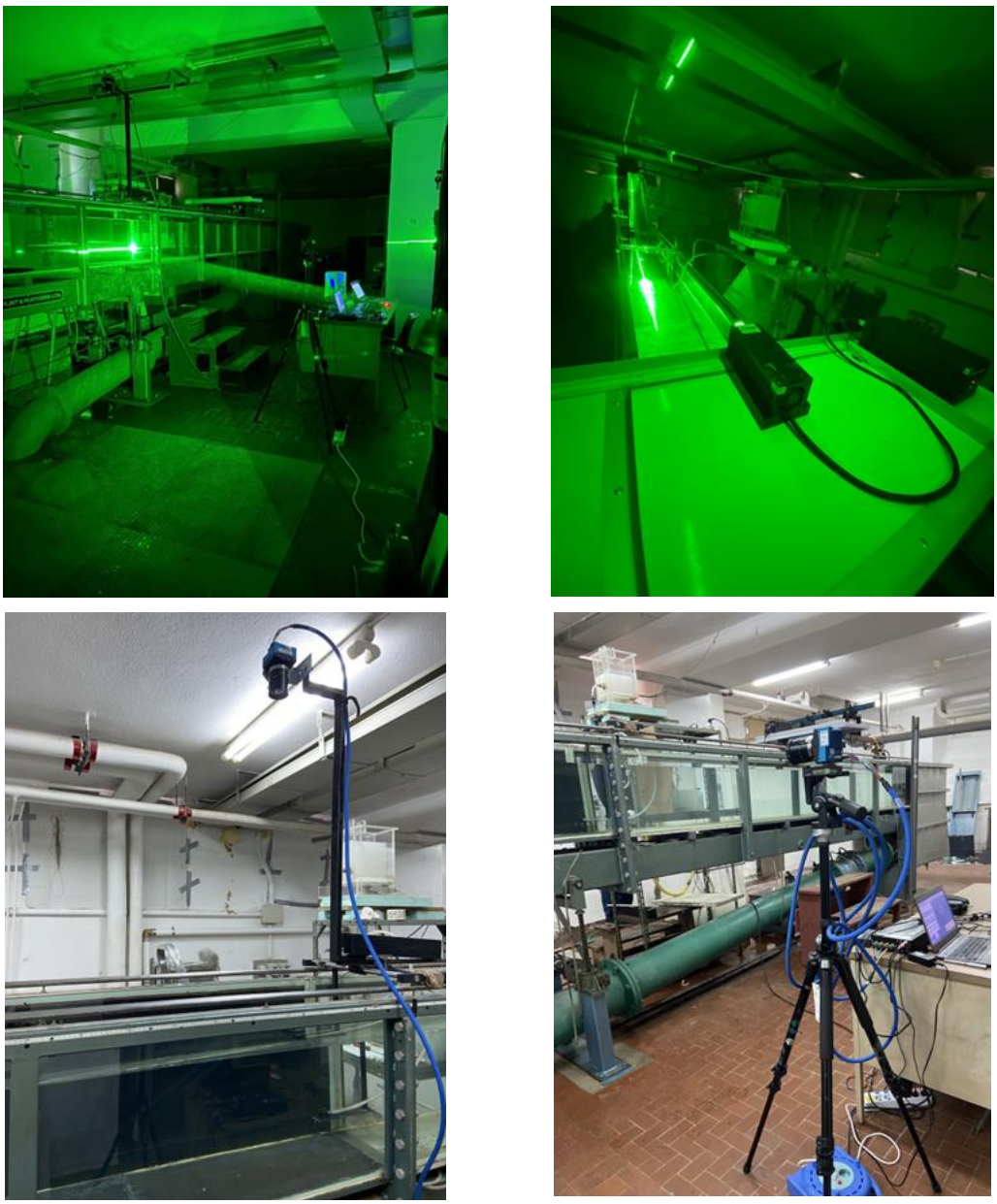

Figure B-1 Hydraulics laboratory at the University of Cagliari, Italy, showing LIF setup

Figure B-2 5-W diode-pumped solid-state (DPSS) continuous green laser

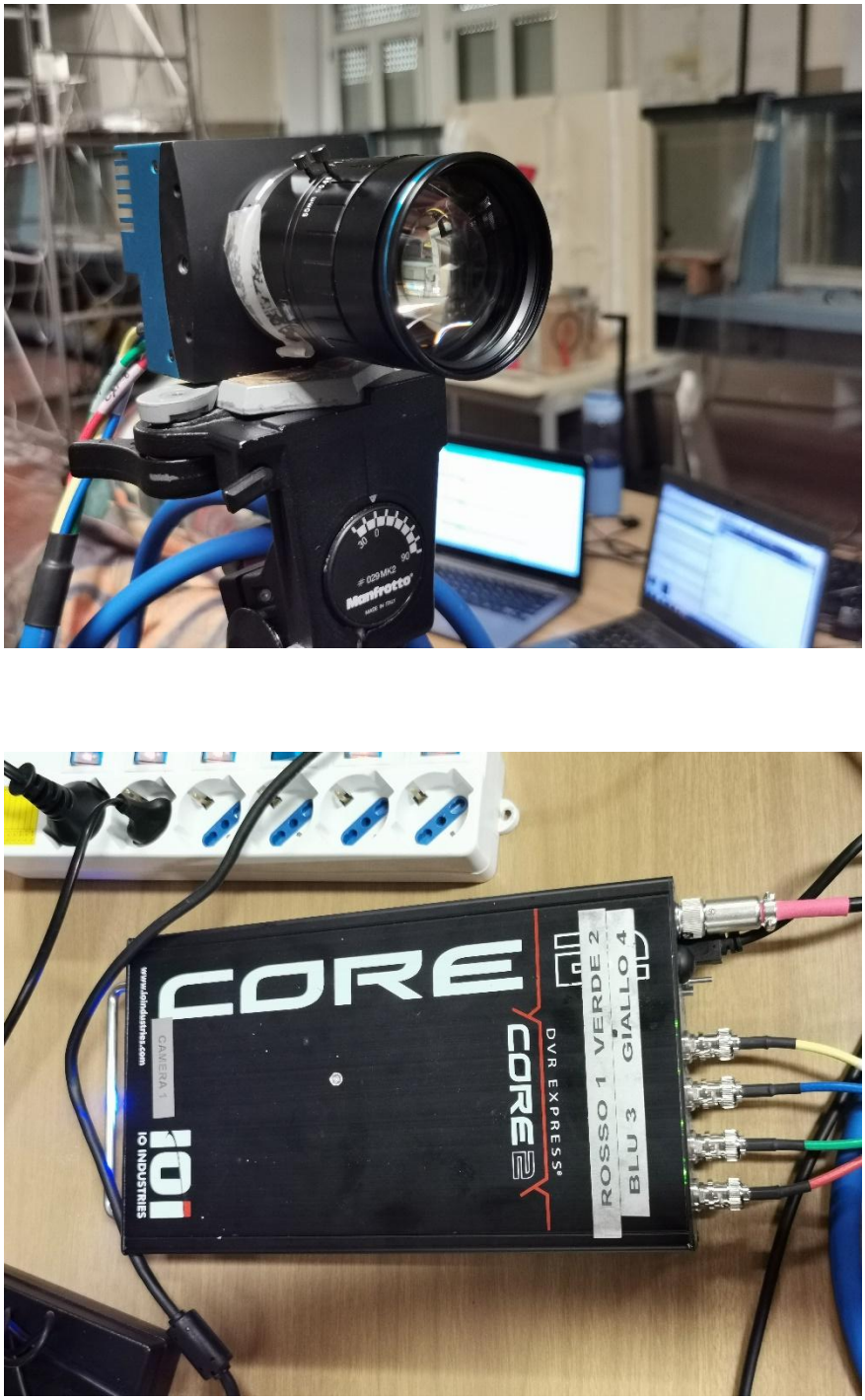

Figure B-3 Digital charge-coupled device (CCD) camera, Mikrotron EoSens 4CXP CoaXPress

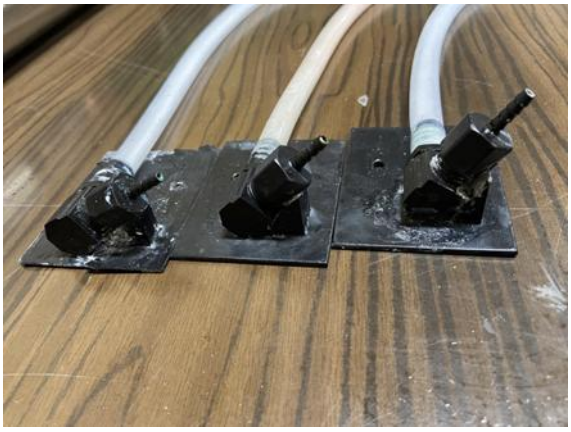

Figure B-4 Designed diffusers with the discharge angles of 30°, 45°, and 60°

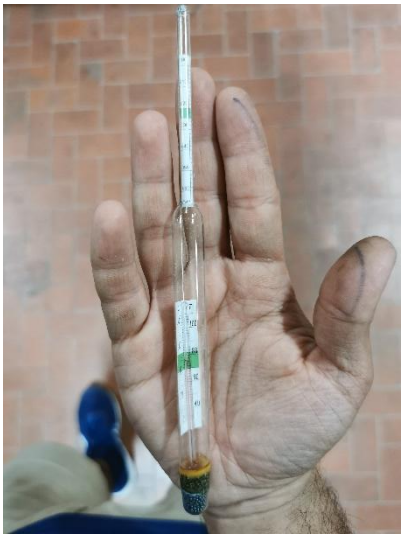

(a)

(b)

Figure B-5 (a) Gravity hydrometer and **(b)** flow meter

Figure B-6 Tool used to move the laser sheets, showing the laser setup

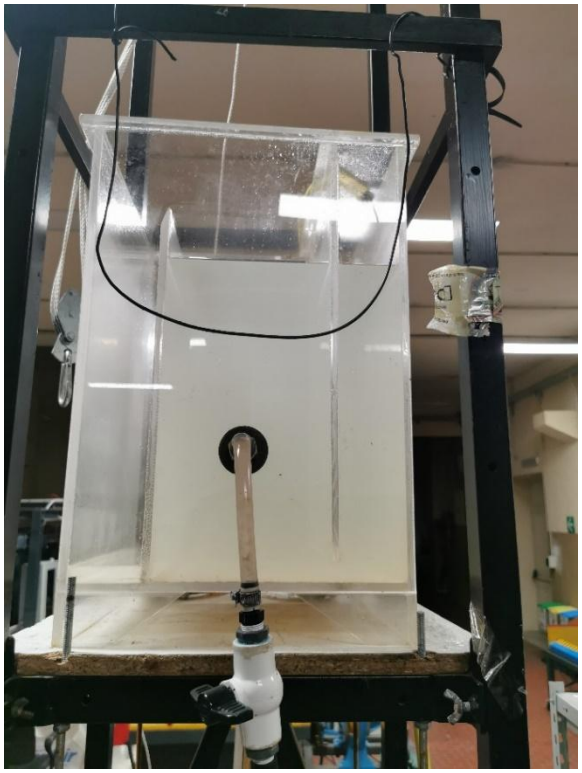

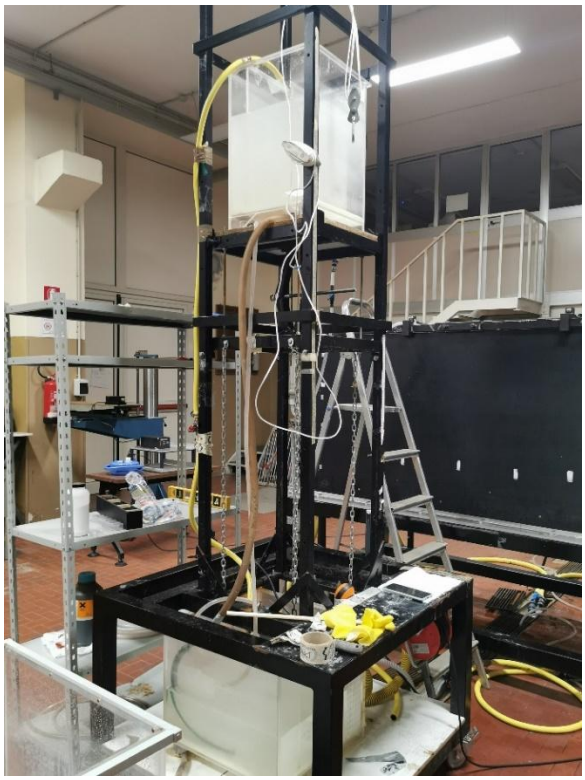

Figure B-7 Discharge tank and its setup